Linking distal volcaniclastic sedimentation and stratigraphy with the growth and development of stratovolcanoes, Ruapehu volcano, New Zealand

A thesis presented in partial fulfilment of the requirements for the degree of

Doctor of Philosophy

in

Earth Sciences

at Massey University, Palmerston North, New Zealand.

Manuela Tost

2015

"Look deep into Nature, and then you will understand everything better"

~ Albert Einstein

ABSTRACT

Large, long-lived stratovolcanoes are inherently unstable, and commonly experience large-scale flank collapse. The resulting debris avalanches permanently alter the edifice and the valleys they impact. New mapping reveals that at least six hitherto unknown debris avalanches occurred from Mt. Ruapehu, New Zealand. They collectively inundated >1,200 km^2 and ranged between 1.3 and >3 km^3 in volume, the latter being the largest debris avalanche known from the volcano. Constriction of the sliding debris avalanches into deep river valleys enhanced basal erosion, incorporation of water-saturated substrate and formation of a basal lubrication zone. This led to runouts of up to 100 km, 2 - 3 times longer than expected for equivalent unconfined dry landslides. Two of the seven river catchments affected by debris avalanches were truncated from the volcano by proximal debris choking. The debris avalanches commonly coincided with warming from glacial into interglacial periods and rapid deglaciation of Mt. Ruapehu. A loss of ice-armouring of the slopes and increased water saturation likely weakened the edifice. At least two of the debris avalanches were triggered by intrusion of new magma into the mountain. The highly resistant debris-avalanche deposits form distinctive plateaus at the highest topographic elevations along present eroding river valleys, in places reflecting earlier drainage pathways. Deposit ages and those from lower climate-controlled (non-volcanic) fluvial aggradational terraces allowed calculation of regional uplift rates, which varied between 1.3 ± 0.5 mm yr^{-1} to 5 ± 1.3 mm yr^{-1} over the last c. 125 ka. Each major flank failure led to decompression of the Mt. Ruapehu magmatic system, triggering pulses of numerous large-scale eruptions and syn-eruptive lahars. Ar-Ar dating of lava clasts within the debris avalanche deposits provided evidence of volcanic episodes that are not exposed on the present edifice. The oldest deposits from Mt. Ruapehu are now identified at ≥340,000 ka and show that a complex multi-stage storage magma system was operating, similar to that of the present day. Hornblende-bearing xenoliths from these lavas show that a magmatic crustal underplate at >40 km depth existed beneath the volcano by ~486.5 ± 37.6 ka. Combined, samples from the mass-flow deposits and the cone lavas show more complex variation over time than previously thought, but generally reflect a progressively increasing heat flux and a shift of the magma-storage system from the lower crust to mid- and upper-crustal levels.

ACKNOWLEDGEMENTS

This research would not have been possible without the assistance of my chief-supervisor Prof Shane Cronin. He suggested my research project and helped me receive a Massey Doctoral scholarship as well as other financial assistance during the course of my PhD. I would also like to thank him for helpful discussions and new ideas during my Doctorate, as well as his thorough reviews of my thesis, manuscripts, and conference abstracts. Most importantly, I'm incredibly grateful that he's always been supportive of me; whether I needed advice and/or someone to talk to in professional as well as private matters.

I also wish to thank my co-supervisors Dr Jonathan Procter and Prof Vince Neall (Massey University), Prof Richard Price (Waikato University) and Assoc Prof Ian Smith (The University of Auckland) for their fruitful discussions over the last four years. I especially want to thank Prof Richard Price for the thorough revision of major parts of my thesis and his helpful criticism. I am grateful to Assoc Prof Ian Smith (University of Auckland) for arranging the use of the XRF-equipment at The University of Auckland. I would also like to thank Dr Alan Palmer (Massey University) for his field assistance, and Dr Bob Stewart, and Dr Georg Zellmer (Massey University) for helpful discussions regarding the Turakina debris flow. Mr. John Wilmshurst (The University of Auckland) is thanked for his helpful assistance in XRF analysis and sample preparation, and Mr Gordon Holms (ANU, Canberra, Australia) for his beautiful thin section preparation. Furthermore, I would like to thank Prof Anthony Koppers and Mr Dan Miggins (Oregon State University, USA) for preparation of suitable samples for $^{40}Ar/^{39}Ar$-dating, as well as their determination in getting the best possible results, even though it mend re-analyzing 12 out of 20 samples. Furthermore, I would like to thank Dr Gert Lube (Massey University) and Dr Pilar Villamor (GNS, Wellington) for helpful discussions regarding the physical parameters of debris avalanches, and regional tectonic fault systems. I furthermore want to thank Dr Gert Lube for making me visit the 2012 Tongariro debris avalanche in order to gain insights into the proximal features of confined landslides, but most importantly I thank him for his friendship and for believing in me.

I furthermore want to thank my fellow postgraduate students, Dr Gabor Kereszturi, Dr Natalia Pardo, Dr Marco Brenna, Gaby Gomez, Rafael Torres-Orozco, Szabolcs Kosik, Eric Breard, and Adam Neather for sharing our "PhD experience", and helping each other during harder times. I furthermore would like to thank Eric Breard for a fun collaboration during the November 2012 eruption of Mt. Tongariro, and for numerous useful late-night scientific discussions.

I would also like to thank Kate Arentsen (Massey University), the true angel of the VRS department. She has always been helpful, thorough, understanding, and supportive in every single matter one can think of, ranging from car bookings down to correcting manuscripts and theses. I am sure without her, and her constant good spirits, I would have had a much harder time during my PhD.

Of the Soil and Earth Sciences Group I would further especially like to thank Matthew Irvin, Bob Toes, Ian Furkert, David Feek, and Dr Anja Möbis. All of them introduced me to the labs (and 4WD driving) at the start of my PhD and helped me out whenever I had difficulties during sample preparation processes, or GIS-data processing. But most of all, they always made me laugh, and knew when there was nothing else needed but a big supportive hug. I especially would like to thank Dr Anja Möbis for all the time we shared: the coffee breaks, the lunch breaks, the

dinners at her or my home; for her friendship and her constant support. I am not sure I would have made it through the four years without her by my side.
I also want to thank the examiners of my thesis: Assoc Prof Ian Fuller, Prof Timothy Davies, and Prof Claus Siebe for their thorough and constructive review of this study. I highly appreciated the discussion with them during my oral, especially regarding potential future research collaborations. They made me feel like I'm already part of the scientific community rather than a student nervous about the outcome of her examination. Overall, they made this final hurdle a very pleasant and fun experience.

I am also grateful to all the farmers on the Ruapehu ring plain who allowed me access to their land. I especially thank Jeff Williams at Mataroa who invited me to stay with him, prepared homemade sandwiches and coffee to share for lunch, and became a true and close friend.

My PhD was funded by a scholarship granted by the Institute of Natural Resources and a Massey Doctoral Scholarship. Furthermore this work was supported by the New Zealand Natural Hazard Research Platform. I would also like to thank the IAVCEI committee for their travel grant, which allowed me to attend the 1st International Conference on Volcano Geology in Madeira, Portugal.

My life would definitely not have been the same without all the amazing people I met in Palmerston North who became friends and made my time spend here truly memorable. Of these I would especially like to thank Chris Prentice, Callum Gibbins, Julie Morris, Kristi Tungatt, Ruthie Henchman, Angela Denes, Daniel Farley, Friederike von Schlippe, Andrew Penwarden, Ana Maria Ramirez, Dylan Ball, Gaby Gomez, Omar Cristobal, Zsuzsa Smolinka, Diana Cabrera, Sophie Staniforth, Jonathan Parsons, Cormac Chalmers, and Claire Black who were my Kiwi-family, far away from my original one. Feeling their support, encouragement, and love was all I ever needed after a hard day to lift me up again. I further would like to thank them for having shown me an amazing life outside of work, filled with exploring the most beautiful places all over New Zealand.

I am extremely grateful to my family and friends in Germany who have supported and encouraged me before and during my entire PhD study, even from the other side of the globe. They gave me the courage to move to New Zealand in the first place, and always made me believe that I can achieve anything for as long as they are part of my life. Of all those beautiful overseas people, I would especially like to thank Anne Deremetz, Arndt Morgenroth, Maximilian Hansen, Swantje and Wendelin Teschemacher, Katrina Weber, Bastian Schwarz, Martin Laudel, Benedikt Lerch, Steffen and Jens Moser, Alexander and Claudia Karaula, Peter and Birgit Niedner, and Brigit, Renate, Friedel, Annette, and Wilhelm Sander for their constant support, their friendship, and for always being there when really needed, even if it involved last-minute 32-hour flights.
I'm incredibly thankful to my parents and my brother without whom I would have never made it here, who always tried their hardest to find solutions to "overseas"-problems and always had time to listen to all those stories I told, whether they were good or low-spirited.

Last but most importantly, I would like to thank Stefanie van Büren, who had been my first true friend and family member here in New Zealand. She was one of the most admirable people I

had ever met. Seeing the way she faced her life, always impressed me and made me feel so much braver than I truly was. She was my climbing, surfing, horse-back riding, and tramping buddy during weekends and public holidays, and my coffee drinking buddy during times of hard work at the department. She always had an open ear for my struggles, and I am incredible grateful for the support, understanding, loyalty and friendship I had received from her over the years. This thesis is dedicated to her.

TABLE OF CONTENTS

LIST OF TABLES

LIST OF FIGURES

sourced from the stratovolcano, form a distinct aggradational terrace at the highest elevation of the valley margins. The extremely high sediment flux generally resulted in blockage of the original river path. Subsequently, up to four non-volcanic fluvial aggradational terraces are exposed on lower altitudes.

Rhyolitic caldera formation in the TVZ. (A) The TVZ (yellow field) is a c. northeast-trending magmatic system divided into three individual magmatic zones, based on the chemical composition of the volcaniclastics. Rhyolitic volcanism is limited to the central part of the TVZ (red rectangle). (B) Localities of the major rhyolitic calderas in the central TVZ that erupted large amounts of volcaniclastic material over the last 340 ± 10 ka (Table), which was likely associated with enhanced regional tectonic activity.

Development of New Zealand's climate over the last 400 ka, modified after Beau and Edwards (1983). The red-shaded areas represent the approximate timing of flank failures at Mt Ruapehu. Syn-eruptive events are marked (*). Most of the post-eruptive large-scale (>1 km^3) flank failures of Mt. Ruapehu (Tost et al., 2014) occurred during transitions between cold stages and interstadial climates.

CHAPTER 1: INTRODUCTION

1.1 Introduction

Since the beginning of written records, reports of volcanoes have reflected the opposing feelings of fascination and unease they create within the people living in their proximity (e.g., Empedocles, 490 - 430 BC; Plato, 428 - 348 BC; Aristotle, 384 - 322 BC). Weathering of their sedimentary products yields extremely fertile and highly sought-after soils for husbandry, even though their eruptions pose great risks to civilization, cultivation, waterways, infrastructure and the climate. Large eruptions can even have worldwide impacts, such as the 1600 eruption of Huaynaputina, Peru, the 1815 eruption of Mt. Tambora, Indonesia, the 1912 eruption of Novarupta, Alaska, and the 1991 eruption of Mt. Pinatubo, Phillippines (e.g., McCormick et al., 1995; Briffa et al., 1998; De Silva & Zielinski, 1998; Oppenheimer, 2003). Of all the various types of volcanoes, outbursts from stratovolcanoes are among the most hazardous due to their generally highly explosive plinian to subplinian eruptive style and their characteristically long periods of quiescence followed by sudden eruptions. The commonly plinian eruptions are characterized by extremely rapid (100 - 400 m/s) discharge of gas- and particle-laden mixtures, which form high (typically between 6 km and >25 km) eruption columns that are dispersed widely by the local wind system, and/or collapse under gravity to create pyroclastic density currents (Cioni et al., 2000). Furthermore, parts of steep stratovolcanic edifices are prone to collapse either during or between eruptions to produce catastrophic, rapid debris avalanches, which bury and bulldoze the landscape they are emplaced upon (Siebert, 1984; McGuire, 1996; Zernack et al., 2012; Tost et al., 2014). In addition, stratovolcanoes are prone to lahars caused by rainfall-induced remobilization of sediment, crater-lake outbreaks, or eruption-induced snow melting. These sediment-laden mudflows and debris flows descend the steep volcanic flanks up to hundreds of kilometres from the edifice (e.g., Mothes, 1992; Rodolfo, 2000; Lecointre et al., 2004; Doyle et al., 2009).

Due to the wide hazard range of stratovolcanoes, the most fatal volcanic eruptions known are related to their eruptive activity. The eruption of Mt. Tambora, Indonesia, in 1815, for example, caused the imminent death of 92,000 people (Oppenheimer, 2003), while the famous eruptions of Krakatoa, Indonesia, in 1883, and Mt. Pelée, Martinique, in 1902 killed 36,000 and 33,000 people, respectively (Symons, 1888; Heilprin, 1903). The 1980 Mt. St Helens eruption was probably the first extremely well documented eruption of a stratovolcano, involving both plinian and debris avalanche processes. Following the intrusion of a cryptodome into the edifice, an earthquake caused multiple failures of the northern flank, which subsequently triggered a northward-directed blast and associated pyroclastic flows, along with a 6 - 8 km^3 debris avalanche and a subsequent plinian eruption (Christiansen & Peterson, 1981; Voight et al., 1983).

Mt. Ruapehu is one of several stratovolcanoes located on New Zealand's North Island. It is frequently active, with major recent eruptions occurring in fifty-year intervals (1895, 1945, and 1995 - 1996) (e.g., Johnston et al., 2000; Price et al., 2012). These were typically associated with lahars descending its eastern and northern flanks (e.g., Nairn et al., 1979; Hackett & Houghton, 1989; Cronin et al., 1997a; Cole et al., 2009; Lube et al., 2009; 2012). These sediment-water mass flows can occur even during periods of eruptive quiescence, as shown tragically in 1953, when 151 people lost their lives in the Tangiwai Railway Disaster. This was caused by a post-eruptive

lake-breakout lahar that spilled into the Whangaehu River and damaged the railway bridge, which subsequently collapsed under the weight of the arriving train (e.g., O'Shea, 1954).
At present, Mt. Ruapehu's activity is characterized by relatively small "blue-sky"-eruptions (~0.05 km^3 magma batches; Price et al., 2012), which deposit pyroclastic and volcaniclastic material dominantly on the volcano flanks (e.g., Kilgour et al., 2010; Christenson et al., 2010). In 1945 and 1995 - 1996 larger subplinian eruptions occurred, distributing tephra to much wider areas around New Zealand (Johnston et al., 2000; Cronin et al., 2003). Numerous exposures of pyroclastic and volcaniclastic sediments, up to 100 km from the volcano, hold evidence that larger-magnitude events have occurred frequently in the history of this stratovolcano. With the population of New Zealand and the number of visitors constantly rising and infrastructure increasing in value (Johnston et al., 2000), assessment and quantification of these hazards are critical in order to develop accurate volcanic event scenarios for future emergency management and hazard mitigation planning (Blong, 1984).

1.2 Objectives of this study

Mt. Ruapehu has a well established historic and geological record (e.g., Palmer, 1991; Cronin et al., 1996; Cronin & Neall, 1997; Lecointre et al., 1998; Gamble et al., 1999; Waight et al., 1999; Donoghue & Neall, 2001; Pardo et al., 2012). Nonetheless, there are huge gaps in its older eruptive and construction history. Previous studies of lahar and other volcaniclastic deposits exposed on the eastern Ruapehu ring plain, mapped in detail by Donoghue (1991), Hodgson (1993) and Cronin (1996), amongst others, concentrated on the last c. 50 ka and thus have only just scratched the surface of the potential geological record contained in the ring plain. The Ruapehu edifice is at least 300 ka in age (Gamble et al., 1993), whereas the ring plain volcaniclastic history has only been well documented back as far as c. 50 ka. A more complete knowledge of the nature and frequency of past activity is necessary to robustly judge the context of recent eruptions of Mt. Ruapehu and more clearly outline its full potential range of future hazards and eruptive behaviour. A major key to this understanding is beyond the cone, because more recent lava-flows dominate the proximal volcanic record and allow little chance for dating and evaluation of long histories. Mass-flow deposits, accumulating in river valleys and overlapping fans (ring plains) around the volcano, provide scope for a longer-term view of the ancient volcanic history, allowing dating and interpretation of the style and magnitude of volcanism, cone collapse and climate interaction (e.g., Cronin et al., 1996). In addition, detailed research on the laharic sequences exposed on the western side of Ruapehu has never been carried out. In order to gain insights into the growth and development of this explosive volcano, a new integration of the geological history contained in the ring plain with that of the cone record is required.

Hence, the aims of this study are to:
1. Construct a full stratigraphic record of the volcaniclastic deposits surrounding Mt. Ruapehu, concentrating especially on the oldest exposed sequences extending from the near-edifice sequences to those down the Hautapu, Turakina, Whangaehu, Mangawhero, Manganuioteao, Whakapapa and Whanganui River valleys.
2. Use geochemistry and petrology to correlate the volcaniclastic sequences to the known and dated lava-flow history on Mt. Ruapehu (e.g., Hackett & Houghton, 1989; Waight et al., 1999;

Gamble et al., 2003) to integrate the ring plain and edifice growth, as well as destruction records.
3. Apply $^{40}Ar/^{39}Ar$-dating of targeted volcaniclastic sequences to:
   a. Reconstruct the older (>50 ka) eruptive history of Mt. Ruapehu, including defining periods of high-frequency and high-magnitude explosive volcanic activity, episodes of intense ring-plain aggradation, and identification of major edifice failures;
   b. Quantify the numbers and rates of different types of volcanic mass-flow events (lahars, debris avalanches) in different sectors of the ring plain;
   c. Provide insights into the palaeo-tectonic/uplift history and rates of erosion in the major catchments draining the Central Plateau area; and
   d. Develop a holistic model of the interaction of the factors that lead to the development, sudden change and evolution of paired stratovolcano-ring plain systems.

1.3 Geological Setting

1.3.1 Taupo Volcanic Zone (TVZ)

The c. 300 km long and up to 50 km wide TVZ (Fig. 1) is the dominant locus of late-Pliocene to Quaternary volcanic activity in New Zealand (Graham & Hackett, 1987; Wilson et al., 1995). It is one of the most productive magmatic systems on Earth, and erupted 15,000 - 20,000 km^3 of volcaniclastics during the past 2 Ma (e.g., Wilson et al., 1995; Price et al., 2005). The TVZ includes central North Island rhyolitic eruptive centres, and andesitic volcanism in its north eastern (Bay of Plenty) and south western (Tongariro Volcanic Centre) subdivisions (e.g., Graham et al., 1995; Houghton et al., 1995; Wilson et al., 1995; Price et al., 2005). The composition of andesitic volcaniclastics varies widely within any particular time period, with no apparent geographical control (e.g. Graham & Hackett, 1987). The TVZ volcanism results from oblique subduction (1.27°/Ma) of the oceanic Pacific Plate beneath the continental crust of the Australian Plate and this becomes progressively more oblique towards the south (Graham et

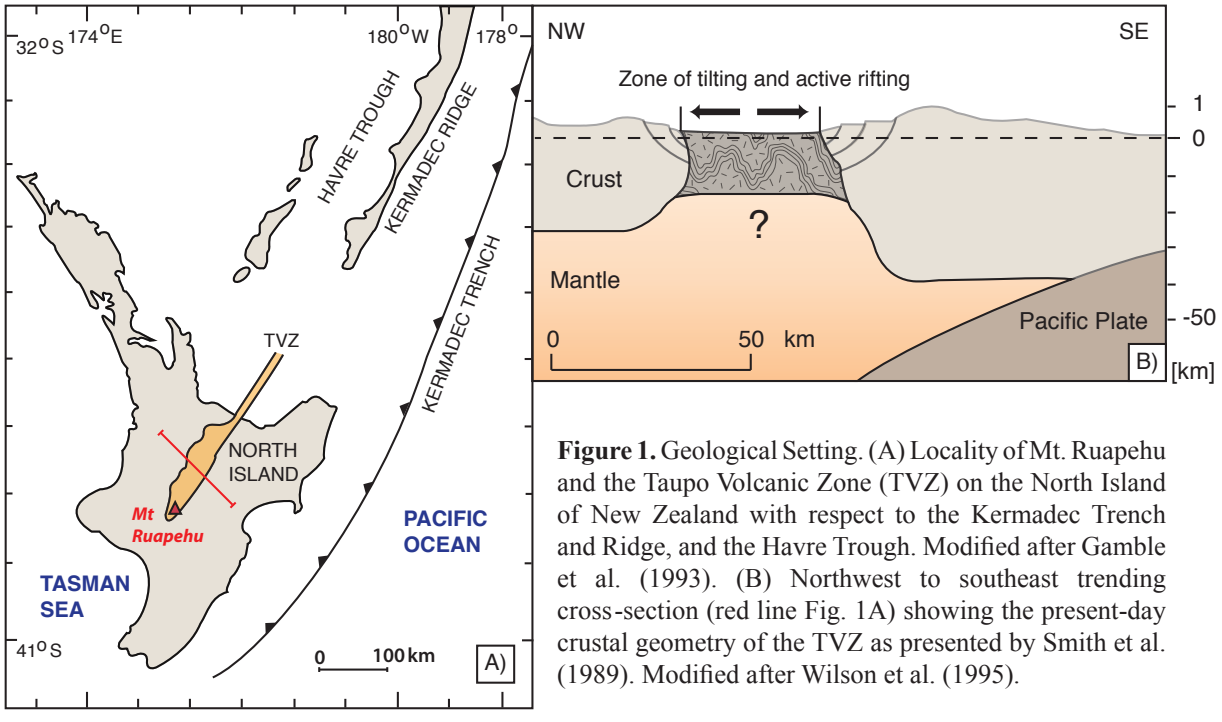

Figure 1. Geological Setting. (A) Locality of Mt. Ruapehu and the Taupo Volcanic Zone (TVZ) on the North Island of New Zealand with respect to the Kermadec Trench and Ridge, and the Havre Trough. Modified after Gamble et al. (1993). (B) Northwest to southeast trending cross-section (red line Fig. 1A) showing the present-day crustal geometry of the TVZ as presented by Smith et al. (1989). Modified after Wilson et al. (1995).

al., 1995; Wilson et al., 1995). The TVZ extends through the central part of the North Island from Ohakune to White Island and beyond to the edge of the continental shelf, forming a NNE-SSW-trending zone of late-Pliocene to Quaternary arc volcanoes (Fig. 1A) (Wilson et al., 1995). The present TVZ is thought to be actively widening, which is primarily caused by rifting rather than spreading (e.g., Sissons, 1979; Grindley & Hull, 1986; Walcott, 1987; Nairn & Beanland, 1989; Darby & Williams, 1991). It is characterized by a thin (12 - 15 km), stretching (~8 - 10 mm/a on average) continental crust, high ^{3}He flux, and extremely high heat flow (~700 mW/m^2) (e.g., Hochstein, 1995; Houghton, 1995; Price et al., 2005). In the onshore TVZ, the seismic basement is usually inferred to lie below 2.0 - 2.2 km depth (e.g., Robinson et al., 1981; Stern & Davey, 1987), but the nature of this basement is ambiguous and it cannot be correlated with any particular lithology (Fig. 1B) (Bibby et al., 1995). To the east and west of the TVZ, pre-volcanic sediments (greywacke), largely of Mesozoic age, crop out at the surface in the axial Hauhungaroa Ranges (Wilson et al., 1995).

1.3.2 Tongariro Volcanic Centre (TgVC)

The TgVC lies at the southwestern end of the TVZ and contains six major andesite massifs: Mt. Maungakatote, Mt. Kakaramea, Mt. Pihanga, Mt. Hauhungatahi, Mt. Tongariro and Mt. Ruapehu (Fig. 2) (Cole, 1978). Of these the currently most active are Mt. Tongariro and Mt. Ruapehu, which shape vast aggradational ring plains composed of tephra, pyroclastic-flow deposits, as well as laharic and fluvial deposits (e.g., Cole et al., 1986; Hackett & Houghton, 1989; Donoghue et al., 1995; Graham et al., 1995). The andesitic lavas exposed within the TgVC are generally porphyritic with a dominant phenocryst assemblage of plagioclase + orthopyroxene + clinopyroxene + titanium magnetite ± olivine ± hornblende (e.g., Cole, 1978; Graham & Hackett, 1987; Price et al., 2005; 2012). Graham and Hackett (1987) identified six different andesite types within the region: plagioclase-pyroxene-phyric (Type 1), plagioclase-phyric (Type 2), pyroxene-(olivine)-phyric (Type 3), pyroxene-phyric (Type 4), olivine-pyroxene-phyric (Type 5), and rare hyprid andesites exhibiting equilibrium textures (Type 6). Labradorite and labradorite-pyroxene andesites are the most voluminous lava types occurring in the TgVC (Cole, 1978) and were interpreted to have formed by assimilation of granitic material by basaltic magma (e.g. Steiner, 1958; Clark, 1960; Stipp, 1968).

The onset of volcanism in the TgVC is still not clearly understood. The oldest lavas sampled and dated from the cones of Mt. Tongariro and Mt. Ruapehu are 0.26 ± 0.003 Ma, and 0.23 ± 0.01 Ma, respectively (Stipp, 1968). Pebbles of labradorite-pyroxene andesite, on the other hand, occur in Lower Pleistocene conglomerates within the marine sequence of the Wanganui District c. 100 km south west of Mt. Ruapehu, and deposited c. 0.3 Ma ago (Fleming, 1953; Cole, 1978; Tanaka et al., 1997; Gamble et al., 2003), but the oldest dated lava (Tama Lakes) is 0.26 ± 0.003 Ma in age (K/Ar date; Stipp, 1968).

1.3.3 Mount Ruapehu

Mt. Ruapehu (2,797 m) is a ~300,000-year old andesitic stratovolcano, sited within an active graben in the centre of New Zealand's North Island. Ongoing normal and strike-slip faulting occurs on the Raurimu Fault to the west, and the Rangipo Fault (750 ± 50 m vertical displacement) to the east, of the composite cone (Villamor & Berryman, 2006a). Numerous normal minor strike-slip

faults are generally downthrown to the distal southern side of the southern Ruapehu area and produce crosscutting geometries with the marginal rift-boundary faults (Villamor & Berryman, 2006b). Seismic (Villamor & Berryman, 2006a; 2006b; Salmon et al., 2011), as well as petrologic xenolith studies suggest that the basement beneath the volcano is c. 40 km thick and made up of Mesozoic greywacke (upper to middle crust) underlain by meta-igneous lower crust (e.g., Graham & Hackett, 1987; Adams et al., 2007; Price et al., 2012).

Permanent glaciers blanket parts of the composite cone and its active vent is filled by an acidic Crater Lake, which has caused more than 60 syn- and post-eruptive lahars since 1861 (e.g., Nairn et al., 1979; Cronin et al., 1997a; Cole et al., 2009; Lube et al., 2012). Prior to this study, hydrothermal alteration and substrate weakening have been interpreted as the pre-conditioning mechanism for five flank-failure events at the volcano (Palmer & Neall, 1989; Hodgson, 1993; Lecointre et al., 1998; Donoghue & Neall, 2001; Keigler et al., 2011). Erosion on the composite

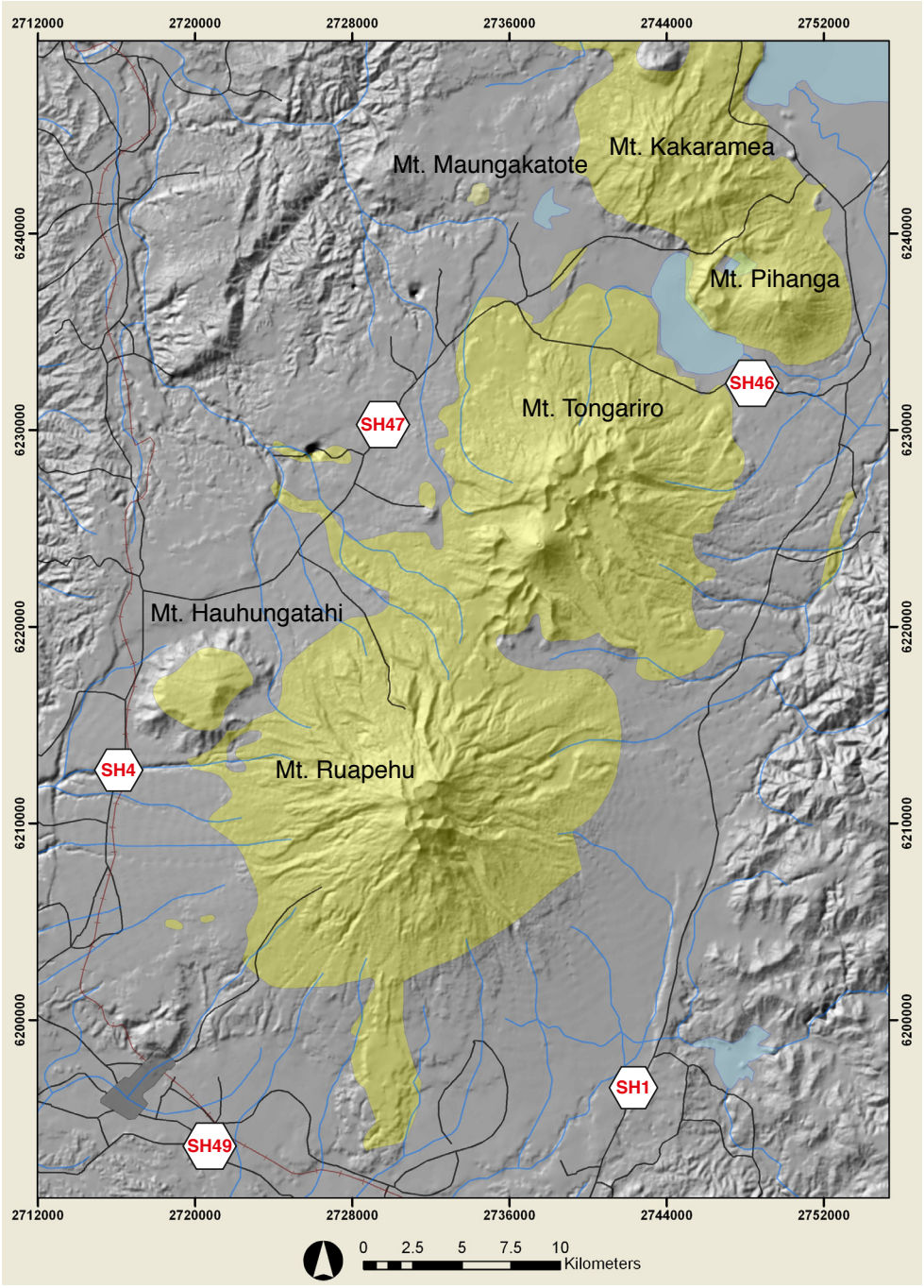

Figure 2. Digital elevation model of the Tongariro Volcanic Centre outlining the major andesite massifs Kakaramea, Pihanga, Tongariro and Ruapehu, as well as the minor volcanic centres Maungakatote and Hauhungatahi.

cone has resulted in strong dissection, forming deep gorges on the upper flanks, as well as on the surrounding proximal and distal ring plain (Gamble et al., 2003). The landscape in the proximity of the stratovolcano is made up of 110 km^3 of stacked laharic, fluvial, and tephra deposits, which are primarily <27.1 ka in age, with longer runout mass-flow deposits infilling and lining the margins of surrounding river catchments up to 200 km from source (e.g., Cronin et al., 1997b; Lecointre et al., 1998).

The stratovolcano itself is made up of variably dipping lava-flow sequences, autoclastic breccias, and pyroclastic, epiclastic, and glacial deposits (Hackett & Houghton, 1989; Smith et al., 1999). Petrologically, the Mt. Ruapehu lava-flow sequences comprise dominantly plagioclase-pyroxene-phyric, plagioclase-phyric, and pyroxene-(olivine)-phyric lavas, although pyroxene-phyric, olivine-pyroxene-phyric, and rare hyprid andesite rock types are also found and correspond to particular growth stages represented as cone-building formations (Graham & Hackett, 1987; Graham et al., 1995; Gamble et al., 2003; Price et al., 2012). The dominant phenocryst assemblage of the lavas is plagioclase + clinopyroxene + orthopyroxene + Fe-Ti-oxides, along with rare olivine and amphibole (Graham & Hackett, 1987; Gamble et al., 2003; Price et al., 2012). The rarity of hornblende in Mt. Ruapehu lavas has been interpreted to indicate that crystallisation occurred from water-undersaturated melts (2 - 5 wt.%) (Graham et al., 1995). Petrological and geochemical studies suggest that crystallization temperatures ranged between 1050°C and 1200°C and crystallization pressures were below 10 kbar (Green & Hibberson, 1969; Lindsley, 1983; Graham & Hackett, 1987).

Four major cone-building episodes were identified and mapped by Hackett & Houghton (1989) on the edifice, and subsequently dated (Fig. 3) (Gamble et al., 2003). These are, from oldest to youngest: the Te Herenga Formation (250 - 180 ka; Gamble et al., 2003), the Wahianoa Formation (c. 120 - 150 ka; Price et al., 2005), the Mangawhero Formation (55 - 15 ka; Gamble et al., 2003), and the Whakapapa Formation (<15 ka; Gamble et al., 2003). The lavas have become progressively more enriched in SiO_2, K, Rb, and Sr over time, although the geochemistry varies widely within each of the major eruptive episodes, apart from the Te Herenga Formation (Fig. 4) (Gamble et al., 2003; Price et al., 2005; 2012). The temporal geochemical and petrographic variations at Mt. Ruapehu have been interpreted to reflect open-system processes within a complex plumbing system, comprising numerous small dykes and sills distributed throughout the crust and upper mantle beneath the volcano (Price et al., 1997; Gamble et al., 1999; 2003; Price et al., 2005; 2007; 2012). This is consistent with seismic anisotropy measurements, which suggest dyke-like structures at less than 10 km beneath the edifice (Miller & Savage, 2001; Gerst & Savage, 2004). Stagnant melt is thought to crystallize and fractionate in these small isolated pockets, assimilating surrounding wall rock, xenoliths and xenocrysts, and mingling with fresh magma intrusions (Graham & Hackett, 1987; Gamble et al., 1999; Price et al., 2005; 2012). Disequilibrium in Th and U isotopic disequilibrium has been used to argue that these processes operate in magmas over tens of thousands of years prior to their eruption (Price et al., 2007). The magma associated with the oldest Te Herenga Formation apparently records the first stage of mantle/crust interaction as magma migrated into the lower crust and small magma chambers began to evolve at different levels within the middle and upper crust (Price et al., 1997; Gamble et al., 1999; Price et al., 2005). As described above, the precise timing for the onset of volcanism of Mt. Ruapehu is not unequivocally established, with on-cone dates extending to 0.23 ± 0.01 Ma (Stipp, 1968), and pebbles of labradorite-pyroxene andesite occurring within distal mass-flow deposits exposed c. 100 km southwest of Mt. Ruapehu dated at c. 300 ka

(Fleming, 1953; Cole, 1978; Tanaka et al., 1997; Gamble et al., 2003).

1.4 Age control - cover bed stratigraphy, aggradational terrace formation, and rhyolitic tephra marker beds

Within the study area, river and marine terraces are dated by their cover-bed sequences, which include a named series of loess/soils and dated tephra horizons (Milne, 1973a; 1973b; Pillans, 1994). The loess sequences, which were deposited during periglacial climatic periods, consist of wind-blown silt- and fine-sand particles of quarzo-feldspathic or volcanic origin. On undisturbed terrain, e.g., along the river catchments studied, or on the Ruapehu and Tongariro ring plains, the loess horizons and the corresponding accretionary soils form a distinctive sequence of unweathered/weathered units that mark alternating stadial/interstadial periods of cool/dry and warm/humid climate.

In most of the area studied the loess horizons correspond to specific aggradational river terraces, which formed during glacial periods when the colder climate caused lower tree lines and high rates of physical weathering in the uplands and mountains (e.g. Milne, 1973a; Pillans, 1994). This fed huge supplies of sediment into river valleys, building broad braided river terraces of gravels and sands (Milne, 1973a). During interglacial periods increased precipitation and vegetation cover in the uplands reduced the sediment supply and resulted in rapid down-cutting of rivers in narrow channels through their former braided gravel deposits. Overall, ongoing tectonic uplift in this area has meant that aggradation surfaces produced during each successive stadial were elevated to form terraces, at progressively higher elevations (Milne, 1973a; Berryman et al., 2000). In total, seven alluvial aggradational terraces are identified in the South Wanganui Basin and along the Rangitikei River, which are, from youngest to oldest: i) the Ohakea Terrace

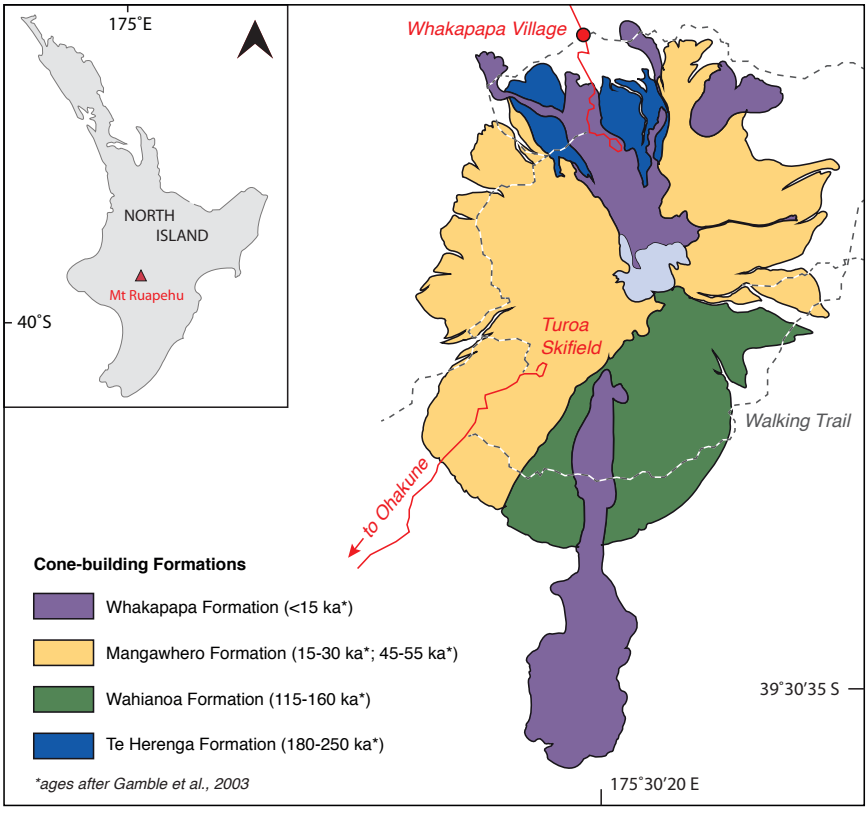

Figure 3. The individual cone-building formations exposed on the Mt. Ruapehu edifice, mapped and identified by Hackett and Houghton (1989).

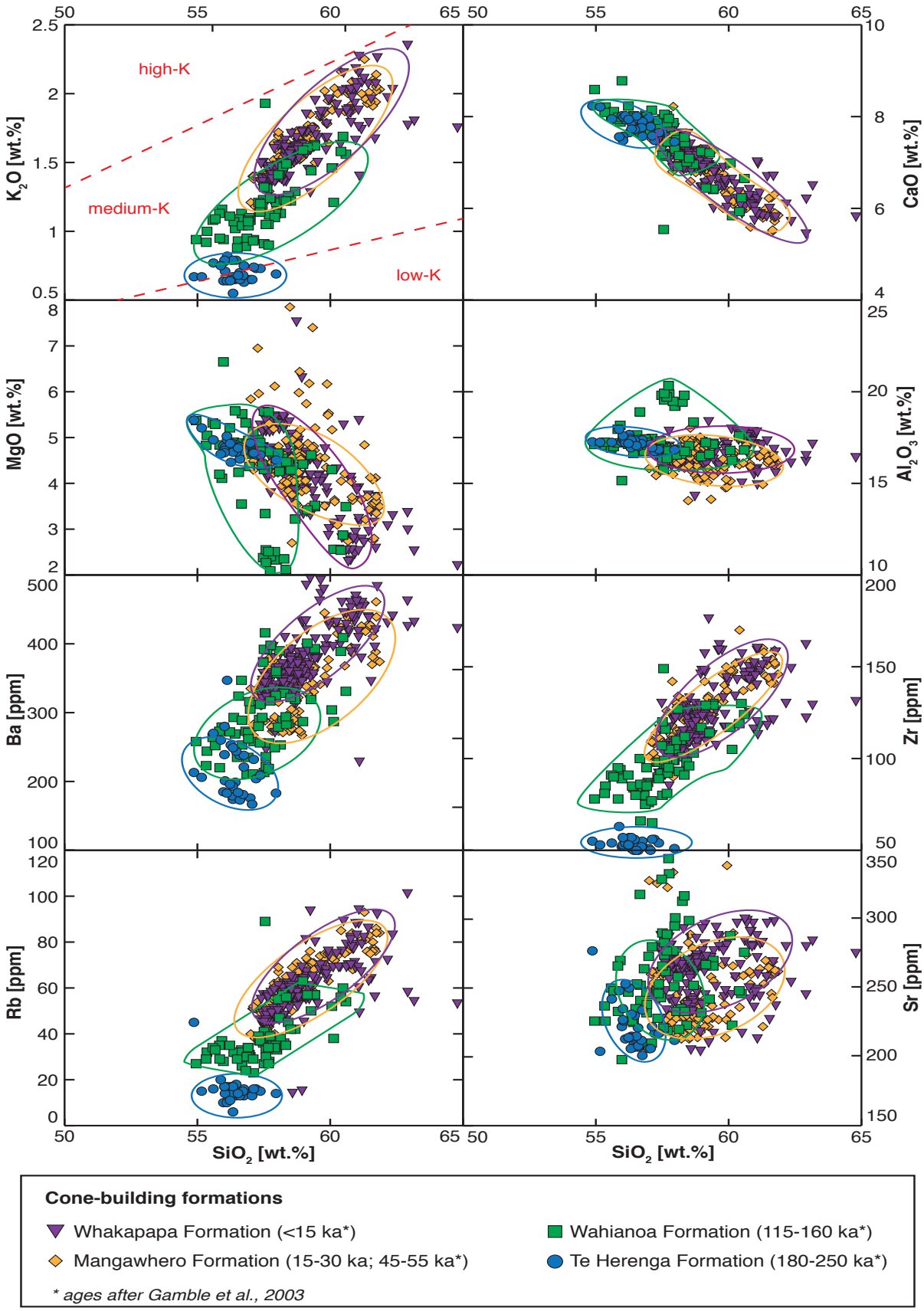

Figure 4. SiO_2 variation diagrams for selected major components and trace elements showing variation in whole rock compositions for individual Ruapehu cone building formations. Labels are colour-matched to Fig. 3 and fields are drawn for the bulk composition of each formation. Data from Price et al. (2012) and ages after Gamble et al. (2003). Potassium fields are after LeMaitre (1989).

(10 - 18 ky BP), the Rata Terrace (30 - 50 ky BP), the Porewa Terrace (70 - 80 ky BP), the Greatford Terrace (110 - 120 ky), the Marton Terrace (140 - 170 ky), the Burnand Terrace (240 - 280 ky), the Aldworth Terrace (340 - 350 ky), and the Waituna Terrace (360 - 370 ky). All ages are from Pillans (1994).

Sequences of marine terraces are limited to the southwestern sector of the study area, between Wanganui and Marton. They are interpreted to have formed during glacio-eustatic changes, with shallow marine sediments deposited during interglacial periods/higher sea levels, and intervening unconformities during glacial periods/lower sea levels (Beu & Edwards, 1984). In total twelve aggradational marine terraces were identified and subsequently dated by Pillans (1983), which are, from youngest to oldest: the Rakaupiko Terrace (60 ky), the Hauriri Terrace (80 ky), the Inaha Terrace (100 ky), the Rapanui Terrace (120 - 135 ky), the Ngarino Terrace (210 ky), the Brunswick Terrace (310 ky), the Braemore Terrace (340 ky), the Ararata Terrace (400 ky), the Rangitatau Terrace (450 ky), the Ball Terrace (420 ky), the Piri Terrace (600 ky), and the Marorau Terrace (680 ky). In each case the ages correspond to the termination of terrace-formation phases.

Another important tool for correlation and age control within the marine and river aggradational terraces are prominent marker beds of rhyolitic tephra layers, which are, from youngest to oldest: the Kawakawa Tephra (27.1 ± 1 ky; Lowe et al., 2008), the Rotoehu Ash (64 ± 4 ky; Wilson et al., 1992), the Fordell Ash (300 ky; Bussell & Pillans, 1992), the Griffins Road Tephras (300 - 340 ky; Bussell & Pillans, 1992), and the Rangitawa Tephra (340 ± 40 ky; Kohn et al., 1992).

1.5 Geography of the study area

This study extended from the southeastern to northwestern sector of the Ruapehu and Tongariro ring plains and covered an area of c. 4,000 km^2 (Fig. 5). The south eastern boundary of volcaniclastics is located c. 2.5 km south of Utiku where the Hautapu River joins the Rangitikei River, and the south western volcaniclastic border is at the Tasman Sea south of Wanganui. The northern extent of the volcaniclastic deposition area lies between the settlements Moerangi and Taumarunui. Field work was focussed along seven major river catchments, which dissect the Mt. Ruapehu and Mt. Tongariro ring plains. These are, from southeast to northwest: the Hautapu River, the Turakina River, the Whangaehu River, the Mangawhero River, the Manganuioteao River, the Whakapapa River and the Whanganui River.

The major settlements (>1,000 citizens) in the area are, from north to south: Taumarunui with a population of 4,503 (Statistics New Zealand), Piriaka with 1,743 inhabitants (Falling Rain Genomics), Raetihi with 1,002 inhabitants (Statistics New Zealand), Taihape with 1,509 residents (Statistics New Zealand), Marton with a population of 4,548 (Statistics New Zealand), and Wanganui with currently 38,094 inhabitants (Statistics New Zealand). Moderate sized settlements (100 - 1,000 citizens) include Owhango (189 inhabitants; Statistics New Zealand), National Park (240 inhabitants; 2006 Census Ruapehu District Council), Ohakune (987 inhabitants; Statistics New Zealand), Waiouru (738 residents; Statistics New Zealand), and Mataroa (149 inhabitants; Falling Rain Genomics). Additional small settlements (<100 inhabitants) occur throughout the study area and were generally established by communities of Maori tribes and/or the farming industry.

1.5.1 The Hautapu River

The present Hautapu River winds its way through the southeastern distal Ruapehu ring plain (Fig. 5). Today it rises in native grasslands east, and 640 ha of wetlands southwest, of Waiouru, e.g. the Ngamatea Swamp (Rogers, 1993). From there it meanders south besides Taihape, the largest town in the valley (Ogle, 2000). The town is located c. 47 km southeast of Mt. Ruapehu, with the Hautapu River running just east of Taihape incising into the late-Pliocene Taihape Mudstone and joining the Rangitikei River c. 2.5 km south of Utiku.
The overall remnants of one of the early eruptive episodes of Ruapehu volcano are volcaniclastic boulders, up to 4 m in diameter, exposed in the Taihape-Mataroa area (Tost et al., 2015). They are scattered around the landscape between Haeremai and Turangarere and outline the course taken by the Hautapu River during a period of volcaniclastic deposition. The andesitic boulders are most common around Mataroa, generally re-deposited on seven individual river terraces (aggradational and degradational). South of Mataroa, the exposure of boulders suggests the former river course turned east towards Taihape. Around Taihape andesitic boulders are generally limited to the area west of State Highway 1. The furthest southern extent of the reworked volcaniclastic boulders is a hilltop at Haeremai.

1.5.2 The Turakina River

The present Turakina River dissects the southern distal Ruapehu ring plain and is not currently sourced from the stratovolcano. Instead it originates from a swamp area c. 4.5 km south-southwest of Tangiwai at an elevation of 740 m a.s.l. (Fig. 5). From there it winds its way south, passing the farming community Rangiwea Junction, as well as the minor settlements Turakina, Ratana and Koitiata, before joining the Tasman Sea c. 15 km southeast of Wanganui. The river incises solely into late-Pliocene mudstones and muddy sandstones.
A debris-flow deposit related to early andesitic eruptive activity is exposed at a road cut c. 1.5 km northwest of Turakina at an elevation of 65 m a.s.l., and is over- and underlain by rhyolitic tephra layers, the Middle and Lower Griffin Road tephra, deposited at c. 310 ka, and c. 340 ka respectively (Bussell & Pillans, 1992). The debris flow was most likely emplaced within a now abandoned proto-Turakina River catchment, which was located c. 1.5 km west of the present one. The deposit is exposed only at this locality and is overlain by significantly younger deposits on the proximal Ruapehu ring plain, and completely eroded on the distal Ruapehu ring plain.

1.5.3 The Whangaehu River

The Whangaehu River catchment has been studied in detail by Hodgson (1993) and also by Keigler et al. (2011). It is the only river system that presently drains the south eastern Ruapehu ring plain and is sourced from Crater Lake, a body of acidic water 0.16 km^2 in area, at an altitude of c. 2,530 m a.s.l. (Houghton et al., 1987). On its way southward it passes, among others, the settlements of Tangiwai, Te Tui, Manawaimai and Mangamahu before entering the Tasman Sea c. 12 km southeast of Wanganui (Fig. 5). It is joined by the major tributary of the Mangawhero River, c. 12 km southwest of Mangamahu, which supplies fresh water to the otherwise acidic river system (Hodgson, 1993). Exposures along the catchment comprise marine Pliocene-Pleistocene sediments overlain by Quaternary volcaniclastic deposits, the oldest of

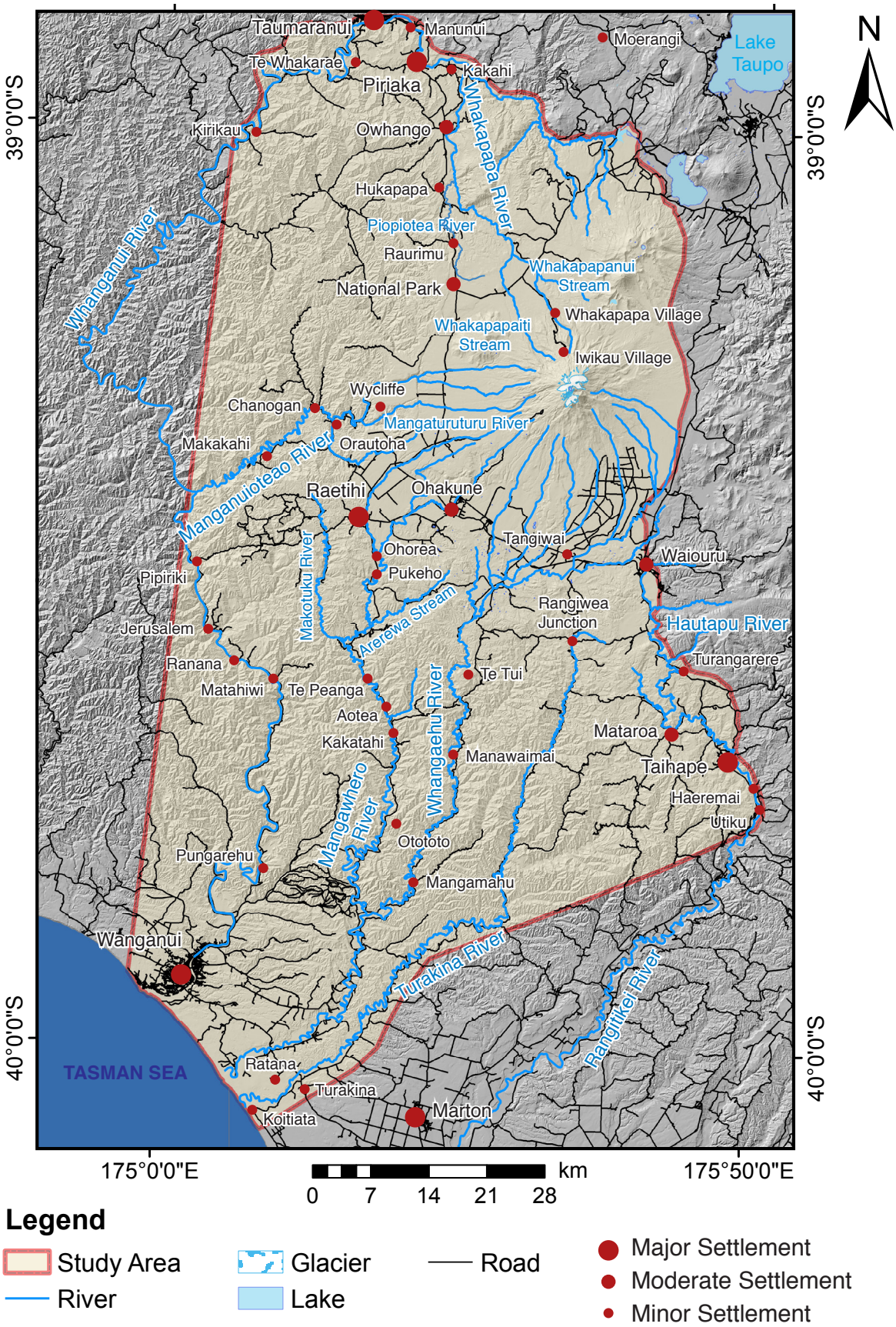

Figure 5. Digital elevation model of the proximal and distal Ruapehu ring plain showing the study area and the key settlements along the seven major river systems focussed on in this research.

which were mapped as the Whangaehu Formation (Hodgson, 1993). Hodgson (1993) identified eight volcaniclastic formations within the Whangaehu catchment, which were also mapped by Donoghue and Neall (2001) over the southeastern ring plain. The volcaniclastic sediments are confined to the river catchment and unconformably overlie late-Pliocene marine mudstones and muddy sandstones (Keigler et al., 2011). In its lower reaches (>140 km), the river incises into late Quaternary river and marine aggradational terraces, as well as underlying Pleistocene marine gravels, sands and silts that are capped with volcaniclastic deposits (Hodgson, 1993; Deely & Sheppard, 1996).

1.5.4 The Mangawhero River

The Mangawhero River rises at 1,840 m a.s.l. from a small stream on the southern flank of Mt. Ruapehu and is part of the Whangaehu River system, which enters the Tasman Sea c. 12 km south east of Wanganui (Michaelis, 1983). On its way southward, it passes the townships of Ohakune, Raetihi (Makotuku River) and Kakatahi before joining with the Whangaehu River 7 km southwest of Mangamahu (Fig. 5). The present Mangawhero River cuts solely into late-Pliocene mudstones. The proximal volcaniclastics exposed along the Mangawhero catchment are part of the Mangawhero cone-building formation (Hackett & Houghton, 1989), whereas the distal volcaniclastics have not been previously studied. The most common relicts of an earlier eruptive episode of Mt. Ruapehu are volcaniclastic boulders up to 3 m in diameter, which are most frequent in the area between Aotea and Ohorea and generally limited to the eastern side of the present Mangawhero River catchment. Further downstream they become rare landscape features, cropping out more frequently again c. 3 km south of Otototo on the eastern side of State Highway 4, where they are exposed along a small valley between Tertiary mudstone mounds. The andesitic boulders have been re-deposited on aggradational terraces with the oldest deposits being exposed on the highest elevation in the landscape. The oldest volcaniclastics are generally exposed at an altitude of 440 - 460 m a.s.l. between Te Peanga and the upper Mangawhero Bridge along State Highway 4, and form an aggradational terrace with exposures on farmland. The key location for the overall stratigraphy of the oldest diamictons in the area is exposed along a cliff at Pukeho, c. 50 m northwest of Arerewa Stream, which is a minor tributary to the Mangawhero River.
Additional volcaniclastics are exposed along the Makotuku River, which joins with the Mangawhero River c. 1.2 km north of Ohorea, as well as close to the present Mangawhero River catchment in the proximity of the volcano.

1.5.5 The Manganuioteao River

The Manganuioteao River is presently sourced from various small streams descending the western flanks of Mt. Ruapehu (Fig. 5). It incises into Quaternary volcaniclastics on the proximal western Ruapehu ring plain and into late-Pliocene mudstone and sandstone on the distal southwestern Ruapehu ring plain, as it passes the minor settlements of Orautoha and Makakahi before joining the Whanganui River c. 10 km north of Pipiriki. The river is protected against development by a National Water Conservation Order and is inhabited by the endangered blue duck species. The area adjacent to the river system is sparsely populated and dominantly used for farming. On the proximal ring plain the Manganuioteao River incises into Quaternary volcaniclastic deposits,

which are part of the Mangawhero cone-building formation (Hackett & Houghton, 1989). On the distal Ruapehu ring plain, the river meanders through the strongly tilted and uplifted Tertiary hill country made up of late-Pliocene mudstones and sandstones, intermittently overlain by Quaternary volcaniclastics of a hitherto unknown eruptive episode of Mt. Ruapehu. The most common relics of this earlier eruptive period are volcaniclastic boulders ≤5 m in diameter, which are scattered throughout the countryside adjacent to the steep Manganuioteao River catchment up to >45 km from the volcano and re-deposited on three aggradational terraces. The oldest volcaniclastic deposits are exposed in road cuts between the farming communities of Wycliffe and Clanogan.

1.5.6 The Whakapapa River

The Whakapapa River is currently fed by numerous streams at the foot of Mt. Ruapehu (800 m a.s.l.) that descend from its steep northwestern flanks, as well as the proximal northwestern Ruapehu ring plain (Fig. 5). Among these are the Piopiotea, Whakapapiti and Whakapapanui Streams. The Piopiotea Stream currently originates from several swamps c. 2.5 km north east of National Park. From there it runs northwards, incising into Quaternary volcaniclastics sourced from Mt. Ruapehu, and passes the settlement of Raurimu before joining the Whakapapa River c. 1.5 km east of Hukapapa. The Whakapapaiti Stream is sourced from the Whakapapa Glacier on the northwestern summit of Mt. Ruapehu at an elevation of 1,940 m a.s.l. On the northwestern slopes of the volcano it incises into the volcaniclastics of the Whakapapa and Mangawhero cone-building episodes (Hackett & Houghton, 1989) before joining the Whakapapa River c. 10 km northeast of National Park. The Whakapapanui Stream originates at an elevation of 2,270 m a.s.l. from several small glaciers descending the Summit Plateau at the northern crest of Mt. Ruapehu. Descending the steep mountain flanks, it passes Iwikau and Whakapapa Village, and incises into the volcaniclastics of the Whakapapa and Te Herenga cone-building episodes (Hackett & Houghton, 1989) before joining the Whakapapa River c. 10 km northeast of National Park.

The Whakapapa River dissects the northwestern distal Ruapehu ring plain, and passes the settlement of Owhango before joining the Whanganui River c. 1.7 km northeast of Kakahi. On its way northwards it dominantly incises into Taupo ignimbrite underlain by Tertiary mudstones and muddy sandstones. Exposures of volcaniclastics related to an older eruptive episode of Mt. Ruapehu are limited to road cuts c. 1 km southwest and c. 2 km south-southeast of Kakahi on the distal Ruapehu ring plain; whereas the oldest volcaniclastic deposits exposed at the headwaters of the present Whakapapa River catchment are related to the Murimotu Formation (9.5 ka; Palmer & Neall, 1989). Closer to the volcano the same volcaniclastics as at Kakahi, as well as significantly younger ones, are exposed within several outcrops along the Piopiotea Stream.

1.5.7 The Whanganui River

The Whanganui River is currently sourced from the western flanks of Mt. Tongariro at an altitude of 1,900 m a.s.l., and joined by numerous streams on the volcano's proximal ring plain (Fig. 5). It dissects the steep flanks of the composite cone towards the north, before flowing in a northwesterly direction c. 1 km north of the Te Whaiau Dam, along the way incising into

Quaternary volcaniclastics sourced from Mt. Tongariro, as well as Taupo ignimbrite. It winds its way through the Pukepoto and Tongariro Forests, incising into Triassic to Jurassic greywacke, late-Pliocene mudstone and sandstone, and Recent Taupo ignimbrite before being joined by the Whakapapa River c. 1.7 km northeast of Kakahi. On its northwestern route, it passes the settlements of Piriaka, Manunui and Taumarunui and dominantly incises into late-Pliocene mudstones and sandstones, Quaternary diamicton deposits sourced from Mt. Ruapehu, and Taupo ignimbrite. From this point onwards, the river turns towards the south and passes the minor settlement of Kirikau before crossing the Whanganui National Park and continuing southwards through the minor settlements of Pipiriki, Jerusalem, Ranana, Matahiwi, and Pungarehu, incising into late-Pliocene mudstones and muddy sandstones before joining the Tasman Sea south of Wanganui where it additionally incises into Quaternary volcaniclastic diamictons potentially sourced from Mt. Ruapehu (e.g., Gamble et al., 2003).
The diamictons focussed on in this study are exposed in road cuts at the Piriaka Lookout (State Highway 4) and Piriaka, where they form a distinctive plateau between Piriaka and Te Whakarae. Andesitic boulders >1 m in diameter are scattered around the countryside until c. 3 km north of Kirikau where they were re-deposited on individual aggradational river terraces and outline the approximate inundation area of the initial deposit.

1.6 Climate and land use

The area studied varies widely in physiography and altitude, ranging from the summit of Mt. Ruapehu, with an elevation of 2,797 m a.s.l., the highest point on New Zealand's North Island, to the coastal regions (0 m a.s.l) at the Tasman Sea southwest of the stratovolcano. Thus, the climate ranges from alpine to coastal. The temperatures within the alpine region (Tongariro National Park) range between -7°C (winter) and 15°C (summer), and westerly winds prevail with speeds of dominantly <11 knots, which can turn to gales of >30 knots at higher altitudes (Thompson, 1984). Rainfall is high overall; on average 3,965 mm fall each year on the northwestern slopes of Mt. Ruapehu (NZ Meteorological Service, 1973). During the winter season heavy snowfalls are common at altitudes ≥1,400 m a.s.l. (Thompson, 1984), and these feed the up to 18 glaciers that cover the summit of Mt. Ruapehu (Chinn, 2001). These ice fields strongly influence the level and acidity of Crater Lake, which was over the past several decades the source for at least two major lahars including the one that caused the 1953 Tangiwai disaster (Odell, 1955; Hodgson, 1993; Cronin et al., 1997a).
Most of the field work for this study has been carried out on well-developed pastoral lands at lower, more temperate altitudes dominantly between 700 m a.s.l. (Taihape region) and 120 m a.s.l. (Taumarunui region). The annual mean temperature of the Taihape region ranges between 6.4°C (winter) and 16.6°C (summer), and the mean monthly precipitation between 59 mm (February) and 100 mm (December) (climate-data.org). The climate in the Taumarunui region is milder than is the case for Taihape due to the lower altitude, with the mean annual temperature ranging between 7.3°C (winter) and 18.4°C (summer) and the mean monthly precipitation varying between 81.3 mm (February) and 141.6 mm (July) (NOAA Global Climate Normals 1961 - 1990; climate-charts.com).
The coastal climate of the well-developed Wanganui region is dominated by comparatively mild mean annual temperatures, which range between 5°C (winter) and 13°C (summer). The mean annual precipitation rate is the lowest of the study area, with monthly values varying between

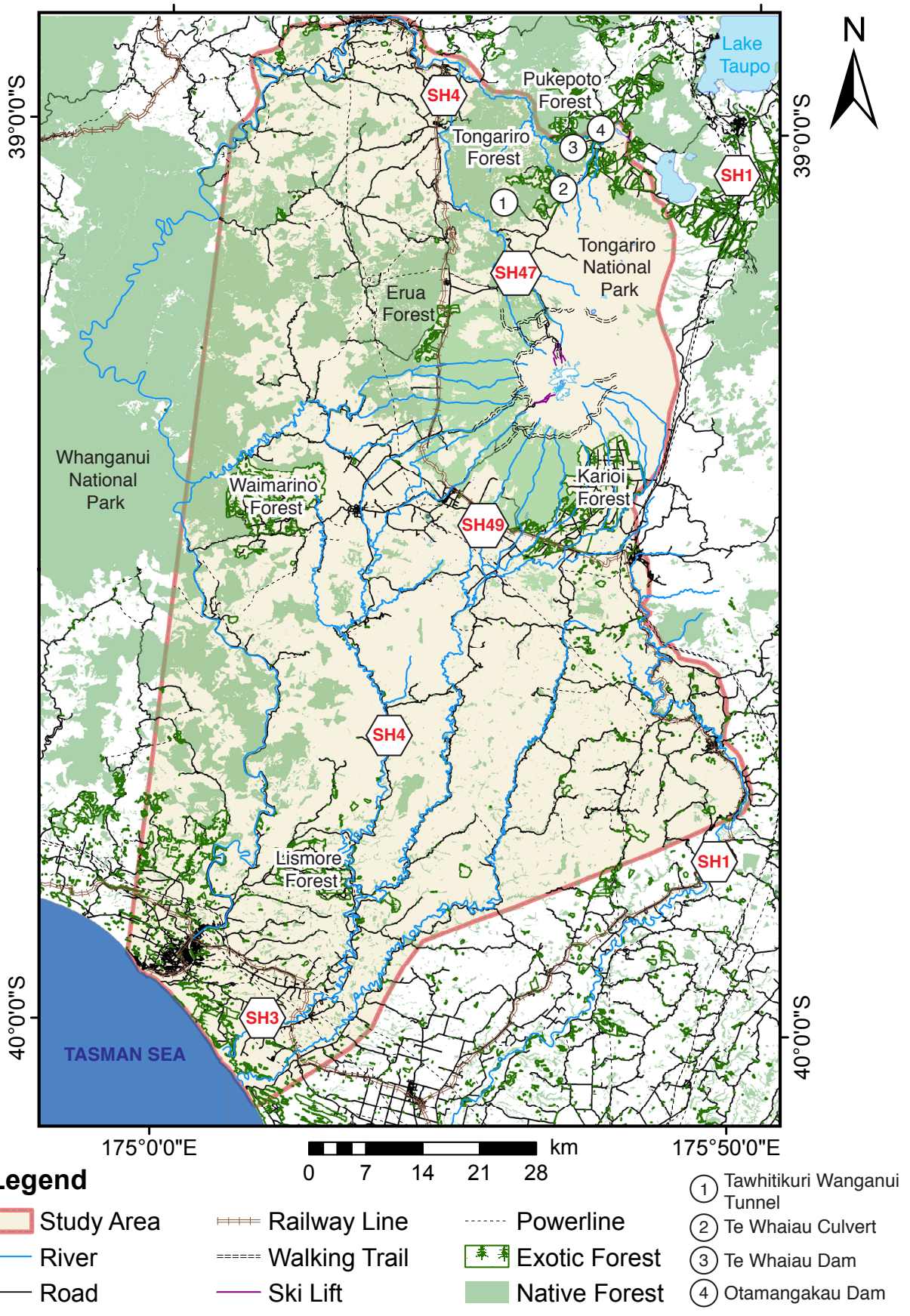

Figure 6. Major land use within the study area.

45 mm (January) and 87 mm (June) (worldweatheronline.com).
The central district of the area studied contains the Tongariro National Park (Fig. 6), which covers an area of 796 km^2 and was founded in 1887; it is therefore the oldest National Park in New Zealand (e.g., Greenway, 1998; Harlen, 1999). In 1993 it became a UNESCO World Heritage Site for both its geological and ecological value and it currently receives c. 800,000 visitors per year (Harry Keys, DOC, personal communication). The land within the Tongariro National Park is undeveloped and extensively used for tourism, especially hiking (e.g., Tongariro Alpine Crossing c. 80,000 annual visitors 2013/14; Harry Keys, DOC, personal communication; Tongariro Northern Circuit c. 12,000 annual visitors 2013/14; Johnson, 2014) and skiing (450,000 visitors 2013/14; Harry Keys, DOC, personal communication).
The western border of the study area crosses into the Whanganui National Park, which was established in 1986, covers an area of 742 km^2 and is visited by c. 200,000 people per year (Rundle, 2008).
The study area also comprises six forest parks, which are used for extensive exotic forestry planting: the Tongariro Forest, the Pukepoto Forest, the Erua Forest, the Waimarino Forest, the Karioi Forest, and the Lismore Forest (Fig. 6).
Several major transport routes including State Highway 1, State Highway 3, State Highway 4, State Highway 47, and State Highway 49 run through the area, as well as the North Island Main Trunk railway line, which connects Auckland and Wellington (Fig. 6). Additionally, several sets of high voltage electricity transmission lines are contained in its north western and south eastern sectors.
The Whanganui, Whakapapa and Whangaehu Rivers provide energy for the Tongariro Power Scheme, which contributes 4% of New Zealand's electricity generation (Martin, 1991). The water is sent through several tunnels, canals, and dams (e.g., Tawhitikuri Wanganui Tunnel, Te Whaiau Culvert, Te Whaiau Dam, Otamangakau Canal, Otamangakau Dam), which are also located within the study area, before it is eventually drained into Lake Taupo (Fig. 6).

1.7 Nomenclature

The outcrops studied along the catchments described in section 1.5 comprise deposits of sediment-water mass flows, which range from debris avalanches to debris flows and hyperconcentrated flows. Additional deposits reflecting "normal" stream-flow behaviour and reworking of these initial volcaniclastics have also been identified.
Sediment-water mass flows from volcanoes (lahars) are among the most hazardous processes occurring during or after volcanic eruptions (e.g., Scott et al., 1995). Their sediment concentrations generally exceed 60 vol.%, which is a major factor in their flow behaviour and mechanics (e.g., Costa, 1984; Coussot, 1995; Scott et al., 1995; Iverson, 1997). Trigger mechanisms of lahars include rainfall-induced remobilization of sediment, crater-lake outbreaks, eruption-induced snow melting, or edifice failure (Rodolfo, 2000; Lecointre et al., 2004; Doyle et al., 2009). Based on their clay content, they are generally divided into two types: i) syn-eruptive "non-cohesive" lahars (≤3 - 5 vol.% clay), which start and end as watery, low-sediment-content flows, and ii) "cohesive" lahars (≥3 - 5 vol.% clay), which generally originate from volcanic edifice failures (e.g., Scott et al., 1995; Cronin et al., 1999). Interaction with stream water often results in rapid dilution and transformation of both types downstream into sand- and pebble-rich hyperconcentrated flows (Cronin et al., 1999; Doyle et al., 2009).

1.7.1 Debris avalanches

Volcanic debris avalanches are extremely rapid flows of partially or fully saturated debris (Hungr et al., 2005), generated by failure of part of a volcanic cone, which results in rapid gravitational acceleration of large masses of material (Siebert, 1984). These are the largest and most violent processes known from stratovolcanoes (Ui, 1983; Siebert, 1984; Glicken, 1991; Palmer, 1991). Debris avalanche triggering mechanisms include tectonic movements (e.g., faulting, earthquakes), explosive eruptions, high-level magma intrusion, extensive hydrothermal alteration of the volcanic edifice, or the migration of vents (Siebert, 1984; McGuire, 1996; Zernack et al., 2012). Their deposits are commonly massive, poorly sorted, contain “megaclasts” (large fragments of the volcanic edifice up to several hundred metres in size), and typically comprise jigsaw-fractured clasts (Fig. 7A) (Mimura et al., 1982; Ui, 1983; Ui et al., 2000). A further distinctive feature of these deposits is a hummocky topography with longitudinal and transverse ridges (Siebert, 1984). Volcanic debris-avalanche deposits significantly change the landscapes they are emplaced upon and induce a different range of sedimentary processes as the landscape recovers and drainage systems re-adjust after their occurrence (e.g., Manville & Wilson, 2004; Procter et al., 2009).

1.7.2 Debris flows

Debris flows are saturated slurries of water and rock debris that can be triggered by, among other processes, intense rainfall, breakouts of crater lakes, (O’Shea, 1954; Ulate & Corrales, 1966; Suryo & Clarke, 1985; Arguden & Rodolfo, 1990; Rodolfo & Arguden, 1991; Pierson et al.,

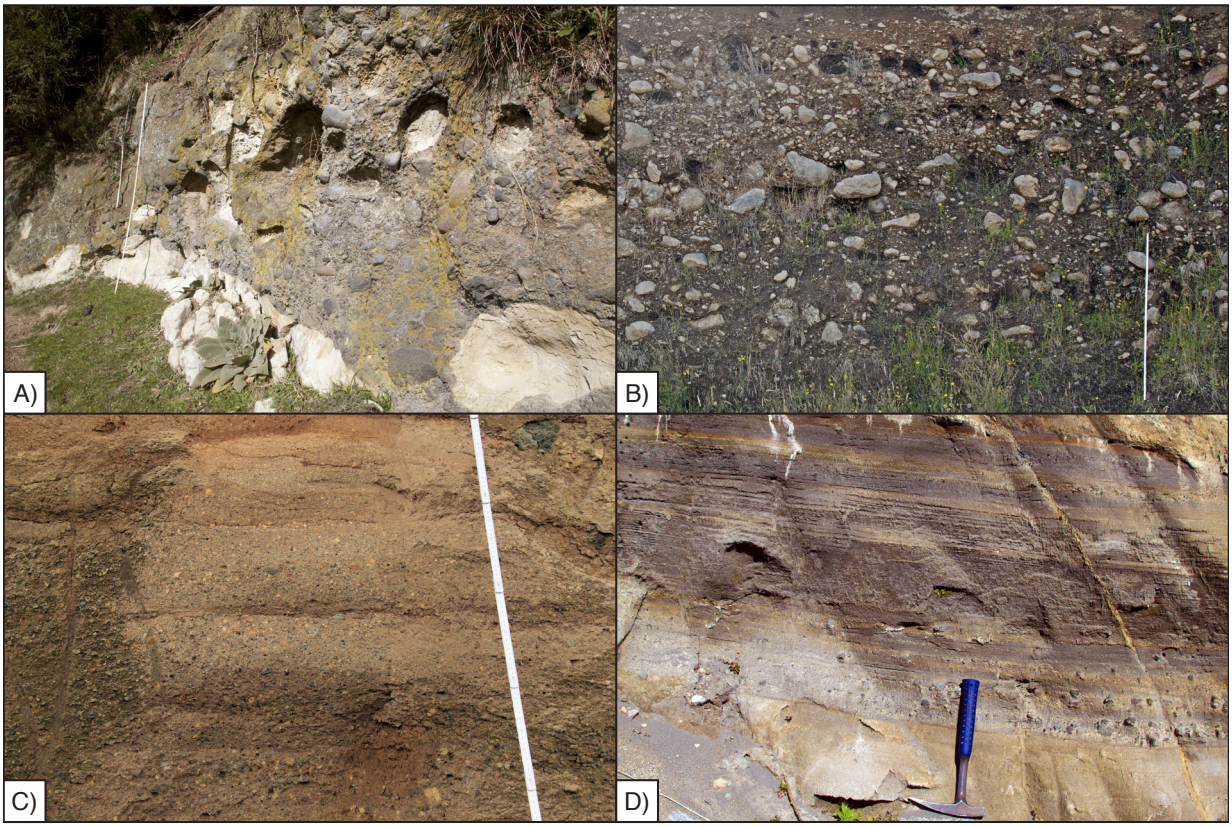

Figure 7. The dominant volcaniclastic deposit types exposed within the individual river catchments on the distal Ruapehu ring plain. (A) Debris-avalanche deposits, (B) debris-flow deposits, (C) hyperconcentrated-flow deposits, and (D) “normal” stream-flow deposits.

1992), and rapid melting of large amounts of snow and ice (Major & Newhall, 1989).
The flow mechanics of debris flows are extremely complex and include combinations of physical particle interactions (friction and momentum transfer between coarse particles), electrochemical particle interactions (double-layer and van der Waals attractions between fine particles), and physical interactions between sediment grains and fluid (Coussot & Piau, 1994; Coussot, 1995; Iverson, 1997).
"Cohesive" debris flows generated by landslides, debris avalanches, or explosions from geothermal/hydrothermal areas commonly contain 80 wt.% sediment and >3 - 5% clay (e.g., Scott et al., 1995). They vary little in character throughout their runout (Vallance & Scott, 1997), and thus typically deposit massive unsorted diamictons of clasts with variable lithologies within a sand, silt and clay-rich matrix (Fig. 7B) (Scott et al., 1995).

1.7.3 Hyperconcentrated flows

Beverage and Culbertson (1964) were the first to define the term "hyperconcentrated flow" as water floods with suspended sediment concentrations of at least 20 vol.% and not more than 60 vol.%, which can be further distinguished from water floods due to i) the bulk rheological properties of the suspension, and ii) how the sand is suspended and deposited in the flow. Generally, large quantities of sand and occasional fine gravel are transported in full dynamic suspension once minimum concentrations of fines (clay and fine silt) are achieved (Cao & Qian, 1990; Cronin et al., 1999; Dinehart, 1999). Hyperconcentrated flows are common in semi-arid and arid regions (e.g., Laronne et al., 1994) and can be triggered during intense rainstorms (Beverage & Culbertson, 1964; Major et al., 1996; Pierson et al., 1996), lake-breakout floods (Rodolfo et al., 1996; O'Connor et al., 2001), glacier-outburst floods (Maizels, 1989), dilution and/or selective deposition at the heads and tails of debris flows (Pierson, 1986; Pierson & Scott; 1985; Cronin et al., 1999; 2000) and inputs of large sediment volumes to water floods by landslides (Kostaschuk et al., 2003).
Hyperconcentrated flows generally have a clast-supported texture with local dewatering structures and in part, well-developed inverse or normal grading (Fig. 7C) (Scott et al., 1995). Hyperconcentrated flows also commonly form during downstream transformation of debris flows. This "transition facies" is characterized by downstream-thickening of hyperconcentrated-flow deposits overlain by downstream-thinning debris-flow deposits (e.g., Scott, 1988).

1.7.4 "Normal" stream flow deposits

"Normal" stream flow behaviour is controlled by tractive-dominated, grain-by-grain sediment deposition, since the river system transports relatively small quantities (<4 vol.%) of fine suspended sediment, which have little effect on its overall flow behaviour (e.g., Waananen et al., 1970; Smith, 1986). The fluid mechanics are hence dominated by inertial fluid forces, which act on the channel boundaries and on the individual entrained sediment grains that have little meaningful interaction with each other (Pierson, 2005). Generally turbulence serves as the major sediment support and transport mechanism and typically results in well developed i) cross bedding of silt- to sand-sized sediments, and ii) imbrication in pebble- to boulder-sized deposits (Fig. 7D) (e.g., Smith, 1986).

CHAPTER 2: METHODS

2.1 Field studies

Detailed field work was carried out within the study area in order to unravel the complex stratigraphy and the approximate emplacement ages of the mass-flow deposits within each river valley and correlate these between catchments, as well as to the stratigraphy identified and mapped on the Mt. Ruapehu edifice (e.g., Hackett & Houghton, 1989; Gamble et al., 2003). In total, five mass-flow formations were studied in detail, which are, from southeast to northwest: the Mataroa Formation (Hautapu River), the Whangaehu Formation (Whangaehu River), the Oreore Formation (Mangawhero River), the Pukekaha Formation (Manganuioteao River), and the Piriaka Formation (Whakapapa and Whanganui Rivers) (Fig. 5). Of these, only the Whangaehu Formation has been previously described and studied in detail (Hodgson, 1993; Keigler et al., 2011).

Initial stratigraphic sequences, as well as reworked andesitic boulders related to the primary deposit, were mapped in order to reconstruct i) periods of enhanced volcanic activity, as well as destruction periods, of Mt. Ruapehu, ii) the locations of the river catchments during the time of mass-flow emplacement, and iii) the approximate inundation area and volume of the flows. Each outcrop was GPS referenced and all individual units exposed were subsequently described in terms of thickness, sorting, grain size, texture, matrix, internal bedding/grading, basal boundaries, and content of pumice and exotic clasts (e.g., river gravel). Samples for subsequent geochemical analysis were taken either from road cuts or bluffs on farm land, in order to link the mass-flow deposits with the lava-flow sequences exposed on the cone. In total 103 samples of the freshest available clasts ≥10 cm in diameter were used for geochemical and petrographic studies: 19 from the Mataroa Formation, 20 from the Whangaehu Formation, 22 from the Oreore Formation, 22 from the Piriaka Formation, and 16 from the Pukekaha Formation. Additional four samples were taken from a debris-flow deposit exposed only in a road cut c. 1.5 km northwest of Turakina. The least rounded clasts were chosen for sampling to ensure a close relationship to the timing of the volcanic deposit unit studied, rather than during an earlier episode that could have been subsequently reworked and incorporated into the specific deposit. Comparatively large (≥10 cm) and poorly altered samples were preferred to avoid leached compositions (e.g., reduced K, Fe, Ti).

2.2 Petrography

Polished thin sections for petrographic analysis and electron microprobe analysis of selected minerals were prepared at the University of Ballarat, Victoria, Australia. Images of thin sections were obtained with a Nikon DS-U1 digital camera attached to a Nikon Eclipse E600 POL microscope and elaborated with NIS-Elements version 3.22.00 at Massey University, Palmerston North, New Zealand.

2.3 X-ray Fluorescence Spectroscopy

In total, 103 samples were cut with a rock saw at Massey University, Palmerston North, New Zealand and the central ~3 x 3 x 3 cm portions (to exclude material possibly affected by

alteration) were crushed and ground in a tungsten carbide ring mill at The University of Auckland, New Zealand in order to obtain major (e.g., Si, Al, Mg, Fe, Ca, K, Na) and minor whole rock element concentrations (e.g., Ti, Mn, P and S) by X-ray fluorescence (XRF) analysis as oxide components. Contamination of trace elements during the crushing process is limited to W and Co, while contamination of Ta and particularly Nb is negligible (Roser et al., 2003; Martin et al., 2013). Element concentrations were measured with a Siemens SRS 3000 sequential X-ray spectrometer containing a Rhodium tube, and the analysing methods were similar to those described by Norrish & Hutton (1969). In general, precision for each major or minor element is better than ±1% (1σ) of the reported value.

2.4 Laser ablation inductively coupled plasma mass spectrometry (LA-ICP-MS)

Trace elements were measured on the fused glass discs obtained from the XRF-analysis at the Research School of Earth Sciences, Australian National University by laser ablation inductively coupled plasma mass spectrometry (LA-ICP-MS), using an Excimer LPX120 laser (193 nm) and an Agilent 7500 mass spectrometer. Trace element concentrations were evaluated following the method of Eggins et al. (1998). Precision for trace elements is better than ±4% (RSD), and the accuracy better than 5% at the 95% confidence level.

2.5 Electron microprobe analysis

Hornblende analyses were obtained from petrographic thin sections with a JEOL JXA-840A electron microprobe (EMP) at Massey University, Palmerston North, New Zealand using a LINK systems LZ5 detector, a QX2000 pulse processor, and a ZAF-4/FLS matrix correction software. Standard operating conditions include an accelerating voltage of 15 kV, a beam current of 0.5 nA, a beam diameter of 3 µm, and a live count time of 100 s. Calibration was obtained by a suite of AstimexTM mineral standards, which reveals an estimated precision for oxide analyses better than ±3%.

2.6 $^{40}Ar/^{39}Ar$-Dating

Sample preparation for high precision dating was done at the OSU Argon Geochronology Lab, Oregon, USA and groundmass ages were obtained using an ARGUS VI multi-collector mass spectrometer. The samples were crushed and subsequently sieved to extract groundmass grains that range between 200 - 300 µm in size. Groundmass separates were primarily obtained by hand-picking, as well as magnetic and heavy-liquids separation, followed by acid treatment. Subsequently, the samples were leached in an ultrasonic bath with ~5% HNO_3 for 20 minutes, followed by distilled water for 20 minutes. Finally, the samples were dried in an oven at a temperature of 80°C. The separated groundmass samples were irradiated using laser step-heating in a resistance furnace. Groundmass ages were obtained using an ARGUS VI multi-collector mass spectrometer connected to an all-metal extraction system for $^{40}Ar/^{39}Ar$ age determinations that has five fixed Faraday detectors and one ion-counting CuBe electron multiplier. The system is equipped with a 25 W Synrad CO_2 laser with an industrial Synrad XY scan head for carrying out gas extractions while steering the laser beam during sample heating. This has the advantage of heating the sample evenly by setting up a beam-raster pattern that

moves continuously up and down at speeds of ≤300 in/s while keeping the sample housing stationary. This ultimately allows the entire sample to be analysed using the Multi-collector Mode, which simultaneously collects all masses m/e = 36, 37, 38, 39 and 40 on the 1012 Ohm Faraday collector array. The resulting custom-made extraction line features two laser chambers, three SAES getters, and two air pipette systems (one for air and one for an ^{38}Ar spiked air standard). After the measurements all resulting ages were calculated using the ArArCALC v2.5.2 software package (Koppers, 2002), and precision is generally within ±2σ.

CHAPTER 3: THE HAUTAPU RIVER – POTENTIAL IMPLICATIONS OF MASS WASTING INTO RIVER CATCHMENTS SOURCED FROM ACTIVE VOLCANOES

3.1 Introduction

The Hautapu River originates from native grasslands and wetlands east of Ruapehu. It dissects the volcano's southeastern distal ring plain and runs through Taihape before joining the Rangitikei River c. 2.5 km south of Utiku (Fig. 5). Exotic boulders ≤4 m in diameter and scattered across the landscape in the Taihape area have long been noted and were first described by Park (1910), who interpreted them to be of glacial origin. Te Punga (1952) later re-interpreted the boulders as a package of lahar deposits sourced from Mt. Ruapehu and referred to them as the "Hautapu Valley Agglomerate". Grindley (1960) termed the volcaniclastics "Hautapu lahars" and was the first to divide them into three stratigraphic units. He interpreted the andesitic boulders scattered on aggradational river terraces along the Hautapu River valley to represent initial emplacement of different lahar events, which resulted in a total thickness estimation of ≥45 m.

Even though these earlier publications noted the occurrence of the volcaniclastic deposits and their origin from Mt. Ruapehu, there have been no detailed studies published regarding lithology, stratigraphy, number of events, trigger and emplacement mechanisms, duration, volume and inundation area, as well as linking to the deposits exposed within the adjacent Whangaehu River catchment.

This chapter, based on the manuscript Tost et al. (2015), provides a detailed stratigraphic and lithologic description of the volcaniclastics exposed along the Hautapu River. The volcanic hazards and the interface between the volcanic and the surrounding geomorphic processes in an uplifting, eroding sedimentary terrain, which can result in short- as well as long-term changes in river systems in the proximity of active volcanoes, are also discussed. Recognising the interplay between volcanic activity and the response in surrounding landscape is essential for improving future volcanic hazard assessments and planning for long-term recovery. Landscape impacts, as shown in the example of the Hautapu River, include damming and permanent alteration of river paths and alteration of catchment susceptibility to subsequent volcanic mass flows.

3.2 Contributions of co-authors

"Impacts of catastrophic volcanic collapse on the erosion and morphology of a distal fluvial landscape: Hautapu River, Mount Ruapehu, New Zealand"

Geological Society of America Bulletin, 127(1-2), 266-280.

M. Tost: Principal Investigator
Carried out: Field studies
Sampling and laboratory preparation of clasts
Manuscript preparation and writing

S. J. Cronin: Co-Investigator
Carried out: Introduction to field sites
Discussion of results and methods
Editing and discussion of the manuscript

J. N. Procter: Co-Investigator
Carried out: Discussion of results and methods
Editing of the manuscript

I. E. M. Smith: Adviser
Carried out: Aided the study by editing the manuscript

V. E. Neall: Adviser
Carried out: Aided the study by editing the manuscript

R. C. Price: Adviser
Carried out: Aided the study by editing the manuscript

3.3 Impacts of catastrophic volcanic collapse on the erosion and morphology of a distal fluvial landscape: Hautapu River, Mount Ruapehu, New Zealand

M. Tost[1], S. J. Cronin[1], J. N. Procter[1], I. E. M. Smith[2], V. E. Neall[1], R. C. Price[3]

[1]Volcanic Risk Solutions, Massey University, Palmerston North 4442, New Zealand
[2]School of Environment, The University of Auckland, Auckland 1142, New Zealand
[3]Faculty of Science and Engineering, University of Waikato 3105, Hamilton, New Zealand

Abstract

Debris avalanches caused by the collapse of volcanic flanks pose a great risk to inhabited areas and may permanently change the surrounding landscape and its drainage systems. In this research we explored the interplay between a debris avalanche and a tectonically uplifting surrounding landscape, providing insights into the long-term consequences of volcanic edifice failures. Exposures of coarse volcaniclastic sediments along the Hautapu River c. 50 km southeast of Mt. Ruapehu, New Zealand evidence the largest known collapse event of the stratovolcano, which was followed by a vigorous regrowth phase that produced numerous pyroclastic eruptions and pumice-rich lahars. Similar diamicton deposits are exposed within the adjacent river catchment to the west. Coverbed stratigraphy as well as geochemical correlation of andesitic lava blocks within the debris-avalanche deposit with dated lavas exposed on the cone, indicate that deposition occurred between 125 to 150 ka ago. The collapse took place during the shift from a glacial to an interglacial climate, when glaciers on the cone were in retreat, and high pore-water pressures combined with deep hydrothermal alteration weakened the cone; the collapse may have been accompanied by magmatic unrest. The c. 2 - 3 km^3 debris avalanche inundated an area of >260 km^2, and entered the proto-Hautapu catchment where it was channelized within the deeply entrenched valley. Mass-wasting events associated with post-collapse volcanism continued to be channelled into the proto-Hautapu River for another c. 10 ka producing long-runout lahars. Subsequently, the river catchment was isolated from the volcano by incision of the intervening Whangaehu River into the proximal volcaniclastic sediments, accompanied by regional faulting and graben deepening around Ruapehu. At present the volcaniclastic deposits form a distinctive plateau on the highest topographic elevation within the Hautapu valley, forming a reversed topography caused by preferred incision of the Hautapu River into softer late-Tertiary sediments concurrent with constant uplift.

3.3.1 Introduction

Mountain-building volcanoes dominate landscape processes in their vicinity and overprint earlier surrounding landscapes at long distances (>30 km) from their summits. Active stratovolcanoes produce high fluxes of volcaniclastic material that may blanket the surrounding landscape (e.g., tephra layers), fill valleys (e.g. pyroclastic flows, lahars, gradual fluvial aggradation), or even completely reshape drainage patterns (e.g. debris avalanches). Even in the absence of volcanic eruptions, ongoing mass wasting occurs, along with sporadic major edifice flank failures that generate huge debris avalanches (Siebert, 1984; Tibaldi et al., 2005; Tibaldi & Lagmay, 2006; Zernack et al., 2012). Volcanic construction and destruction episodes result in much higher

material accumulation rates than almost all other geological settings (Tibaldi et al., 2008). Major “catastrophic” edifice failures are perhaps the most sudden agents of landscape change, producing debris-avalanche deposits that almost instantaneously transform the surrounding geomorphology by valley infilling, fan creation, surface hummock formation, damming and diversion of rivers, and subsequent injection of high sediment loads into impacted catchments (Voight et al., 1981; Crandell et al., 1984; Procter et al., 2009). The most voluminous case known is exposed in the Shasta Valley, California, where c. 26 km^3 of volcaniclastic material, associated with the collapse of the ancestral Mt. Shasta, form hundreds of surface mounds and ridges in the >450 km^2 affected area (Crandell et al., 1984). Repeated sector collapses are common at large stratovolcanoes, with 2 to 14 events recorded during their typical active lifetime (10 - 500 ka; Begét & Kienle, 1992; Tibaldi et al., 2005; Zernack et al., 2009; Roverato et al., 2011). Volcano instability is enhanced by active rifting, hydrothermal alteration, weather and climate impacts and is often pre-conditioned by gradual volcano-spreading due to the inter-layering of hydrothermally altered weak pyroclastics and solid lava flows. Such circumstances are described from the simplest types of stratovolcanoes, such as Stromboli (Italy), through to high, complex and long-lived volcanoes, such as Ollagüe (Bolivia-Chile) and Planchon (Chile) (Tibaldi et al., 2005; 2007). New Zealand stratovolcanoes are also extremely unstable, with both Mt. Taranaki (Zernack et al., 2012) and Mt. Ruapehu (Hodgson, 1993; Cronin et al., 1996) experiencing regular mass failures. Ruapehu marks the southern terminus of the Taupo Volcanic Zone, and lies near the southern extreme of active extension caused by transtensional rifting (Sissons, 1979; Walcott, 1984; Nairn & Beanland, 1989; Darby & Williams, 1991; Acocella et al., 2002). Southwards, the Taupo Volcanic Zone passes into the South Wanganui Basin, where in the northern sector, marine sedimentary sequences are currently up-doming and normal and reverse faulting and synclinal and anticlinal folding are taking place (Kamp et al., 2004, Pulford & Stern, 2004; Villamor & Berryman, 2006b). Ruapehu is thus in a unique position where volcanic landscapes abut non-volcanic terrains and subduction tectonics give way to strike-slip faulting to the south (Wood & Davy, 1994; Stratford & Stern, 2006).

The purpose of this research was to examine the interface between the volcanic and the surrounding geomorphic processes in an uplifting, eroding sedimentary terrain. This was carried out through the geologic reconstruction of one of the largest flank-collapse episodes known from Mt. Ruapehu, as well as evaluating the immediate and long-term impacts of the sudden volcanic sediment influx into a complex eroding catchment. The single deposition episode described provides a key to examining the tectonic history of an active continental margin environment, including elucidating rates of uplift, fluvial erosion and mass-wasting.

Large flank collapses of volcanoes and their associated debris avalanches pose a great risk to inhabited areas many tens to hundreds of kilometres from volcanoes (Siebert, 1984; Begét & Kienle, 1992; Tibaldi et al., 2005; Zernack et al., 2012). Confinement of pore-water rich debris-avalanches enriched in hydrothermal clays causes transformation into cohesive debris flows that spread significantly farther than “dry” debris avalanches of similar volume (Vallance & Scott, 1997). Detailed knowledge regarding the interaction between volcanism and fluvial landscapes will provide better understanding of cascading geological hazards during and following debris avalanches. Recognising the interplay between volcanic activity and the surrounding landscape response is essential to improve future volcanic hazard assessment and

plan for long-term recovery. Landscape impacts include damming and permanent alteration of river paths and alteration of catchment susceptibility to subsequent volcanic mass flows.

3.3.1.1 Geological Setting

Mt. Ruapehu (2,797 m) is sited within an active graben, with ongoing normal and strike-slip faulting on the Raurimu Fault to the west, and the Rangipo Fault (750 ± 50 m vertical displacement) to the east, of the composite cone (Villamor & Berryman, 2006a). Numerous normal minor strike-slip faults are generally downthrown to the distal side of the southern Ruapehu area and produce crosscutting geometries with the marginal rift-boundary faults (Villamor & Berryman,

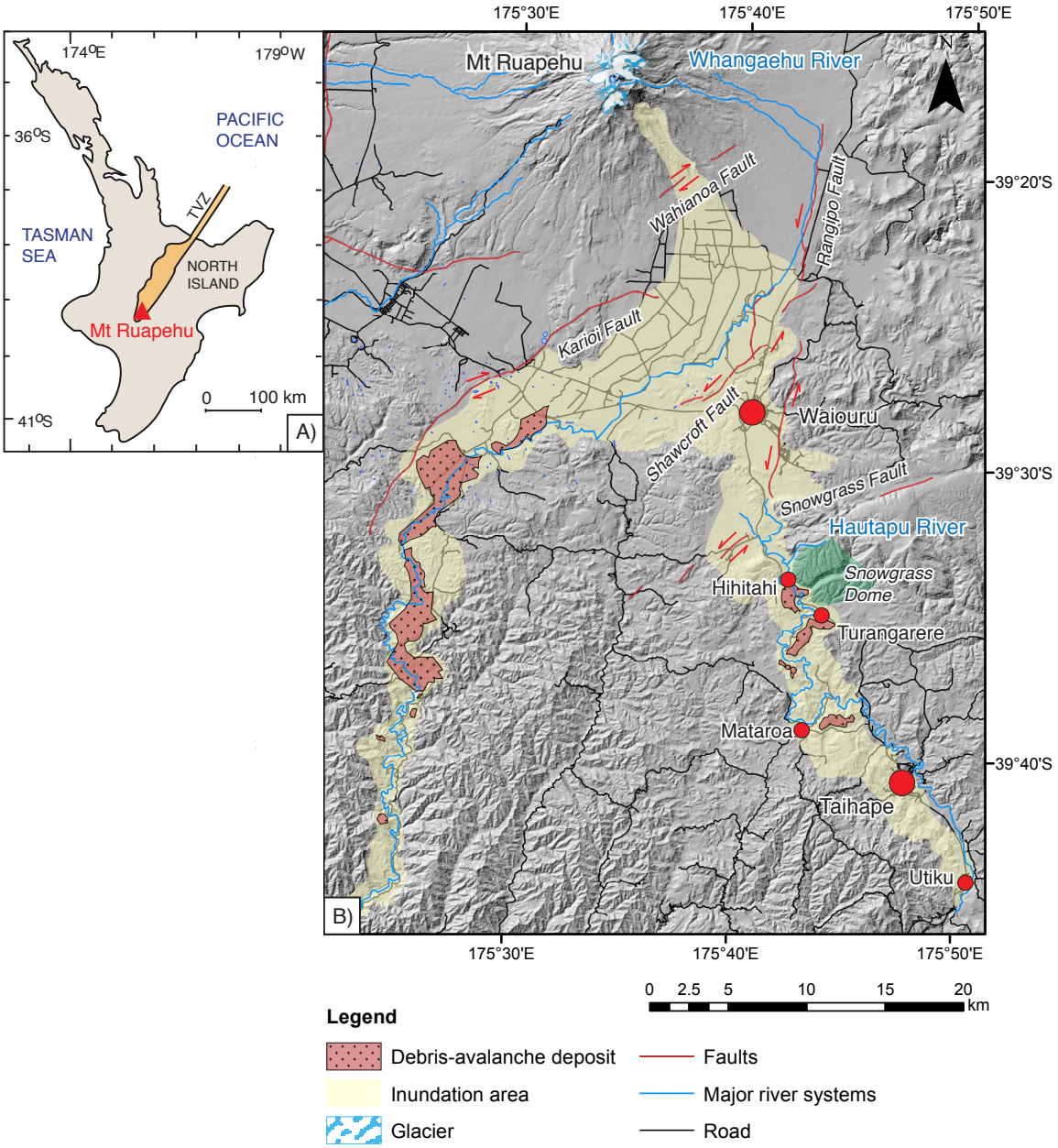

Figure 8. Geological setting. (A) Mt. Ruapehu is located in the centre of New Zealand's North Island at the southern terminus of the subduction-related Taupo Volcanic Zone (modified after Wilson et al., 1995; Smith et al., 1999). (B) The Whangaehu River currently incises into the southeastern Ruapehu ring plain, whereas the Hautapu River arises from wetlands southeast of Waiouru. Debris-avalanche deposits are exposed along these river catchments (red fields) up to 60 km from source, and reworked andesitic boulders >1.5 m in diameter, related to the diamictons, outline their approximate inundation area (yellow fields). The landscape in this region is dominated by constant uplift associated with subduction-zone related strike-slip faulting. Five major fault systems (Villamor et al., 2006a) strongly influence the present route of the two river systems.

Table 1. Volume, age, and magma flux of the four cone-building formations exposed on Mt. Ruapehu. Table after Gamble et al., 2003.

Cone-building formation	Volume* [km^3]	Approximate age** [ka]	Magma flux** [km^3/ka]
Te Herenga	65	250 - 180	0.93
Wahianoa	45	60 - 115	1
Mangawhero	35	55 - 45	0.88
		30 - 15	
Whakapapa	2.6	<15	0.17

*after Hackett & Houghton, 1989

**after Gamble et al. 2003

2006a). The stratovolcano is composed of variably dipping lava-flow sequences, autoclastic breccias, and pyroclastic, epiclastic, and glacial deposits (Hackett & Houghton, 1989; Smith et al., 1999). Petrologically, Mt. Ruapehu lavas comprise porphyritic basaltic andesites, andesites, and rare dacites, with a dominant phenocryst assemblage of plagioclase + clinopyroxene + orthopyroxene + Fe-Ti-oxides, along with rare olivine and amphibole (Graham & Hackett, 1987; Gamble et al., 2003; Price et al., 2012). Four major cone-building episodes were identified and mapped by Hackett & Houghton (1989) and subsequently dated, leading to modified definitions (Table 1). The oldest units are mapped as the Te Herenga Formation (200 - 300 ka; Tanaka et al., 1997), followed by the Wahianoa Formation (c. 120 - 150 ka; Price et al., 2005), the Mangawhero Formation (55 - 15 ka; Gamble et al., 2003), and the Whakapapa Formation (<15 ka; Gamble et al., 2003) (Fig. 3). In general, the whole-rock composition of the Mt. Ruapehu lavas shows a distinct compositional evolution toward more K_2O and SiO_2-rich compositions in the younger cone-building episodes (Price et al., 2005; 2012). The major and trace element compositions of the lavas indicate geochemical variation due to fractional crystallization, crustal assimilation, and magma mixing (Graham & Hackett, 1987; Gamble et al., 1999; Nakagawa et al., 1999; 2002; Price et al., 2005; 2012).

Erosion on the composite cone, which currently supports a number of small glaciers, has resulted in strong dissection, forming deep gorges on the upper flanks of Mt. Ruapehu as well as on its surrounding landscape (Gamble et al., 2003). Hydrothermal alteration and substrate weakening has been interpreted as the pre-conditioning mechanism for at least five flank failure events recognised to have occurred at Mt. Ruapehu (Palmer & Neall, 1989; Hodgson, 1993; Lecointre et al., 1998; Donoghue & Neall, 2001; Keigler et al., 2011). The proximal Ruapehu ring plain comprises volcaniclastic deposit sequences, which are primarily <27.1 ka, with longer run-out mass-flow deposits infilling and lining the margins of surrounding river catchments up to 200 km from source (Cronin et al., 1997). The persistent summit crater lake has been the source of many lahars, both during and between eruptions, with more than 60 lahars descending the flanks of the volcano into the Whangaehu River since 1861 alone (Nairn et al., 1979; Cronin et al., 1997; Cole et al., 2009).

3.3.1.2 Southeastern Ruapehu drainage system

The Whangaehu River is the only system that presently drains the southeastern Mt. Ruapehu ring plain (Fig. 8). This river is sourced from Crater Lake at an altitude of c. 2,530 m. Exposures along the catchment comprise marine Pliocene-Pleistocene sediments overlain by Quaternary volcaniclastic deposits, the oldest of which were mapped as the Whangaehu Formation (Hodgson, 1993). The base of the Whangaehu Formation is a c. 120 to 140 ka debris-avalanche deposit formed by a massive collapse of the southern proto-Ruapehu edifice, which was termed

the Lower Whangaehu Formation by Keigler et al. (2011). The volcaniclastic sediments are confined to the river catchment and unconformably overlie late Tertiary marine mudstones and muddy sandstones, with the contact generally exposed c. 10 - 30 m above the valley floor (Keigler et al., 2011). In the lower reaches (>137 km south of Mt. Ruapehu), the Whangaehu River has incised into late Quaternary river terraces and underlying Pleistocene marine gravels, sands, and silts that are capped with volcaniclastic deposits (Hodgson, 1993; Deely & Sheppard, 1996).

In addition to the Whangaehu River, the southeastern Ruapehu ring plain was also once drained by the proto-Hautapu River, which is the main focus of this study. The Hautapu River currently rises in native grasslands and 640 ha of wetlands east of Ruapehu, southwest of the town of Waiouru (Fig. 8) (Rogers, 1993). It flows southward through the major regional settlement of Taihape (c. 47 km linear distance from Mt. Ruapehu) before joining the Rangitikei River c. 2.5 km south of Utiku. The river has incised into the soft Taihape Mudstone, a massive siliciclastic partly concretionary siltstone of Upper Pliocene age, which formed in a continental shelf environment (Fleming, 1953; Ker, 1970). Large exotic volcaniclastic boulders within non-volcanic gravels, sands and silts are scattered across the landscape in the Taihape area, where they rest on, and between, four aggradational (gravel) river terraces and the valley floor (Fig. 9). The “erratic” volcanic boulders are most frequent in the Mataroa area, where the most elevated terrace sequences occur between 693 and 703 m above sea level (Fig. 10A). Park (1910) was the first to describe the diamicton sourcing the huge boulders (henceforth referred to as the Mataroa Formation), and interpreted it to be of glacial origin. Te Punga (1952) later described the unit as the “Hautapu Valley Agglomerate” and, in the light of knowledge of the periglacial conditions of this region, re-interpreted it as a package of lahar deposits sourced from Mt. Ruapehu. This now volcanically isolated catchment and its volcaniclastic sequence was targeted for further study in order to define the timing, duration and mechanisms of volcanic sedimentation, and its subsequent landscape impact.

3.3.1.3 Nomenclature

Sediment-water mass flows from volcanoes (lahars) are among the most hazardous processes occurring during or after volcanic eruptions (Scott et al., 1995). Lahars may be triggered by rainfall-induced remobilization of sediment, crater-lake outbreaks, eruption-induced snow melting, or edifice failure (Rodolfo, 2000; Lecointre et al., 2004; Doyle et al., 2009). Syn-eruptive lahars are typically “non-cohesive”, i.e., with low clay contents, and start and end as watery, low-sediment content flows (Scott et al., 1995; Cronin et al., 1999). Interaction with stream water often results in rapid dilution and transformation downstream into sand- and pebble-rich hyperconcentrated flows (Cronin et al., 1999; Doyle et al., 2009). Hyperconcentrated flows generally have a clast-supported texture with local dewatering structures and in parts well-developed inverse or normal grading (Scott et al., 1995).

Inter-eruptive lahars generated by landslides, debris avalanches, or explosions from geothermal/hydrothermal areas, may contain higher clay contents, and produce “cohesive” debris flows that vary little in character throughout their runout (Vallance & Scott, 1997). Cohesive debris flows commonly contain 80 wt.% sediment and >3 - 5% clay. Consequently they typically deposit massive unsorted diamictons of clasts with variable lithologies within a sand-, silt- and clay-rich matrix (Scott et al., 1995).

Volcanic debris avalanches are extremely rapid flows of partially or fully saturated debris

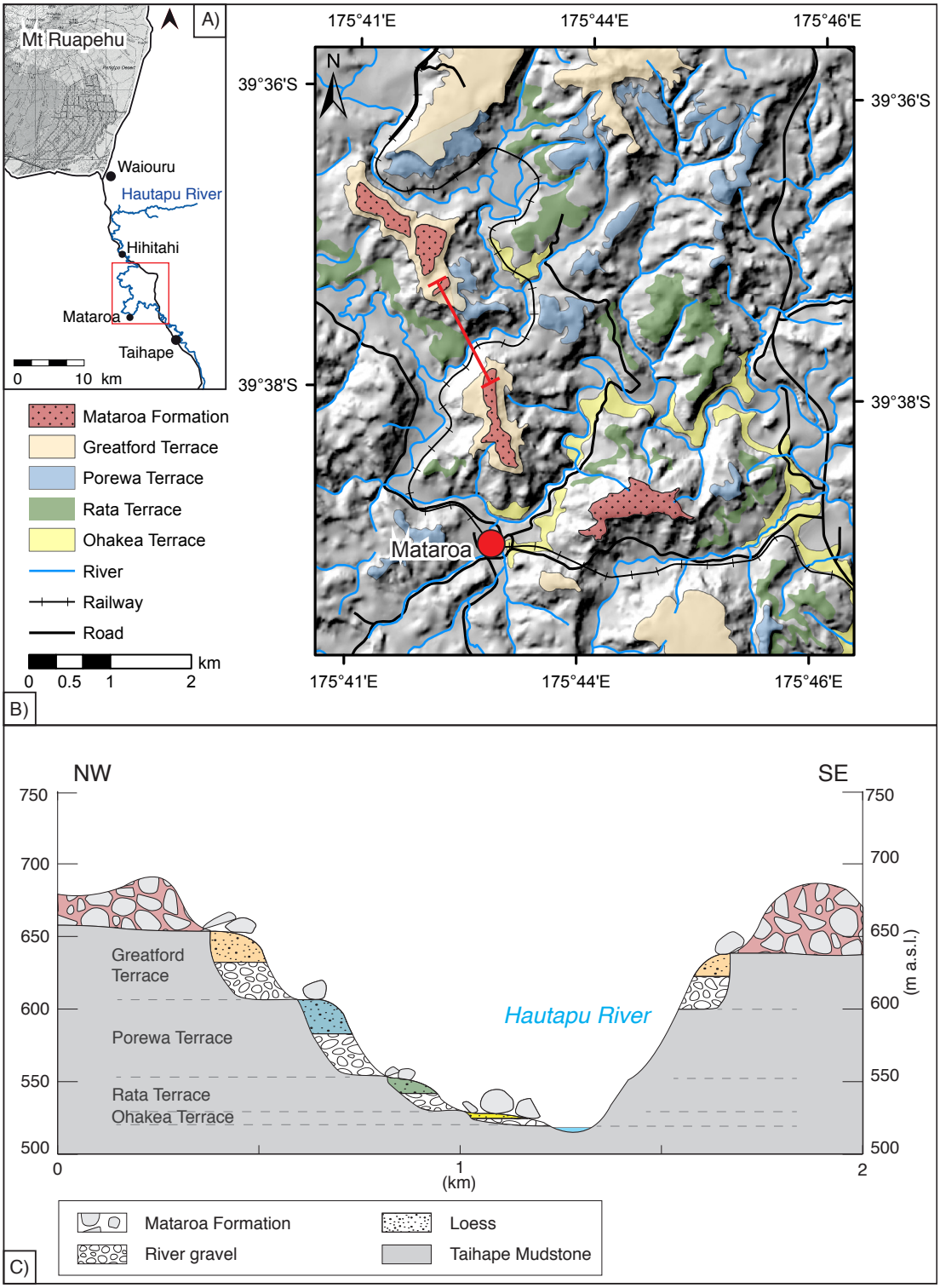

Figure 9. Site of study. (A) The site of study is located c. 40 km southeast of Mt Ruapehu (rectangle). (B) Volcaniclastic diamictons sourced from the composite cone are exposed along the Hautapu River with major outcrops located between Hihitahi and Mataroa, c. 40 km southeast of the volcano (rectangle in A). The Mataroa Formation (red) is exposed at the highest topographic elevation in the area and forms a distinct plateau. (C) Present-day landscape in the Mataroa area (section line in B), where colours of loess layers are consistent with the timing of their source gravels, as represented by the aggradational terraces in Fig. 9B. The Mataroa Formation forms a distinct plateau that armours the softer Taihape Mudstone from erosion. Ongoing uplift and river incision, overprinted by climate- induced erosion cycles formed four aggradational river terraces. Andesitic boulders of the Mataroa Formation are redeposited on top of these and reflect the course of the proto-Hautapu River during the time of volcaniclastic emplacement.

(Hungr et al., 2005), typically generated by failure of part of the volcanic cone, leading to rapid gravitational acceleration of large masses of material (Siebert, 1984). These are the largest and most violent of all processes known from stratovolcanoes (Ui, 1983; Siebert, 1984; Glicken, 1991; Palmer et al., 1991). The potential hazards associated with them were demonstrated during the 18th May 1980 Mt. St Helens eruption, when intense seismicity accompanied with magmatic injection resulted in multiple retrogressive slope failures, rapidly followed by explosive eruptions, including the fatal lateral blast that mantled and mixed with the preceding debris-avalanche deposit (Voight et al., 1981). Debris avalanche triggering mechanisms include tectonic movements (e.g. faulting, earthquakes), explosive eruptions, high-level magma intrusion, extensive hydrothermal alteration of the volcanic edifice, or the migration of vents (Siebert, 1984; McGuire, 1996; Zernack et al., 2012). Their deposits commonly contain "megaclasts" (large fragments of the volcanic edifice up to several hundred metres in size), are massive, poorly sorted, and typically comprise jigsaw-fractured clasts (Mimura et al., 1982; Ui, 1983; Ui et al., 2000). A further distinctive feature of these deposits is a hummocky topography with longitudinal and transverse ridges (Siebert, 1984). Volcanic debris-avalanche deposits significantly change the landscapes they are emplaced upon and induce a different range of sedimentary processes as the landscape recovers and drainage systems re-adjust after their occurrence (e.g., Manville & Wilson, 2004; Procter et al., 2009).

3.3.1.4 Methods

Angular to sub-rounded and unweathered andesitic clasts, ≥10 cm in diameter, were sampled from the Mataroa and Whangaehu Formations for petrological studies and geochemical analysis. Polished thin sections for petrological studies were prepared at the University of Ballarat, Victoria, Australia. Forty two samples (21 each of the Mataroa and Whangaehu Formations) were cut and the central c. 3 x 3 x 3 cm portions were crushed and ground in a tungsten carbide mill. At The University of Auckland, 2 g of ignited sample material were subsequently prepared with 6 g of 12:22 flux to produce glass disks for X-ray fluorescence analysis (XRF). Whole-rock geochemical data were acquired using a Siemens SRS 300 X-ray spectrometer containing a Rh-tube. XRF-calibration is based on 34 international standards, and the Brucker SPECTRA-plus software (V1.51), which uses variable alphas as a matrix correction method, and is calibrated for all elements using three multi-element glass beads and a graphite disk.

3.3.2 Results

3.3.2.1 The Mataroa Formation – stratigraphy and sedimentology

The overall stratigraphy of the Mataroa Formation is reconstructed from several sites (Fig. 11), with the type locality situated beside an airstrip c. 1.5 km east-northeast of Mataroa (175°44'30.5902 E, 39°38'35.7641 S; 692 m a.s.l.). Basal units of this volcaniclastic sequence crop out at three further localities in the area and unconformably overlie the Upper-Pliocene Taihape Mudstone (Fig. 10D). The deposit comprises two massive, unbedded diamicton facies, primarily distinguished by the maximum-clast size of andesite boulders and rip-up clasts of the underlying Taihape Mudstone.

Facies 1 – Debris Avalanche Deposit (DAD)

The lowermost Facies 1 shows no bedding structures and contains moderate- to well-rounded

pebble- to boulder-sized clasts of andesite lava (50 - 60 vol.%, <4 m), along with rip-up clasts of Taihape Mudstone (5 - 15 vol.%, <5 m), supported by a firmly consolidated matrix (making up 25 - 35 vol.%) (Fig. 10C; Fig. 12). The hardened inter-block matrix is dominated by silt to fine sand, but is coarser sand or pebbly in places. Several clasts show distinctive jigsaw-fractures. The clast assemblage is dominated by andesite lava fragments (80 - 90 vol.%), Taihape Mudstone (10 - 15 vol.%), soft and hydrothermally altered andesitic clasts (≤5 vol.%), and Mesozoic greywacke gravel (<5 vol.%). Some of the Taihape Mudstone rip-up clasts are up to 5 m long and in places deformed. Facies 1 varies in exposed thickness between 0.5 m to >6 m. Facies 1 deposits locally pass laterally into channels of <1.5 m thick fluvial clast-supported gravels. In other cases “blocks” of sandy-pebbly planar-bedded volcaniclastic deposits occur out of stratigraphic context (Fig. 12). At the basal contact, Facies 1 overlies Taihape Mudstone (exposed at S1 and S3; Fig. 11) with either a sharp and smooth, or irregular contact, where the underlying rock was ripped up.

Facies 2 – Lahar Deposits

Above the basal massive and coarse deposit, thick, pumice-rich, pebbly and sandy volcaniclastic diamictons occur (Facies 2). Up to 15 individual units are recognised across all localities, with some individual sites exposing up to six stacked flow units, totalling 3 to 11 m in thickness. These deposits contain the same rock types as Facies 1, but are rich in weathered pumice pebbles, yellow-brown, reddish, grey or white in colour, depending on the site hydrology. Clasts are sub-rounded to angular, varying with grain size and sorting in each individual unit. Deposits are mostly massive and unbedded, with pebble- to cobble-sized clasts within a sandy-silt matrix, or they verge on being clast-supported and show faint planar bedding. Finer grained (pebble-sand dominated) and better-sorted deposit units generally contain more angular clasts. In the most commonly exposed units, clasts are dominantly <0.1 m in diameter. In some locations, thicker, channelized deposits occur with clasts up to 0.75 m in diameter. The pumice clast component is dominantly pebble-sized and ranges from 10 vol.% in basal units up to c. 30 vol.% in the uppermost deposits (Fig. 11B; 11D). The matrix is usually sand to silt, although in rare cases it also contains up to 40% clay. Some units show reverse grading, particularly seen by increasing contents of pumice clasts towards the top. Rare horizontally bedded and low-angle cross-laminated horizons <40 cm thick occur at one site (Section 2). Basal contacts are planar with occasional erosional features noted. A fine-grained pebble-dominated and weakly planar-bedded deposit at Section 4 also contains distinctive charcoal fragments (≤5 cm) in its upper third.

3.3.2.2 Age Control

Cover-bed stratigraphy

In the most complete cover-bed sequence (Section 4), up to four loess horizons and associated buried soils occur on top of the volcaniclastic deposits, with the Kawakawa Tephra (27.1 ± 1 ka cal. BP; Lowe et al., 2008) occurring within the uppermost loess (Fig. 11E). In areas to the south of the studied sequences, river and marine terraces are dated by their cover-bed sequences, particularly a named series of loess/soils and dated tephra horizons (Fig. 9) (Milne, 1973; Pillans, 1994). North of this area, within the volcanic ring plain, loess/soil sequences also provide age control on the oldest volcaniclastic surfaces (Cronin et al., 1996). Here, the loess/soil sequences are made up of wind-blown silt- and fine-sand particles sourced from quarzo-feldspathic or volcanic surfaces, with rates of accumulation particularly high during periglacial climates. On

undisturbed landscapes adjacent to rivers or ring plains, these are accretionary soils, forming a distinctive sequence of weathered/unweathered units with gradational contacts marking stadial/interstadial periods of cool/dry and warmer/wetter climates. The three youngest undisturbed loess units (Ohakean, Ratan and Porewan Loess) are associated with accumulation during the three main stadials of the last glaciation (post-80 ka) (Milne, 1973). Below these, many further loess units occur, capped by a very distinctive Last Interglacial paleosol. Each aggradational terrace is followed by development of a paleosol during interglacial periods. At Section 4 (Hihitahi; Fig. 11E), the upper three Last Glaciation loess units are identified, with associated interstadial soils. Below this is a thick paleosol, which may be developed into a fourth loess layer. The oldest loess could be the Greatford Loess from the penultimate glaciation (Milne, 1973), or it may have formed during the early part of the last interglacial. Either way, the well-developed paleosol is highly distinctive and represents the Last Interglacial. This implies an age for the underlying

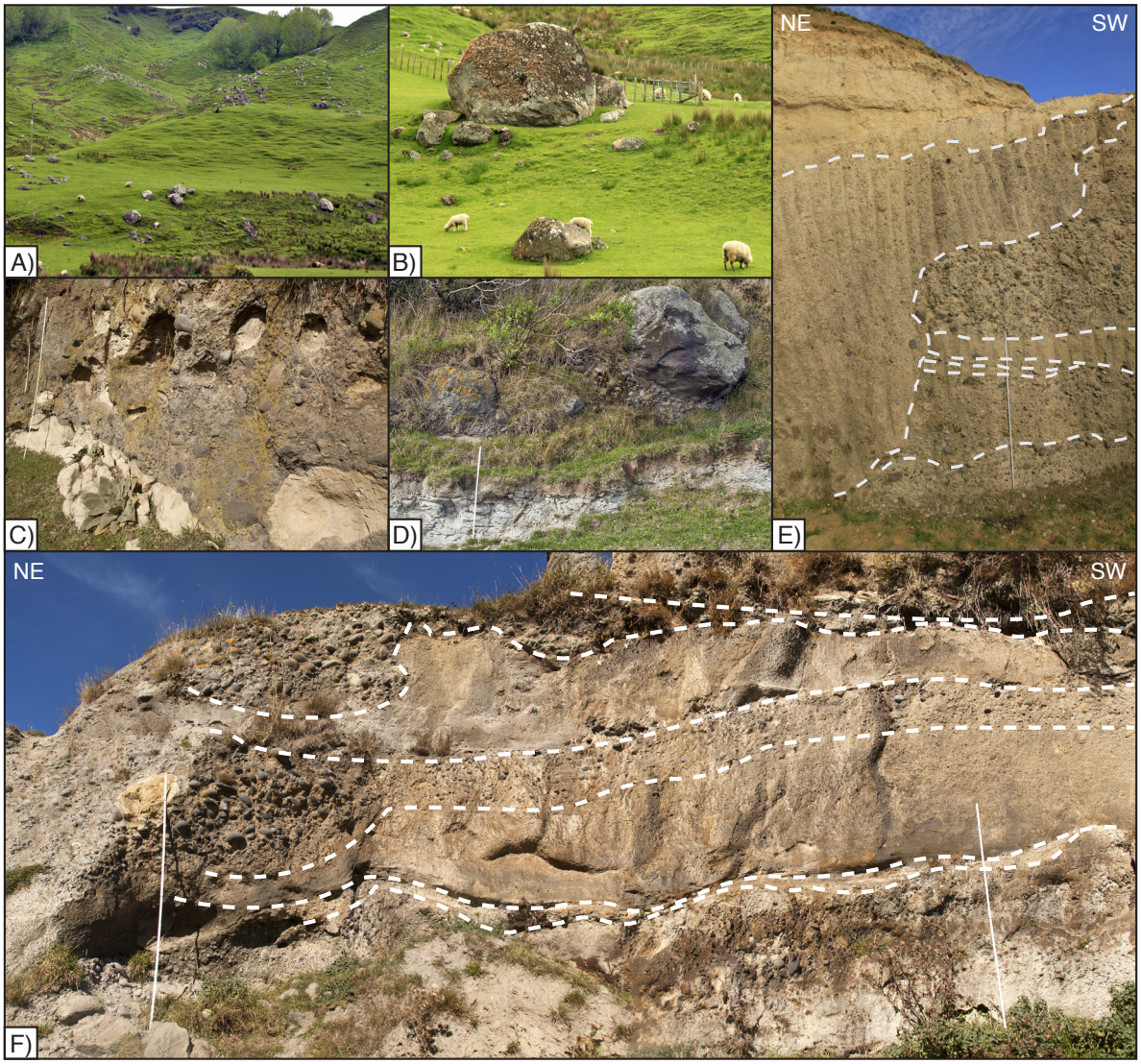

Figure 10. Lithological characteristics of the Mataroa Formation. (A) Preferred incision of the Hautapu River into the soft Taihape Mudstone resulted in reworking and re-deposition of andesitic boulders related to the Mataroa Formation on top of aggradational river terraces and the valley floor. (B) Subrounded andesitic boulders up to 4 m in diameter are reworked from Facies 1 of the Mataroa Formation and remain scattered around the countryside. (C) Facies 1 of the Mataroa Formation is heterolithologic, poorly sorted and massive. The light-coloured clasts are Taihape Mudstone rip-up clasts (Scale: 2 m). (D) The Mataroa Formation overlies Taihape Mudstone, reflecting the onset of volcaniclastic deposition within the Hautapu River catchment (Scale: 1 m). (E-F) The sequence of hyperconcentrated-flow and debris-flow deposits (Facies 2) differs between locations, and reflects the formation of a braided river system after deposition of Facies 1 (Scale: 2 m).

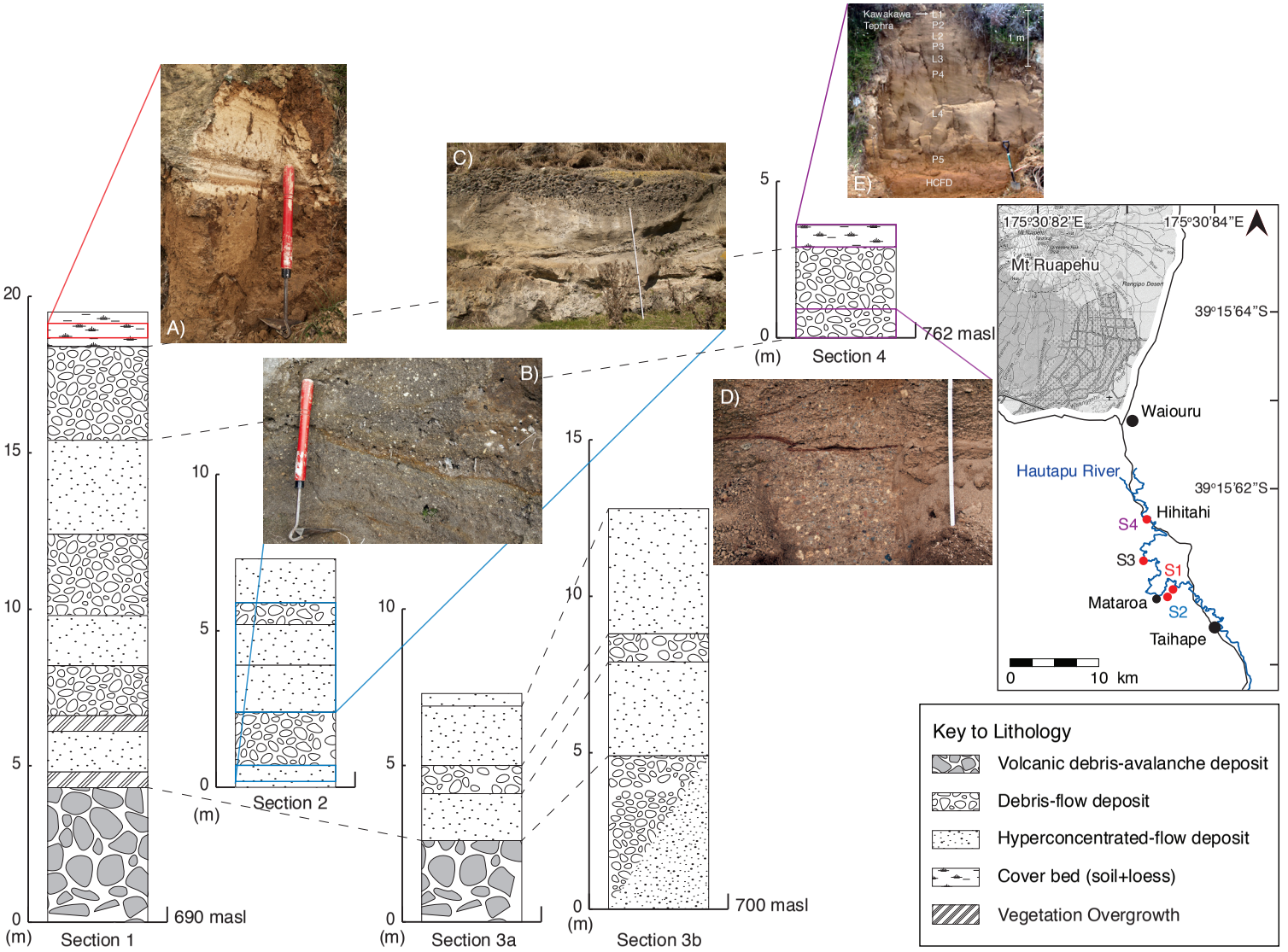

Figure 11. Stratigraphic correlation of the Mataroa Formation. Facies 1 is best exposed at two localities and overlain by sequences of hyperconcentrated -flow and debris-flow deposits that comprise various amounts of pumice (Inset map: locality of exposures). (A) The rhyolitic Kawakawa Tephra (27.1 ka cal. BP; Lowe et al., 2008) is exposed within the top loess unit of Section (S) 1 and S4. (B) The lowermost hyperconcentrated-flow deposit at S2 contains c. 10 vol.% pumice clasts and indicates eruptive activity of Mt. Ruapehu after Facies 1 emplacement. (C) Several flow units can be distinguished at S2 in part eroding into, and incorporating the underlying flow unit (Scale: 2 m). (D) The uppermost lahar deposit comprises c. 30 vol.% angular pumice clasts. It is overlain by cover-beds at S1 (A) and S4 (E), and marks the end of volcaniclastic deposition within the Hautapu River catchment.

volcaniclastic sequence of >125 ka.

Correlation using petrology and geochemistry

Whole-rock chemical compositions of Mt. Ruapehu lavas show a distinctive trend towards higher incompatible element and silica contents over time (Price et al., 2005; 2012). Based on published data, the most mafic eruptives refer to the Te Herenga Formation with 54.87 - 57.96 wt.% SiO_2 and 0.55 - 0.82 wt.% K_2O, and the most evolved to the Whakapapa Formation with 55.50 - 64.79 wt.% SiO_2 and 1.23 - 2.35 wt.% K_2O (Price et al., 2012). This evolutionary geochemical sequence provides the opportunity to link the distal Mataroa Formation deposits (and other units of similar age, e.g., the Whangaehu Formation) to specific lava flow sequences exposed on the volcanic edifice (Fig. 13).

In all samples, simple to polysynthetic twinned plagioclase is the predominant phenocryst phase, followed by zoned clinopyroxene, and orthopyroxene. Fe-Ti-oxides and olivine phenocrysts are rare (≤1 vol.%), as is accessory zircon. Fluid and melt-inclusions are dominant along cleavages or in the centre of feldspar and pyroxene phenocrysts. Phenocrysts are up to 4 mm across and make up ≤50 vol.%. All samples also contain small (≤3 mm) xenoliths of exotic (underlying basement) origin. The ≤40 vol.% groundmass comprises feldspar and clinopyroxene microlites within a glassy matrix. Irregularly rounded vesicles ≤5 mm in diameter make up ≤50 vol.% of the studied samples.

Whole rock compositions of the Mataroa Formation are andesites and basaltic andesites (56 - 61 wt.% SiO_2; 3.9 - 5.0 wt.% $K_2O + Na_2O$; Table 2) with intermediate to low Si and K contents (0.64 - 1.5 wt.% K_2O) relative to Mt. Ruapehu volcanic rocks. Concentrations of incompatible trace elements, such as Ba (189 - 355 ppm), Rb (14 - 47 ppm), and Zr (53 - 110 ppm), are also at the low end of the Ruapehu volcanic rock compositional spectrum (Table 2). Correlation of the Mataroa (and Lower Whangaehu) Formation to the lavas exposed on the Mt. Ruapehu edifice focuses on the two oldest eruptive episodes (Te Herenga and Wahianoa Formations) since the cover-bed stratigraphy overlying the mass-flow deposits relates to significantly younger cone-building formations (Mangawhero and Whakapapa Formations). The data indicate that the volcaniclastic deposits of the Mataroa Formation are geochemically more evolved than the oldest Mt. Ruapehu volcanic suite (the Te Herenga Formation lavas) (Fig. 13C). The Mataroa Formation samples, hence, have compositions that correlate best with those of lavas from the Wahianoa Formation, which were erupted between 120 - 150 ka ago (Gamble et al., 2003; Price et al., 2005). This correlation is also consistent with the known distribution of the Wahianoa Formation on the southern flanks of Mt. Ruapehu (Fig. 13A). Less evolved samples similar to Te Herenga compositions could represent materials from the deepest and oldest parts of the failed flank generating the debris avalanche.

Geomorphic evidence from Fluvial Aggradational Terraces

Another set of constraints on the emplacement time of the Mataroa Formation in the proto-Hautapu valley can be obtained from estimates for the time of formation of aggradational-gravel terraces in the region (e.g. Milne, 1973; Pillans, 1994). During glacial periods the periglacial climate of the central and southern North Island caused lower tree lines and high rates of physical weathering in the uplands and mountains. This fed huge supplies of sediment into river valleys, building broad braided river terraces of gravels and sands (Milne, 1973). During interglacial periods increased precipitation and vegetation cover in the uplands reduced the sediment supply and resulted in

rapid down-cutting of rivers in narrow channels through their former braided gravel deposits. Overall, ongoing tectonic uplift in this area has meant that aggradation surfaces produced during each successive stadial were elevated to form terraces, at progressively higher elevations than subsequent terraces (Milne, 1973; Berryman et al., 2000). In total, seven alluvial aggradational terraces are identified in the South Wanganui Basin and along the Rangitikei River, which are, from youngest to oldest: i) the Ohakea Terrace (10 - 18 ka BP), the Rata Terrace (30 - 50 ka BP), the Porewa Terrace (70 - 80 ka BP), the Greatford Terrace (110 - 120 ka), the Marton Terrace (140 - 170 ka), the Burnand Terrace (240 - 280 ka), and the Aldworth Terrace (340 - 350 ka). All given ages are obtained from Pillans (1994) . Correlating the terraced landscape of the Hautapu River tributary with the well-defined Rangitikei Terrace sequence 10 km south of Taihape, the Mataroa Formation occurs above the Greatford Terrace (four loess- and corresponding soil

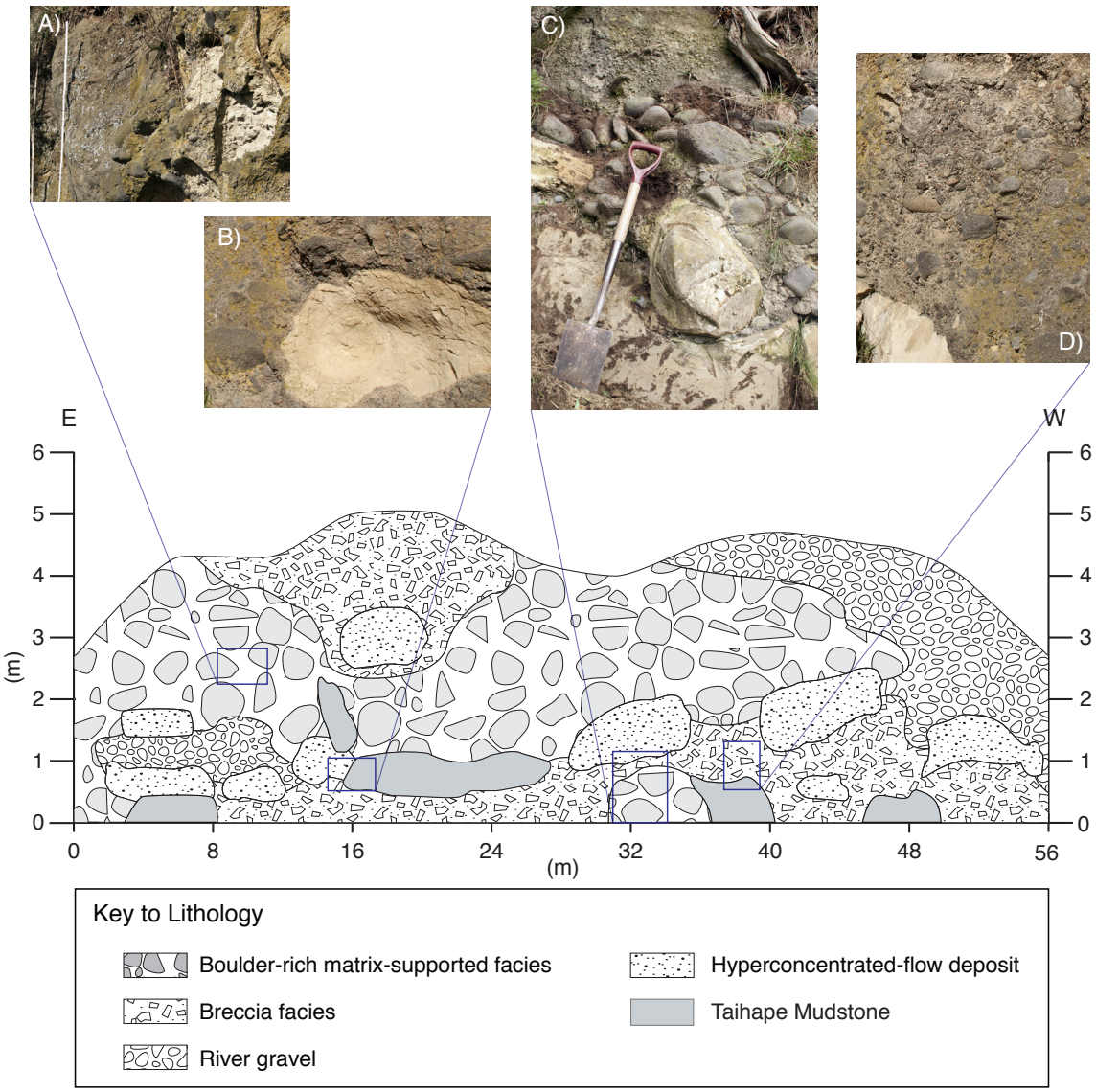

Figure 12. Profile of Facies 1 at Section 1. The deposit contains domains of a boulder-rich, matrix-supported facies, comprising jig-saw fractured clasts up to 2 m in diameter. Volcaniclastic clasts of brecciated material and hyperconcentrated-flow deposits were either derived from the collapsing flanks or incorporated during runout. "Pockets" of exotic material comprise river gravel and Taihape Mudstone, most likely ripped-up from the river bed during runout. (A) Subrounded andesitic boulders within a consolidated matrix-supported framework (Scale: 1 m). (B) Taihape Mudstone rip-up clast within Facies 1 (Scale: 50 cm). (C) Facies 1 is emplaced on top of Taihape Mudstone. In areas of decreasing thickness clasts are generally well-rounded. (D) The dominant lithology of Facies 1 comprises angular to subrounded andesitic clasts within a firmly consolidated inter-block matrix of dominantly silt to fine sand (Scale: 70 cm).

horizons) and forms the highest units in the landscape (Fig. 9). Thus the Mataroa Formation volcaniclastic deposits must be older than 110 ka.

3.3.3 Discussion

3.3.3.1 Mataroa Debris Avalanche Triggering

The flank collapse generating the Mataroa debris avalanche may have been pre-conditioned by the growing Ruapehu edifice loading and deforming its weak Tertiary rock substrate. Indications of a cryptodome intrusion, implicated as a trigger mechanism for a 10 ka debris avalanche on the western slopes of Ruapehu volcano (Palmer & Neall, 1989; McClelland & Erwin, 2003), are absent, although the pumice-rich Facies 2 might reflect an earlier intrusion of melt prior to collapse. Alternatively, intense hydrothermal alteration may have weakened the rocks of the edifice, or major regional tectonic motion associated with the Taupo Volcanic Zone, especially along the Wahianoa Fault (Fig. 8B), could have triggered failure. The lack of known large-scale eruptions from the rhyolitic Taupo Volcanic Zone anywhere near this time, however, may rule out a regional volcano-tectonic correlation. Instead, this collapse appears to be coincident with the end of the Penultimate Glaciation (120 ka; Milne, 1973) and an onset of warmer, wetter conditions during the Last Interglacial period. A formerly ice-armoured edifice, responding to a warming climate, may have become infiltrated by melt water, leading to weakening and ultimately collapse. Similar climate-preconditioned or climate-triggered volcanic collapses have been suggested for several Mexican volcanoes (Carrasco-Núñez et al., 2006; Roverato et al., 2011; Capra et al., 2013).

3.3.3.2 Emplacement Mechanisms of the Mataroa Formation volcaniclastic deposits

The sedimentology and lithology of Facies 1 show properties that are attributed to a distal debris avalanche (Fig. 14B). Along its flow path, from proximal to medial reaches, the debris avalanche eroded and entrained gravel, as well as the soft Taihape Mudstone. The common sub-rounded and moderately- to well-rounded andesitic boulders within the deposit were either sourced from the partly glaciated collapsing volcano flanks, or were eroded from abundant deposits of this kind on the surface of the proximal ring plain.

The debris avalanche passed through a narrow reach of the proto-Hautapu River between Hihitahi and Turangarere (30 km from source), as it travelled over Snowgrass Dome, which is composed of Pliocene sedimentary beds (Fig. 8) (Feldmeyer et al., 1943; Ker, 1991; Villamor & Berryman, 2006a). After emerging from this narrow neck, the flow spread out between Turangarere and Taihape (Fig. 14B). Here, the greatest width of deposition is seen in both primary deposits as well as the residual boulders scattered across the eroded terrain (Fig. 10A; B). These boulders are too large to have been moved by subsequent streamflow processes. This zone of major deposition probably relates to a local widening of the valley plus a small break in slope from 0.012° to 0.002° between Hihitahi and Mataroa. Once the volcanic debris avalanche reached the Mataroa area, it had entered an incised proto-Hautapu River course. This was located to the west of the present deeply incised channel and may have been in a braided, aggraded state at the time of collapse (Fig. 14B). Overall, the debris-avalanche deposit, which forms Facies 1 of the Mataroa Formation, has an approximate runout of >60 km, and inundated an area of at least 220 to 260 km^2 (Fig. 8). Using these constraints, its original volume can be estimated as 2.0 - 3.0 km^3.

The high energy of the flow is attested by the transport of huge (>4 m) dense lava boulders over 50 km from Ruapehu. Locally, the extremely violent and erosional behaviour of the flow is shown by the common rip-up and incorporation of the underlying Taihape Mudstone. Further distinctive characteristics of the debris-avalanche deposit include common jig-saw jointed clasts, still coherent, or slightly dispersed within the matrix, and the presence of mega-clasts or blocks of other volcaniclastic lithologies that must have been carried along within the moving mass (Siebert, 1984; Palmer & Neall, 1989; Gaylord & Neall, 2012). Debris avalanches typically carry large quantities of pore water within the collapsing mass but their motion is usually dominated by granular and frictional processes (e.g., Iverson, 2012). However, once the debris avalanche became confined to a valley, compression may have enhanced the internal pore fluid pressures, and, along with the high silt-content in the matrix, caused the debris avalanche to transform into a flow regime similar to a cohesive debris flow. The mechanism envisaged is similar to that proposed for the debris avalanche induced Osceola Mudflow at Mt. Rainier, USA (Vallance & Scott, 1997). An increase in pore pressure within the channelized Mataroa debris avalanche likely transformed it into a viscous flow by 50 km from source, contributing to its long runout.

On top of the debris-avalanche deposit, the Facies 2 deposits are characterized by a sequence of units interpreted as debris-flow and hyperconcentrated-flow deposits (Fig. 10). They all contain pumice, but the upper units are progressively finer-grained and contain greater pumice contents. Thick, coarse channel-fill deposits occur as well as thinner, flat-lying tabular deposits, which indicates deposition within a complex braided and aggrading river system forming above and beside the volcanic debris-avalanche deposit (Fig. 10; 14B). The large quantity (up to 30 vol.%) of pumice sand and pebble fragments in Facies 2 is typical of Ruapehu lahar deposits associated with explosive sub-plinian to plinian volcanism (Cronin et al., 1997; 1999; Lecointre et al., 2004). The contact between Facies 1 and Facies 2 is sharp, with no paleosol present (Fig. 11). Hence these deposits might hint at a pulse of explosive volcanism, which began soon after the major flank collapse and debris-avalanche emplacement (Fig. 14B). The pyroclastic material associated with the eruptive events was presumably deposited on the proximal Ruapehu ring plain, and subsequently reworked and incorporated into the lahars. Eruptive activity associated with subsequent lahar formation has also frequently been observed at Mt. St Helens, USA, where syn-eruptive lahar deposits are exposed within numerous river catchments dissecting the steep flanks of the stratovolcano (e.g., the Kalama and Lewis River; Crandell & Mullineaux, 1973; Hyde, 1975, or the North and South Fork Toutle River; Mullineaux & Crandell, 1962; Lipman & Mullineaux, 1981). Charcoal fragments ≤5 cm in size in the uppermost flow unit of Facies 2 of the Mataroa Formation suggest that pyroclastic-flow deposits on the volcano and the proximal ring plain were reworked into the lahars. This also indicates that woody vegetation was present on intact portions of the edifice and/or most proximal parts of the ring plain, consistent with a warm, interglacial climate. Even under the present warm climate, vegetation within the range of the largest known Ruapehu pyroclastic flows (c.f., Pardo et al., 2012) is present only on some sectors of the volcano. The sequence of likely syn-eruptive lahars within Facies 2 leads to a smoothing and mantling of the distal valley landscape after volcanic debris-avalanche emplacement.

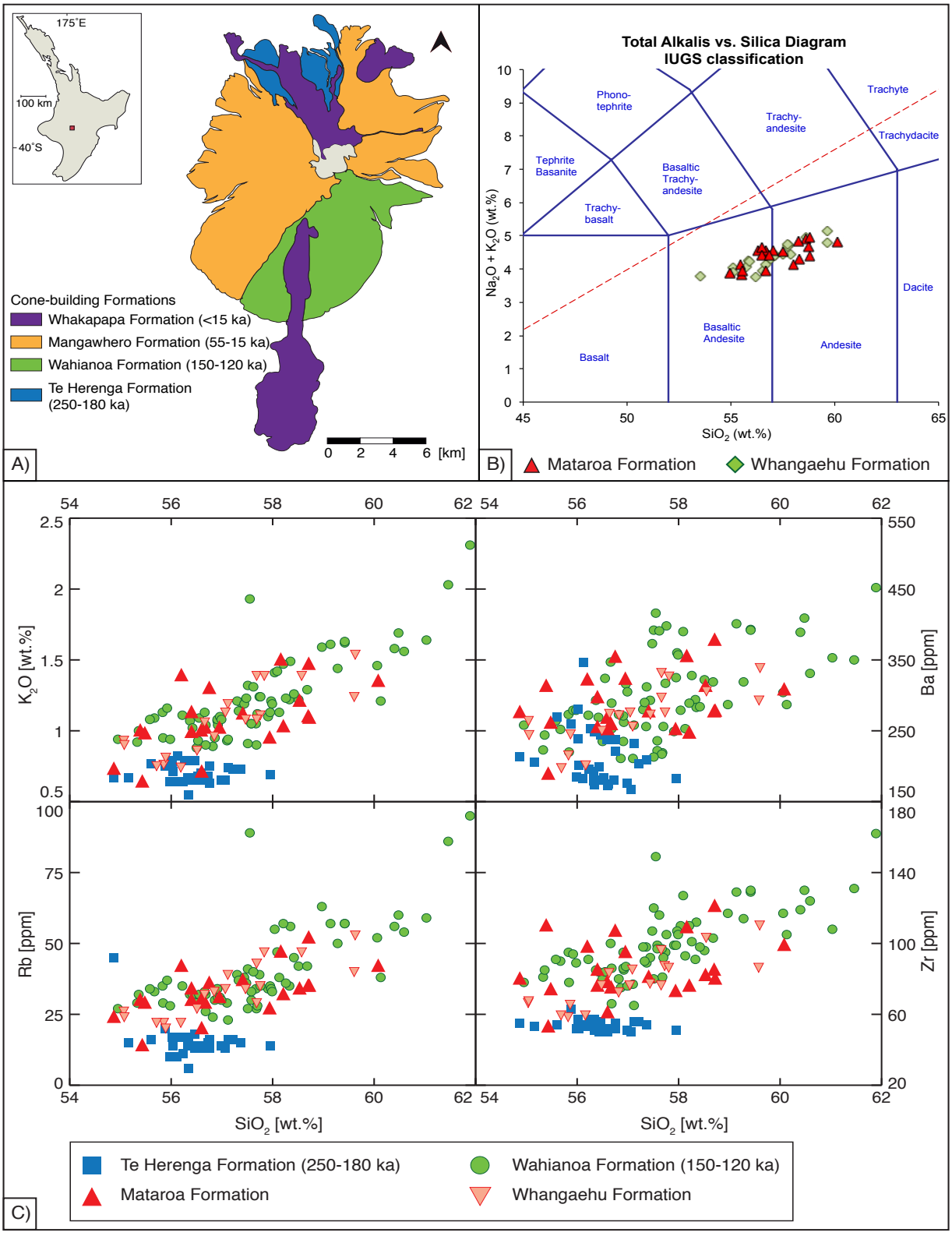

Figure 13. Representative whole-rock composition of the Mataroa and Whangaehu Formation sin relation to the lavas exposed on the Mt. Ruapehu cone (Price et al., 2012). Ages from Gamble et al. (2003) and Price et al. (2005). (A) The four major cone-building formations as mapped by Hackett and Houghton (1989). (B) Total-alkali compositions of the Mataroa and Lower Whangaehu Formations reflect basaltic andesites and andesites. Nomenclature after LeBas et al. (1986), IUGS – International Union of Geosciences. (C) In comparison to the Ruapehu lavas (Price et al., 2012), whole-rock compositions of the Mataroa and Whangaehu Formations are similar to those of the Wahianoa cone-building formation. Cone-building formation colours are the same as in A.

Table 2. Representative whole rock composition of the Mataroa Formation. Th, La, and Ce concentrations are measured for overlap corrections.

	1	2	3	4	5	6	7	8	9	10	11	12	13	14	15	16	17	18	19	20	21
Sample	Man-1	Man-2	Man-3	Man-4	Man-5	Man-6	Man-7	Man-8	Man-9	Man-10	Man-11	Man-12	Man-13	Man-14	Man-15	Man-16	MT-01	MT-02	MT-03	MT-04	MT-05
wt.%																					
SiO_2	60.08	58.21	56.67	58.53	58.70	56.59	58.16	56.95	56.60	56.20	55.39	55.43	58.72	57.94	55.48	56.40	54.87	56.40	58.71	56.75	57.41
TiO_2	0.57	0.60	0.67	0.60	0.65	0.66	0.69	0.64	0.64	0.76	0.85	0.61	0.58	0.61	0.74	0.72	0.68	0.67	0.73	0.71	0.66
Al_2O_3	16.29	16.68	18.69	19.25	17.56	19.36	17.96	18.88	17.81	17.95	17.73	16.95	17.22	17.27	17.29	16.63	17.76	18.54	17.90	17.56	17.51
Fe_2O_3	6.55	7.61	7.46	5.78	6.87	6.95	7.38	6.48	7.26	8.17	8.65	8.16	7.06	7.81	9.05	8.56	8.23	7.76	6.95	7.75	8.22
MnO	0.11	0.13	0.12	0.09	0.11	0.11	0.12	0.10	0.13	0.12	0.14	0.13	0.13	0.13	0.15	0.14	0.13	0.12	0.11	0.12	0.13
MgO	3.50	4.47	3.47	2.08	3.73	2.81	3.14	3.08	4.37	3.79	4.59	5.87	3.91	4.21	4.35	4.32	4.69	3.61	2.91	4.26	4.03
CaO	6.59	7.37	7.94	7.33	7.16	7.93	6.45	6.82	8.06	7.28	7.71	8.24	7.06	7.07	7.88	8.18	6.70	7.97	5.97	6.35	7.35
Na_2O	3.48	3.27	3.48	3.70	3.58	3.53	3.34	3.53	3.24	3.16	3.12	3.21	3.29	3.18	2.96	3.51	3.15	3.43	3.49	3.11	3.40
K_2O	1.35	1.03	1.02	1.21	1.10	1.00	1.50	1.02	0.71	1.39	1.00	0.64	1.09	0.95	0.98	1.13	0.73	0.99	1.47	1.30	1.12
P_2O_5	0.13	0.11	0.12	0.12	0.11	0.12	0.14	0.11	0.09	0.13	0.14	0.09	0.10	0.10	0.13	0.13	0.09	0.12	0.12	0.13	0.12
H_2O	0.29	0.20	0.04	0.26	0.12	0.52	0.26	0.71	0.53	0.48	0.24	0.18	0.19	0.24	0.34	0.03	1.46	0.27	0.74	1.06	0.24
LOI	0.96	0.24	0.22	0.94	0.20	0.30	0.75	1.56	0.45	0.44	0.33	0.37	0.58	0.37	0.51	0.13	1.41	0.02	0.78	0.77	-0.31
Total	99.89	99.91	99.90	99.89	99.88	99.90	99.89	99.88	99.89	99.88	99.88	99.88	99.91	99.89	99.87	99.88	99.89	99.89	99.88	99.87	99.88
ppm																					
Ba	308	247	259	313	277	268	355	323	252	322	313	189	278	252	261	297	276	255	378	354	277
Rb	42	32	29	34	35	30	47	31	20	42	30	14	35	27	29	34	24	30	52	36	37
Sr	236	224	259	279	247	274	278	260	231	282	268	226	229	232	264	284	220	254	244	244	257
Pb	10	8	5	10	9	7	12	11	5	8	7	5	7	8	7	7	11	5	12	11	11
Th	8	3	4	0	8	5	6	7	1	2	2	0	1	0	2	3	4	1	6	3	7
Zr	99	76	75	82	85	78	109	95	61	98	110	53	80	73	74	85	80	76	121	107	81
Nb	5	3	4	4	4	4	5	4	4	5	5	3	5	4	5	5	3	4	5	6	3
Y	22	19	21	19	18	21	22	21	23	24	21	18	19	17	21	22	17	20	21	23	17
V	150	178	184	149	173	162	165	159	205	204	244	203	173	197	237	215	205	188	175	192	208
Cr	44	87	46	16	88	28	14	43	41	26	52	175	67	68	48	70	86	51	32	57	43
Ni	12	36	18	7	32	13	8	14	15	12	13	67	22	15	68	29	29	16	15	16	10
Cu	25	44	48	33	37	54	28	39	40	32	47	26	30	19	31	63	53	46	28	34	38
Zn	65	75	74	66	73	74	83	66	85	80	87	76	84	86	93	85	82	74	72	79	77
La	11	9	12	6	7	10	17	11	9	14	11	4	9	7	12	10	17	8	13	11	11
Ce	20	0	13	14	9	8	20	8	2	18	22	9	7	7	6	14	3	6	19	3	8

3.3.3.3 Relationship to the Whangaehu Formation

Towards the west, the catchment adjoining the Hautapu River hosts the Whangaehu River, which is the current route for the majority of lahars descending the southern and eastern slopes of Mt. Ruapehu. At present, the route of the Whangaehu River is dominantly controlled by the Karioi Fault (Fig. 14C). The oldest volcaniclastic unit exposed in its valley is the 10 - 30 m-thick Lower Whangaehu Formation (Hodgson, 1993; Keigler et al., 2011), which is a channel-confined debris-avalanche deposit with sedimentary and lithological characteristics similar to those of the Mataroa Formation. The loess and soil cover-bed stratigraphy above the Whangaehu Formation and its relationship to the Rapanui interglacial marine-cut terraces in the lower river imply a depositional age of ≥120 ka (Hodgson, 1993). In addition, the andesitic clasts within this deposit occupy the same compositional field as the Mataroa Formation and the corresponding Wahianoa cone-building lavas on Mt. Ruapehu (Fig. 13). Geochemically, the clasts of the Lower Whangaehu Formation represent basaltic andesites and andesites (53.5 - 63.3 wt.% SiO_2; 3.8 - 6.1 wt.% $K_2O + Na_2O$; Table 3). As is the case for the Mataroa Formation, the chemistry of clasts from the Lower Whangaehu Formation shows intermediate to low Si and K contents (0.7 - 1.5 wt.% K_2O) compared with those of Mt. Ruapehu volcanic rocks. Concentrations of incompatible trace elements such as Ba (195 - 337 ppm), Rb (19 - 46 ppm), and Zr (58 - 110 ppm) are also similar (Table 3). Thus, the age estimates and clast chemistry from these two debris avalanches overlap (Fig. 13) and indicate that either two rapidly successive collapses occurred from the southern Ruapehu flanks within <30 ka of each other (Price et al., 2005), or two depositional lobes were formed from a single collapse. This bifurcation occurred at the edge of the ring plain where separate channels are split by the graben structure associated with the 22 km long Karioi Fault (Villamor & Berryman, 2006a) (Fig. 8; 14). Villamor and Berryman (2006a) suggest an average displacement rate of 0.4 mm/yr and an approximate initial age of >100 ka for the normal fault. Assuming the Karioi Fault was already active at the time of debris-avalanche emplacement and with the same average-displacement rate, the Karioi Fault scarp would have been up to 40 m high prior to the flank failure. Such an offset could have been easily buried by the mass-wasting events descending the southeastern slope of Ruapehu volcano. The Tertiary hill country located south of Mt. Ruapehu is very likely to have prevented unconfined spreading of the deposit, instead forcing the debris avalanche into the Whangaehu and Hautapu River catchments.

The runout of the Whangaehu debris avalanche is estimated at >60 km (Keigler et al., 2011). The deposit covers an area of c. 80 - 120 km^2 and has an approximate volume of 2.4 - 5.3 km^3. If both the Whangaehu and Mataroa Formation debris-avalanche deposits were derived from a single large flank collapse of the Wahianoa cone-building lavas, the total volume of this volcanic debris avalanche may have been between c. 4.4 - 8.2 km^3 (Fig. 8). Either singly or combined, these units represent the largest debris avalanches recognised at Mt. Ruapehu so far (c.f., Murimotu Formation, 0.2 km^3; Palmer & Neall, 1989; Mangaio Formation, 0.034 km^3, Donoghue & Neall, 2001). These volume estimates are, however, well within the sizes estimated for debris avalanches from the 2,518 m-high andesitic stratovolcano Mt. Taranaki, 100 km to the west of Mt. Ruapehu (Zernack et al., 2012).

3.3.3.4 Landscape and sedimentological response to a catastrophic debris avalanche

Emplacement of the Mataroa Formation within the proto-Hautapu River catchment has affected the landscape to the present day (Fig. 14). The current course of the deeply entrenched Hautapu River in the Mataroa-Taihape area lies east of the Mataroa Formation volcaniclastic deposits

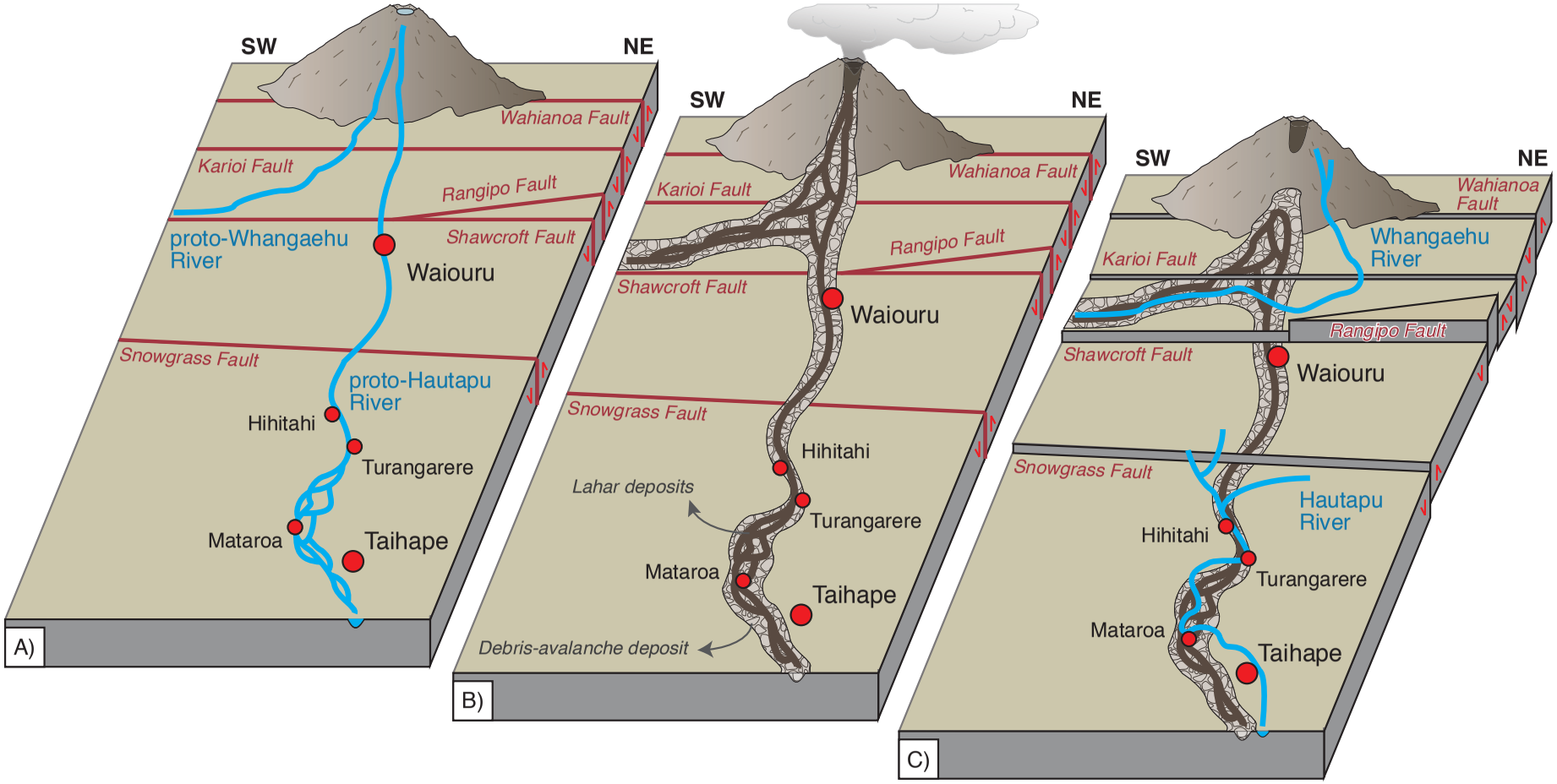

Figure 14. Depositional model of the Mataroa Formation. (A) Prior to emplacement of the Mataroa and Lower Whangaehu Formations (>150 ka), the proto-Hautapu River very likely arose either from the flanks of the Mt. Ruapehu edifice, or the proximal ring plain. A braided river system developed between Turangarere and Taihape. The origin of the proto-Hautapu River on the volcanic edifice implies the source of a proto-Whangaehu River to be located further southwest than at present. Exposures of volcaniclastic deposits along the Whangaehu River, as well as regional strike-slip faulting indicate that the majority of its course has been consistent over time. (B) Substrate-weakening and hydrothermal alteration on the cone resulted in partial collapse of the southeastern Wahianoa flank 125 - 150 ka ago, which produced a debris-avalanche deposit that spilled into the Hautapu (and Whangaehu) River catchment. Sub-plinian to plinian eruptions produced vast amounts of pyroclastic material, which was reworked into lahars that descended the volcanic flanks and were emplaced on top of the debris-avalanche deposit. (C) The Whangaehu River emerged at the eastern flank of the volcanic edifice <125 ka ago. Its course is dictated by regional strike-slip faulting, especially the Rangipo and Karioi Fault, which results in it running southwards and incising into the mass-flow deposits of the Mataroa and Lower Whangaehu Formations. At the same time, the proto-Hautapu River was cut off from the proximal Ruapehu ring plain and presently arises from wetlands south of Waiouru.

Table 3. Representative whole rock composition of the Lower Whangaehu Formation. Th, La, and Ce concentrations are measured for overlap corrections.

	1	2	3	4	5	6	7	8	9	10	11	12	13	14	15	16	17	18	19	20	21
Sample:	MT-06	MT-07	MT-08	MT-09	MT-10	MT-11	MT-12	MT-13	MT-14	MT-15	MT-16	MT-17	MT-18	MT-19	MT-20	MT-21	MT-22	MT-56	MT-57	MT-58	MT-59
wt.%																					
SiO_2	57.71	53.44	55.80	55.66	56.46	57.64	57.64	56.80	57.79	59.57	55.01	56.14	57.07	57.42	59.59	57.02	55.02	63.27	58.53	55.84	56.61
TiO_2	0.72	0.81	0.62	0.61	0.55	0.75	0.64	0.65	0.60	0.55	0.77	0.62	0.71	0.63	0.63	0.65	0.69	0.63	0.74	0.65	0.67
Al_2O_3	18.62	17.59	18.28	17.93	17.84	17.64	19.24	17.88	16.30	17.08	17.56	16.91	17.00	17.62	18.52	17.77	17.15	16.47	17.89	17.74	17.11
Fe_2O_3	7.39	10.05	8.02	8.21	7.38	7.82	6.68	8.40	7.67	6.53	9.55	8.88	8.15	8.01	6.58	7.96	9.02	5.05	7.28	8.63	8.55
MnO	0.11	0.15	0.13	0.13	0.12	0.12	0.10	0.13	0.13	0.11	0.14	0.14	0.13	0.13	0.11	0.12	0.14	0.09	0.11	0.11	0.13
MgO	3.02	5.01	4.41	4.69	3.88	3.54	2.74	4.01	4.75	3.76	4.52	5.25	4.53	4.15	2.24	3.85	5.08	1.82	2.87	4.14	4.34
CaO	7.42	8.61	7.97	7.87	6.82	6.95	7.83	7.75	7.27	6.75	8.40	8.21	7.32	7.46	6.24	7.37	8.43	4.81	6.84	7.60	7.92
Na_2O	3.60	2.94	3.49	3.33	3.11	3.31	3.67	3.34	3.05	3.55	3.12	3.03	3.21	3.36	3.60	3.27	3.01	3.90	3.57	3.41	3.08
K_2O	1.10	0.85	0.75	0.74	0.85	1.38	1.07	0.95	1.38	1.23	0.92	0.73	1.18	1.07	1.53	1.12	0.89	2.24	1.38	0.80	1.05
P_2O_5	0.12	0.10	0.09	0.09	0.11	0.12	0.13	0.12	0.11	0.10	0.11	0.10	0.10	0.11	0.13	0.11	0.11	0.15	0.13	0.10	0.11
H_2O	0.25	0.33	0.33	0.33	0.53	0.32	0.21	0.17	0.25	0.32	0.14	0.12	0.20	0.12	0.18	0.36	0.16	0.39	0.21	0.59	0.23
LOI	-0.18	0.00	0.02	0.33	2.26	0.30	-0.06	-0.32	0.58	0.35	-0.36	-0.23	0.30	-0.20	0.56	0.33	0.20	1.07	0.36	0.29	0.10
Total	99.89	99.89	99.90	99.90	99.90	99.88	99.88	99.88	99.87	99.89	99.88	99.89	99.91	99.89	99.91	99.91	99.89	99.88	99.90	99.91	99.89
ppm																					
Ba	274	265	213	195	248	295	330	270	325	291	262	199	254	271	337	274	242	437	304	243	272
Rb	34	21	21	21	26	42	28	32	46	39	25	21	38	33	52	33	23	75	46	19	31
Sr	279	271	233	214	248	262	300	234	259	246	264	215	224	238	275	238	235	230	269	238	239
Pb	12	6	11	11	8	10	8	10	13	11	10	8	10	8	12	9	9	14	10	7	6
Th	5	3	2	2	1	4	0	11	5	6	5	3	1	4	4	4	0	4	5	0	2
Zr	87	62	58	59	76	96	76	72	86	86	66	59	85	77	110	76	67	146	103	65	83
Nb	5	3	3	3	3	4	4	3	3	4	3	3	5	3	5	4	4	6	5	2	4
Y	19	20	16	18	18	20	17	18	18	16	18	17	19	18	20	18	18	24	21	16	20
V	187	294	200	205	165	223	179	202	187	156	277	207	221	202	132	196	234	106	198	210	218
Cr	40	46	46	50	61	15	34	63	86	67	36	87	71	59	4	38	60	15	13	59	59
Ni	16	11	23	24	18	1	11	25	23	19	9	31	13	16	0	12	27	2	3	33	20
Cu	40	47	59	51	36	23	45	65	23	32	46	48	26	33	10	38	77	13	34	41	68
Zn	76	87	73	75	76	78	69	78	83	65	84	76	77	79	73	79	79	63	74	71	79
La	11	12	13	5	13	12	12	15	13	12	9	9	14	10	18	13	7	17	12	8	9
Ce	8	10	0	0	10	12	8	15	11	0	18	0	9	11	21	8	0	33	12	8	4

and has been dominantly controlled by incision into the softer Taihape Mudstone (Fig. 14C). In the Hihitahi region the proto-catchment was constrained by the surrounding Tertiary hill country, especially the Pliocene Snowgrass Dome, which forms a natural barrier towards the east and directed the Hautapu River southwards towards Mataroa and Taihape (Fig. 14).

Previous studies have concluded that the Hautapu River was cut off from the proximal Ruapehu ring plain due to movement on the Wahianoa Fault <27.1 ka BP ago, or movement on the Rangipo Fault >20 ka ago (Hodgson, 1993; Donoghue & Neall, 2001; Villamor & Berryman, 2006a; Villamor et al., 2007; Keigler et al., 2011). The Wahianoa Fault, however, displaces the southeast flank of Mt. Ruapehu with downthrow to the southeast of the proximal Ruapehu ring plain (Fig. 14) (Villamor & Berryman, 2006a). Thus volcaniclastic deposition in the Wahianoa Fault region is dominantly controlled by the angle of slope, and mass flows could have easily overrun and/or infilled any offset caused by fault displacement. Although we cannot exclude movement along the Rangipo Fault to be responsible, displacement due to this fault system was likely small (only <15 m since debris-avalanche emplacement) in the Hihitahi area. Thus, larger mass wasting events, as seen within the Mataroa Formation, would have easily overtopped the fault scarp.

There is no evidence for volcaniclastic deposition in the Hautapu catchment after 125 ka, thus we propose an alternative model for the geological evolution of the proto-Hautapu River. In this model, the proto-Hautapu catchment formerly ran from the southeastern Ruapehu ringplain through the town of Waiouru, towards Hihitahi (Fig. 14A). Volcaniclastic input into the proto-Hautapu River was limited to rare hyperconcentrated-flow deposits, likely emplaced in the proximity of the volcano, which were easily eroded and reworked into fluvial sequences further downstream. The failure of the southeastern flank of the southern Mt. Ruapehu generated the first major volcaniclastic sediment influx into the Hautapu and Whangaehu River catchments, and affected vast areas of the proximal Ruapehu ring plain (Fig. 14B). In the proto-Hautapu catchment it formed a short-term route for lahars formed during explosive eruptions of the decapitated volcano. However, soon after deposition of Facies 2 lahars, the Hautapu River was cut off from further volcaniclastic input from Mt. Ruapehu by incision of the Whangaehu River into the proximal ring plain, augmented by ongoing movement along the Karioi Fault (Fig. 14C). This area presently forms a natural depression hosting the Whangaehu River on the proximal Ruapehu ring plain. Subsequent faulting along the Shawcroft/Rangipo Fault intersection and deepening of the graben enclosing Mt. Ruapehu have made it unlikely that future lahars (apart from catastrophic flank failures) will enter the Hautapu catchment. Thus the catchment was beheaded and is now mostly fed by the wetlands south of Waiouru (Fig. 14C). Low sediment supply has led to deep incision of the Hautapu River into the Taihape Mudstone during warm climates, exceeding the deposition of alluvium during glacial periods. Simultaneous and constant uplift (c. 0.4 mm/a; Pulford & Stern, 2004) together with river incision, have resulted in elevation of the aggradational surfaces as terraces and thus an inverted stratigraphy, with the Mataroa Formation forming a distinct plateau at topographic elevations >690 m, well above the present river (Fig. 9C). No major faulting can be observed after volcanic debris-avalanche emplacement in the Mataroa area. The low-sediment supply and dominantly fluvial processes have not been energetic enough to remove large andesitic boulders from original areas of debris-avalanche deposition, hence these remain scattered on top of the aggradational terraces throughout the landscape from Hihitahi to Utiku.

3.3.4 Conclusions

Volcanic debris avalanches are a common feature of active stratovolcanoes and pose a great risk for populated areas. They also dramatically change the landscape upon which they are emplaced and lead to long-term changes in drainage systems in both proximal and distal areas (e.g., Procter et al., 2009). In this study we demonstrated how major debris avalanches may spill into new catchments previously unaffected by volcanism, creating new pathways for lahars and their deposits. In this case, because the volcaniclastic deposits were substantially more resistant to erosion than the rest of the catchment's geological substrate, an inverted topography was formed, so that the formerly infilled river valley is now located several hundred metres higher and several kilometres offset from the present channel.

Sedimentological and geomorphological features of the Mataroa Formation suggest three stages of volcanic impact and subsequent landscape response on the southeastern Ruapehu ring plain. (1) Partial collapse of the southeastern Wahianoa flank produced a voluminous debris avalanche that descended the slopes of the volcano between c. 125 - 150 ka. As this debris avalanche entered the Hautapu (and Whangaehu) catchment, confinement generated elevated pore pressures in the flowing mass, transforming it into a cohesive debris flow and promoting a long runout. A similar conclusion has been drawn for the Osceola Mudflow, which originated from a flank failure of water-saturated debris at Mt. Rainier, USA, and spilled into the White River catchment (Vallance & Scott, 1997). (2) The flank collapse likely caused rapid decompression of the magmatic system, triggering sub-plinian to plinian eruptions that produced vast amounts of pumice lapilli on the volcano's slopes. These were incorporated into lahars that mantled and infilled the irregular topography of the debris-avalanche deposit, forming a smooth, broad braided aggradational surface. (3) After this pulse of rapid sedimentary accumulation within the Hautapu River catchment, the drainage system was completely cut off from the proximal Ruapehu ring plain and starved of sediment supply, which caused rapid down cutting of the river at the eastern margins of volcaniclastic deposits, primarily within the Pliocene mudstones. This was accompanied by constant uplift and the climatic-induced aggradation-degradation cycles, producing a terraced landscape.

This study shows that river catchments long distances from active volcanoes can be affected by major geomorphological changes caused by large-scale flank failures and debris avalanches. Infilling and damming of river catchments by volcaniclastic deposits affects the inundated landscape for thousands of years and can result in complete truncation of drainage systems from their original sources. Subsequently these landscapes can be influenced by other geological activity (e.g., faulting, erosion). In the case of Mt. Ruapehu, one of its most voluminous volcanic debris avalanches known completely changed the landscape by armouring it and thus protecting it from erosion associated with uplift and cyclic climate-change induced aggradational terrace formation. The longer-term post-event hydrogeological consequences of major debris avalanches need to be considered for comprehensive hazard evaluations from mountain-building volcanoes worldwide.

3.3.5 Acknowledgements

Manuela Tost is supported by a Massey University Doctoral Scholarship, and we all gratefully acknowledge support from the New Zealand Natural Hazards Research Platform project "Living

with Volcanic Risk". We thank the local land owners of the Mataroa area, in particular Jeff Williams, for access to the reference sites. We would also like to thank Jon Wilmshurst for running the XRF-analyses, Dr Pilar Villamor for useful discussions regarding the tectonics of this area, and Dr Lucia Capra and Dr Vern Manville for helpful revisions of the original manuscript.

CHAPTER 4: GEOMORPHOLOGICAL CONTROLLED RUNOUT OF LARGE-SCALED MASS WASTING EVENTS AT MOUNT RUAPEHU, NEW ZEALAND

4.1 Introduction

Failures of steep volcanic flanks are among the most hazardous processes known. They can produce debris-avalanche deposits that almost instantaneously change the landscape upon which they are emplaced by valley infilling, fan creation, surface hummock formation, damming and diversion of rivers and subsequent high sediment loads into impacted catchments (Voight et al., 1981; Crandell et al., 1984; Procter et al., 2009). Deposits of four partial edifice failures have been recognized at Mt. Ruapehu. These are the basal facies of the Mataroa Formation (c. 125 ka, 2.0 - 3.0 km^3; Tost et al., 2015), the Lower Whangaehu Formation (120 - 180 ka, 0.7 - 1.2 km^3; Keigler et al., 2011), the Murimotu Formation (9.5 ka, 0.2 km^3; Palmer & Neall, 1989), and the Mangaio Formation (4.6 ka, 0.034 km^3; Donoghue & Neall, 2001). While the Murimotu and the Mangaio Formations form fans on the proximal Ruapehu ring plain, the larger Mataroa and Lower Whangaehu Formations flowed farther into the deep catchments of the Hautapu and Whangaehu Rivers and were emplaced up to 60 km from source (Keigler et al., 2011; Tost et al., 2015).

This chapter is based on an article by Tost et al. (2014), published in Bulletin of Volcanology, in which another four debris-avalanche deposits are identified and described on the western distal ring plain of Mt. Ruapehu. These deposits were generated by major flank failures on the volcano and they occur within the Oreore (Mangawhero River), Pukekaha (Manganuioteao River) and Piriaka Formations (Whakapapa and Whanganui River). Their sedimentological characteristics are strikingly similar to the Mataroa and Lower Whangaehu Formations and suggest that large-scale (>1 km^3) collapse events of Mt. Ruapehu commonly result in debris-avalanche confinement within the catchments of major river systems. It is important to recognize the transport and emplacement mechanisms controlling these channelized long-runout mass-wasting events in order to improve the future volcanic hazard assessment of Mt. Ruapehu and prepare for recovery in case of future large-scale flank failures of the stratovolcano.

4.2 Contributions of co-authors

“Transport and emplacement mechanisms of channelized long-runout debris avalanches, Ruapehu volcano, New Zealand”

Bulletin of Volcanology, 76(12), 1-14.

M. Tost: Principal Investigator
Carried out: Field studies
Manuscript preparation and writing

S. J. Cronin: Co-Investigator
Carried out: Field assistance
Discussion of results
Editing and discussion of the manuscript

J. N. Procter: Advisor
Carried out: Aided the study by editing the manuscript

4.3 Transport and emplacement mechanisms of channelized long-runout debris avalanches, Ruapehu volcano, New Zealand

M.Tost, S.J. Cronin, J.N. Procter

Volcanic Risk Solutions, Massey University, Palmerston North, New Zealand

Abstract

The steep flanks of composite volcanoes are prone to collapse, producing debris avalanches that completely reshape the landscape. This study describes new insights into the runout of large debris avalanches enhanced by topography, using the example of six debris-avalanche deposits from Mt. Ruapehu, New Zealand. Individual large flank collapses (>1 km^3) produced all of these units, with four not previously recognised. Five major valleys within the highly dissected landscape surrounding Mt. Ruapehu channelled the debris avalanches into deep gorges (≥15 m), and resulted in extremely long debris-avalanche runouts of up to 80 km from source. Classical sedimentary features of debris-avalanche deposits preserved in these units include: very poor sorting with a clay-sand matrix hosting large subrounded boulders up to 5 m in diameter, jig-saw fractured clasts, deformed clasts, and numerous rip-up clasts of late-Pliocene marine sediments. The unusually long runouts led to unique features in distal deposits, including a pervasive and consolidated interclast matrix, and common rip-up clasts of Tertiary mudstone, as well as fluvial gravels and boulders. The great travel distances can be explained by the debris avalanches entering deep confined channels (≥15 m), where friction was minimised by a reduced basal contact area along with loading of water-saturated substrates which formed a basal lubrication zone for the overlying flowing mass. Extremely long-runout debris avalanches are most likely to occur in settings where initially partly saturated collapsing masses move down deep valleys and become thoroughly liquified at their base. This happens when pore water is available within the base of the flowing mass, or in the sediments immediately below it. Based on their H/L ratio, confined volcanic debris avalanches are 2 - 3 times longer than unconfined, spreading flows of similar volume. The hybrid qualities of the deposits, which have some similarities to those of debris flows, are important to recognise when evaluating mass-flow hazards at stratovolcanoes.

4.3.1 Introduction

Flank failure of composite cones (stratovolcanoes) may produce large (>10^7 m^3) sliding and granular landslides, known as debris avalanches. Debris avalanches are among the most hazardous phenomena known from stratovolcanoes, and they almost instantaneously affect edifice configuration, reshape river drainages, and form hummocky topographies (Voight et al., 1981; Crandell et al., 1984; Procter et al., 2009). Many debris avalanches travel much farther than simple friction laws would suggest (e.g., Scheidegger, 1973), but observations of their motion are rare, and thus there is no single accepted theory for their behaviour (e.g. Kent, 1966; Davies, 1982; Sassa, 1988; Campbell, 1989; van Gassen & Cruden, 1989; Davies et al., 1999; Legros, 2002; Collins & Melosh, 2003; Hungr & Evans, 2004; Davies & McSaveney, 2012; Iverson, 2012). No single mechanism has unequivocally been shown to explain how debris avalanches achieve the very long runouts seen from the geologic record. Here we examine

cases where the pre-existing topography, especially channel confinement, and the entrainment of water and saturated sediment along the flow path may have enhanced debris avalanche travel distance.

The two largest stratovolcanoes in humid-temperate New Zealand, Ruapehu (2,797 m) and Taranaki (2,518 m) have both collapsed frequently. Taranaki produced at least 12 debris avalanches of 0.5 km^3 to 7 km^3 during the last 130,000 years, forming a surrounding debris fan (ring plain) (e.g., Zernack et al., 2012). Mt. Ruapehu has also produced several large debris avalanches (e.g., Palmer & Neall, 1989; Keigler et al., 2011; Tost et al., 2015), but rather than spreading around the volcano, they flowed beyond the volcaniclastic ring plain (e.g., Hodgson, 1993; Cronin et al., 1997a) and into deeply incised valleys radiating from it (Fig. 15). Mt. Ruapehu is situated at the southern end of the subduction-related Taupo Volcanic Zone (Nairn & Beanland, 1989; Acocella et al., 2002). To the south the volcano abuts the Miocene-

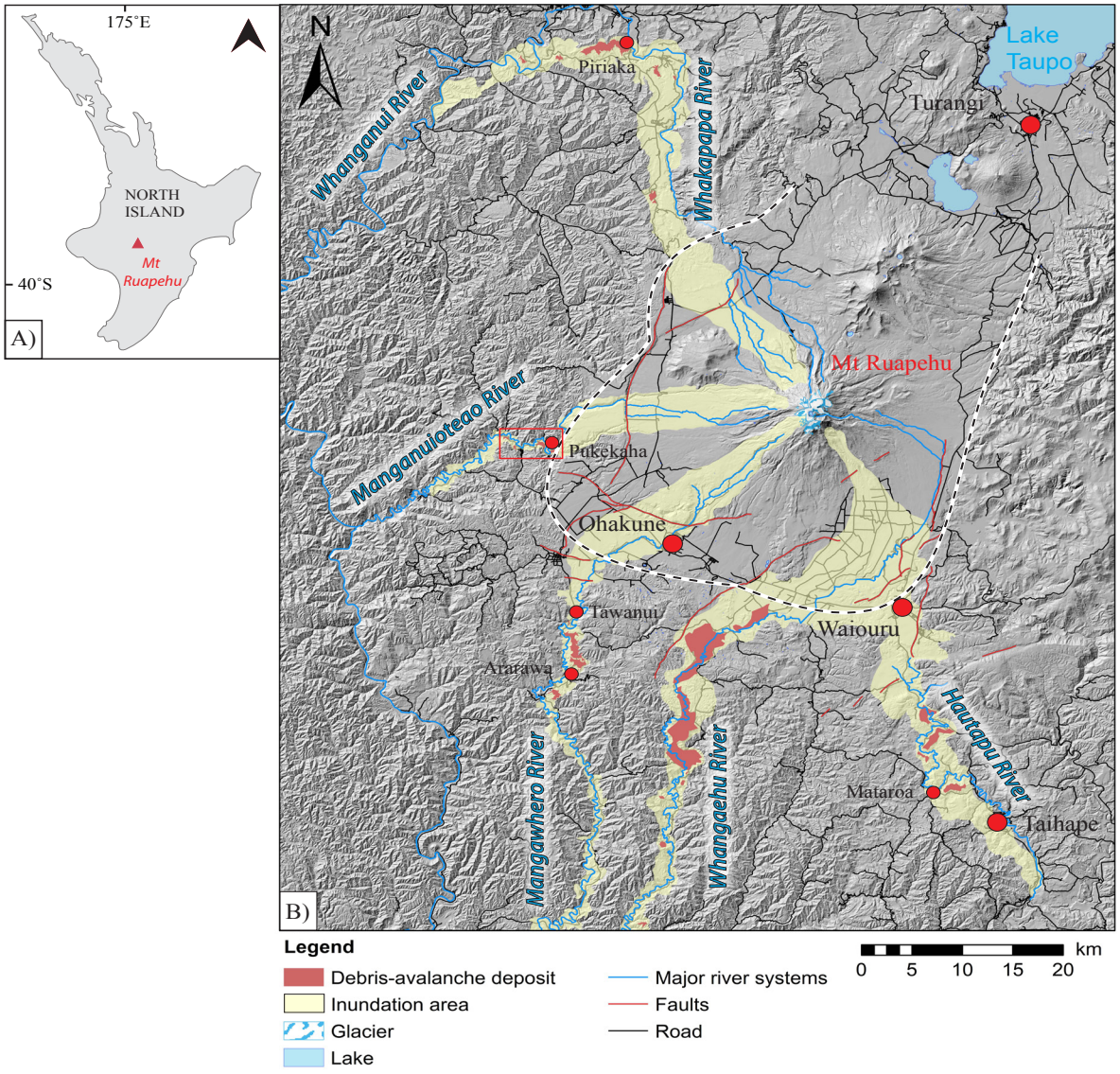

Figure 15. (A) Outline of New Zealand's North Island with Mt. Ruapehu located near its centre. (B) Digital elevation model of the proximal and distal Ruapehu ring plain. Note the difference in geomorphology where an aggradation-dominated landscape changes into an erosive one (dashed line). Six debris-avalanche deposits crop out along five major river catchments that drain the stratovolcano. Basal outcrops of debris-avalanche deposits are limited to the landscape adjacent to the drainage systems and distances >30 km. Scattered andesitic boulders >1.5 m in diameter scattered around the countryside indicate the extent of flow inundation.

Quaternary South Wanganui Basin, made up of marine sedimentary sequences, which are currently being uplifted and dissected by numerous faults (Kamp et al., 2004; Pulford & Stern, 2004; Villamor & Berryman, 2006). The geology and climate has produced a topography that provides an ideal setting in which to examine the influence of channelization and interstitial fluids on debris-avalanche runout and the sedimentary properties of the deposits. Many sedimentological studies of debris-avalanche deposits (Siebert, 1984; Francis et al., 1985; Ui et al., 1986; Glicken, 1991; Palmer et al., 1991; Procter et al., 2009; Roverato et al., 2011; Zernack et al., 2012) have focused on unconfined/spreading volcanic debris avalanches, which form fans and characteristic hummocky landscapes. The few examples of confined/channelised debris avalanches studied show above-average runout lengths (e.g., Stoopes & Sheridan, 1992; Takarada et al., 1999), and properties that are similar to clay-rich debris flows generated from flank collapses of hydrothermally altered edifices (e.g., Vallance & Scott, 1997).

This study describes, for the first time, the sedimentary properties of four of the six largest debris-avalanche deposits known from Mt. Ruapehu. These units are used to derive insights into debris avalanches in humid environments and their transport and emplacement onto dissected fluvial landscapes. We evaluate future volcanic hazards and interpret landscape change following large-scale debris-avalanche inundation.

4.3.1.1 Geological Setting

Mt. Ruapehu is a c. 300,000-year old andesitic stratovolcano, sited within an active graben (Hackett & Houghton, 1989; Gamble et al., 2003; Villamor & Berryman, 2006). Permanent glaciers partially cover the composite cone and the acidic Crater Lake occupies its active crater, resulting in many syn- and post-eruptive lahars (Cronin et al., 1997b; Lube et al., 2012). The stratovolcano comprises variably dipping lava flow sequences, autoclastic breccias, and pyroclastic, epiclastic, and glacial/moraine deposits (Hackett & Houghton, 1989; Smith et al., 1999). A large ring plain, made up of stacked laharic, fluvial, and tephra deposits surrounds the stratovolcano (Cronin et al., 1997a; Lecointre et al., 1998). Previous workers identified five flank-collapse debris-avalanche events caused by hydrothermal alteration accompanied by substrate weakening (Palmer & Neall, 1989; Hodgson, 1993; Lecointre et al., 1998; Donoghue & Neall, 2001; Keigler et al., 2011; Tost et al., 2015). In addition, four newly discovered deposits related to hitherto unknown collapse events are described here. The latter are exposed along five major river catchments, radiating from the distal Ruapehu ring plain (Fig. 15). Four of the five drainage systems currently originate from the upper flanks of Mt. Ruapehu. The Hautapu River, on the other hand, presently originates from native grasslands and wetlands southwest of Waiouru (Rogers, 1993), as a result of landscape modification and stream-capture following the Mataroa debris avalanche (Tost et al., 2015). Exposures along the river catchments show that the debris-avalanche deposits overlie Pliocene-Pleistocene marine mudstones, sandstones and rare limestones (Naish & Kamp, 1997; Kamp et al., 2004; Keigler et al., 2011).

4.3.2 Results

4.3.2.1 Deposits of long-runout Ruapehu debris avalanches

Deposits of six individual long-runout mass flows from Ruapehu volcano were studied on the distal Ruapehu ring plain, primarily in locations >35 km from source. Four of them have not been

identified before, whereas the Whangaehu and Mataroa Formation were previously described (Hodgson, 1993; Keigler et al., 2011; Tost et al., 2015). The ongoing uplift of the area, associated with incision of the river systems into the underlying soft late-Pliocene marine mud- and sandstones means that the debris-avalanche deposits outcrop at the highest elevated margins of the valleys. Scattered, reworked large andesitic boulders 2.5 to 5 m in diameter occur along the younger surfaces of the catchments up to 80 km from source. These stranded boulders, too large to move in normal fluvial processes, are the only relics of debris-avalanche deposits that have been eroded (along with underlying mudstones) from the central parts of the growing valleys (Fig. 16) (Tost et al., 2015). Previous studies have described confined long-runout debris-avalanche deposits along the Hautapu and Whangaehu Rivers (Fig. 15) (Park, 1910; Te Punga, 1952; Hodgson, 1993, Keigler et al., 2011; Tost et al., 2015). New mapping has revealed four similar deposits along the Mangawhero, Manganuioteao, and Whanganui Rivers. The sedimentary character of these debris-avalanche deposits is similar, comprising landslide features such as matrix-supported, jig-saw fractured clasts, and megaclasts, as well as unusual features, including subrounded boulders and eroded/entrained river gravels (Fig. 17; Table 4). The debris avalanches were emplaced between 70,000 and 200,000 years ago, most likely during the shift from a glacial to an interglacial climate. The approximate ages are obtained from coverbed sequences overlying the individual formations, their position in the glacio-fluvial terraced landscape (Table 5), and the geochemical correlation of clasts to cone-building formations on the volcano (Tost et al., 2015).

Mataroa Formation (Tost et al., 2015)

Over 11 m of the Mataroa Formation deposit unconformably overlies late-Tertiary Taihape Mudstone in the Mataroa area southeast of Mt. Ruapehu and forms an undulating plateau (Fig. 15; 16). The deposit is massive, poorly sorted, and contains c. 50 - 60 vol.% of pebble to boulder-sized clasts, reaching over 2 m in diameter, supported in a consolidated matrix (25 - 35 vol.% <0.6 mm) (Fig. 17C). The well- to subrounded and in part jig-saw fractured clasts are composed of 80 - 90 vol.% andesite lava, 10 - 15 vol.% Taihape Mudstone, and

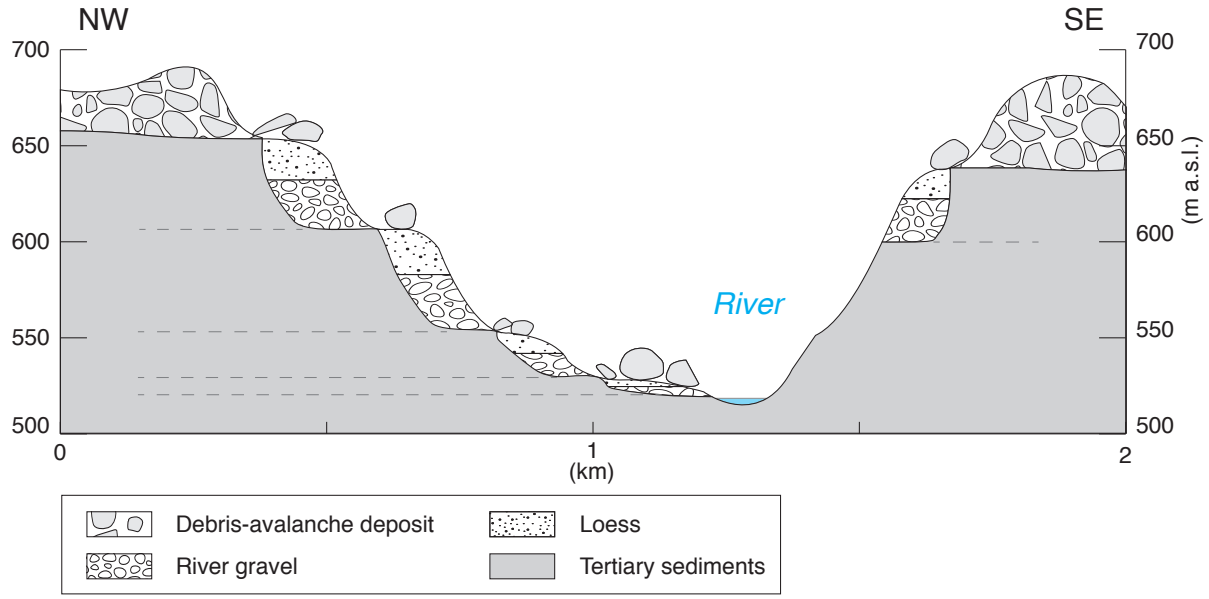

Figure 16. The Ruapehu debris avalanches form a distinctive high terrace in valleys of each river catchment due to uplift and river incision. Glacial and interglacial periods have resulted in the formation of river terraces on which reworked andesitic boulders related to the collapse events were emplaced. Modified after Tost et al., 2015.

Table 4. Major depositional characteristics of unconfined and channelized volcanic debris avalanches.

Lithological features	**Unconfined subaerial volcanic landslides**	**Confined subaerial volcanic landslides**
Hummock formation	A hummocky morphology with longitudinal and transverse ridges is common (Glicken, 1982).	Hummocks occur but can be less prominent.
Megaclasts	Megaclasts are common and usually exposed as exotic breccia-blocks within hummocks; the maximum clast-size decreases with distance from source (Siebert 1984).	Megaclasts occur either as exotic blocks, or as strongly deformed and sheared areas of exotic material; megaclast-size decreases with distance from source.
Jig-saw fractures	Common as fragments of boulders and megablocks of the former cone (Ui, 1983).	Common as fragments of boulders and megaclasts of entrained path material or breccia sourced from the former cone. Frequently, the individual fragments are spread apart within the intra-block matrix.
Matrix	The deposits usually contain a vast amount of crushed rock fragments (matrix) in sharp contact with blocks and/or megaclasts of either similar or differing composition (Coates, 1977).	The matrix is made up of crushed rock fragments which are in sharp contact with blocks and/or megaclasts of similar or differing composition. The matrix/clast-ratio can be comparatively low.
Clast-assemblage	The clast assemblage is dominated by a hetero-lithologic mixture of locally homogeneous units, including undisturbed massive segments of the former cone (e.g., Mimura et al., 1982).	The clast assemblage is dominated by a chaotic mixture of locally homogeneous units made up of megaclasts of entrained path material. Larger clasts (>1 m in diameter) sourced from the former cone area are generally subrounded.
Path material	Path material is dominantly entrained at the base, or at the front as the flows descend steep slopes; additional minor entrainment occurs at the margins; the material entrained reflects the lithology of the overridden bed and can comprise e.g., glacial till, alluvium, or residual soil (e.g., McDougall and Hungr, 2005).	Path material is entrained at the front as the landslide descends steep slopes, but dominantly occurs at the base and the margins of the flows as soon as confinement occurs. Additional loading due to bank failures is common at the flow/catchment interface. Sediments deposited via fluvial processes within the valleys/ catchments form the majority of the entrained path material.
Shearing	Shearing occurs but plays a secondary role in respect to “brittle”-rock fracturing. Megablocks generally show rotation in a horizontal but not a vertical plane (e.g., Mimura et al., 1982).	Shearing is extremely distinctive at the base and the margins of the flows. Depending on the fluidization-state of the landslide, shearing and rotation of megaclasts occurs in a horizontal as well as in a vertical plane. Towards the top fluidization and thus shearing decreases and “brittle”-rock fracturing becomes more prominent.

<5 vol.% Mesozoic greywacke gravel. Angular rip-up clasts of Taihape Mudstone over 5 m long occur in the lower half of the deposit and are in places contorted and sheared (Fig. 18A). Additionally, large-scale lithofacies of deformed and sheared patches of Recent river gravel and hyperconcentrated-flow deposits also occur out of stratigraphic context within the lower half of the deposit (Fig. 18A). Fractures are common throughout the entire deposit but are most prominent in the lower region that includes entrained substrate. This facies is interpreted to represent deposition from the basal, highly sheared parts of a distal debris-avalanche deposit.
The extent of the Mataroa Formation is >256 km^2, with the runout exceeding 60 km. Its estimated thickness indicates an approximate volume of 2.9 km^3. Geological mapping and dating of the oldest cone-building lavas exposed on the uppermost slopes of Mt. Ruapehu (Hackett and Houghton, 1989; Gamble et al., 2003) indicate that it was always at least of similar height to the present day. Thus, the H/L ratio of the Mataroa Formation is 0.03 (Fig. 15; Appendix I).

Lower Whangaehu Formation

Hodgson (1993) and Keigler et al. (2011) described the Lower Whangaehu Formation as a <18-m-thick, clast- to matrix-supported, boulder-rich, poorly sorted, and massive diamicton. It unconformably overlies Tertiary sand- and mudstone and is exposed within the steep walls of the Whangaehu valley and locally forms hummocks (Fig. 15). The Lower Whangaehu Formation is a megaclast-rich breccia in the proximal and marginal regions, but transforms downstream into ungraded beds of subrounded boulders, pebbles and cobbles (Keigler et al., 2011). Overbank facies differ from axial ones by the presence of megaclast breccias stacked up into ramp-like structures (Keigler et al., 2011). The main distal exposures of the Lower Whangaehu Formation include subrounded andesitic boulders ≤1.5 m in diameter that are embedded in a poorly sorted, consolidated, matrix-supported (35 - 50 vol.%; <0.6 mm) framework (Fig. 17D). Common ripped-up and deformed clasts of Tertiary mud- and sandstone as well as deformed and sheared domains of Quaternary river gravel and hyperconcentrated-flow sediments are especially apparent within the basal parts of the deposit. Pebble to boulder-sized clasts are commonly well to moderately rounded and composed of 80 - 90 vol.% andesite lava, 10 - 15 vol.% Tertiary mudstone, 3 vol.% hydrothermally altered clasts, and <2 vol.% Mesozoic greywacke gravel. Distinctive jig-saw jointing is present, with clasts either still held together or spread slightly within the matrix, and generally increases towards the base of the deposit (Keigler et al., 2011). Fractures occur throughout the deposit but are generally most prominent at interfaces of differing lithofacies (Fig. 17). The Lower Whangaehu Formation has an approximate runout of >60 km, a volume of c. 2.4 km^3, an H/L ratio of 0.04, and inundated an area of >120 km^2 (Fig. 15; Appendix I).

Oreore Formation

The basal facies of the Oreore Formation forms a distinct plateau with undulating topography between Tawanui and Ararawa (Fig. 15) and is exposed in numerous road cuts. The massive diamicton deposit is very poorly sorted and contains c. 60 - 65 vol.% angular to well-rounded clasts, with rounding generally increasing downstream. Clasts comprise 70 - 75 vol.% andesitic lava, pebble- through to boulder-sized, reaching up to 3 m in diameter, along with 10 - 15 vol.% pumice ≤0.3 m in diameter. Exotic clasts include c. 5 - 10 vol.% Tertiary mud- and sandstone rip-up clasts up to 1 m in diameter, c. 5 - 8 vol.% hydrothermally altered clasts ≤0.5 m in diameter, and 1 - 2 vol.% Mesozoic greywacke gravel. In addition, this unit contains jigsaw-fractured andesitic clasts including re-deposited bombs and cooling-fractured andesitic lava blocks. The

Table 5. Approximate depositional ages of the Ruapehu debris avalanches in relation to the four cone-building formations identified and mapped on the edifice by Hackett and Houghton (1989).

Debris-avalanche deposits	Cone-building formations
Mangaio Formation (4.6 ka)* Murimotu Formation (9.5 ka)**	Whakapapa Formation (<15 ka)***
	Mangawhero Formation (15 - 55 ka)***
Pukekaha Formation (c. 80 - 90 ka)	
Piriaka Formation (A & B) Mataroa Formation Lower Whangaehu Formation	Wahianoa Formation (119 - 160 ka)***
Oreore Formation	Te Herenga Formation (180 - 250 ka)***

*after Donoghue and Neall, 2001 **after Palmer and Neall, 1989
***after Gamble et al., 2003

consolidated sand-dominated matrix makes up c. 35 - 40 vol.% of the deposit. Fining-upwards, dish-like structures occur within the matrix, below andesitic boulders >1 m in diameter (Fig. 19E). Contorted and sheared domains of pre-existing sandy-pebbly planar-bedded volcaniclastic deposits (>8 m in length) and Quaternary river gravel also occur sporadically throughout the unit (Fig. 18D). In places the deposit laterally abuts <0.5 m thick channel-form deposits of cross-laminated fluvial sands, which represent post-depositional marginal re-mobilisation and reworking. Fractures appear within clasts throughout the deposit, but are generally more common in the areas around domains of contrasting lithofacies (Fig. 18). The Oreore Formation debris avalanche has an approximate runout of >80 km, a volume of c. 3 km^3, an H/L ratio of 0.03, and inundated an area of >200 km^2 (Fig. 15; Appendix I).

Pukekaha Formation

Outcrops of a coarse diamicton within the Pukekaha Formation are located around Pukekaha Road (Fig. 15). The massive diamicton deposit is poorly sorted and contains angular to well rounded pebble- to boulder-sized clasts of andesitic lava (50 - 60 vol.%, <2.5 m), c. 20 vol.% dense pumice <5 cm in diameter, c. 10 vol.% sintered claystone, and <5 vol.% hydrothermally altered clasts. The angular to well-rounded clasts are supported by a consolidated silty-sand matrix of fragmented pumice (c. 30 - 40 vol.%). Jigsaw-fractured clasts are common, with individual fragments separated by the intra-clast matrix. Subrounded andesitic lava boulders show distinctive cooling joints (Fig. 18C). The deposit abuts Tertiary sandstone, and deformed, sheared lithofacies of Recent river gravel and hyperconcentrated-flow deposits occur in the lower half of the unit (Fig. 18C). Fractures are common in clasts throughout the facies, but are most common in the lower regions of the deposit. The Pukekaha Formation debris avalanche has an approximate runout of >50 km, a volume of c. 1.56 km^3, an H/L ratio of 0.04, and inundated an area of >120 km^2 (Fig. 15; Appendix I).

Piriaka Formation

Major outcrops of two separate debris-avalanche deposits, lower Piriaka-A and an upper Piriaka-B, are exposed within a volcaniclastic sequence at road cuts in the Piriaka region (Fig. 15) and form a distinct plateau alongside the Whakapapa River (Fig. 18C). Both diamictons are unbedded and poorly sorted with angular to subrounded clasts supported by a firmly consolidated matrix. The silt to fine-sand matrix of the lower >2.5-m-thick Piriaka-A diamicton makes up 30 - 50 vol.%

of the deposit and is cemented by secondary calcite. The clasts comprise 85 - 90 vol.% andesitic lava pebbles and boulders (<1.5 m in diameter), 10 - 15 vol.% hydrothermally altered andesitic clasts, <1 vol.% pumice, and <1 vol.% Tertiary mudstone. Several clasts show distinctive jigsaw-fractures, with some fragments slightly separated and infilled by the inter-block matrix. The Piriaka-A debris-avalanche deposit has an approximate volume of 1.35 km^3, an H/L ratio of 0.03, and inundated an area of >225 km^2 (Fig. 15; Appendix I). The upper >5-m-thick Piriaka-B diamicton is very coarse grained with common large boulder-sized clasts between 1 and 4 m in diameter (40 - 50 vol.%), supported by a consolidated fine sand matrix (making up 50 - 60 ol.%), which is cemented by secondary calcite (Fig. 17A). The clast assemblage is mainly andesite lava (>95 vol.%), accompanied by <5 vol.% Tertiary mud- and sandstone rip-up clasts. The

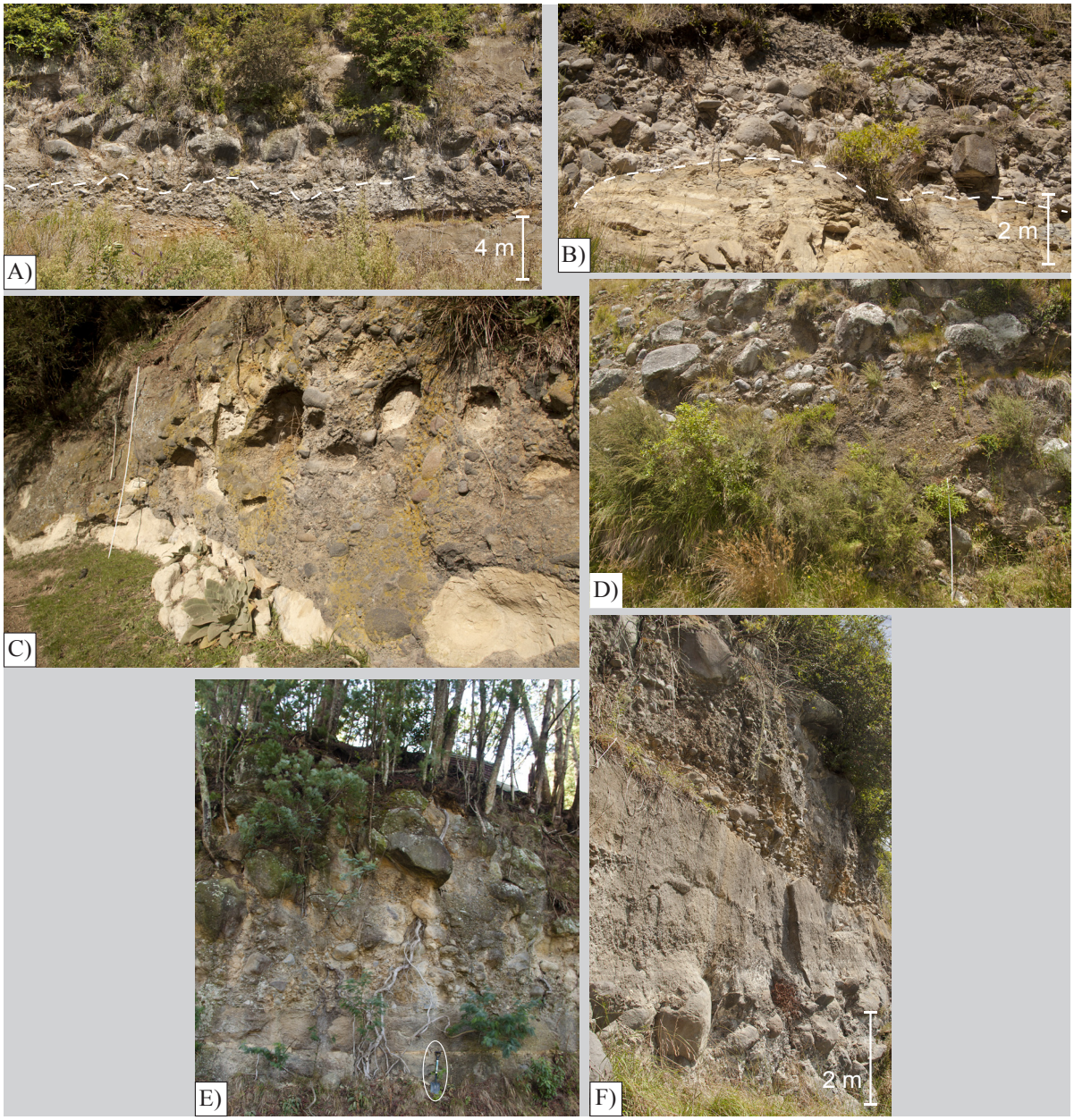

Figure 17. Six individual debris-avalanche deposits were identified on the distal Ruapehu ring plain and show strikingly similar sedimentological characteristics. (A) The Piriaka-B debris avalanche is inversely graded and unconformably overlies Quaternary river gravel. (B) The basal facies of the Oreore Formation is made up of a debris avalanche deposit unconformably overlying late-Pliocene mudstone. (C) The basal facies of the Mataroa Formation (Scale: 2 m), (D) The Lower Whangaehu Formation (Scale: 2 m), (E) The debris-avalanche deposit exposed within the Pukekaha Formation, and (F) The Piriaka-A debris-avalanche deposit.

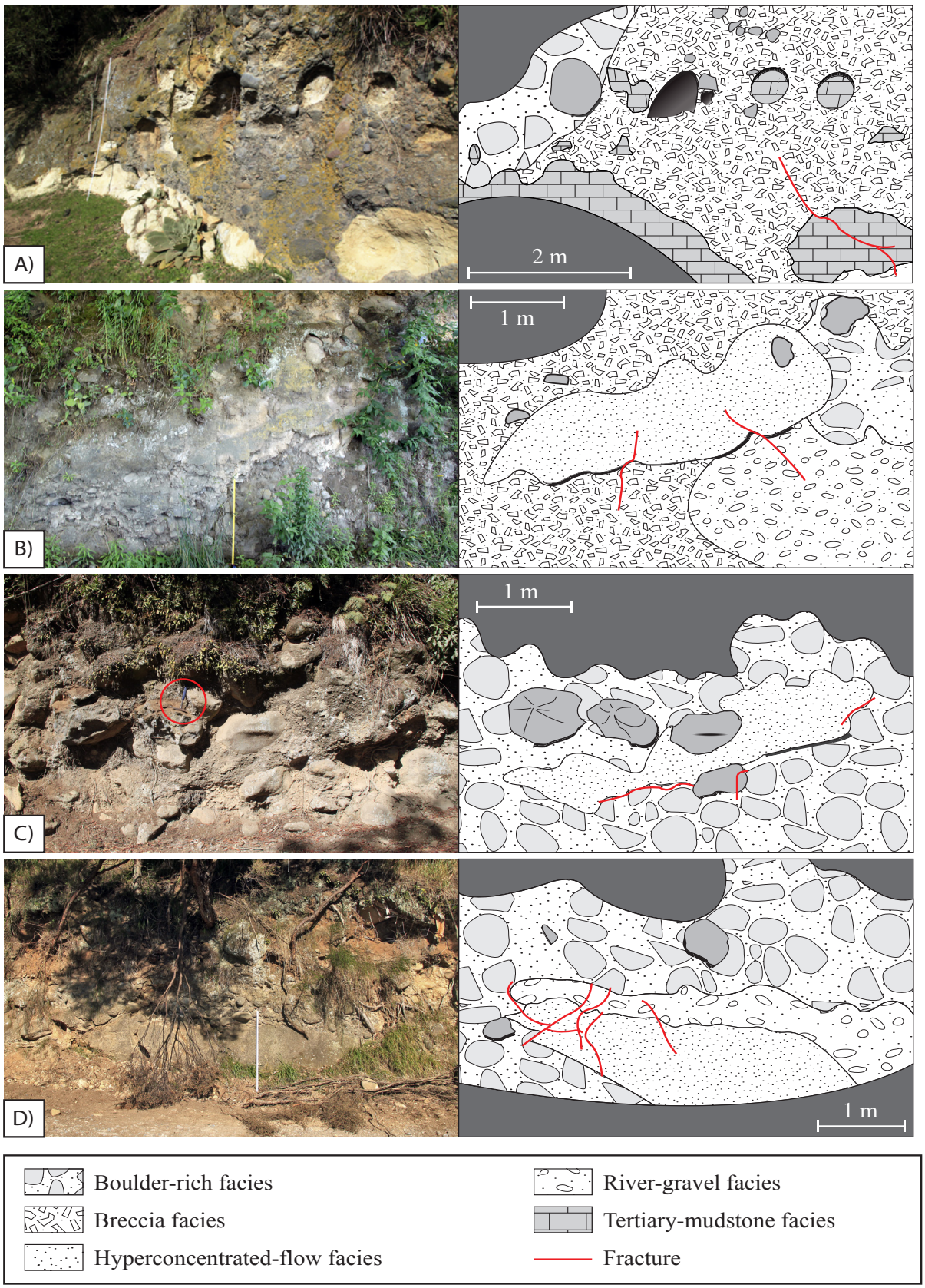

Figure 18. Textural features of the Ruapehu debris avalanches. The deposits are hetero-lithologic and comprise various amounts of incorporated path material, such as (A) Tertiary marine sediments; (B), (D) River gravel; and (B), (C), (D) Hyperconcentrated-flow deposits. Fractures, probably due to increased shear stresses, are common within the exposures, especially at interfaces of differing lithofacies. Highlighted clasts within the sketches serve as orientation-points.

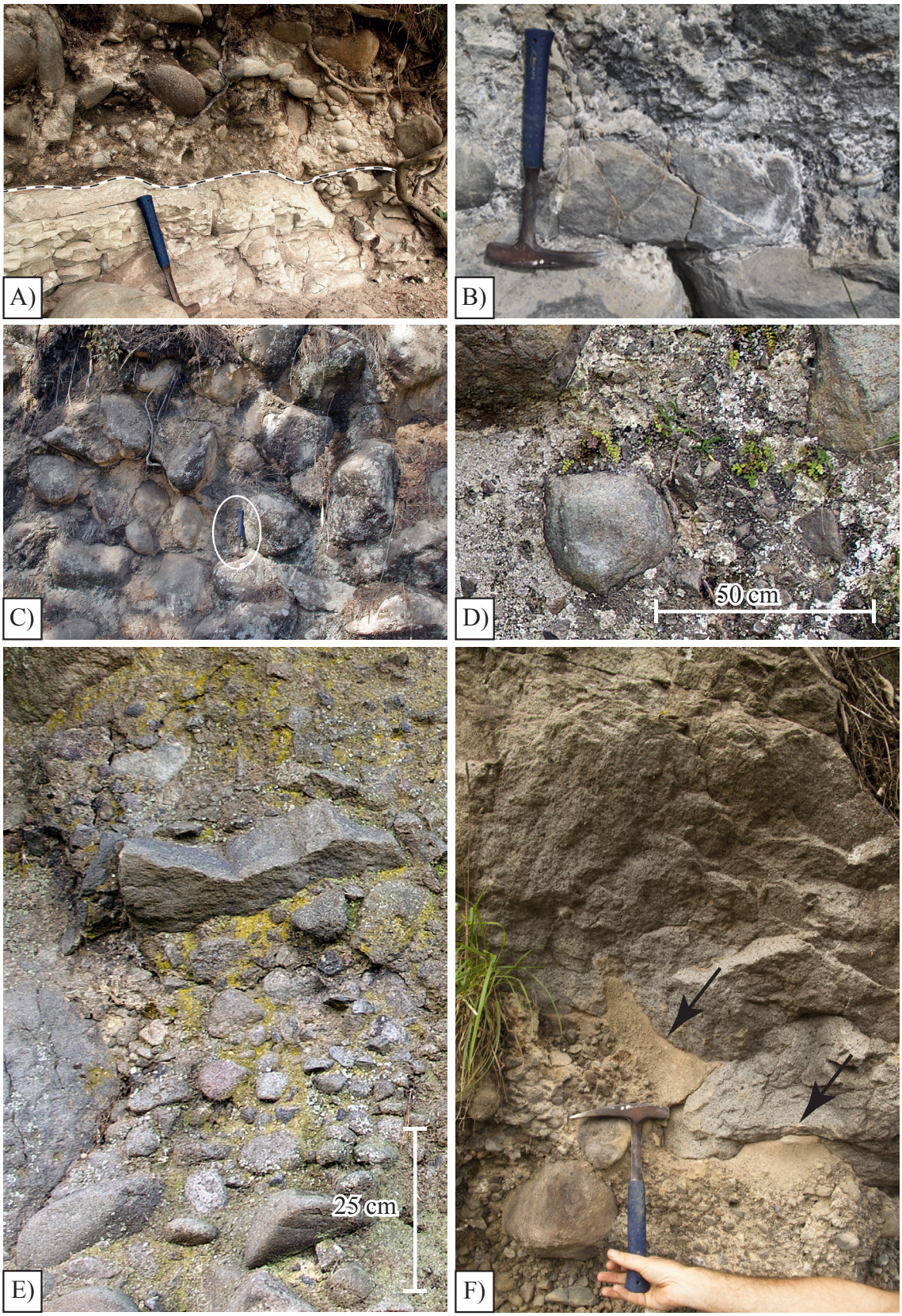

Figure 19. Lithological features of the Ruapehu debris-avalanche deposits. (A) The flows overran and incorporated various amounts of path material including river gravel and late-Pliocene mudstones and muddy sandstones. (B) Fractured clasts are generally not common but present within all grain sizes. (C) Larger boulders within the Ruapehu debris-avalanche deposits are generally subrounded. (D), (E) The intra-block matrix is consolidated and generally consists of the fine-sand to silt. (F) Dish-like structures (arrows) exposed within the basal facies of the Oreore Formation.

deposit shows inverse grading, with boulders exceeding 2 m in diameter limited to the upper half of the unit. The diamicton has an irregular basal contact onto river gravels, which are also ripped up and incorporated into the lower portion of the deposit. Fractures within the clasts can be observed throughout the facies, but are more frequent around domains of differing lithofacies. The Piriaka-B debris-avalanche deposit has an approximate volume of 1.4 km^3, an H/L ratio of 0.03, and inundated an area of >260 km^2 (Fig. 15; Appendix I).

4.3.2.2 Debris-avalanche runout and mobility

We compiled data from subaerial volcanic landslides (confined and unconfined), non-volcanic landslides, submarine landslides, block-and-ash flows, and pumice flows, in order to form a basis for comparison to the confined Ruapehu debris avalanches (Fig. 20; Appendix I). As has been noted in previous studies, the total runout of landslides in all environments is proportional to their volume (e.g., Voight, 1978; Crandell et al., 1984; Stoopes & Sheridan, 1992; Dade & Huppert, 1998; Davies & McSaveney, 1999; Collins & Melosh, 2003). The mass of a landslide strongly affects its i) inundation area, ii) mean flow depth, iii) mean basal shear stress, and iv) mobility (Pudasaini & Miller, 2013). In general, debris avalanches show a positive correlation between the approximate landslide volume and mapped inundation area (Fig. 20B). This relationship has been previously interpreted to reflect a constant shear stress that limits the overall runout of such flows (Dade & Huppert, 1998; Kelfoun & Druitt, 2005). Most volcanic debris avalanches (unconfined and confined), including the Ruapehu events, show high mobilities (i.e., high area/volume), which are equivalent to pumice flows and the most mobile block-and-ash flows (Fig. 20A). Using a common descriptor of flow mobility introduced by Dade and Huppert (1998), the $A/V^{2/3}$ ratio (A = area of deposition; V = volume of deposit), there is no significant difference between unconfined and confined debris avalanches. This ratio is highly suited to examining spreading, fan-like flows, but it does not distinguish narrow flows that may have extremely long runouts. Likewise, no significant difference can be observed between unconfined and channelized subaerial volcanic landslides in respect to their area and volume (Fig. 20B).

It has been widely observed that there is a correlation between landslide volume and the corresponding net efficiency (L/H; where L = runout length and H = drop height), as well as its inverse quantity, the apparent coefficient of friction (H/L) (e.g., Hayashi & Self, 1992; Davies & McSaveney, 1999; Legros, 2002). The Ruapehu debris avalanches have comparatively low H/L ratios at given volumes with respect to non-volcanic, and unconfined subaerial landslides (Fig. 20C). This is also true for other known channelized/confined subaerial volcanic landslides. The comparatively lower apparent coefficients of friction for channelized subaerial volcanic landslides follow the same trend as that for non-volcanic and unconfined subaerial volcanic landslides. Others have suggested that the H/L ratio decreases with availability of water or clay (Vallance & Scott, 1997; Legros, 2002; Pudasaini & Miller, 2013). Hence, submarine landslides reflect the lowest apparent coefficients of friction in respect to their volume (although large scatter obscures a clear trend) (Fig. 20C).

Some studies argue that the coefficient of friction is better represented by the runout and drop height of the centre of mass, which considers spreading of the flows (e.g., Davies, 1982; Hayashi & Self, 1982; Legros, 2002; Davies & McSaveney, 2012). Applying this approach to the Ruapehu debris avalanches, assuming runout within v-shaped valleys, results in much

Table 6. Approximate runout and apparent coefficient of friction of the confined Ruapehu debris avalanches considering spreading of the mass within a v-shaped valley, calculated after Legros (2002). Assuming linear thickness decrease, the author suggests that the center of mass (L*) travels about one quarter of the total runout distance (L_{max}) of the flow, resulting in significantly higher apparent coefficients of friction (H/L*) than calculated using total runout distance (L_{max}) and total drop height (H).

	V [km^3]	L_{max} [km]	H [km]	A [km^2]	L* [km]	H/L*
Mataroa Formation	2.9	64.0	2.1	256	16.00	0.13
Pukekahu Formation	1.56	56.0	2.4	120	14.00	0.17
Oreore Formation	3	80.0	2.3	200	20.00	0.12
Piriaka-A Formation	1.35	72.0	2.5	225	18.00	0.14
Piriaka-B Formation	1.4	75.0	2.5	260	18.75	0.13
Lower Whangaehu Formation	2.4	60.0	2.3	120	15.00	0.15

* calculated runout and apparent coefficient of friction after Legros, 2002

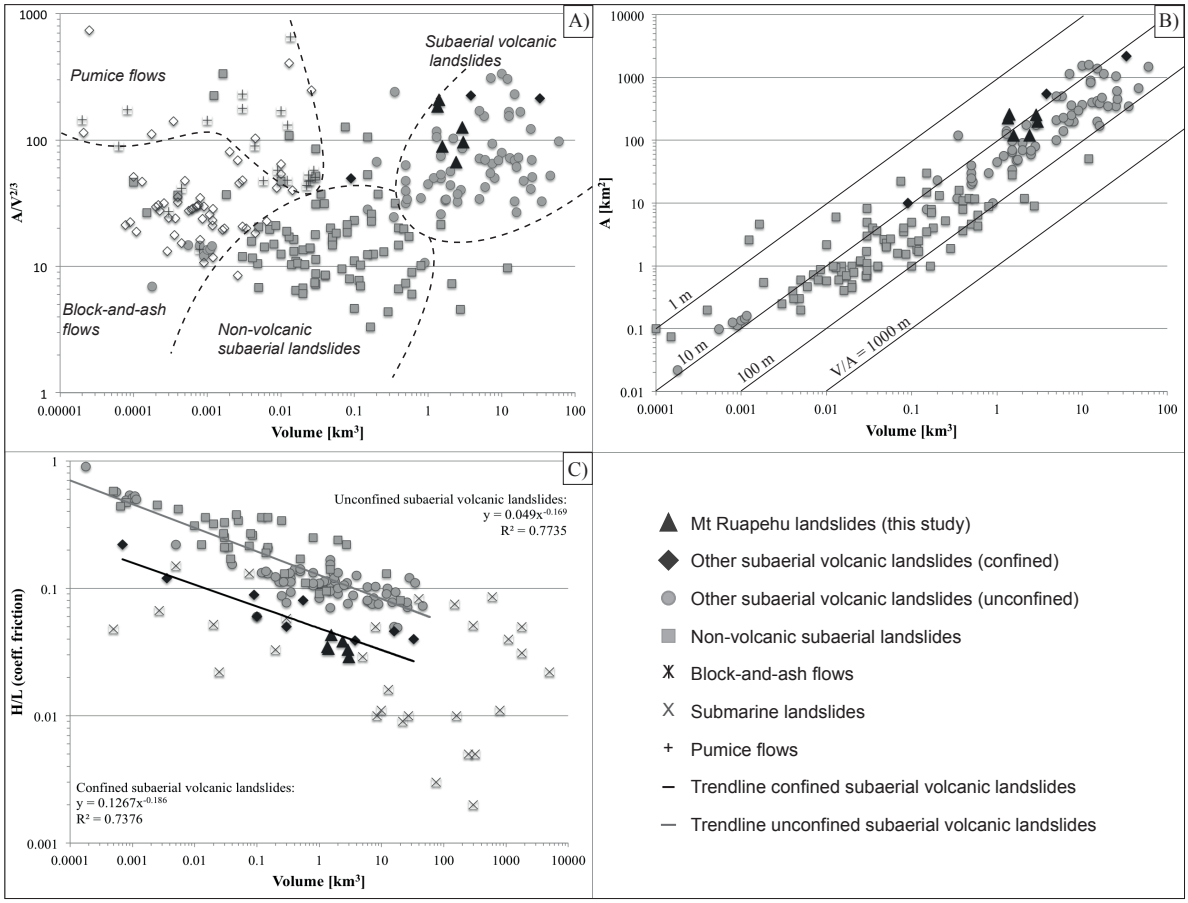

Figure 20. Parameters of the Ruapehu debris avalanches in relation to non-volcanic landslides, subaerial volcanic landslides (confined and unconfined), submarine landslides, block-and-ash flows, and pumice flows (see Appendix I for data).

higher H/L ratios than using deposit limits and indicates that the bulk of deposition was near the volcano (Table 6). Nonetheless, coefficients of apparent friction of the Ruapehu debris avalanches calculated in this manner are significantly lower (0.12 - 0.17) than those of rockfalls (~0.6; Hsü, 1975; Davies, 1982).

4.3.3 Discussion

The coarse diamictons exposed at >35 km along five major river catchments on the distal Ruapehu ring plain were emplaced by six long-runout debris avalanches that were formed by flank-sector failures of Ruapehu volcano between 70,000 and 200,000 years ago, and collectively inundated an area of c. 1,200 km^2. The fine-sand to silt matrix of the Ruapehu debris avalanches is firmly consolidated and prohibits detailed grain size analyses. The notably high content of pumice lapilli and cooling-jointed block and bomb clasts within the deposits of the Oreore and Pukekaha Formations suggest syn-eruptive failures of the Mt. Ruapehu edifice. The other four Ruapehu debris-avalanche deposits lack evidence for abundant fresh eruptive components, but instead contain common hydrothermally altered clasts. This indicates that the Mataroa, Whangaehu, and Piriaka debris avalanches were likely triggered by failure of a hydrothermally weakened and altered sector of the cone, possibly associated with increasing magmatic unrest. These components of the debris-avalanche deposits also indicate that a hydrothermal system was a long-lived part of the volcano, similar to that on the current volcano (c.f. Christenson & Wood, 1993). In addition, under the current humid (NIWA: National Climate Summary 2013) and past NZ climate conditions, Mt. Ruapehu, like many snow-covered composite volcanoes (e.g., Glicken, et al. 1995; Cashman et al., 2009), is partially saturated with water. Thus, landslides from Mt. Ruapehu contained significant internal water from the onset.

All six Ruapehu debris-avalanche deposits have very similar field appearances and sedimentary properties. They exhibit classical features of debris avalanches such as very poor sorting, entrained and contorted path material, jig-saw fractured clasts, boulders up to 5 m in diameter, megaclasts, sheared and deformed weaker clasts (Fig. 18). However, in addition to these properties, there are several features that are atypical of proximal to medial debris-avalanche deposits (c.f., Siebert, 1984; Ui et al., 1986; Palmer & Neall, 1989), including a great abundance of rounded clasts, entrained river gravels, and evidence for water-saturated zones. The combination of these features indicates that the Ruapehu debris avalanches contained significant water, and that they entrained large volumes of basement mudstones and river gravels (Fig. 18). Gradual downstream transformation of debris-avalanche deposits in wet environments into cohesive debris flows has been previously described (e.g., Vallance, 2000), but exposures of debris-flow deposits associated with the Ruapehu collapse events are missing. Furthermore, apart from the Whangaehu Formation, all the channelized debris-avalanche deposits show little lithologic variation with distance from source. These deposits lack a pervasive and uniform-textured loamy matrix, such as that described in the lateral facies of Mt. Taranaki debris avalanches (Ui et al., 1986; Palmer & Neall, 1989; Palmer et al., 1991; Procter et al., 2009). The clay content of the deposits is generally very low, so that they cannot be classified as cohesive debris flows (c.f., Vallance & Scott, 1997). The large rounded andesitic boulders within the debris-avalanche deposits are one to two orders of magnitude larger than the maximum clast sizes within the alluvial deposits emplaced subsequently to the debris avalanches. Their size and shape indicates they were likely derived from moraine or similar outwash deposits on the mid-upper

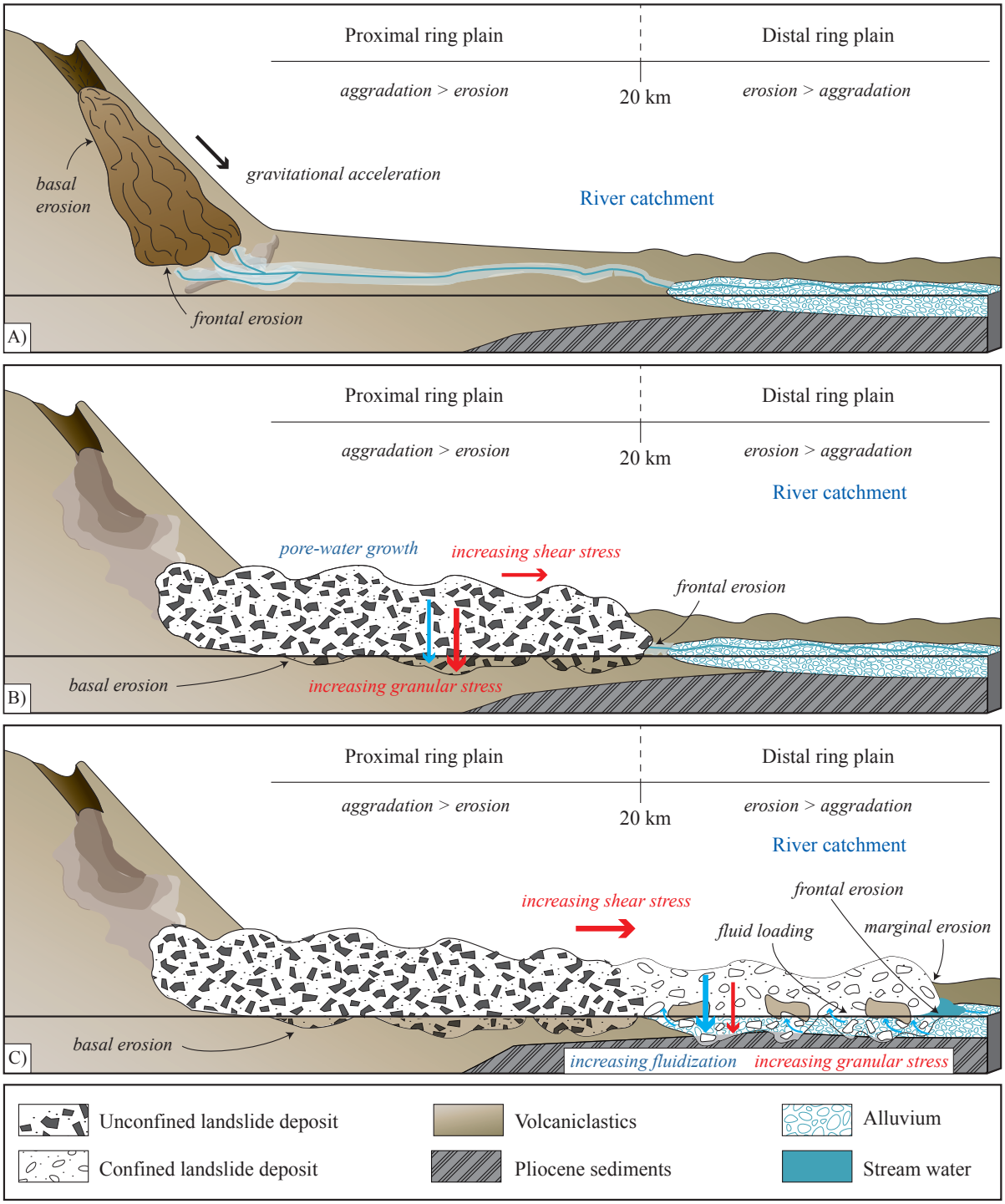

Figure 21. Transport and emplacement-model for the Ruapehu debris avalanches. (A) Gravitational collapse of a volcanic flank and movement of the mass downslope. Erosion is dominant at the base and the front of the flow especially in areas of strongly decreasing slope. (B) The bulk of the mass laterally spreads on the low-topography terrain of the proximal ring plain, whereas minor parts are likely confined to steep river channels. Basal and frontal erosion is dominant, and loose volcaniclastics are easily eroded and loaded into the flow. Interstitial fluids increase the basal pore pressure towards the base of the debris avalanche. The overlying mass facilitates downwards-directed progressive granular stress. (C) The initial topography of the distal ring plain channelizes the flow into major river catchments. Granular stress is overall reduced though erosion continues with path material entrained at the base, the front, and the margins. Stream water as well as saturated river sediments augment the volume of interstitial fluids, and strongly increase shearing and pore pressures towards the base of the flow.

volcano flanks, where Last Glacial moraines are currently common (Hackett & Houghton, 1985). In cases of unconfined subaerial volcanic landslides, the crushing of soft components (e.g., scoria and weathered rock) of the moving mass and the liberation of pore water may generate a distal transition from debris avalanche into a uniform debris flow-like viscous flow (Roverato et al., 2014). In the Ruapehu units examined here, however, the matrix is only a minor component: huge clasts often dominate with many cracked and jig-saw fractured clasts present, even at great distances from source. In the Ruapehu case, abundant basal fluid seems to have played the dominant role in generating these hybrid-sedimentary features, and thus increased the runout distance.

Two main contributing mechanisms led to the unusual debris-avalanche deposit properties and long runouts of the Ruapehu debris avalanches. Firstly, the collapse of ice/snow covered volcano flanks, with voluminous moraine and glacial-margin deposits provided the unusually large content of rounded coarse boulders. In addition, these led to debris avalanches of collapsing masses with considerable pore water. Secondly, the concentration of the debris avalanches into deep, confined valleys as they passed off the ring plain led to a lower surface area of frictional contact. This confinement also led to erosion and entrainment of river water, saturated river gravels and soft Tertiary mudstones. Taranaki volcano, with similar scale debris avalanches of similar age (Zernack et al., 2012), also had high pore-water contents, but the major difference is that they spread across a low-relief ringplain forming broad fans between 20 - 35 km from source. In a few more of the oldest deposits exposed up to 40 km from source, similar deposit features to the Ruapehu debris avalanches occur including an abundance of rounded clasts, and contorted ripped-up Tertiary sediments. These were especially common where deposits were emplaced into a large river valley and were confined (Alloway et al., 2005; Zernack et al., 2009; 2011).

The Ruapehu debris avalanches are an unusually pore-water rich examples of large (≥1 km^3) landslides that entered deeply incised valley systems. Proximal deposits <30 km are now covered by several tens of metres of more recent lahar, fluvial and tephra deposits (Cronin et al., 1997a; Lecointre et al., 1998; Donoghue & Neall, 2001). Significant portions of these flows traversed the ring-plain and entered distal catchments. Comparison with other valley-filling landslide deposits shows that confined subaerial volcanic landslides have, for a given volume, significantly lower H/L ratios compared to unconfined subaerial volcanic landslides and non-volcanic landslides, indicating similar transport and emplacement mechanisms for channelized landslides worldwide (Fig. 20C). Thus volcanic debris avalanches confined to the valleys of major river systems form an intermediate field of behaviour between subaerial “dry” volcanic landslides and submarine landslides. The Ruapehu debris avalanches indicate that the runout of debris avalanches is, apart from volume, influenced by the proportion of water in the flow as well as valley confinement (Fig. 20C) (e.g., Nicoletti & Sorrisco-Valvo, 1991; Legros, 2002; Pudasaini & Miller, 2013). Confined debris avalanches extend to 2.5 times the total length of unconfined subaerial volcanic landslides of similar volume (Fig. 20C). Nicoletti and Sorrisco-Valvo (1991) suggest that the long runout of confined debris avalanches is caused by the very limited dissipation of total mechanical energy during their runout. This relates to the lower basal contact area to volume ratio within channelized flows, in comparison to spreading flows that form broad deposit fans.
In addition to reduction of basal stress and contact surface within steep valleys, Ruapehu

flows may have also concentrated water in their base, especially at the lower boundary to the impermeable Tertiary mudstone substrate. This could also have been augmented by water entrained from saturated fluvial sediments in front of the flow.

4.3.3.1 Long runouts of the Mount Ruapehu debris avalanches

The initial stage of each Ruapehu debris avalanches was likely dominated by rapid sliding and breakage of large slabs of flank material downslope (Fig. 21A). Upon crossing the first 15 - 20 km of broad, flat ring-plain, parts of the debris avalanches descended off the Central Plateau and into deep channels, confining the flows. The effect of this is clearly shown in the sedimentary features of the Ruapehu debris avalanches by their deposition pattern, their very long runouts (>80 km) and the entrained and contorted bedrock sediments, as well as large quantities of rounded river gravels and boulders incorporated within the final deposits (Fig. 18; 21). The flow substrates included Quaternary volcaniclastics and moraine deposits on the proximal ring plain, along with Tertiary marine mudstone and Recent river gravels in distal channel floors (Fig. 18; 21). Entrainment of substrate material was common in deep valley sections (c.f., McDougall & Hungr, 2005). Entrainment of saturated fluvial sediments likely augmented the pore-water contents at the base and the margins of the flows (Fig. 21C) (c.f., Voight & Sousa, 1994; Sassa et al., 2004). The impermeable late-Pliocene mudstone substrate provided ideal conditions to enhance fluid overpressures at the base of the debris avalanche and led to the formation of an efficient shear zone. Transmission of basal shear stress to the river bed, accompanied by liquefaction, drove the entrainment of substrate debris (c.f., Iverson et al., 2010; Iverson, 2012). Unlike more homogenous flows, such as debris flows, the substrate entrainment was restricted only to the basal portions of the Ruapehu debris avalanches (Fig. 17A; 21). This shows that the flows had a mobile saturated base with high shear strain focussed near the boundary. Above this, the unsaturated upper parts of the flow rode along as an agitated granular mass. The deposits contain ubiquitous angular jig-saw fractured pebble to boulder clasts, attesting to the internal vibration and enduring clast-clast contacts (Fig. 19B; D). Basal and marginal stresses were high enough for the flow to incorporate and deform late-Pliocene mudstones and muddy sandstones (Fig. 21). The inverse grading observed within the Piriaka-B Formation (Fig. 17A) suggests higher shear stresses were experienced in the marginal and basal areas, which led to stronger clast-disruption at the base of the flow. The dish-structures exposed within the Oreore Formation (Fig. 19E) were potentially formed post-depositionally during loss of interstitial fluids and excess pore-pressure dissipation during deposit compaction (c.f., Voight & Sousa, 1994; Sassa et al., 2004).

4.3.4 Conclusion

In this study, six individual debris-avalanche deposits of Mt. Ruapehu, exposed from 35 km up to 80 km from the volcano, record major flank collapses, including four that have not been reported before. This shows that major flank collapses of Ruapehu volcano occurred far more frequently than previously known. The huge landslides were confined in distal regions to the valleys of deeply incised river systems, and had volumes estimated between 1.3 and 3 km^3, covering a combined area of >1,200 km^2. The basal deposit features, including common rip-up clasts of basement mudstone and abundant river gravels, show that the flows were highly erosive once concentrated in the deep valleys, with high shear stress.

Channelization resulted in concentration of water at the base of flows as they loaded and entrained path material, especially water-saturated river gravel, causing the basal regions of the debris avalanches to become highly mobile, which reduced the basal friction of the entire flow. Basal and marginal erosion, accompanied by dynamic rock fragmentation within the mass continued as the debris avalanches ran out. As the flows halted, the upward-directed loss of interstitial fluids eventually resulted in compaction and consolidation of the deposits.
The H/L ratios of channelized debris avalanches are far lower than those of non-volcanic and unconfined subaerial volcanic landslides of similar volume. Thus, the hazard evaluation of debris avalanches in humid tropical and temperate climates must take into account both the effects of pore water, and also identify geomorphic conditions that may enhance runout.

4.3.5 Acknowledgements

Manuela Tost is supported by a Massey University Doctoral Scholarship. This work is also supported by the SJC-led New Zealand Natural Hazards Research Platform Project “Living with Volcanic Risk”. We thank the local land-owners, in particular Jeff Williams and Rex Martin, for access to their land. We also like to thank Prof JW Vallance and Prof TR Davies for their helpful and thorough reviews of the manuscript.

CHAPTER 5: LINKING DISTAL VOLCANICLASTIC SEDIMENTATION AND STRATIGRAPHY WITH THE DEVELOPMENT OF RUAPEHU VOLCANO, NEW ZEALAND

5.1 Introduction

Stratovolcanoes are large, complex constructional edifices of lava and pyroclastic deposits with associated reworked volcaniclastic sediments that build up over hundreds of thousands of years from sporadic eruption episodes (e.g., Coats, 1950; Gamble et al., 1999). High precision dating of lavas exposed on composite cones (e.g., Mt. Adams, USA; Hildreth & Lanphere, 1994; Mt. Tongariro, New Zealand; Hobden et al., 1996; 1999; 2002; Tatara-San Pedro Complex, Chile; Singer et al., 1997; Dungan et al., 2001), and integration of this information with stratigraphic and lithological data, is typically the main approach used to examine pre-historic eruptive activity and event periodicity. However, on large volcanic edifices, generally only a small fraction of the total deposits of explosive and effusive eruptions, particularly those of older cone-building episodes, are exposed. Burial or erosion of older stratigraphic units generally masks the earlier history. For example, the upper 1,100 m of the 2,500 m stratovolcano Mt. Taranaki, in western North Island, New Zealand, is made up of units that are all <20 ka in age, whereas the ring plain surrounding the volcano contains deposits up to 170 ka old (Zernack et al., 2011). The bulk of the erupted magma of such volcanoes is found within a broad ring plain, made up of mass-flow deposits, fluvial sediments, and tephra (e.g., Janda et al., 1981; Donoghue et al., 1995; Cronin & Neall, 1997; Zernack et al., 2011). Mass flows from composite cones can extend hundreds of kilometres from source (e.g., Lecointre et al., 2004; Doyle et al., 2009), and their deposits may constitute the only evidence of an older eruptive history that on the edifice has long since been buried and/or eroded (Zernack et al., 2011). High precision dating (e.g., $^{40}Ar/^{39}Ar$-dating) of lavas from distal mass-flow deposits may provide the only means to reconstruct the initial stages of the volcanic growth of composite cones. A more complete knowledge of previous eruptive magnitudes and frequencies is important in order to improve our understanding of the hazards associated with potential future eruptions of these highly explosive, and often unpredictable, volcanoes (Cronin, 2013).

5.1.1 Geological Setting

Mt. Ruapehu, located in the centre of the North Island, is one of the most active stratovolcanoes in New Zealand. The composite massif is made up of lava flow sequences, autoclastic breccias, and pyroclastic, epiclastic, and glacial/moraine deposits (Hackett & Houghton 1989; Smith et al. 1999). Four major cone-building episodes have been previously identified and mapped by Hackett and Houghton (1989) on the edifice, and were subsequently dated (Fig. 4B) (e.g., Tanaka et al., 1997; Gamble et al., 2003). These are, from oldest to youngest: the Te Herenga Formation (250 - 180 ka; Gamble et al., 2003), the Wahianoa Formation (120 - 150 ka; Price et al., 2005), the Mangawhero Formation (55 - 15 ka; Gamble et al., 2003), and the Whakapapa Formation (<15 ka; Gamble et al., 2003). The stratovolcano is surrounded by a large ring plain, which comprises stacked mass flow, fluvial, and tephra deposits (Cronin & Neall 1997; Lecointre et al. 1998). The ring plain is dissected by numerous river systems in which mass-flow deposits

were emplaced up to 100 km from source (e.g., Cronin et al., 1996; Tost et al., 2014). Previous workers have identified mass -flow sequences along the Whangaehu River, the Waimarino River, the Waikato River, and their tributaries (Hodgson 1993; Cronin et al., 1996; Lecointre et al. 1998). This study focuses on the six major river catchments dissecting the Ruapehu ring plain: the Hautapu River, the Turakina River, the Mangawhero River, the Manganuioteao River, the Whakapapa River, the Whanganui River, and their individual tributaries. Four of the six drainage systems currently originate from the steep volcanic flanks of Mt. Ruapehu, whereas the Hautapu River and the Turakina River rise from the distal Ruapehu ring plain (e.g., Tost et al., 2015). Correlating cone-building formations and periods of activity, and comparing them to ring plain volcaniclastic deposit stratigraphy, has never been carried out before. Hence, the aim of this study is to improve the knowledge of the eruptive history of Mt. Ruapehu, especially that of >50,000 years ago. In part this is based on new geological mapping and the collection of 15 new $^{40}Ar/^{39}Ar$ dates of lava clasts sampled from long-runout mass-flow deposits exposed on the distal Ruapehu ring plain, up to 90 km from the volcano (Fig. 22). The new ages are integrated with the observed volcaniclastic deposit stratigraphy along the six individual river catchments and the overlying dated cover-bed sequences (Pillans, 1994). The volcaniclastic units and their lithologies were examined in order to gain insights into eruptive styles and magnitudes (volcanic eruption index or VEI, after Newhall and Self, 1982) of early eruption episodes that are mostly no longer represented in primary deposits (Table 7).

5.2 Methods

Samples selected for petrographic and geochemical analysis and high precision dating were obtained from moderately to poorly rounded, ≥30 cm lava clasts, collected from mass-flow sequences exposed either in road cuts or bluffs on farm land (Fig. 22). The freshest central c. 3 x 3 x 3 cm portion of each clast was crushed and ground in a tungsten carbide ring mill at the University of Auckland, New Zealand, in order to obtain major and minor whole rock element concentrations by X-ray fluorescence (XRF) analysis (see Chapter 6). Samples with K/Ca ratios exceeding 0.18 were further considered for high precision dating. Polished thin sections were prepared at the University of Ballarat, Victoria, Australia, and these were used to select samples with crystalline groundmass for $^{40}Ar/^{39}Ar$-analysis. Twenty samples selected in this way were crushed and sieved to extract groundmass grains that range between 200 - 300 µm in size. Groundmass separates were primarily obtained by hand-picking, as well as magnetic and heavy-liquid separation, followed by acid treatment. The separated groundmass samples were irradiated and dated at the Oregon State University (OSU) Argon Geochronology Laboratory, Oregon, USA, using laser step-heating in a resistance furnace and an ARGUS VI multi-collector mass spectrometer. All resulting ages were calculated using the ArArCALC v2.5.2 software package (Koppers, 2002), with precisions within ±2σ.

Results from five samples (plateau as well as total gas) were rejected because of low precision, and 15 plateau ages, which agree within 2σ uncertainty, were accepted. The results of the 15 analyses are summarized in Table 8. The plateau ages are considered to be accurate estimates for crystallization ages, indicating individual times of eruptive activity of Mt. Ruapehu. These ages were supplemented by stratigraphic ages, based on cover-bed sequences and landscape/terrace development in the river catchments studied.

Table 7. Criteria for estimating the Volcanic Explosivity Index (VEI) of historic eruptions after Newhall and Self (1982).

VEI	**0**	**1**	**2**	**3**	**4**	**5**	**6**	**7**	**8**
Description	non-explosive	small	moderate	moderate-large	large	very large			
Volume of ejecta (m^3)*	$<10^4$	10^4-10^6	10^6-10^7	10^7-10^8	10^8-10^9	10^9-10^{10}	10^{10}-10^{11}	10^{11}-10^{12}	$>10^{12}$
Column height (km)**	<0.1	0.1-1	1-5	3-15	10-25	>25			
Qualitative description	gentle, effusive		explosive		violent, colossal, cataclysmic				
Classification	Hawaiian		Vulcanian			Ultraplinian			
		Strombolian			Plinian				
Duration of continous blast (h)	<1				>12				
			1-6						
				6-12					
Max explosivity***	lava flow	explosion or nuee ardente							
		phreatic							
	dome or mudflow								
Tropospheric injection	negiligible	minor	moderate	substantial					
Stratospheric injection	none			possible	definite	significant			

*Tsuya (1995) classification, assuming all eruptive products are pyroclastic ejecta
**Uses km above crater for VEI's between 0-2; and km above sea level for VEI's between 3-8
***The most explosive activity indicated for the eruption in the Catalogue of Active Volcanoes

5.3 Stratigraphy and sedimentology of the mass-flow deposits

5.3.1 The Turakina debris flow

A road cut c. 1.5 km northwest of Turakina (Fig. 22) exposes a volcaniclastic diamicton intercalated between the Braemore and Brunswick marine terraces, which were formed during periods of sea-level rise, preserved by ongoing tectonic uplift, and are estimated to have formed at 340 ka and 309 ka, respectively (Pillans, 1983). The c. 2.5 m thick volcano-sedimentary deposit is poorly sorted, massive to cross-bedded and contains dominantly well-rounded cobble- to pebble-sized clasts of andesite lava (60 vol.%), pumice lapilli (30 vol.%), and Tertiary mudstone rip-up clasts (10 vol.%). The unconsolidated matrix (70 - 80 vol.%) is silt to fine sand (Fig. 23A). The deposit is overlain by three rhyolitic tephra layers: the Middle Griffins Road Tephra, the Upper Griffins Road Tephra, and the Fordell Ash, dispersed during highly explosive caldera eruptions within the Taupo Volcanic Zone between 340 ka and 300 ka ago (e.g., Pillans et al., 1988; Berger et al., 1992; Bussell & Pillans, 1992).

5.3.2 The Mataroa (and Whangaehu) Formation

The stratigraphy of the Mataroa Formation is outlined in Fig. 11;24 and described in detail by Tost et al. (2015). The volcaniclastic sequence overlies a massive conglomerate that, in-turn, unconformably overlies Miocene Taihape Mudstone. The deposit comprises well-rounded cobble- to pebble-sized clasts of dominantly andesitic lava (>90 vol.%), which as part of this study have been dated at 283.5 ± 6.7 ka (Table 8). The deposit is overlain by a 0.5 to 11 m-thick massive diamicton (the Mataroa debris-avalanche deposit) containing partly- and well-rounded pebble- to boulder-sized clasts of andesite lava (50 - 60 vol.%, <4 m), dated at 236.5 ± 7.2 ka (Table 8), and rip-up clasts of Taihape Mudstone (5 - 15 vol.%, <5 m), in a firmly consolidated silt- to fine sand-sized matrix (making up 25 - 35 vol.%) (Fig. 10C; 12). Several clasts show distinctive jigsaw-fractures and most Taihape Mudstone rip-up clasts are strongly deformed. The diamicton is unconformably overlain by a sequence of varying thickness consisting of up to 15 individual deposits of pumice-rich, pebbly and sandy debris flows and hyperconcentrated flows. Andesite lavas within the basal debris-flow deposit exposed at Mataroa 2 (Fig. 24) are dated at 188.9 ± 11.0 ka (Table 8). The mass-flow deposits are dominantly massive, in rare cases planar-bedded, poorly sorted, and matrix-supported. They are made up of subrounded to well-rounded pebble- to boulder-sized clasts (≤1.2 m) of andesite lava (75 - 80 vol.%), pumice lapilli (15 - 20 vol.%), and exotic Taihape Mudstone rip-up clasts. The mass-flow deposits comprise pebble- to cobble-sized clasts of andesite lava, and up to 30 vol.% pumice. These pumiceous units are commonly reversely graded with increasing contents of pumice clasts towards the top. Finer grained (pebble-sand dominated) and better-sorted units generally contain more angular clasts. A fine-grained pebble-dominated and weakly planar-bedded deposit at Hihitahi (Fig. 22) also contains distinctive charcoal fragments (≤5 cm) in its upper third. The mass-flow sequence exposed at Hihitahi is overlain by four Last Glaciation loess units (each formed during a stadial period of the Last Glaciation; Milne, 1973) and their associated interstadial soils, implying a depositional age for the underlying volcaniclastic sequence of >125 ka (Tost et al., 2015).

A very similar diamicton sequence is exposed within the Whangaehu River valley located to

Table 8. $^{40}Ar/^{39}Ar$-plateau ages of 15 groundmass separates from the studied mass-flow formations exposed along six major river valleys on the distal Ruapehu ring plain.

No.	Sample no.	River valley	Mass-flow form.	Groundm. crystallinity	η	K/Ca ± 2σ	Age (ka) ± 2σ
1	HAU-GWT	Hautapu River	Mataroa	moderately crystalline	15	0.192 ± 0.048	283.5 ± 6.7
2	HAU-GW3gr	Hautapu River	Mataroa	moderately glassy	13	0.234 ± 0.014	236.5 ± 7.2
3	WHA-HAF3	Whangaehu River	Lower Whangaehu	moderately crystalline	11	0.326 ± 0.057	229.9 ± 3.3
4	WHA-MA1	Whangaehu River	Lower Whangaehu	moderately crystalline	11	0.252 ± 0.024	218.7 ± 31.1
5	MAN-KL4	Mangawhero River	Oreore	moderately glassy	11	0.411 ± 0.048	192.0 ± 7.3
6	HAU-MF1b	Hautapu River	Mataroa	moderately glassy	7	0.082 ± 0.049	188.9 ± 11.0
7	WAN-SpU2	Whakapapa River	Piriaka	crystalline	13	0.368 ± 0.053	181.6 ± 5.6
8	MAN-AR1	Mangawhero River	Oreore	moderately crystalline	17	0.198 ± 0.060	178.4 ± 3.3
9	MAN-AI2	Mangawhero River	Oreore	glassy	11	0.258 ± 0.078	162.5 ± 5.2
10	MAN-OH1	Mangawhero River	Oreore	moderately glassy	19	0.212 ± 0.030	160.8 ± 9.6
11	MNT-HR2	Manganuioteao River	Pukekaha	moderately crystalline	16	0.414 ± 0.026	158.8 ± 4.7
12	WAN-KAI1	Whanganui River	Piriaka	moderately crystalline	11	0.218 ± 0.048	146.4 ± 4.9
13	WAN-SH4/1	Whakapapa River	Piriaka	moderately crystalline	16	0.358 ± 0.018	79.0 ± 9.6
14	MNT-RB4	Manganuioteao River	Pukekaha	glassy	16	0.465 ± 0.024	65.0 ± 10.8
15	MNT-MA1	Manganuioteao River	Pukekaha	crystalline	5	0.692 ± 0.095	50.4 ± 10.5

the west. The oldest volcaniclastic unit is the 10 - 30 m-thick Lower Whangaehu Formation (Hodgson, 1993; Keigler et al., 2011), interpreted as a channel-confined debris-avalanche. The massive diamicton deposit, which unconformably overlies Tertiary sand- and mudstone, is clast- to matrix-supported, boulder-rich and very poorly sorted. Well to moderately rounded pebble- to boulder-sized clasts are commonly jigsaw jointed and comprise 80 - 90 vol.% andesite lava dated at 229.9 ± 3.3 ka and 218.7 ± 31.1 ka (Table 8), 10 - 15 vol.% Tertiary mudstone, 3 vol.% hydrothermally altered clasts, and <2 vol.% Mesozoic greywacke gravel. The debris-avalanche deposit is overlain by numerous pumice-rich hyperconcentrated-flow deposits (Fig. 23B). Four Last Glaciation loess units, and the corresponding interstadial soil horizons, were identified on top of the Whangaehu Formation, implying a depositional age of >125 ka (Hodgson, 1993; Keigler et al., 2011; Tost et al., 2015).

5.3.3 The Oreore Formation

The stratigraphy of the Oreore Formation is outlined in Fig. 25. The basal deposit corresponds to a debris-avalanche deposit described in detail by Tost et al. (2014), which contains andesitic lava clasts dated at 192.0 ± 7.3 ka, 178.4 ± 3.3 ka, 162.5 ± 5.2 ka, and 160.8 ± 9.6 ka (Table 8). The deposit is massive, very poorly sorted and contains c. 60 - 65 vol.% angular to well-rounded pebble- to boulder-sized clasts, made up of 70 - 75 vol.% andesite lava (≤3 m in diameter), and 10 - 15 vol.% pumice (≤0.3 m in diameter). Other clast varieties include c. 5 - 10 vol.% Tertiary mud- and sandstone rip-up clasts (≤1 m in diameter), c. 5 - 8 vol.% hydrothermally altered clasts (≤0.5 m in diameter), and 1 - 2 vol.% Mesozoic greywacke gravel. The deposit is overlain by a c. 2 m-thick, massive, fine-grained, consolidated, matrix-supported hyperconcentrated-flow deposit made up of 10 - 20 vol.% angular pebble-sized clasts (≤2 cm in diameter) that comprise andesite lava (80 - 85 vol.%) and pumice lapilli (15 - 20 vol.%) (Fig. 23C). The strongly cemented matrix makes up 80 - 90 vol.% of the deposit and is silt to coarse-sand. The hyperconcentrated-flow deposit is unconformably overlain by a c. 1 m-thick massive, coarse-grained, matrix-supported (c. 50 vol.% fine sand) debris-flow deposit, which contains subrounded to well-rounded pebble- to boulder-sized clasts (≤40 cm in diameter) made up of andesite lava (>90 vol.%), pumice lapilli (7 vol.%), and non-volcanic material (<3 vol.%) of late-Pliocene mudstone and Jurassic greywacke gravel (Fig. 23D). Above the

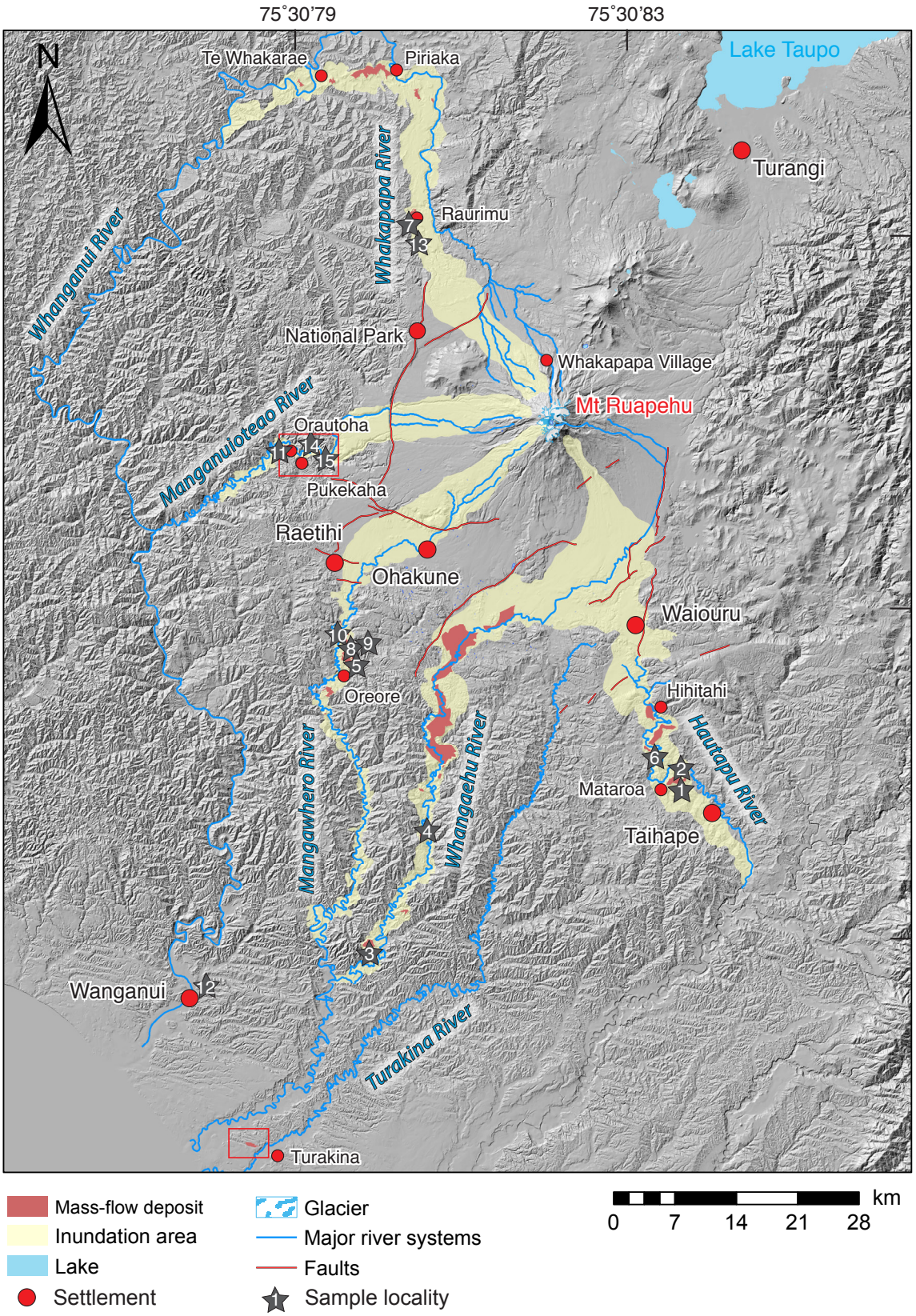

Figure 22. Digital elevation model of the proximal and distal Ruapehu ring plain including tectonic faults (red lines) after Villamor and Berryman (2006a; 2006b). Exposures of the mass-flow deposits studied are limited to the proximal ring plain (red field and rectangles). Reconstruction of the approximate inundation area (yellow fields) of the flows is based on reworked andesitic boulders (≥1 m in diameter) associated with the initial event and scattered around the landscape adjacent to the river valleys. The stars represnt sampling sites for Ar-dating and the numbers correspond to Table 8. Modified after Tost et al., 2014.

debris-flow deposit is a >5 m-thick sequence of numerous pumiceous, well-sorted, fine-grained (0.2 - 5 mm), and in part planar- to cross-bedded hyperconcentrated-flow deposits (Fig. 23E).

5.3.4 The Piriaka Formation

The volcaniclastic stratigraphy of the Piriaka Formation, exposed along the Whakapapa and Whanganui River valleys, is outlined in Fig. 26. The basal part of the sequence exposed at Piriaka comprises a >2.5 m-thick unbedded and poorly sorted debris-avalanche deposit, described in detail by Tost et al. (2014), containing angular to subrounded clasts supported by a firmly consolidated matrix (30 - 50 vol.%). The clast assemblage is made up of 85 - 90 vol.% andesitic lava pebbles, cobbles and boulders (<1.5 m in diameter), 10 - 15 vol.% hydrothermally altered andesitic clasts, <1 vol.% pumice, and <1 vol.% Tertiary mudstone. The deposit is unconformably overlain by a c. 1.4 m-thick massive hyperconcentrated-flow deposit, which is made up of 80 - 90 vol.% fine sand- to silt-sized grains, and 10 - 20 vol.% angular to well-rounded pebble- to cobble-sized clasts (<13 cm) of andesite lava (Fig. 23F). A sandy c. 8 cm-thick, commonly eroded, planar- to cross-bedded layer overlies the hyperconcentrated-flow deposit and hints at a period of normal stream-flow sedimentation processes. The fluvial layer is, in-turn, unconformably overlain by another c. 1 m-thick massive hyperconcentrated-flow deposit, which comprises >90 vol.% silt, and <10 vol.% angular to well-rounded andesite lava pebbles (≤2 cm in diameter). Above is a 1.2 m-thick massive, poorly sorted volcaniclastic conglomerate. The deposit is strongly weathered, matrix-supported (60 - 75 vol.% fine sand), and contains 25 - 40 vol.% pebble- to boulder-sized subrounded to well-rounded clasts (≤1 m in diameter). These are made up of 60 vol.% andesite lava, 10 vol.% pumice lapilli, and 30 vol.% late-Pliocene mudstone and Jurassic greywacke gravel rip-up clasts. On top of the deposit is a >5 m-thick very coarse grained, unbedded and poorly sorted debris-avalanche deposit described in detail by Tost et al. (2014), which contains boulder-sized clasts between 1 and 4 m in diameter (40 - 50 vol.%), supported by a consolidated fine-sand matrix (Fig. 17A). The clast assemblage comprises andesite lava (>95 vol.%) and <5 vol.% Tertiary mud- and sandstone rip-up clasts. The deposit shows inverse grading, with boulders exceeding 2 m in diameter limited to the upper half of the unit. Above the debris-avalanche deposit is a c. 5 m-thick sequence of hyperconcentrated-flow deposits, which correspond to a c. 10 m-thick hyperconcentrated-flow sequence exposed in a road cut along State Highway 4 at Raurimu (Fig. 23G; 26). At Raurimu, the sequence is overlain by a massive, poorly sorted, matrix-supported diamicton, made up of subrounded to well-rounded pebble- to boulder-sized clasts (≤1.2 m) of andesite lava (75 - 80 vol.%) dated at 181.6 ± 5.6 ka (Table 8), pumice lapilli (15 - 20 vol.%), and exotic late-Pliocene mudstone rip-up clasts (Fig. 23H).

At Piriaka, the massive >5 m-thick hyperconcentrated-flow sequence is stratigraphically overlain by a c. 0.8 m thick sequence of fluvial deposits. The lowermost unit is fine-grained, planar- to cross-bedded and contains pebbles. The deposit fines upwards and contains 30 - 35 vol.% of strongly weathered pumice lapilli. The layer is unconformably overlain by two massive, consolidated, poorly sorted and matrix-supported conglomerate units, which contain 70 - 90 vol.% andesite lava pebbles (≤5 cm in diameter) and 10 - 20 vol.% strongly altered pumice lapilli (≤7 cm in diameter). The uppermost unit also contains 10 vol.% hydrothermally altered clasts. The conglomerate is overlain by a >6 m-thick fine-grained, planar- to cross-bedded fluvial deposit, reflecting a return to normal stream-flow behaviour of the proto-Whanganui River.

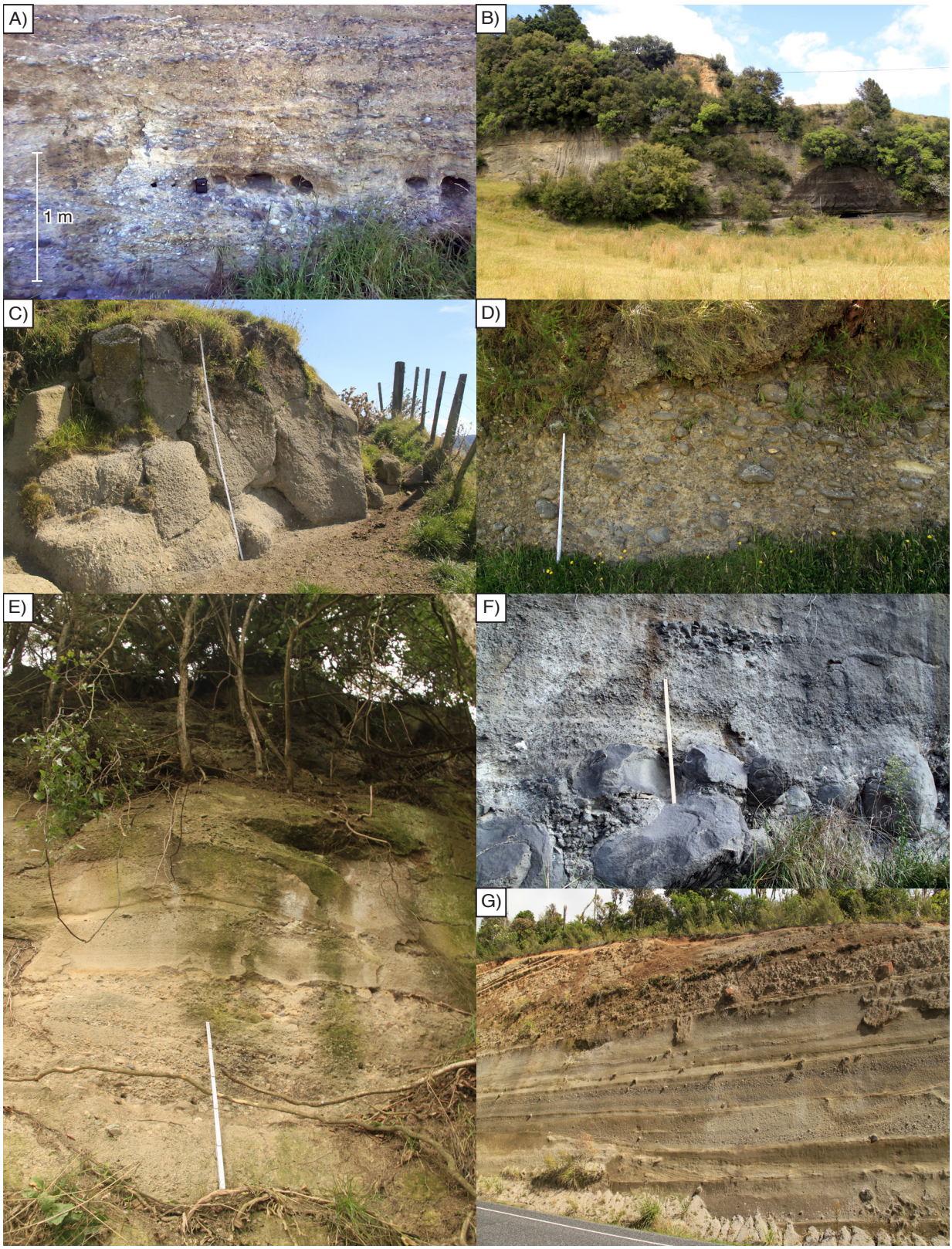

Figure 23. Field observations. (A) The Turakina debris-flow deposit is massive to cross bedded and dominantly contains well-rounded pebble-sized clasts. (B) A sequence of hyperconcentrated-flow deposits overlies the Lower Whangaehu Formation along the Whangaehu River valley. (C) The conglomerate exposed within the Oreore Formation (Scale: 1 m). (D) The lowermost consolidated pumiceous hyperconcentrated-flow deposit of the Oreore Formation (Scale: 2 m). (E) The uppermost sequence of the Oreore Formation is made up of numerous fine-grained pumiceous hyperconcentrated-flow deposits (Scale: 1 m). (F) The basal debris-avalanche deposit of the Piriaka Formation is unconformably overlain by two hyperconcentrated-flow deposits (Scale: 1 m). (G) The c. 10 m thick sequence of hyperconcentrated-flow deposits of the Piriaka Formation exposed in a road cut along State Highway 4 at Raurimu.

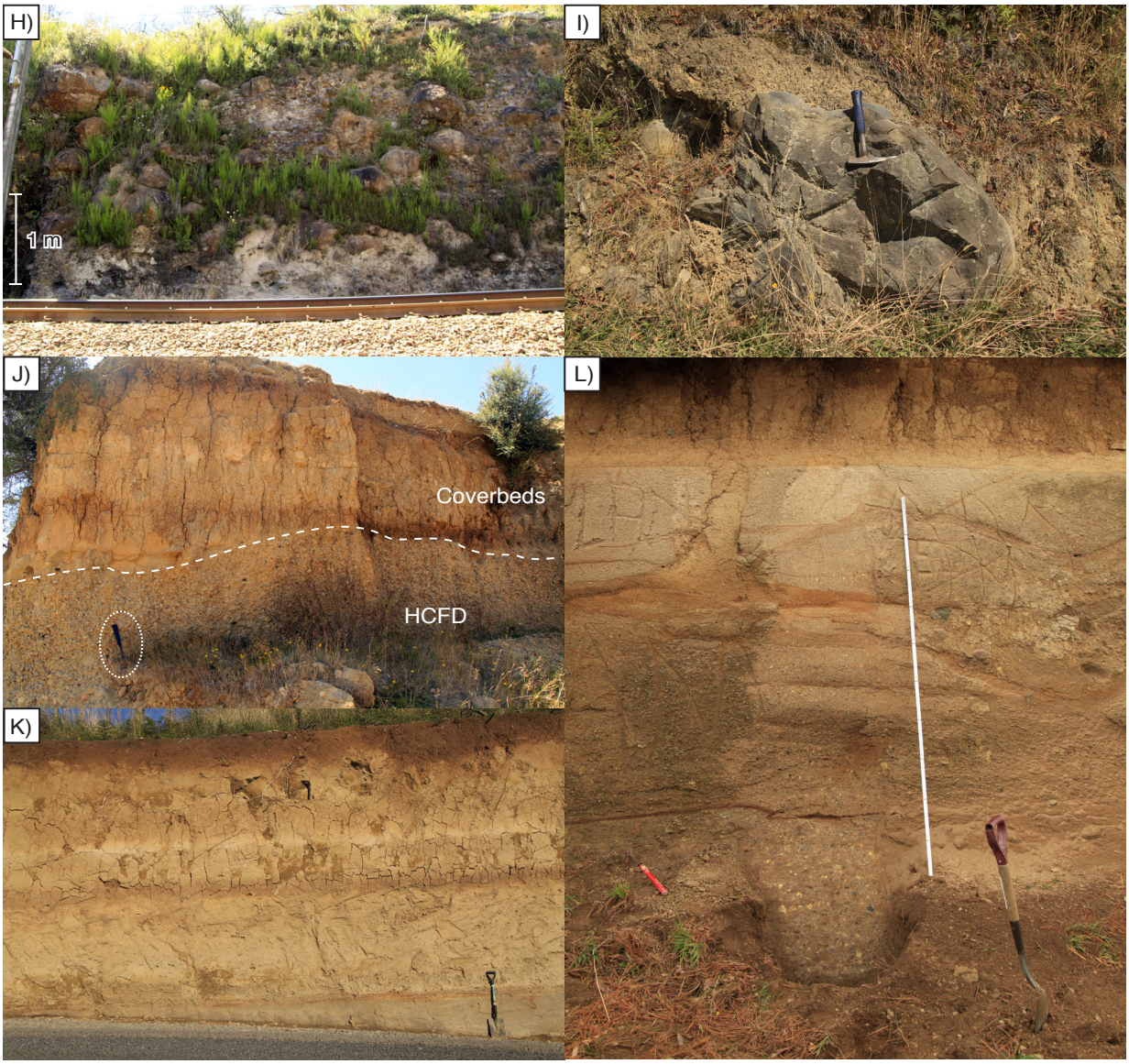

Figure 23 (continued). Field observations. (H) The debris-flow deposit overlying the previous sequence of hyperconcentrated-flow deposits along the Main Trunk Railway Line at Raurimu. (I) Heat-fractured boulder within a strongly weathered diamicton deposit exposed in a road cut along the Manganuioteao River valley. (J) Hyperconcentrated-flow deposits and overlying coverbeds of the Pukekaha Formation exposed in a quarry along the river valley. (K) Basal hyperconcentrated-flow deposit (HCFD) and overlying coverbed sequence exposed in a road cut along State Highway 4 c. 4 km south of Raetihi. (L) Pumiceous sequence of seven hyperconcentrated-flow deposits exposed in a road cut along State Highway 1 at Hihitahi (Scale: 2 m).

Two individual mass-flow deposits are exposed in a road cut along a farm track c. 1.5 km southeast of Te Whakarae (Fig. 22; 26). The lowermost unit is a >5 m-thick, massive, matrix-supported (60 - 80 vol.% silt-sized material), fine-grained, hyperconcentrated-flow deposit, which contains angular to subrounded pebbles of andesite lava (60 - 70 vol.%), pumice lapilli (20 - 25 vol.%), and hydrothermally altered volcanic lithologies (10 - 15 vol.%). Additionally, the deposit contains c. 10 vol.% of free pyroxene crystals. The central part of the hyperconcentrated-flow deposit is unconformably overlain by a 1.9 m-thick massive, silty matrix-supported, consolidated and strongly weathered debris-flow deposit. The poorly sorted, inversely graded unit comprises clasts of subrounded to well-rounded pebbles to cobbles (≤22 cm in diameter) of andesite lava (>80 vol.%), pumice lapilli (15 vol.%), and Tertiary mudstone (<5 vol.%). Above this sequence is a >1 m-thick unit of planar- to cross-bedded, well-sorted fluvial sands.

A related volcaniclastic conglomerate is exposed at Kaimatira Bluff, along State Highway 4 at Wanganui (Fig. 22), and contains well-rounded pebble-sized clasts of andesite lava dated at 146.4 ± 4.9 ka (Table 8). This was identified within the sequence described by Kershaw (1989). Parish (1994) noted the same volcaniclastic conglomerate on farmland c. 6 km northeast of Wanganui and named it after its landowners. Stratigraphically, the O'Leary Conglomerate overlies the Brunswick marine aggradational terrace (309 ka; Pillans, 1983), and has, therefore, been previously interpreted to be emplaced c. 300 ka ago (Parish, 1994; Gamble et al., 2003). Along the Whakapapa River catchment, andesitic lavas sampled from diamictons exposed in road cuts along State Highway 4 (Fig. 22; 26) are dated at 79.0 ± 9.6 ka (Table 8). The consolidated debris-avalanche deposit is coarse-grained, matrix-supported (50 - 60 vol.% fine sand), poorly sorted, and contains angular to subrounded pebble- to boulder-sized andesite lava (>95 vol.%), and Tertiary mudstone rip-up clasts (<5 vol.%).

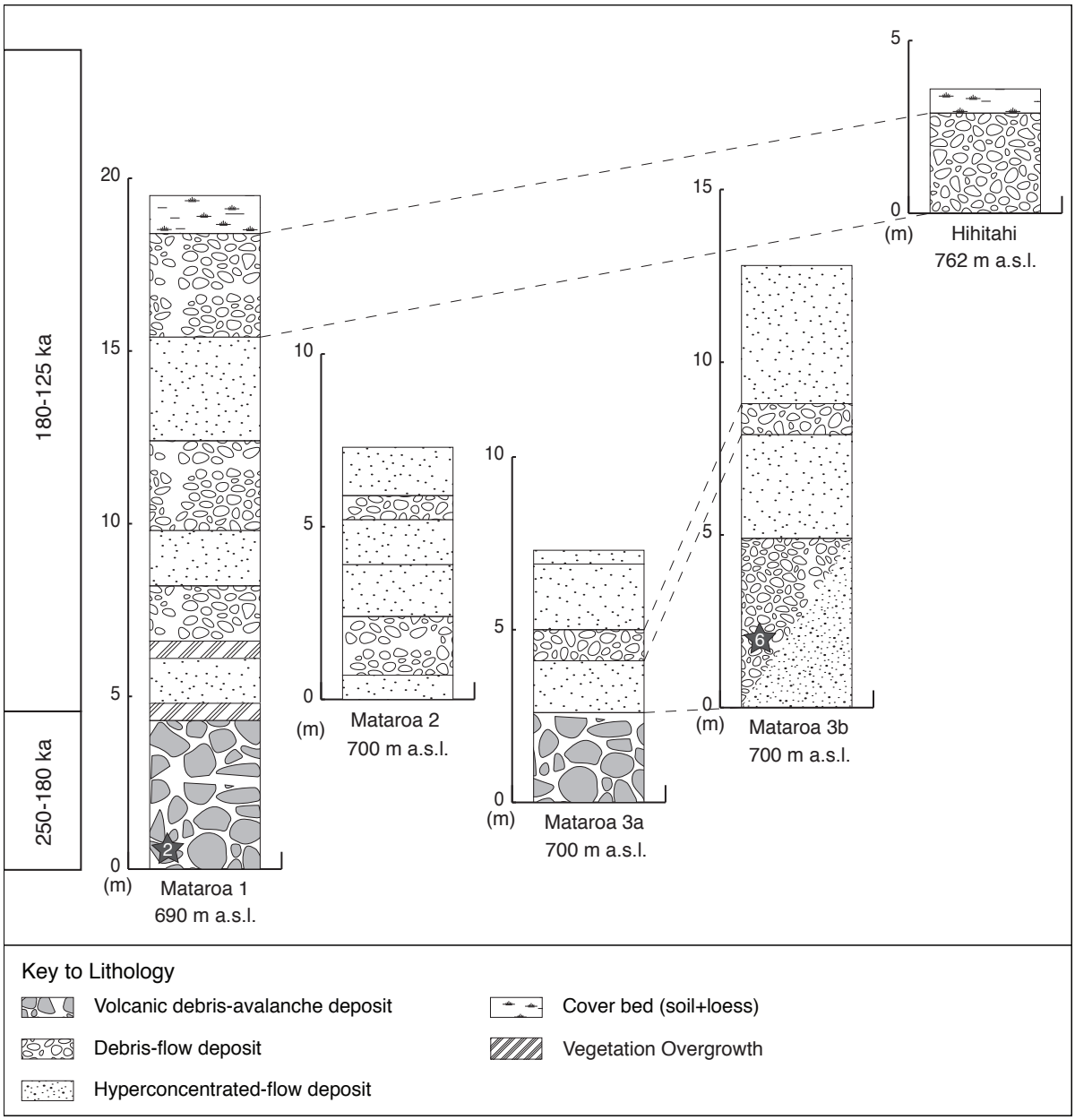

Figure 24. Stratigraphy of the Mataroa Formation modified after Tost et al. (2015). The base of the sequence holds a debris-avalanche deposit with its undulating topography being subsequently infilled and smoothed by at least 15 lahar deposits (hyperconcentrated flows and debris flows). The stars outline mass-flow units sampled for Ar-dating, and the given numbers correspond to Table 8 and Fig. 22.

5.3.5 The Pukekaha Formation

Numerous exposures of diamictons and stream-flow deposits along the Manganuioteao River reveal a complex volcaniclastic stratigraphy (Fig. 27). The following section is focused on mass flows that were emplaced before 50 ka.

The oldest volcaniclastic deposit, exposed in a road cut c. 1 km northwest of Orautoha along the Manganuioteao River catchment, is a strongly weathered diamicton deposit, which incorporates heat-fractured andesite lava blocks ≤3 m in diameter dated at 158.8 ± 4.7 ka (Table 8; Fig. 23I). The deposit is stratigraphically overlain by a 85 cm-thick hyperconcentrated-flow deposit, an intercalated 2 cm-thick andesitic lapilli-tephra layer and another 71 cm-thick hyperconcentrated-flow deposit (Fig. 27). Both mass-flow deposits are massive, consolidated, matrix-supported (60 - 70 vol.% silt), well-sorted, and comprise angular to subrounded pebble- to cobble-sized clasts (≤5.2 cm) made up of 80 - 85 vol. % andesite lava, 10 - 15 vol.% primary pumice lapilli, and 5 vol.% hydrothermally altered andesite. At the top is a debris-avalanche deposit described in detail by Tost et al. (2014), which comprises heat-fractured andesite lava boulders dated at 65.0 ± 10.8 ka and 50.4 ± 10.5 ka (Table 8) (Fig. 18C). The massive and poorly sorted deposit contains angular to well-rounded pebble- to boulder-sized clasts of andesitic lava (50 - 60 vol.%, <2.5 m), c. 20 vol.% dense pumice <5 cm in diameter, c. 10 vol.% sintered claystone, and <5 vol.% hydrothermally altered clasts supported in a sand-sized matrix of fragmented pumice (c. 30 - 40 vol.%). The debris-avalanche deposit is stratigraphically overlain by a >2 m thick sequence of volcaniclastic deposits exposed within two disused quarries along the Manganuioteao River valley (Fig. 23J; 27). The basal cover-beds comprise a >30 cm-thick massive silty clay with c. 2 vol.% strongly altered pumice. The unit is overlain by a 34 cm-thick laminated fluvial silty sand. The sequence is capped by a 1.5 m-thick, massive, matrix-supported debris-flow deposit, which contains angular to subrounded pebble- to cobble-sized clasts (≤5.7 cm in diameter) made up of >92 vol.% andesite (c. 15 vol.% glassy,

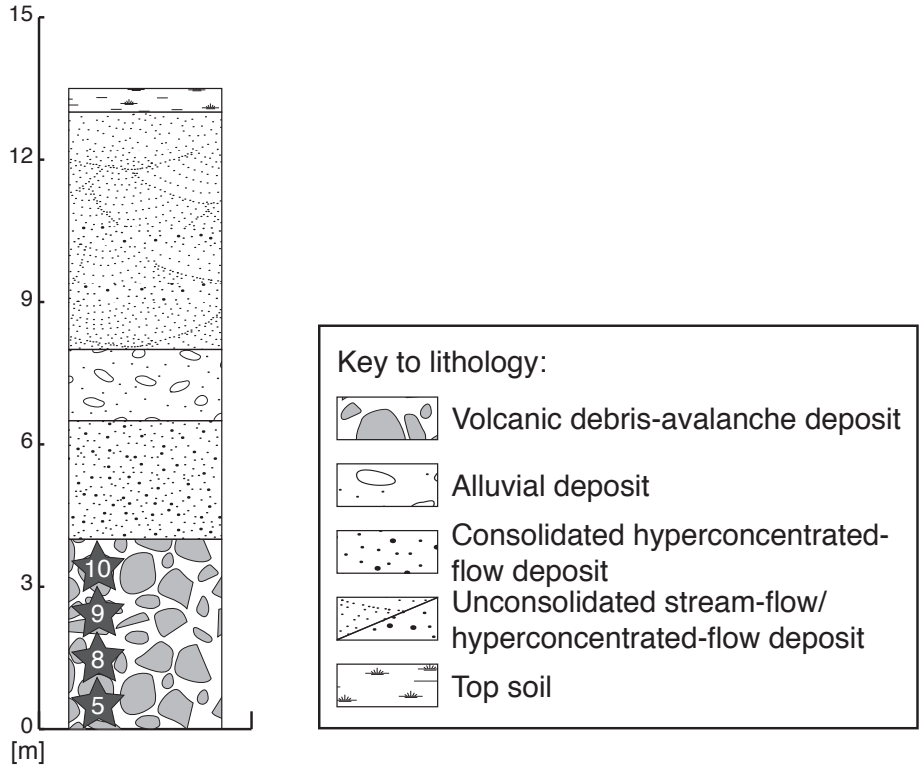

Figure 25. Stratigraphy of the Oreore Formation. The type locality for the syn-eruptive mass-flow sequence is exposed on farmland c. 2 km northeast of Oreore. The basal debris-avalanche deposit forms an undulating topography in the area which is infilled and smoothed by the overlying lahar deposits, forming a distinctive plateau between Ohorea and Oreore (see Fig. 22 for localities). The stars outline mass-flow units sampled for Ar-dating, and the given numbers correspond to Table 8 and Fig. 22.

highly vesicular, phenocryst-rich), <5 vol.% dense pumice, 1 - 2 vol.% hydrothermally altered material, and ≤1 vol.% charcoal. These occur within a pumice-dominated sand-silt matrix (50 - 60 vol.%). The mass-flow deposits form a distinctive plateau on top of the Ratan-aged (30 - 50 ka; Pillans, 1994) aggradational river terrace (c.f., Milne, 1973a) and are overlain by two loess layers, with the upper containing Kawakawa Tephra (27.1 ka; Lowe et al., 2008), which indicates an emplacement age of >50 ka during a warm and humid climate.

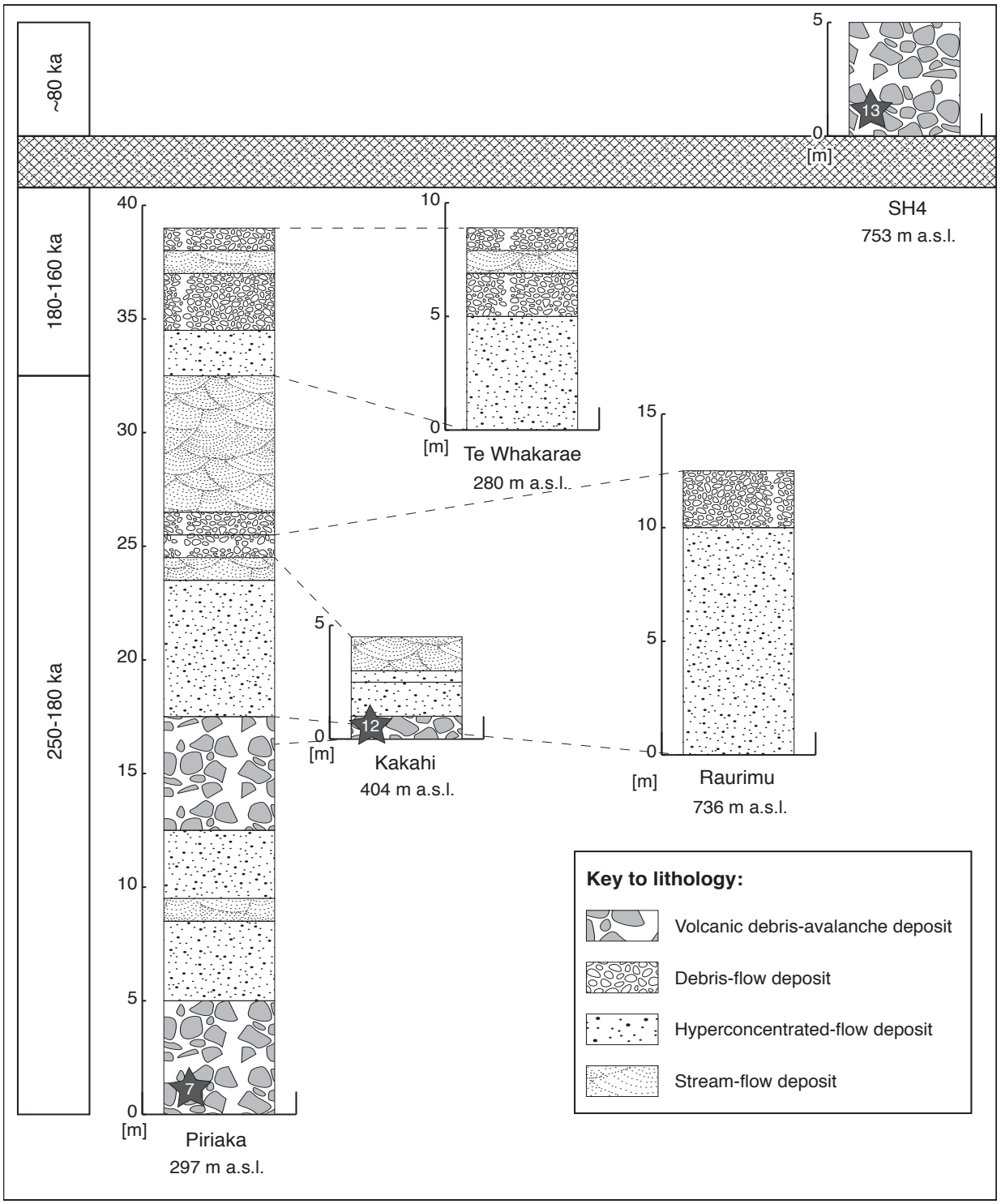

Figure 26. Stratigraphy of the Piriaka Formation. The c. 40 m thick sequence forms a distinctive plateau between Piriaka and Te Whakarae. The lithology of the individual units reflects several large-scale sub-plinian to plinian eruptions of Mt. Ruapehu, which were followed by periods of subdued volcanic activity. The stars outline mass-flow units sampled for Ar-dating, and the given numbers correspond to Table 8 and Fig. 22.

5.4 Reconstruction of cone-building and collapse with new volcaniclastic stratigraphy

This study demonstrates how $^{40}Ar/^{39}Ar$ dating of coarse-grained volcaniclastic mass-flow deposits, along with stratigraphic and lithologic analyses, allows the reconstruction of >50 ka eruption episodes of Mt. Ruapehu. The stratigraphic record exposed within river valleys on the distal Ruapehu ring plain reveal hitherto unknown periods of constructional eruptive activity and subsequent destructive collapse phases of the stratovolcano. The ages obtained with the $^{40}Ar/^{39}Ar$ method correspond to the time of crystallization of the individual clasts, not the emplacement of volcaniclastic mass-flow sequences within the river valleys. The mass-flow deposition ages can, however, be estimated in a number of cases from cover-bed stratigraphy and the terrace level (e.g., Milne, 1973; Pillans, 1983; 1994). This study has enabled the identification of three hitherto unknown eruptive episodes of Mt. Ruapehu, as well as periods of rapid ring-plain aggradation during the earlier history of the composite cone (Fig. 28). A more detailed understanding has been obtained of the eruptive intervals within individual cone-building episodes. The detailed mass-flow chronology of Mt. Ruapehu >50 ka is outlined in Table 9.

5.4.1 The Turakina eruptive interval (340 - 280 ka)

The pumice-rich lithology and stratigraphic position of the debris-flow deposit exposed c. 1.5 km northwest of Turakina are evidence that major plinian to sub-plinian eruptions of Mt. Ruapehu occurred 340 - 310 ka ago. This hitherto unknown explosive period of the stratovolcano will be referred to as the Turakina eruptive interval (Fig. 28A). The debris-flow deposit is located c. 90 km south of the stratovolcano, which indicates voluminous remobilisation of volcaniclastic material (>1 km^3), potentially associated with syn-eruptive collapse of a southern ancestral Mt. Ruapehu flank. The collapse generated a debris avalanche, which was likely channelized within the proto-Turakina valley, leading to a long runout (c.f., Tost et al., 2014). The extent of the deposit suggests the existence of a mature ancestral Mt. Ruapehu edifice >340 ka ago. The Turakina eruptive interval was followed by a period of eruptive quiescence, although smaller-scaled activity (VEI ≤2) may have occurred, depositing tephra and volcaniclastics near the volcano.
A conglomerate underlying the Mataroa Formation, with clasts dated at 283.5 ± 6.7 ka represents the next Ruapehu mass-flow deposit preserved. This occurs within the Hautapu River system. The well-sorted, clast-supported deposit with well-rounded clasts indicates a very water-saturated post-eruptive mass flow, originating from rainfall-induced remobilisation of eruptive products or glacial deposits.

5.4.2 The Te Herenga cone-building episode (250 - 180 ka)

Mass-flow deposits emplaced between 280 - 250 ka are not exposed within the volcaniclastic formations studied. Either the eruptive activity of Mt. Ruapehu was subdued during this period, depositing volcaniclastics solely in the proximity of the volcano, or mass-wasting deposits were subsequently eroded on the distal Ruapehu ring plain.
The oldest dated andesite lavas of mass-flow deposits related to the Te Herenga cone-building episode (250 - 180 ka; Gamble et al., 2003) are exposed within the proto-Hautapu River and the Whangaehu River catchments on the distal Ruapehu ring plain (Fig. 28B). Both deposits correspond to destabilisation of an ancestral Mt. Ruapehu edifice, which produced the

debris-avalanche deposits within the Mataroa Formation (Fig. 24) and the Lower Whangaehu Formation (Keigler et al., 2011; Tost et al., 2015). $^{40}Ar/^{39}Ar$-dating of lava clasts taken from the debris-avalanche deposits reveal ages of 236.5 ± 7.2 ka (Hautapu River), and 229.9 ± 3.3 ka and 218.7 ± 31.1 ka (Whangaehu River) (Table 8). The lithology of the deposits indicates that the mass flow was most likely triggered by weakening of the southeastern proto-Mt. Ruapehu flank

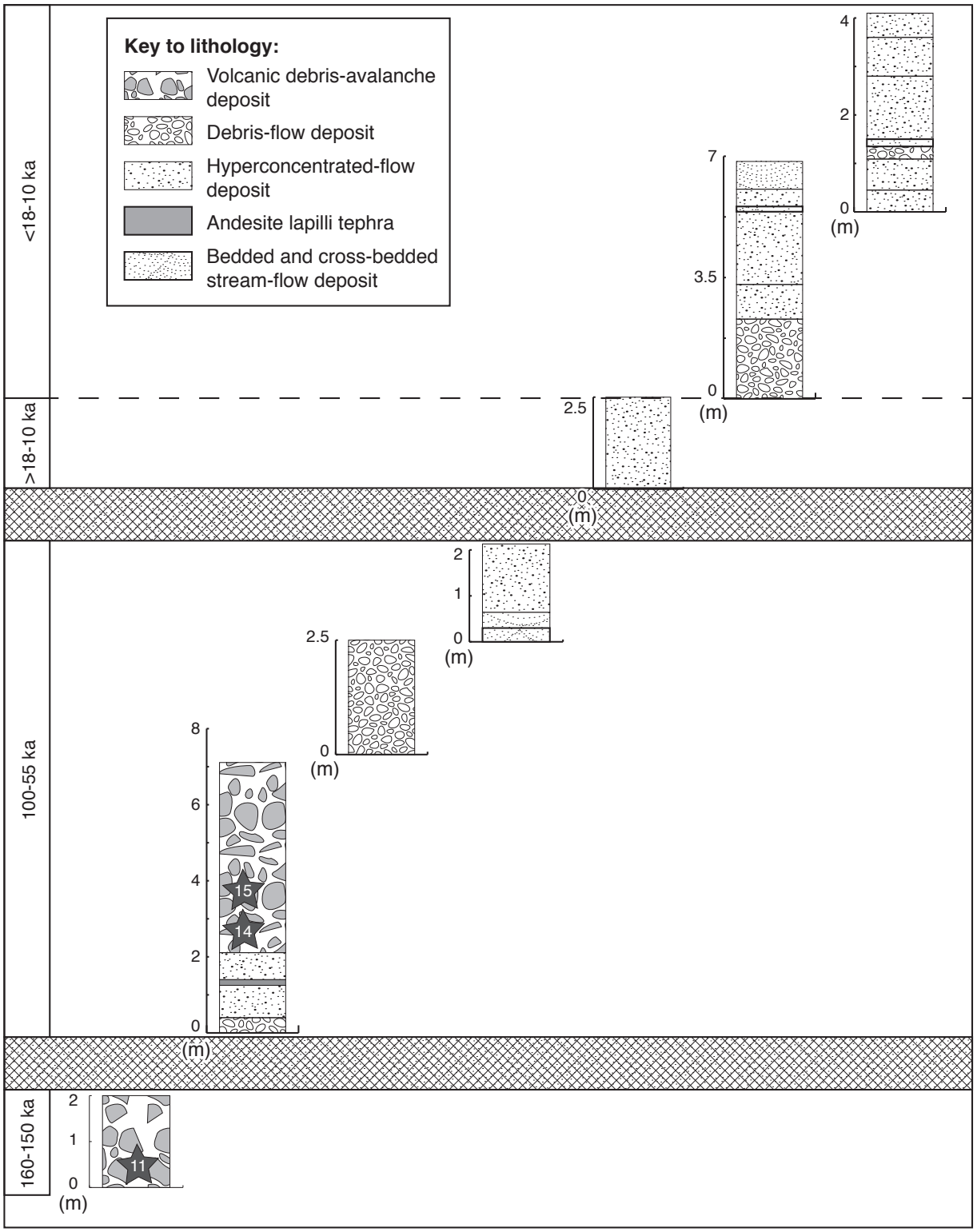

Figure 27. Stratigraphy of the Pukekaha Formation. Several exposures of volcaniclastics along the Manganuioteao River valley reveal that syn- as well as post-eruptive mass-flow deposits have been spilled into the river catchment between 160 ka ago and the present. The stars outline mass-flow units sampled for Ar-dating, and the given numbers correspond to Table 8 and Fig. 22.

due to hydrothermal alteration. The collapse could possibly have been caused by magmatic unrest (Tost et al., 2015). The debris-avalanche deposits in the Whangaehu catchment directly overlie late-Pliocene mudstones and were the first known to have reached the distal Ruapehu ring plain. Above these chaotic mass-flow units, numerous pumice-rich hyperconcentrated-flow deposits occur in both river valleys (Hautapu and Whangaehu) (Fig. 23A), and indicate that vigorous explosive activity of the stratovolcano began after cone collapse. Rapid unloading of a large part of the proto-Ruapehu edifice could have decompressed the magmatic system, triggering large pumice-producing eruptions (VEI 3 - 4).

The debris-avalanche deposit that makes up the basal unit of the Piriaka Formation must relate to a post-eruptive failure of an ancestral northwestern Mt. Ruapehu flank >180 ka ago (Tost et al., 2014). The absence of primary pumice within the deposit implies that the edifice collapsed due to weakening by hydrothermal alteration, potentially triggered by magmatic intrusion or large-scale tectonic activity. The overlying hyperconcentrated-flow deposits contain little or no pumice and appear to be sourced from ongoing remobilisation of material from the collapse scarp by heavy rainfall. Pumice lapilli occur within an overlying volcaniclastic conglomerate, suggesting a return to large, likely sub-plinian, eruptions at Mt. Ruapehu (producing pumice types and textures similar to those identified in the younger Bullot Formation, Pardo et al., 2014).

The early Piriaka episode of volcanic activity was followed by a period of eruptive quiescence, or at least only small-scaled eruptions (VEI ≤2) that were not recorded in the ring-plain stratigraphy. Ongoing weathering and hydrothermal alteration eventually led to a second collapse of the northwestern proto-Ruapehu flank, producing a second debris avalanche within the upper Piriaka Formation (Tost et al., 2014). Rapid unloading of the edifice resulted in a sudden highly explosive eruption.

On the southwest ring plain, a debris-avalanche deposit (within the Oreore Formation) with a similar age range to the Piriaka sequence contains a clast dated at 192.0 ± 7.3 ka and this was probably incorporated into the deposit during flank failure. Also at this time explosive sub-plinian eruptions deposited pumice on the proximal Ruapehu ring plain, and this material was incorporated in syn- and post-eruptive lahars that flowed down the proto-Hautapu (188.9 ± 11.0 ka) and the Whakapapa River catchments (181.6 ± 5.6 ka) (Fig. 28B).

5.4.3 The Oreore eruptive interval (180 - 160 ka)

Ruapehu was thought to have been dormant between 180 and 160 ka, or at least it was considered that there was little cone-building activity (Gamble et al., 2003). Deposits exposed within the Oreore Formation along the Mangawhero River and the Piriaka Formation along the Whanganui River (Fig. 28C) indicate, however, that large-scale volcanism continued during this period. This hitherto unknown eruptive episode is referred to here as the Oreore eruptive interval. The basal unit of the Oreore Formation is a syn-eruptive debris-avalanche deposit, containing many chilled-margin bomb clasts and pumice, as described in detail by Tost et al. (2014). The fresh clasts within this unit were dated at 178.4 ± 3.3 ka, 162.5 ± 5.2 ka, and 160.8 ± 9.6 ka, (Table 8). Magma ascent and inflation of Mt. Ruapehu are likely to have led to instability and collapse of the hydrothermally altered volcanic flanks, triggering a concurrent large sub-plinian

eruption (c.f., Mt. St. Helens, Voight et al., 1981). The freshly erupted pyroclastic material was incorporated into the debris avalanche and deposited along the proto-Mangawhero River, creating a localized hummocky topography. Sub-plinian to plinian eruptions (VEI 3 - 4) must have continued, with pumice re-deposited by lahars and hyperconcentrated flows, which buried the debris-avalanche deposit and smoothed its upper surface.

Stratigraphically correlated deposits of a similar pumice-rich nature occur along the proto-Whanganui River and Whakapapa catchments, indicating that much of the western ring plain was affected (Fig. 28C).

5.4.4 The Wahianoa cone-building episode (160 - 119 ka)

A major cone-building episode built up the southeastern sector of Mt. Ruapehu between 160 and 119 ka (e.g., Hackett & Houghton, 1989; Gamble et al., 2003). On the distal Ruapehu ring plain, mass flows associated with the Wahianoa cone-building formation are limited to the Manganuioteao, Whanganui, and Hautapu River catchments (Fig. 28D). Hodgson (1993) noted that lahar deposits emplaced between 140 - 25.5 ka ago are absent in the Whangaehu River valley and concluded that syn- as well as post-eruptive mass flows from Mt. Ruapehu solely spilled into the Hautapu River during this time. Tost et al. (2015) showed, however, that this was not the case, with deposits <125 ka being absent from the Hautapu catchment.

In the Manganuioteao River catchment (west of Mt. Ruapehu), a strongly weathered diamicton includes fresh, heat-fractured andesite lava blocks up to 3 m in diameter, which have been dated at 158.8 ± 4.7 ka, and this would indicate that eruptive activity was occurring at the stratovolcano at this time. The O'Leary Conglomerate in the Whanganui catchment has been interpreted to originate from a sector collapse of Mt. Ruapehu at 300 ka, based on the marine terrace chronology (Parish, 1994). However, our new age of 146.4 ± 4.9 ka for a lava clast within the unit indicates that the volcaniclastic deposit was emplaced within a channel cut into the older marine sequence.

At Hihitahi along the Hautapu River valley, the exposed upper portion of the Mataroa Formation is overlain by four paleosol and four loess layers (Fig. 24), indicating that numerous syn-eruptive lahars spilled into the Hautapu River >125 ka ago (Tost et al., 2015). The volcaniclastics here consist of several pumice-rich hyperconcentrated-flow deposits (Fig. 23L) that also include appreciable charcoal, likely resulting from re-deposition of pyroclastic fall and flow deposits from large-scale sub-plinian to plinian activity of Mt. Ruapehu (VEI 4).

5.4.5 The Waimarino eruptive interval (100 - 55 ka)

Cone-building lavas emplaced between 119 ka and 55 ka ago are absent on the Mt. Ruapehu massif; therefore, this was interpreted to indicate an interval of volcanic dormancy (Hackett & Houghton, 1989; Gamble et al., 2003). Several lahar sequences are known to have been emplaced on the surrounding Ruapehu ring plain during this period (Fig. 28E) (e.g., Hodgson & Neall, 1993; Cronin et al., 1996; Lecointre et al., 1998). Dated andesitic lavas from the Pukekaha and Piriaka Formations, in addition to the stratigraphy of mapped mass flows

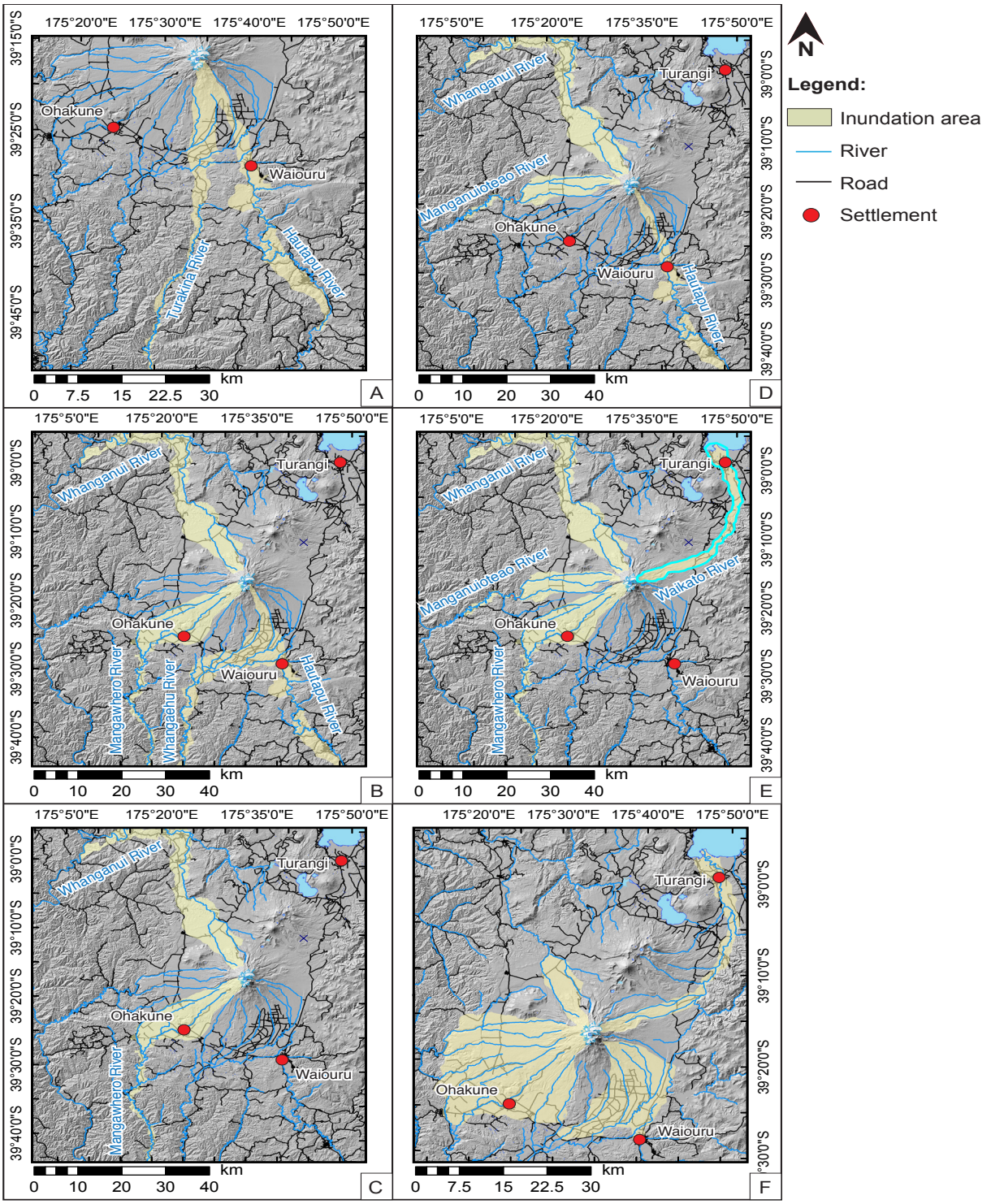

Figure 28. Digital elevation model of the Ruapehu ring plain outlining the mass-flow inundation areas during individual eruptive episodes. (A) Mass flows spilled into the Turakina and Hautapu River valleys during the Turakina eruptive interval 280-340 ka ago. (B) Mass-wasting events during the Te Herenga cone-building formation (250-180 ka; Gamble et al., 2003) were confined to the Hautapu, Whangaehu, Mangawhero, Whakapapa and Whanganui River valleys. (C) During the Oreore eruptive interval (180 - 160 ka) diamictons were emplaced in the Mangawhero, Whakapapa and Whanganui River catchments. (D) Mass-wasting deposits related to the Wahianoa cone-building formation are exposed along the Hautapu, Manganuioteao, Whakapapa and Whanganui River valleys. (E) Rapid ring-plain aggradation occurred in the southwestern to northeastern sector of the Ruapehu ring plain during the Waimarino eruptive interval (100-55 ka ago). (F) Post-50 ka mass-wasting events are generally limited to the proximal Ruapehu ring plain.

around the volcano, reveal three individual episodes of Ruapehu activity between 100 ka and 55 ka ago. These are collectively referred to here as the Waimarino eruptive interval. The first stage occurred >80 ka ago and is associated with emplacement of a coarse, pumice-rich diamicton unit, within the upper Tongariro River catchment (Cronin et al., 1996). The lithology of the unit suggests a syn-eruptive origin. This unit is overlain by a c. 1 m-thick lignite sequence, indicating a period of subdued volcanic activity (Cronin et al., 1996). The authors noted several tephras within the paleo-swamp deposit, but interpreted them as Mt. Tongariro units, due to significant hornblende-content.

The second stage of the Waimarino cone-building formation, between 80 - 65 ka ago, is represented by a rapid volcaniclastic aggradation of lahar deposits into the Tongariro catchment (Cronin et al., 1996), the Whakapapa River (this study), the Waimarino River (e.g., Grindley, 1960; Hay, 1967; Lecointre et al., 1998), the Manganuioteao River (Lecointre et al., 1998; this study), and the Mangaturuturu River (e.g., Grindley, 1960; Hay, 1967; Lecointre et al., 1998). A major diamicton sequence exposed along State Highway 4 contains a clast dated at 79.0 ± 9.6 ka. The absence of pumice within the sequence suggests it was formed either by remobilisation of dome-forming deposits or fractured lavas.

On the western Ruapehu ring plain, the stratigraphically corresponding sequence of mass-flow deposits was mapped as the Waimarino Formation (Grindley, 1960; Hay, 1967; Lecointre et al., 1998). This forms a distinctive terrace between Whakapapa Village and National Park to the north, and Ohakune and Raetihi to the south (Fig. 22; 28E). The 50 m-thick deposit covers an area of 60 km^2, with a combined volume of 12 km^3 (Lecointre et al., 1998). The mix of boulder-rich debris-flow units and sandy pebble- and cobble-rich hyperconcentrated-flow deposits indicate a period of rapid aggradation associated with extensive volcanic activity at Mt. Ruapehu. A similar suite of deposits estimated to be between 80 - 65 ka in age was described on the northeastern ring plain, although these occur on the down-wind side of the volcano, and are poor in pumice (Cronin et al., 1996).

The third stage of the Waimarino cone-building episode, between 65 and 55 ka, was related to major eruptive activity of the composite massif. The diamicton sequence exposed within the upper Waikato River (upper Tongariro catchment) is intercalated with numerous andesitic pumice-lapilli fall units, indicating explosive subplinian to plinian activity of Mt. Ruapehu (Cronin et al., 1996). These authors interpreted a gradual reduction in magnitude and/or frequency of the eruptions. At the same time, identical loess cover-bed stratigraphy shows that multiple fine-grained, hyperconcentrated-flow deposits were emplaced in the proto-Mangawhero and Makotuku River catchments (Fig. 23K; 28E).

Also belonging to this time interval, the Pukekaha debris-avalanche deposit emplaced to the west of Ruapehu has a high content of chilled-margin blocks and pumice, with clasts dated at 65.0 ± 10.8 ka and 50.4 ± 10.5 ka ago. These lithological characteristics and the subsequent pumice-rich (and charcoal-bearing) hyperconcentrated-flow deposits indicate an origin during large-scale sub-plinian eruptions. This deposit also includes common hydrothermally altered clasts and dark-red sintered clay (Tost et al., 2014), indicating the presence of an active hydrothermal system on the proto-Mt. Ruapehu. Bertolani and Loschi-Ghittoni (1986) concluded

Table 9. Stratigraphic column of mass-flow deposits emplaced on the proximal and distal Ruapehu ring plain between 340 - 55 ka (RPA = ring-plain aggradation).

Cone-building formation	Eruptive interval	Eruptive activity	River valley	Volcaniclastics
	Turakina (340-280 ka)	Plinian	Turakina River	debris-flow deposit
		RPA	Hautapu River	conglomerate
Te Herenga (250-180 ka)		RPA	Hautapu River & Whangaehu River	debris-avalanche deposit hyperconcentrated-flow deposit
		Sub-plinian		debris-flow deposit debris-flow deposit hyperconcentrated-flow deposit debris-flow deposit hyperconcentrated-flow deposit
		RPA	Whanganui River	debris-avalanche deposit hyperconcentrated-flow deposit fluvial deposit hyperconcentrated-flow deposit
		Sub-plinian		debris-avalanche deposit hyperconcentrated-flow deposit fluvial deposit debris-flow deposit debris-flow deposit fluvial deposit
	Oreore (180-160 ka)	Plinian to sub-plinian	Mangawhero River	debris-avalanche deposit hyperconcentrated-flow deposit conglomerate hyperconcentrated-flow deposit
			Whanganui River	hyperconcentrated-flow deposit debris-flow deposit fluvial deposit hyperconcentrated-flow deposit
Wahianoa (180-119 ka)		Sub-plinian to plinian	Manganuioteao River	diamicton
			Whanganui River	debris-flow deposit
			Hautapu River	hyperconcentrated-flow deposit
	Waimarino (100-55 ka)	Sub-plinian	Waikato River	debris-flow deposit
		RPA	Waikato River	individual sequences of debris-flow and hyperconcentrated-flow deposits
			Whakapapa River	
			Manganuioteao River	
			Waimarino River	
			Mangaturuturu River	
		Plinian	Manganuioteao River	hyperconcentrated-flow deposit tephra deposit hyperconcentrated-flow deposit debris-avalanche deposit fluvial deposit hyperconcentrated-flow deposit
		Sub-plinian	Waikato River	tephra deposit
			Mangawhero River	hyperconcentrated-flow deposit

that residual clays could derive from hydrothermal or lateritic transformation of volcanic and sedimentary rocks, and noted that these are generally kaolinitic and frequent in still-active hydrothermal systems. When heated above 1250°C, the residual clays become dark-red in colour and show melting along cracks.

5.4.6 Post-50 ka ring-plain stratigraphy

Numerous stacked volcaniclastic sequences, made up of laharic, fluvial, as well as tephra deposits, were previously identified within steep river catchments on the proximal Ruapehu ring plain and date back as far as 50 ka (e.g., Palmer, 1991; Donoghue et al., 1995; Cronin & Neall, 1996; Lecointre et al., 1998; Donoghue & Neall, 2001; Pardo et al., 2012). These deposits indicate frequent and ongoing eruptive activity of the stratovolcano during the Mangawhero and Whakapapa cone-building formations, 55 - 15 ka and <15 ka, respectively (Gamble et

al., 2003). The most violent activity of the stratovolcano known during this episode occurred between 14.7 ka and 11.9 ka and produced the pumiceous tephra sequence of the Bullot Formation, as well as pumice-rich syn-eruptive hyperconcentrated flows that spilled into the Tongariro and Whangaehu Rivers (e.g., Cronin & Neall, 1996; Donoghue & Neall, 2001; Pardo et al., 2012). Rapid volcaniclastic aggradation due to mass wasting occurred in all sectors of the proximal ring plain (Fig. 28F). Mass-flow deposits emplaced on the distal Ruapehu ring plain, however, are rare and limited to the Whangaehu River and Tongariro River valleys (e.g., Campbell, 1973; Hodgson, 1993; Cronin & Neall, 1996). The extent of the mass flow and tephra deposits emplaced post-50 ka reflect the modern record of Ruapehu activity and, moreover, indicate the magnitude of eruptive activity and mass wasting associated with the mass-flow formations of the older volcaniclastic record (>50 ka).

5.5 Conclusions

Mt. Ruapehu is a complex and long-lived composite cone made up of lava-flow sequences interlayered with primary and reworked volcaniclastic units (e.g., Gamble et al., 1999). The historic and geological record of the stratovolcano <50 ka is well known (e.g., Palmer, 1991; Cronin et al., 1996; Cronin & Neall, 1997; Lecointre et al., 1998; Gamble et al., 1999; Waight et al., 1999; Donoghue & Neall, 2001; Pardo et al., 2012), whereas its older explosive eruptive history is not well understood. Present eruptions of Mt. Ruapehu are produced by small (~0.05 km^3) magma batches, and deposition of volcaniclastic material is restricted to the proximity of the volcano (e.g., Christenson et al., 2010; Kilgour et al., 2010; Price et al., 2012). Our new geological mapping, however, shows numerous exposures of volcaniclastics, up to 90 km from the edifice in all main catchments radiating from the edifice. These show evidence that multiple phase, larger-magnitude eruptions have been frequent in the history of the stratovolcano. These periods of activity have an analogy in the c. 10 - 30 ka episode of volcanism at Mt. Ruapehu, where hundreds of large sub-plinian eruptions occurred (e.g., Pardo et al., 2012), along with widespread deposition of debris flows and hyperconcentrated flows, rich in pumice.

Intercalating with these deposits of redistributed pumice are periodically emplaced major debris-avalanche units. Dating of fresh clasts from the debris-avalanche deposits and examining the deposit lithology allow development of a new timing and reconstruction of volcanic growth periods and identification of formerly unknown phases of activity and cone-growth at Mt. Ruapehu.

Three hitherto unknown eruptive episodes have been identified by this study: the Turakina eruptive interval (340 - 310 ka); the Oreore eruptive interval (180 - 160 ka); and the Waimarino eruptive interval (100 - 55 ka). The distal mass-flow deposits are generally only diagnostic for periods of large-volume (0.5 - 1 km^3) pumice lapilli producing sub-plinian eruptions of VEI >3 (i.e., similar to those known from the 30 - 10 ka Bullot Formation). Our results show that the eruptive activity of Mt. Ruapehu has been continuous since >340 ka, in contrast to conclusions reached by dating lavas on the cone, where large gaps in the chronology have been interpreted to indicate quiescent periods. The difference between the ring plain and lava flow sequence records is explained by periodic massive flank collapses, which would erase evidence of eruption episodes on the cone, but deposit re-worked material on the distal ring plain.

This work shows how edifice-based radiometric studies must be combined with parallel work on the distal ring plain in order to construct a comprehensive eruptive history of long-lived stratovolcanoes. The repeating sequence shown at Mt. Ruapehu leads to a new view of ongoing growth and destruction of this volcano, with periods of explosive volcanism following major collapse events. The periodicity of these large-scale episodes is roughly 60 - 90 kyr.

CHAPTER 6: NEW INSIGHTS INTO THE EVOLUTION OF THE MOUNT RUAPEHU MAGMATIC SYSTEM REVEALED BY DISTAL MASS-FLOW DEPOSITS

6.1 Introduction

Stratovolcanoes are large, complex constructional edifices of lava and pyroclastic deposits, with associated reworked volcaniclastic units that build up over hundreds of thousands of years from sporadic eruption episodes (e.g., Coats, 1950; Gamble et al., 1999). These large mountains, however, generally only represent a fraction of the underlying long-lived magmatic system. The bulk volume of magma erupted from stratovolcanoes is typically found within volcaniclastic and pyroclastic deposits that make up their surrounding ring plains or fans (e.g., Mt. Ruapehu and Tongariro, New Zealand, Donoghue et al., 1995, Cronin & Neall, 1997; Mayon, Phillippines, Arguden & Rodolfo, 1990; Mt. St Helens, USA, Janda et al., 1981; and Mt. Taranaki, Zernack et al., 2011). In particular, lahars and volcanic debris avalanches can transport eruptive products hundreds of kilometres from their volcanic source (e.g., Mothes et al., 1998; Rodolfo, 2000; Lecointre et al., 2004; Doyle et al., 2009). For much of the early geological history of stratovolcanoes, these distal deposits may represent the only record of volcanism, with deposits on the edifice buried, eroded, or hydrothermally altered (Zernack et al., 2011). On the Mt. Taranaki edifice in the western North Island of New Zealand, for example, lavas up to 14 ka B.P. in age are exposed, whereas the ring plain deposits extend to at least 170 ka (Zernack et al., 2009).

Mt. Ruapehu is one of the most active composite cones in New Zealand and its magmas have petrological characteristics similar to those of continental arc lavas worldwide, with an ultimate origin from mantle-derived basaltic melts (e.g., Graham & Hackett, 1987; Gamble et al., 1999; 2003; Price et al., 2005; 2007; 2012). All petrological and geochemical studies on Mt. Ruapehu have focused on the lava-flow sequences exposed on the cone, which extend to a maximum age of c. 250 ka (e.g., Cole et al., 1983; Graham & Hackett, 1987; Hackett & Houghton, 1989; Price et al., 1999a; Gamble et al., 2003; Price et al., 2012). The stratigraphy and chronology developed for Mt. Ruapehu from the cone lavas show several gaps or periods for which there is little information. A more detailed chronology has been recently established based on dated mass-flow deposits exposed within river catchments dissecting the volcaniclastic ring plain surrounding the composite massif (Chapter 5). Presented here is new information on parts of the geochemical record not previously described for Ruapehu volcano. These data have been obtained through sampling and analysis of lava clasts from newly mapped and dated long-runout mass-flow deposits. In particular, the new data provide further insights into the older (>50 ka) volcanic record of Mt. Ruapehu. This rarely used approach enables significant extension of magmatic histories at long-lived stratovolcanoes. Lava fragments within distal volcaniclastic deposits may provide the only means of sampling the initial stages of magma development of such composite cones, as well as large parts of the cone that have collapsed in debris avalanches.

6.1.1 Geological Setting

In terms of geological structure, Mt. Ruapehu is a typical composite cone/stratovolcano (Cole, 1978; Smith et al., 1999). Its broad summit hosts three explosive vents (Nairn, 1975), but the

Table 10. The eruptive episodes of Mt. Ruapehu in correlation to the depositional ages of the mass-flow deposits sampled.

Eruptive episode	Age (ka)	Mass-flow formation	Sampled deposit	Age (ka)
Turakina	340-280*	Turakina*	Debris flow	340-310*
Te Herenga	250-180**	Mataroa*,***	Debris avalanche; debris flow	230-190*
		Lower Whangaehu****	Debris avalanche; debris flow	230-220*
		Piriaka*,*****	Debris avalanche; debris flow	250-190*
Oreore	180-160*	Oreore*****	Debris avalanche	180-160*
Wahianoa	160-119**	N/A	N/A	N/A
Waimarino	100-55*	Pukekaha*****	Debris avalanche	50-70*
Mangawhero	55-15**	N/A	N/A	N/A
Whakapapa	<15**	N/A	N/A	N/A

*based on stratigraphiy and $^{40}Ar/^{39}Ar$-dating; Chapter 5

**based on K/Ar-dating; Gamble et al. (2003)

***after Tost et al. (2015)

****after Hodgson (1993); Keigler et al. (2011)

*****after Tost et al. (2014)

southernmost of these is the site of hundreds of recent eruptions and is normally filled by the acidic Crater Lake (Cole, 1978). Seismic (Villamor & Berryman, 2006a, 2006b; Salmon et al., 2011), as well as xenolith petrology, studies show that the basement beneath the volcano is c. 40 km thick and made up of Mesozoic greywacke (upper to middle crust) underlain by a meta-igneous lower crust (Graham & Hackett, 1987; Graham et al., 1990; Adams et al., 2007; Price et al., 2012). At present, Mt. Ruapehu's volcanic activity is characterised by frequent small-scale eruptions (<0.05 km^3), occurring at decadal intervals and each lasting for several months (e.g., Lecointre et al., 2004).

Four major cone-building episodes have been identified and mapped on the Mt. Ruapehu edifice (Fig. 3); from oldest to youngest, these are: the Te Herenga Formation (250 - 180 ka), the Wahianoa Formation (160 - 115 ka), the Mangawhero Formation (55 - 45 ka; 30 - 15 ka), and the Whakapapa Formation (<15 ka) (Hackett & Houghton, 1989; Gamble et al., 2003). The precise timing for the onset of volcanism of Mt. Ruapehu is not unequivocally established. The oldest lavas sampled and dated from the cones of Tongariro and Mt. Ruapehu are 260 ± 3 ka, and 230 ± 1 ka in age, respectively (Stipp, 1968). Pebbles of labradorite-pyroxene andesite occur within distal mass-flow deposits exposed c. 100 km southwest of Mt. Ruapehu and hint at an even earlier stage of volcanic activity at c. 300 ka (Fleming, 1953; Cole, 1978; Tanaka et al., 1997; Gamble et al., 2003).

Petrologically, the Mt. Ruapehu lava-flow sequences comprise dominantly plagioclase-pyroxene-phyric, plagioclase-phyric, and pyroxene-(olivine)-phyric lavas, although pyroxene-phyric, olivine-pyroxene-phyric, and rare hybrid andesite rock types have also been found and these seem to correspond to particular cone-building formations (Graham & Hackett, 1987; Graham et al., 1995; Gamble et al., 2003; Price et al., 2012). The lavas become progressively more enriched in SiO_2, K, Rb, and Sr over time, although the geochemistry varies widely within each of the major eruptive episodes, apart from the Te Herenga Formation (Fig. 4) (Gamble et al., 2003; Price et al., 2005; 2012). The calc-alkaline lavas of Mt. Ruapehu have higher alkali and light rare earth element (LREE) concentrations than lavas from the intra-oceanic Tonga-Kermadec arc to the north of New Zealand (Ewart & Stipp, 1968; Cole, 1982). Hence, the temporal geochemical and petrographic variations at Mt. Ruapehu have been interpreted

to reflect open-system processes within a complex plumbing system, comprising numerous small dykes and sills distributed throughout the crust and upper mantle beneath the volcano (Price et al., 1997; Gamble et al., 1999; 2003; Price et al., 2005; 2007; 2012). This is consistent with seismic anisotropy measurements, which suggest dyke-like structures at less than 10 km beneath the edifice (Miller & Savage, 2001; Gerst & Savage, 2004). Stagnant melt is thought to crystallize and fractionate in these small isolated pockets, assimilating surrounding wall rock, xenoliths and xenocrysts, and mingling with fresh magma intrusions (Graham & Hackett, 1987; Gamble et al., 1999; Price et al., 2005; 2012). Disequilibrium in Th and U isotopes shows that these processes operate over tens of thousands of years in magmas prior to their eruption (Price et al., 2007). The magma associated with the oldest Te Herenga Formation apparently records the first stage of mantle/crust interaction as magma migrated into the lower crust and small magma chambers began to evolve at different levels within the middle and upper crust (Price et al., 1997; Gamble et al., 1999; Price et al., 2005). The scarcity of hornblende in Mt. Ruapehu lavas has been interpreted to indicate that crystallization occurred from water-undersaturated melts (2 - 5 wt.%) (Graham et al., 1995). Petrological and geochemical studies suggest that crystallization temperatures ranged between 1200°C and 1050°C and crystallization pressures were below 10 kbar (Green & Hibberson, 1969; Lindsley, 1983; Graham & Hackett, 1987).

6.1.2 Distal mass-flow deposits

Five individual mass-flow deposit sequences from Mt. Ruapehu, which were emplaced between 340 and 60 ka, occur along six major river valleys that radiate outward from the south to west flanks of the volcano (Tost et al., 2014; 2015) (Fig. 22). The mass-flow formations comprise debris-avalanche deposits (Keigler et al., 2011; Tost et al., 2014), overlying and/or underlying debris-flow deposits and hyperconcentrated-flow deposits (Keigler et al., 2011; Tost et al., 2015; Chapter 5). Additionally, outcrops c. 1.5 km northwest of Turakina (Fig. 22) reveal a debris-flow deposit overlain by two dated rhyolitic tephra layers (Middle Griffin Road Tephra and Fordell Ash, 300 ka; Bussell & Pillans, 1992). Some of these older sequences have been cut off from the modern Mt. Ruapehu because of tectonic motion and river capture (Tost et al., 2015). In each case, the main mass-flow deposit of the sequence is poorly sorted and unbedded, with large clasts (≤4 m) supported in a sand-silt matrix (Keigler et al., 2011; Tost et al., 2014; 2015). The deposits contain dominantly volcanic lithologies, including lava blocks and pumice with a range of textures. Several units contain jigsaw fractured angular blocks and poorly to well rounded andesite lava fragments (66 - 90 vol.%), along with hydrothermally altered clasts (≤5 vol.%), ripped up river gravel (≤10 vol.%) and Tertiary sediment (≤15 vol.%). Some units contain variably weathered angular to subrounded pumice (≥20 vol.%). A detailed description of the sampled mass-flow deposits, their age, and relation to the Mt. Ruapehu cone-building formations is outlined in Table 10.

6.2 Analytical methods

Samples for geochemical and petrological analysis were taken from angular to subrounded lava blocks (30 - 200 cm diameter) and the freshest possible angular pumice (≥10 cm) at all of the debris-avalanche sites and the Turakina debris-flow deposits (Fig. 22). Polished thin sections for petrographic and electron microprobe (EMP) analysis were prepared at the University of

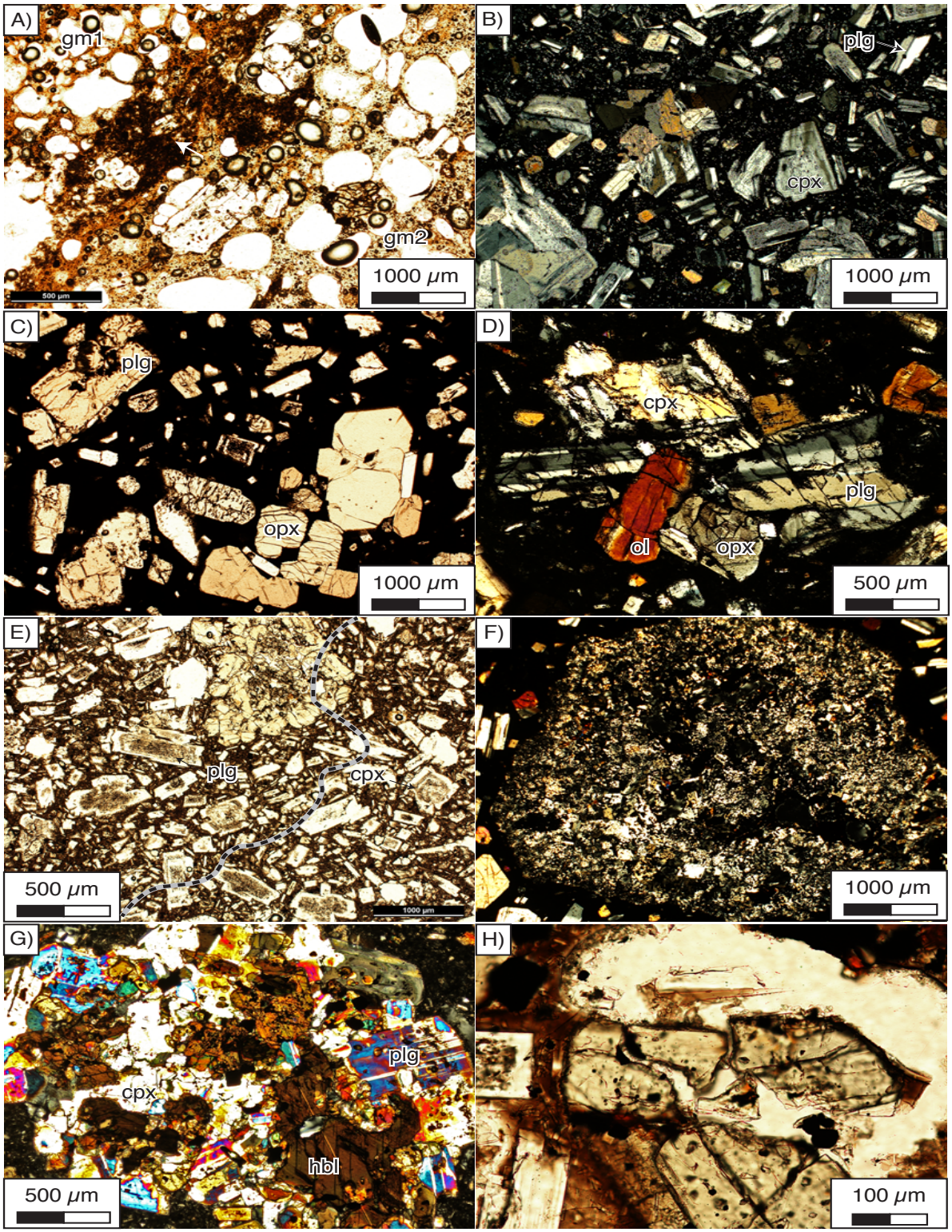

Figure 29. Photomicrographs of clasts from the Ruapehu mass flows. (A) Samples with two different groundmasses are exposed within the Turakina eruptive episode, the Oreore Formation, and the Pukekaha Formation. Pyroclasts contain up to 40% subrounded, and in part elongated vesicles. (B) Typically, phenocrysts are subhedral and the groundmass microcrystalline. (C) A hyaline groundmass is limited to samples taken from initial pyroclasts. (D) Clasts from lava flow sequences are generally porphyritic and comprise sieve-textured plagioclase and pyroxene phenocrysts. (E) Glomerocrysts are made up of plagioclase + orthopyroxene + clinopyroxene + olivine. (F) Fine-grained meta-sedimentary xenolith. (G) Meta-igneous hornblende-bearing xenolith. (H) Ruptured phenocrysts within initial pyroclasts testify to explosive eruptions.

Ballarat, Victoria, Australia. After careful selection of non-weathered samples, 103 rocks were cut and the central c. 3 x 3 x 3 cm portions were crushed and ground in a tungsten carbide ring mill at the University of Auckland, New Zealand. Contamination of trace elements during the crushing process is limited to W and Co, while contamination of Ta and particularly Nb is negligible (Roser et al., 2003; Martin et al., 2013). Images of thin sections were obtained with a Nikon DS-U1 digital camera attached to a Nikon Eclipse E600 POL microscope. Major (e.g., Si, Al, Mg, Fe, Ca, K and Na) and minor element concentrations (e.g., Ti, Mn, P and S) were obtained as oxide components on whole rock samples at the University of Auckland, New Zealand, using X-ray fluorescence (XRF) and methods similar to those described by Norrish and Hutton (1969). In general, precision for each major or minor element is determined by repeated analyses of standard rock, is better than ±4% (RSD), and the accuracy better than 5% at the 95% confidence level.

Hornblende analyses were obtained with a JEOL JXA-840A electron microprobe (EMP) at Massey University, Palmerston North, New Zealand, using a LINK systems LZ5 detector, a QX2000 pulse processor and ZAF-4/FLS matrix correction software. Standard operating conditions include an accelerating voltage of 15 kV, a beam current of 0.5 nA, a beam diameter of 3 μm, and a live count time of 100 s. Calibration was performed using a suite of AstimexTM mineral standards. The estimated precision for oxide analyses obtained by EMP is better than ±3%. The $^{40}Ar/^{39}Ar$-age of hornblende was obtained at the OSU Argon Geochronology Laboratory, Oregon, USA, using an ARGUS VI multi-collector mass spectrometer. The selected sample was crushed and sieved to extract grains between 200 - 300 μm in size. Hornblende separates were obtained by hand-picking. The resulting ages were calculated using the ArArCALC v2.5.2 software package (Koppers, 2002), with precision being within ±2σ.

6.3 Petrology

The clasts sampled from the Ruapehu mass-flow deposits range from dense lava to pumice (up to 40% vesicles; Fig. 29A), but all are porphyritic with up to 10% phenocrysts in pumice and up to 45% in lavas. The phenocrysts vary between 0.4 - 2.0 mm in size, with assemblages including plagioclase + orthopyroxene + clinopyroxene + titanium magnetite ± olivine ± hornblende. Inequigranular and generally hypocrystalline textures dominate, comprising euhedral to subhedral phenocrysts within a microcrystalline and hyaline groundmass (Figs. 29B; 29C). Glomerocrysts are limited to samples from the Oreore and Pukekaha Formations (Fig. 29D). Holocrystalline xenoliths, up to 2 mm across, are common within all samples (2 - 15%) and comprise meta-sedimentary and meta-igneous rocks.

6.3.1 Phenocryst characteristics

Plagioclase is the most abundant mineral phase (60 - 65% on average), forming euhedral to subhedral phenocrysts, as well as groundmass microlites (Fig. 29). Carlsbad and albite twinning in association with oscillatory and complex zoning is common. Larger phenocrysts (>0.6 mm) are sieve textured, with especially strong corrosion in the crystal cores, which are commonly surrounded by fresh rims, although in rare cases the entire crystal shows partial resorption textures. The plagioclase phenocrysts in the Turakina debris-flow samples show the finest phenocrysts (rarely exceeding 0.4 mm) and few, if any, resorption textures (Fig. 29B).

Table 11. Representative major and trace element concentrations of lava and fresh pumice samples from the Ruapehu mass-flow deposits sampled here. A complete database is included in Appendix II.

	1	2	3	4	5	6	7	8	9	10	11	12
Formation	**Mataroa Formation**				**Whangaehu Formation**				**Oreore Formation**			
Sample no.	GW3b	GW3gr	MF3b	JW2b	MP3	MP4	TF2	TF8	KL5	KL6	KL8	KL9
SiO_2	58.53	58.70	58.71	58.72	57.64	57.64	57.79	57.42	53.52	53.64	52.53	52.93
TiO_2	0.60	0.65	0.73	0.58	0.75	0.64	0.60	0.63	0.64	0.69	0.64	0.64
Al_2O_3	19.25	17.56	17.90	17.22	17.64	19.24	16.30	17.62	18.59	18.26	17.04	17.29
Fe_2O_3	5.78	6.87	6.95	7.06	7.82	6.68	7.67	8.01	9.63	8.88	8.36	8.42
MnO	0.09	0.11	0.11	0.13	0.12	0.10	0.13	0.13	0.15	0.14	0.14	0.13
MgO	2.08	3.73	2.91	3.91	3.54	2.74	4.75	4.15	4.98	5.48	6.26	6.32
CaO	7.33	7.16	5.97	7.06	6.95	7.83	7.27	7.46	7.67	7.92	8.15	8.14
Na_2O	3.70	3.58	3.49	3.29	3.31	3.67	3.05	3.36	2.91	2.77	3.11	3.08
K_2O	1.21	1.10	1.47	1.09	1.38	1.07	1.38	1.07	0.29	0.68	0.62	0.58
P_2O_5	0.12	0.11	0.12	0.10	0.12	0.13	0.11	0.11	0.08	0.08	0.06	0.06
H_2O	0.26	0.12	0.74	0.19	0.32	0.21	0.25	0.12	0.43	0.44	1.22	0.84
LOI	0.94	0.20	0.78	0.58	0.30	-0.06	0.58	-0.20	1.03	0.90	1.76	1.44
Total	99.89	99.88	99.88	99.91	99.88	99.88	99.87	99.89	99.90	99.88	99.89	99.87
Be	0.84	0.85		0.92								
Cs	1.65	1.46	2.76	1.79	2.08	1.02	2.36	1.10	0.49	1.50	1.25	1.04
Ba	309	273	402	282	299	338	335	292	236	282	235	260
Rb	30	29	48	30	39	25	39	30	4	19	16	14
Sr	261	229	253	221	266	310	267	253	218	267	257	251
Pb	7.97	7.97	68.20	8.06	10.53	8.58	13.41	31.47	52.54	36.75	28.55	28.66
Th	2.75	2.77	5.53	2.95	4.43	3.39	4.28	3.20	1.84	4.28	3.41	3.43
U	0.85	0.83	1.33	0.89	0.98	0.78	1.08	0.83	0.39	0.85	0.87	0.91
Zr	72	73	126	74	102	80	94	82	64	96	85	84
Nb	3.22	3.39	4.94	3.30	4.14	2.89	3.45	2.98	2.15	3.97	3.23	3.23
Hf	2.00	2.04	3.38	2.08	2.80	2.16	2.54	2.23	1.81	2.67	2.41	2.34
Ta	0.31	0.34	0.41	0.44	0.33	0.21	0.29	0.24	0.17	0.31	0.24	0.26
Y	14	14	20	15	20	17	18	18	16	18	19	16
Sc	16.3	20.4	23.7	23.9	29.3	21.2	30.9	27.8	35.6	34.8	33.2	33.7
V	154	181	188	179	237	193	205	209	252	222	193	194
Cr	20	88	39	66	18	35	91	62	48	108	210	218
Co	58	42	73	95	42	40	48	50	41	54	76	62
Ni	15	35	27	23	11	20	29	23	25	35	65	59
Cu	31	35	28	28	18	41	21	32	48	41	45	40
Zn	72	77	182	90	88	76	97	237	177	180	168	164
Ga	17	17	18	16	18	18	17	17	17	18	17	17
La	8.18	7.73	12.71	7.99	11.12	10.27	11.55	9.02	4.84	11.13	8.77	8.25
Ce	17.79	17.50	27.57	16.99	22.58	19.96	20.96	17.94	11.43	23.54	20.27	20.49
Pr	2.14	2.04	3.27	2.09	2.81	2.63	2.71	2.34	1.77	3.09	2.47	2.45
Nd	9.50	9.06	14.38	9.07	12.38	11.71	11.64	10.39	8.61	13.76	11.25	10.82
Sm	2.45	2.32	3.54	2.39	3.12	2.78	2.82	2.65	2.49	3.35	2.89	2.73
Eu	0.74	0.70	0.90	0.69	0.86	0.89	0.79	0.81	0.85	0.92	0.78	0.82
Gd	2.34	2.25	3.45	2.43	3.15	2.82	3.00	2.67	2.68	3.20	2.88	2.86
Tb	0.39	0.38	0.58	0.39	0.54	0.49	0.50	0.49	0.47	0.57	0.53	2.05
Dy	2.52	2.46	3.69	2.59	3.70	3.24	3.21	3.18	3.19	3.64	3.31	3.29
Ho	0.53	0.55	0.74	0.56	0.77	0.68	0.68	0.69	0.65	0.76	0.74	0.69
Er	1.53	1.60	2.20	1.76	2.20	1.91	1.96	1.99	1.99	2.23	2.19	2.08
Tm	0.25	0.25	0.33	0.27	0.33	0.31	0.32	0.30	0.28	0.33	0.33	0.31
Yb	1.65	1.62	2.25	1.77	2.10	1.90	1.97	2.06	1.96	2.24	2.19	2.06
Lu	0.27	0.25	0.33	0.26	0.33	0.29	0.30	0.32	0.30	0.32	0.32	0.30

Table 11 (continued). Representative major and trace element concentrations of lava and fresh pumice samples from the Ruapehu mass-flow deposits sampled here. A complete database is included in Appendix II.

	13	14	15	16	17	18	19	20	21	22	23	24
Formation	**Piriaka Formation**				**Pukekaha Formation**				**Turakina Formation**			
Sample no.:	PI3	PI4	PL2	KA1	RB2	RB5	MA1	MA3	TUR_01	RAT_01	RAT_02	RAT_03
SiO_2	57.30	57.53	57.28	57.52	58.16	57.91	57.97	57.95	58.65	58.65	56.91	59.31
TiO_2	0.62	0.55	0.58	0.64	0.77	0.72	0.72	0.74	0.64	0.49	0.53	0.49
Al_2O_3	17.43	17.55	16.85	17.35	16.72	14.74	15.20	14.85	17.91	17.77	17.51	16.47
Fe_2O_3	7.88	8.28	7.89	8.07	6.79	7.26	7.27	7.23	6.80	7.00	7.30	6.69
MnO	0.12	0.13	0.13	0.12	0.10	0.11	0.12	0.11	0.11	0.12	0.11	0.11
MgO	4.37	4.16	4.97	4.21	4.19	6.95	6.17	6.63	3.36	3.05	4.22	4.13
CaO	7.41	7.66	7.76	7.02	6.86	7.16	7.50	7.33	7.15	6.67	7.47	6.89
Na_2O	3.37	3.37	3.25	3.42	3.32	2.98	3.03	3.01	3.49	3.45	3.23	3.48
K_2O	1.03	0.64	0.93	1.04	1.78	1.62	1.60	1.60	1.07	0.81	0.77	0.88
P_2O_5	0.11	0.08	0.11	0.11	0.16	0.14	0.14	0.14	0.11	0.10	0.09	0.10
H_2O	0.20	0.15	0.16	0.31	0.40	0.08	0.12	0.19	0.17	0.34	0.44	0.27
LOI	0.06	-0.20	-0.02	0.07	0.63	0.16	0.02	0.04	0.43	1.47	1.31	1.08
Total	99.90	99.91	99.88	99.89	99.87	99.85	99.85	99.84	99.88	99.91	99.88	99.90
Be												
Cs	1.43	0.34	1.24	1.01	3.59	3.56	2.31	3.13	1.75	1.60	1.43	1.32
Ba	264	200	283	260	349	319	337	328	296	234	247	276
Rb	26	14	24	28	61	58	54	55	31	25	22	22
Sr	250	219	249	236	261	218	248	233	265	212	243	247
Pb	24.86	31.45	25.56	5.71	9.44	8.60	8.17	8.50	14.31	23.58	32.63	39.54
Th	2.57	1.25	2.29	2.39	5.94	5.41	5.28	5.14	3.19	2.05	2.31	1.78
U	0.68	0.41	0.64	0.73	1.61	1.53	1.47	1.46	0.79	0.62	0.63	0.58
Zr	74	52	70	70	128	114	115	115	86	68	72	65
Nb	2.67	1.60	2.22	2.41	4.67	4.10	4.07	4.05	3.47	2.80	2.65	2.12
Hf	2.14	1.52	1.87	1.96	3.45	3.17	3.12	3.19	2.38	1.88	1.95	1.80
Ta	0.21	0.11	0.18	0.17	0.35	0.32	0.31	0.32	0.29	0.19	0.21	0.15
Y	17	14	16	18	18	17	17	16	16	15	13	13
Sc	27.0	28.1	28.8	25.1	20.9	25.3	27.3	26.1	23.1	20.3	26.9	24.0
V	201	205	197	200	181	188	195	197	178	147	174	164
Cr	73	44	127	76	88	334	237	309	85	23	142	126
Co	46	41	43	47	63	63	43	40	57	39	67	51
Ni	50	27	42	36	51	125	86	105	33	20	63	51
Cu	35	67	51	46	41	54	45	78	34	27	30	32
Zn	177	236	178	64	54	51	53	54	173	191	203	233
Ga	17	16	17	16	17	15	15	15	17	16	17	15
La	7.30	4.11	7.00	7.26	13.23	11.60	10.93	11.21	8.53	6.11	6.21	5.86
Ce	15.81	9.04	14.84	15.12	28.66	24.74	23.59	24.46	18.49	12.53	13.22	12.57
Pr	1.97	1.23	1.96	2.09	3.48	2.97	2.90	2.94	2.28	1.63	1.62	1.61
Nd	9.40	6.04	9.25	9.59	14.86	13.03	12.43	12.77	9.95	7.38	7.45	7.22
Sm	2.52	1.73	2.53	2.52	3.34	3.15	2.95	2.93	2.51	1.98	1.93	1.94
Eu	0.73	0.58	0.76	0.77	0.83	0.72	0.79	0.75	0.74	0.64	0.64	0.65
Gd	2.60	2.07	2.59	2.68	3.20	3.00	2.86	2.82	2.57	2.18	2.10	1.99
Tb	0.46	0.37	0.41	0.48	0.51	0.49	0.49	0.47	0.46	0.38	0.39	0.34
Dy	2.94	2.50	2.79	2.88	3.25	3.06	3.09	2.97	2.91	2.60	2.39	2.20
Ho	0.62	0.53	0.61	0.63	0.64	0.61	0.62	0.60	0.63	0.60	0.51	0.48
Er	1.88	1.56	1.76	1.89	1.92	1.86	1.84	1.70	1.86	1.74	1.55	1.42
Tm	0.28	0.24	0.27	0.28	0.30	0.26	0.27	0.25	0.29	0.29	0.24	0.22
Yb	1.90	1.66	1.77	1.91	1.95	1.81	1.74	1.70	1.87	1.96	1.55	1.53
Lu	0.29	0.25	0.27	0.29	0.28	0.27	0.26	0.26	0.28	0.31	0.24	0.23

Pyroxene is also ubiquitous (15 - 20% on average) with both ortho- and clinopyroxene being present. Both pyroxene types occur as euhedral to subhedral phenocrysts and as groundmass microlites. Oscillatory, continuous and discontinuous zoning is common. Titanium magnetite is the most abundant mineral inclusion within the pyroxene phenocrysts and it occurs mainly along cleavages and/or phenocryst fractures. Rare inclusions of olivine are also present. Larger clinopyroxene phenocrysts (>0.6 mm) are commonly sieve textured, with corrosion strongest in the crystal cores (Figs. 29B; 29E).

Titanium magnetite is a common mineral phase (5% on average), occurring as euhedral to

subhedral and homogenous phenocrysts and as groundmass microlites. It also occasionally occurs as inclusions within plagioclase and pyroxene phenocrysts.
Olivine is rare to accessory and does not exceed 3% in volume. It is most abundant in samples of the Oreore Formation and almost entirely absent in clasts from the Mataroa, Lower Whangaehu, and Pukekaha Formations. When present, it forms small (<0.4 mm) euhedral phenocrysts or inclusions within clinopyroxene phenocrysts.
Hornblende is only present as an accessory phenocryst phase (≤1%) in some clasts of the Lower Whangaehu Formation, where it forms small (≤0.2 mm) subhedral crystals with thin outer reaction rims.

6.3.2 Groundmass characteristics

In lava samples the groundmass is microcrystalline and hyaline within pyroclast samples. The microcrystalline groundmass is dominantly plagioclase + titanium magnetite ± pyroxene and homogenous in clasts sampled from the Mataroa, Whangaehu, and Piriaka Formations. Samples from the Turakina debris-flow deposit, as well as the Oreore and Pukekaha Formations, show both microlite rich and hyaline textures (Fig. 29F).

6.3.3 Autolith characteristics

Autoliths, up to 2 cm in diameter, occur only in samples from the Piriaka Formation. They consist of inequigranuar textured hypocrystalline clasts with subhedral phenocrysts in a microcrystalline groundmass. The autolith groundmass generally contains more microlites than the surrounding material. The major phenocryst and microlite mineral assemblage includes plagioclase + clinopyroxene + orthopyroxene + titanium magnetite. The phenocrysts show strong marginal resorption, including alteration of rims, as well as strongly altered phenocrysts.

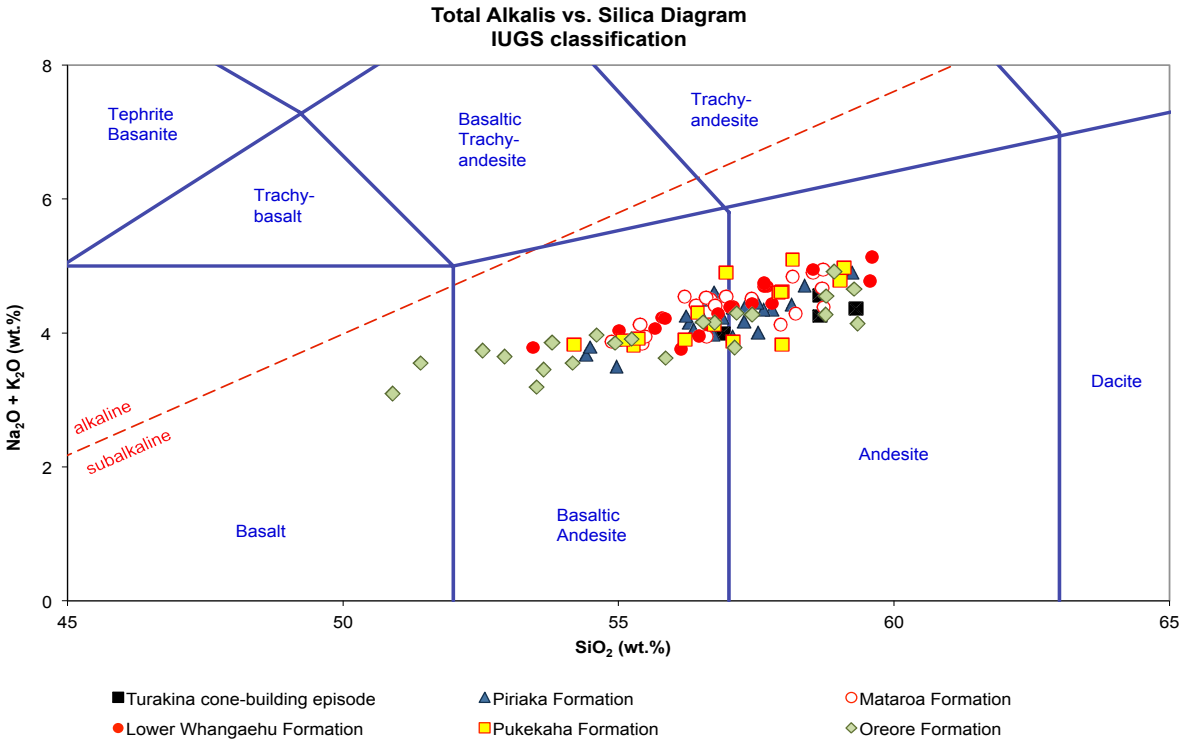

Figure 30. Total alkali vs. silica classification for the Ruapehu mass flows. Nomenclature after LeBas et al. (1986).

6.3.4 Xenolith and xenocryst characteristics

Xenoliths in the samples are small (up to 2 mm) and three distinct types occur; one variety is meta-sedimentary and the other two meta-igneous. The meta-sedimentary xenoliths are fine-grained quartz + granoblastic plagioclase + orthopyroxene + magnetite (Fig. 29F). They occur in samples of all mass-flow units suites with the exception of those from the Turakina mass-flow deposits. One type of meta-igneous xenolith is ubiquitous and generally coarser grained than the meta-sedimentary types. It contains granoblastic plagioclase + orthopyroxene + olivine + clinopyroxene + titanium magnetite. Xenoliths similar to these two types are also common within Mt. Ruapehu edifice lavas (Graham, 1980; Graham et al., 1990; Price et al., 2012). A second type of meta-igneous xenolith that occurs only in the Turakina mass-flow deposit, contains hornblende, which is frequently mantled by clinopyroxene, along with plagioclase + orthopyroxene + olivine + clinopyroxene + titanium magnetite (see above). One example has been dated at 486.5 ± 37.6 ka. Further, hornblende occurs in some lava clasts as up to 2 mm long subhedral xenocrysts (Fig. 29G), some of which show discontinuous zoning and varying degrees of resorption, with reaction rims in which the original crystals have been replaced by opaque phases being common.

6.4 Geochemistry

In the sampled sequences, the abundances of incompatible major and minor elements (e.g., Si, K, Na, Mn) and trace elements (e.g., Rb, Sr, Zr, REE) vary systematically and these trends can be used to define distinctive magmatic cycles or periods. Major and trace element data for representative whole rock samples from the six Ruapehu mass flow suites (Oreore, Mataroa, Lower Whangaehu, Piriaka, Pukekaha and Turakina) are shown in Table 11 and the data from the whole suites are presented in Appendix II. The lava and pumice clast suite is subalkaline and ranges from basalt to andesite (SiO_2 50.89 to 59.59 wt.% and total alkalis from 3.10 to 5.10 wt.%.) (Fig. 30) (LeBas et al., 1986). The clasts from the Turakina mass-flow deposit (340 - 310 ka) are exclusively andesite. The only two basaltic clasts are from the Oreore Formation (180 - 160 ka), which contains a suite dominated by basaltic andesite with less common andesite. The samples taken from the other mass-flow formations are dominantly andesite with minor basaltic andesite.

6.4.1 Major element composition

Silica-variation diagrams for selected major elements are illustrated in Fig. 31. Overall the distal volcaniclastics have medium to low silica contents compared to the lava flow sequences exposed on the flanks of Mt. Ruapehu (Fig. 4). Samples of the Turakina debris-flow deposit plot at the more evolved end of the overall suite, with SiO_2-contents generally exceeding 58 wt.%. Most of the Lower Whangaehu, Mataroa, Piriaka, and Pukekaha Formation samples range between 56 - 58 wt.% SiO_2. The rocks with the lowest silica contents usually correspond to the stratigraphically oldest mass-flow units within each suite, with highest values in the youngest mass-flow units of the suite.

The potassium contents of most mass-flow suites are similar to the Wahianoa Formation on the edifice (160 - 119 ka; Gamble et al., 2003). Low K_2O contents, similar to those of the Te Herenga Formation (250 - 180 ka; Gamble et al., 2003), occur in the Oreore Formation debris-avalanche

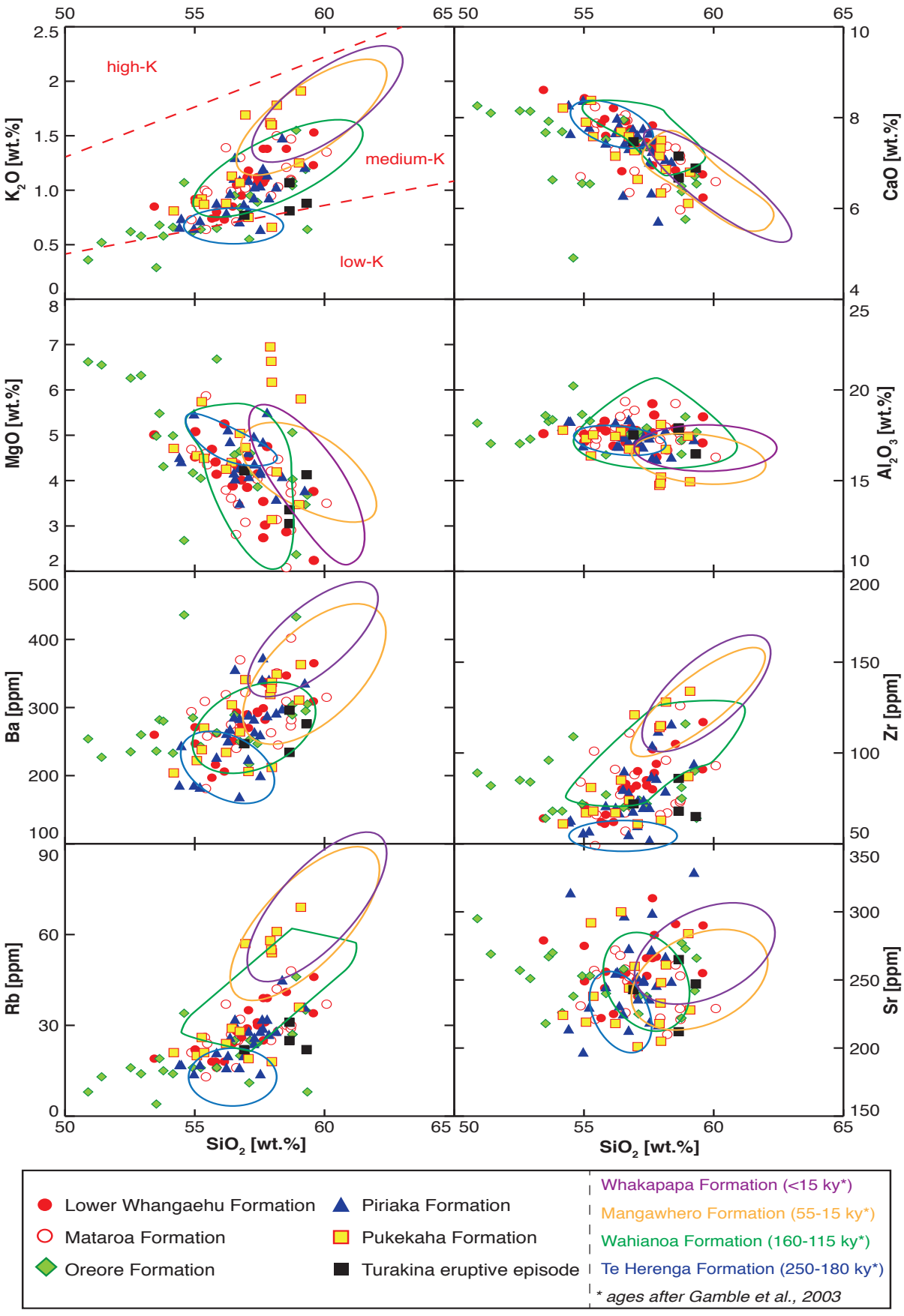

Figure 31. Selected representative major and trace element variation diagrams for the Ruapehu mass flows. Fields drawn for lava flow formations correspond to those shown in Fig. 4 and are colour-matched to Fig. 3. Potassium fields after LeMaitre (1989).

deposits (180 - 160 ka). In the Pukekaha Formation (65 - 55 ka), K_2O content decreases up the mass flow sequence from 1.91 to 1.13 wt.%.
The CaO and MgO contents show a reverse correlation with SiO_2 abundance, as has been found for the edifice lavas (Fig. 4), with phenocryst-poor samples having the highest CaO contents. Variation in Al_2O_3-contents is low (14.74 - 20.22 wt.%), with the concentration decreasing with decreasing age. In the oldest unit (Turakina 340 - 310 ka) medium Al_2O_3 concentrations are found.

6.4.2 Trace element compositions

Systematic variations in trace element concentration reflect the evolution of a magmatic system (e.g., Wager and Mitchell, 1951; Nockolds and Allen, 1954). All samples of the mass-flow suite (Figs. 32 - 34) have similar N-MORB normalized rare earth element (REE) patterns and exhibit the trace element characteristics of magmas from subduction zone settings (c.f., McCulloch & Gamble, 1991; Hawkesworth et al., 1993; Keleman et al., 2005) or continental crust (Weaver & Tarney, 1984; Rudnick & Gao, 2005). Caesium, Rb, Ba, Th, K and U are enriched relative to the light REEs (LREEs), and heavy REEs (HREEs) are depleted compared to LREE and N-MORB abundances. Rubidium is depleted relative to Cs, and Nb is depleted relative to K and La (Fig. 32). Titanium is depleted relative to elements of similar compatibility (Fig. 32) and Eu is depleted relative to the adjacent REEs Sm and Gd (Fig. 33). The bulk of the mass-flow

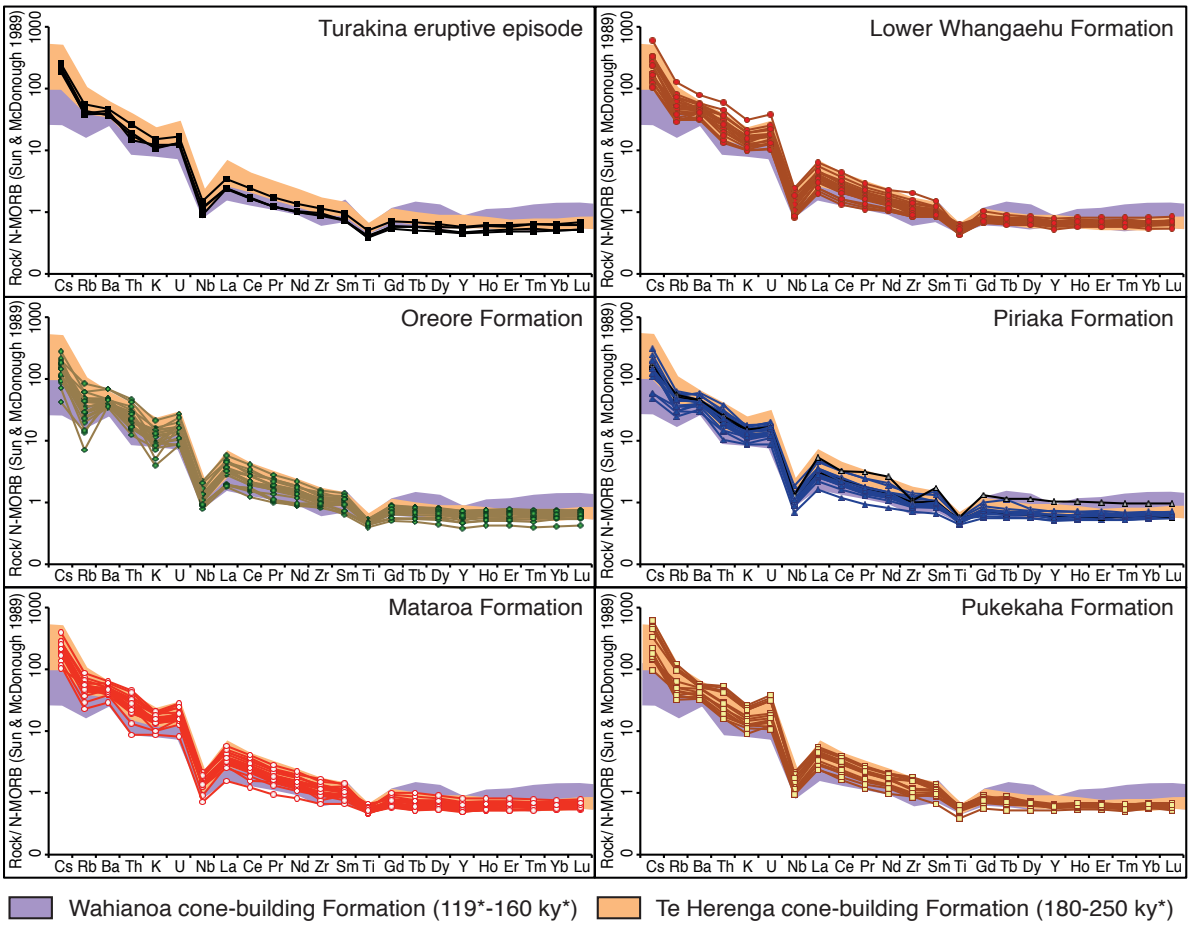

Figure 32. N-MORB normalized (Sun & McDonough, 1989) multi-element plots for the Ruapehu mass-flow deposits in relation to the lavas of the Te Herenga and Wahianoa cone-building formations exposed on the edifice.

deposits display trace-element compositions similar to the Te Herenga (250 - 180 ka; Gamble et al., 2003) and Wahianoa (160 - 119 ka; Gamble et al., 2003) cone-building formations on the Ruapehu edifice. The Ba, Zr, Rb, and Sr contents of all mass-flow samples cover a similar range and vary widely within each mass-flow suite. An exception is the Rb content within the Pukekaha Formation (65 - 55 ka), which follows the same pattern as that described for the K_2O content (see above).

6.4.3 Amphibole composition

Representative amphibole compositions from meta-igneous xenoliths found in the Turakina debris-flow samples are shown in Table 12. According to the classification of Leake et al. (1997), all the analysed amphiboles are pargasite with slight core to rim compositional changes. The amphibole compositions were used with the methods of Anderson and Smith (1995) and Ridolfi et al. (2010) to estimate the approximate depth of origin, as well as the vertical extent of the hornblende stability field and the approximate water content, of the melt in which each amphibole

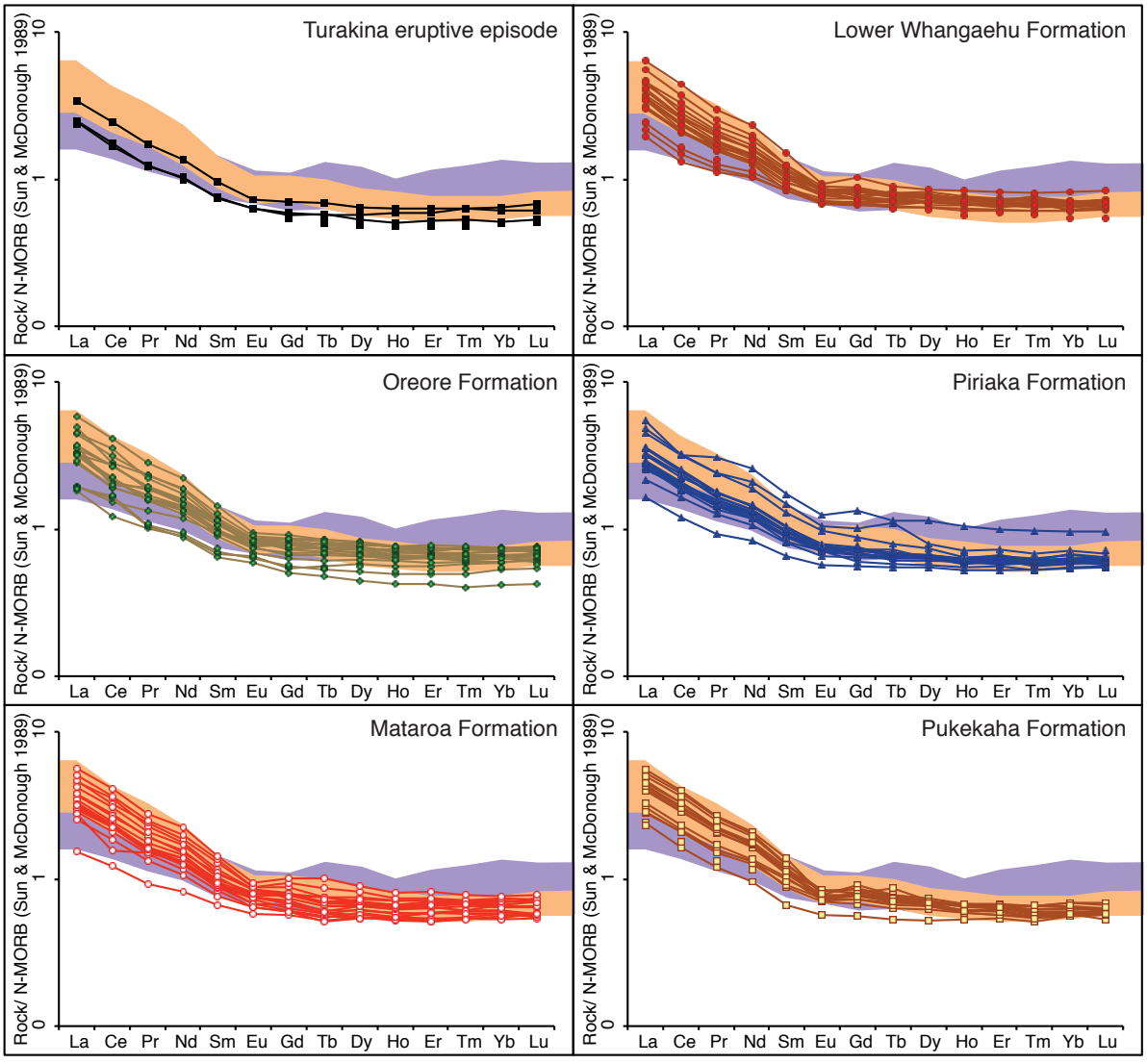

Figure 33. N-MORB normalized (Sun & McDonough, 1989) REE plots for the Ruapehu mass-flow deposits in relation to the lavas of the Te Herenga and Wahianoa cone-building formations exposed on the edifice.

crystal equilibrated. The pargasite from the Turakina samples formed at depths of 49.7 ± 2.27 km (based on the core compositions) to 43.77 ± 2.27 km (rim compositions) at temperatures between 894.37°C (hornblende rim) and 953.56°C (hornblende core), and remained stable within the melt until the magma reached upper crustal levels ranging between 18.0 ± 4.49 km (core) and 10.2 ± 1.12 km (rim). The approximate water content of the underplating melt is estimated to have been between 8.1 ± 1.2 wt.% (hornblende core) and 6.5 ± 1.0 wt.% (hornblende rim).

6.5 Discussion

The petrological and geochemical data from volcanic clasts, 340 - 55 ka in age, obtained from seven mass-flow deposits exposed up to 90 km from Mt. Ruapehu provide new insights into the ancient eruptive history of this stratovolcano. The lava-flow sequences exposed on the Ruapehu edifice were previously separated into four major cone-building episodes (Fig. 3) and these have ages that generally overlap with those of the newly described mass-flow deposits (Figs. 31 - 34). There are also similarities in geochemical composition and petrography between the lavas of the edifice and igneous clasts from the mass-flow deposits. These include similar LIL (large-ion lithophile) element contents (e.g., K, Rb, Sr, Ba), as well as low Nb relative to K abundances. These characteristics are generally interpreted to reflect slab fluid input (Arculus & Powell, 1986; Tatsumi et al., 1986; McCulloch & Gamble, 1991; Hawkesworth et al., 1993), and/or interaction between crust and mantle-derived magma (Graham & Hackett, 1987; Graham et al., 1995; Price et al., 2005; 2012). The negative Ti anomaly, on the other hand, most likely arises from fractional crystallization involving titanium magnetite, and the slight negative Eu anomaly could reflect either fractional crystallization of plagioclase (Graham & Hackett, 1987), or retention of this mineral as a restite phase during crustal anatexis (Price et al., 2012). The porphyritic basalts

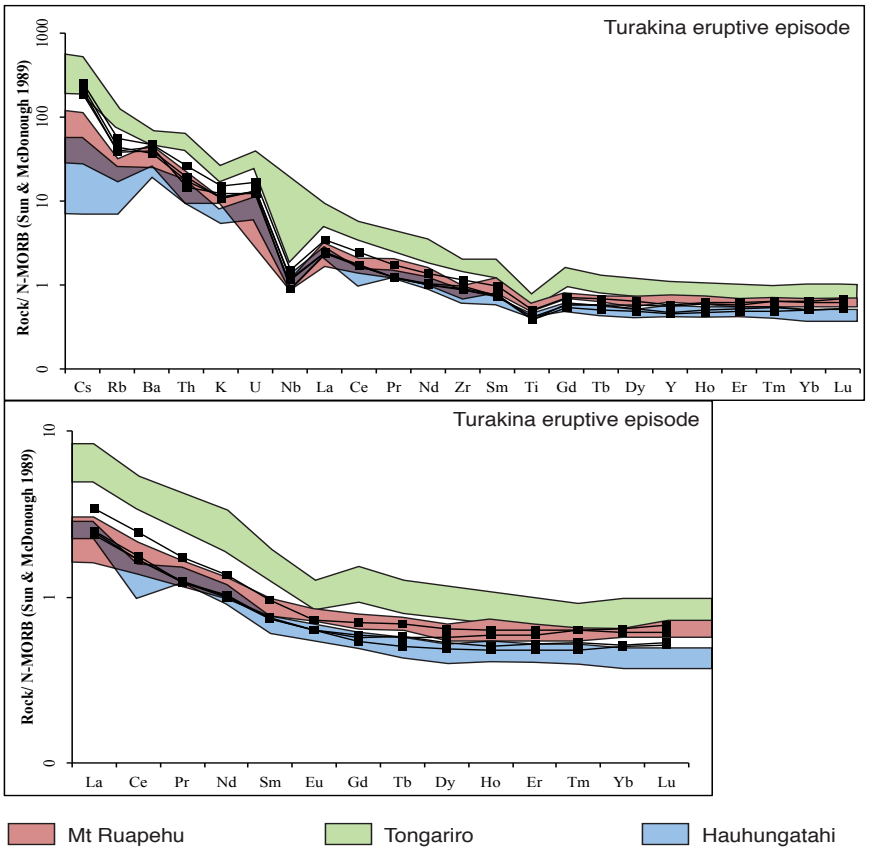

Figure 34. Trace element composition of the Turakina eruptive episode in comparison to the lavas exposed on the volcanic edifices of Mt. Ruapehu (Price et al., 2012), Tongariro (Hobden, 1997) and Hauhungatahi (Cameron et al., 2010).

and andesites typically contain strongly zoned and sieve-textured pyroxene and plagioclase phenocrysts, which were at some stage not in equilibrium with the host melt. Thus, as has been proposed for the edifice lava-flow sequences, the Ruapehu rock suite as a whole reflects open system batch-melting and/or assimilation fractional crystallization processes where repeated cycles of magma replenishment occurred within a complex crustal storage system (c.f., Price et al., 2007; 2012). The progressive shift of the mass-flow igneous clast sample suite towards more primitive compositions between c. 340 and 150 ka likewise suggests magma replenishment of mantle-derived basaltic melts into the mid- to upper crustal Ruapehu storage system. A similar conclusion has been drawn for Mt. Taranaki located c. 130 km west of Mt. Ruapehu (Turner et al. 2008; 2011).

Each of the individual Ruapehu mass-flow formation suites shows a wide range in geochemical variation, which is consistent with the interpretation of geochemical and petrographic data for the cone-building lavas being a reflection of multi-stage mixing processes (e.g., Price et al., 2005). All the mass-flow formations contain meta-igneous and/or meta-sedimentary xenoliths representing fragments of the basement and deep crust (Graham, 1987; Graham et al., 1990; Price et al., 2012), probably from the Cretaceous greywacke-argillite basement (Mortimer et al., 1997; Roser & Korsch, 1999; Adams et al., 2002; 2007). The common meta-igneous xenoliths in Ruapehu andesites have distinctive isotopic compositions that indicate a deeper crust underlying the basement greywackes (Graham et al., 1990; Price et al., 2012).

In order to determine the major petrological processes involved in the evolution of the magmas represented by the new mass-flow samples, the compatible trace element compositions of the igneous clasts were examined with the FC-AFC-FCA (fractional crystallization - assimilation fractional crystallization - fractional crystallization assimilation) and mixing modeler developed by Ersoy and Helvaci (2010) (Fig. 35). The relative ratio of assimilated material to crystallized material (r) and the "increments" value were chosen on the basis of arguments made by Graham and Hackett (1987), who postulated that Ruapehu magmas were most likely generated from primitive mantle-derived melts subjected to 30% crystal fractionation and 6% crustal assimilation. The mass-flow samples indicate an evolution controlled by decoupled assimilation and fractional crystallization processes, accompanied by magma mixing. Thus, wall-rock assimilation dominated fractional crystallization during magma storage in the middle to upper continental crust. Magma mixing was likely to have been more important than expected (c.f., Graham & Hackett, 1987), especially during the Turakina eruptive episode (340 - 310 ka). This indicates that a long-lived, primitive, deep magma-storage system existed from very early in Ruapehu's history, with smaller individual high-level magma reservoirs being repeatedly recharged from the deeper levels of the storage system (c.f., Graham & Hackett, 1987; Price et al., 2005). The dominant magma-modification process within each mass-flow suite appears to have been related to shifts from magma mixing to FCA processes, which may indicate cycles from low to high mantle-magma supply rates.

6.5.1 The Turakina eruptive epoch (340 - 310 ka)

The Turakina mass-flow deposit, located approximately 90 km south-southwest of Mt. Ruapehu (Fig. 22), has a well constrained deposition interval between 340 - 310 ka (Chapter 5). This places it as the oldest known sample suite from Mt. Ruapehu, around 90 ka earlier than the oldest Te Herenga cone-building suite (250 - 180 ka; Gamble et al., 2003). The andesite

Table 12. Representative hornblende composition and thermobarometric calculations for the meta-igneous xenoliths within the samples of the Turakina mass-flow deposit.

Sample	RAT-03	RAT-03	RAT-03	RAT-03	RAT-03	RAT-03	RAT-03	RAT-03	MAN-KL7	MAN-KL7
Label	**hbl1_core**	**hbl1_rim**	**hbl2_rim**	**hbl2_core**	**hbl3_rim**	**hbl3_core**	**hbl4_rim**	**hbl4_core**	**hbl1_core**	**hbl1_rim**
SiO_2 (wt.%)	42.93	42.95	43.03	43.03	42.49	42.90	43.10	42.90	42.90	42.72
TiO_2 (wt.%)	2.03	2.00	1.67	1.67	1.94	1.82	2.03	1.82	1.20	1.23
Al_2O_3 (wt.%)	10.65	10.64	11.45	11.45	11.34	11.14	10.84	11.14	11.65	12.01
Cr_2O_3 (wt.%)	0.11	0.06	0.07	0.07	0.12	0.04	0.05	0.04	0.11	0.10
FeO (wt.%)	15.25	15.24	14.57	14.57	13.92	14.57	14.07	14.57	14.32	14.65
MnO (wt.%)	0.26	0.35	0.38	0.38	0.29	0.34	0.28	0.34	0.31	0.40
MgO (wt.%)	12.50	12.55	12.86	12.86	13.16	13.07	13.16	13.07	13.07	12.88
CaO (wt.%)	10.95	10.95	11.08	11.08	11.09	11.11	11.23	11.11	11.03	10.88
Na_2O (wt.%)	2.04	2.00	2.12	2.12	2.13	2.19	2.04	2.19	2.03	2.03
K_2O (wt.%)	0.37	0.35	0.31	0.31	0.35	0.33	0.34	0.33	0.29	0.33
F (wt.%)	0.00	0.00	0.00	0.00	0.00	0.00	0.00	0.00	0.00	0.00
Cl (wt.%)	0.12	0.13	0.09	0.09	0.07	0.07	0.07	0.07	0.07	0.05
Physical-chemical conditions (Ridolfi et al., 2010)										
T (°C)	904.07	903.80	919.27	919.27	928.74	920.16	915.39	920.16	919.46	924.23
uncertanty (σest)	22.00	22.00	22.00	22.00	22.00	22.00	22.00	22.00	22.00	22.00
P (MPa)	270.40	269.28	322.03	322.03	318.93	299.37	280.85	299.37	339.44	367.47
uncertanty (Max error)	29.74	29.62	35.42	35.42	35.08	32.93	30.89	32.93	84.86	91.87
oceanic depth (km)	9.54	9.50	11.36	11.36	11.25	10.56	9.91	10.56	11.98	12.97
continental depth (km)	10.21	10.17	12.16	12.16	12.05	11.31	10.61	11.31	12.82	13.88
ΔNNO	0.71	0.75	0.83	0.83	0.87	0.87	0.84	0.87	1.05	1.00
logfO2	-11.07	-11.04	-10.67	-10.67	-10.47	-10.63	-10.74	-10.63	-10.44	-10.40
uncertanty (σest)	0.40	0.40	0.40	0.40	0.40	0.40	0.40	0.40	0.40	0.40
H2Omelt (wt.%)	6.48	6.56	7.16	7.16	6.68	6.60	6.54	6.60	7.47	7.62
uncertanty*	0.97	0.98	1.07	1.07	1.00	0.99	0.98	0.99	1.12	1.14
Physical conditions (Anderson & Smith, 1995)										
P (MPa)	1203.51	1204.18	1243.42	1243.42	1159.07	1184.32	1164.83	1184.32	1275.06	1303.98
uncertanty (Max error)	1.12	1.12	1.34	1.34	1.32	1.24	1.17	1.24	3.20	3.47
oceanic depth (km)	42.46	42.49	43.87	43.87	40.90	41.79	41.10	41.79	44.99	46.01
uncertanty (Max error)	2.12	2.12	2.12	2.12	2.12	2.12	2.12	2.12	2.12	2.12
continental depth (km)	45.45	45.48	46.96	46.96	43.77	44.73	43.99	44.73	48.16	49.25
uncertanty (Max error)	2.27	2.27	2.27	2.27	2.27	2.27	2.27	2.27	2.27	2.27

Table 12 (continued). Representative hornblende composition and thermobarometric calculations for the meta-igneous xenoliths within the samples of the Turakina mass-flow deposit.

Sample	MAN-KL7	MAN-KL7	MAN-KL7	MAN-KL7	MAN-KL7	MAN-KL7	MAN-OH4	MAN-OH4	MAN-OH4	MAN-OH4
Label	**hbl2_rim**	**hbl2_core**	**hbl3_rim**	**hbl3_core**	**hbl4_rim**	**hbl4_core**	**hbl1_core**	**hbl1_rim**	**hbl2_rim**	**hbl2_core**
SiO_2 (wt.%)	43.69	42.89	43.54	42.65	43.58	42.86	42.93	42.58	43.00	43.34
TiO_2 (wt.%)	1.26	1.28	1.10	1.29	1.23	1.31	1.21	1.23	1.27	1.24
Al_2O_3 (wt.%)	10.70	11.54	11.10	11.77	10.98	11.42	10.86	11.75	11.19	11.12
Cr_2O_3 (wt.%)	0.09	0.06	0.16	0.07	0.09	0.01	0.05	0.13	0.15	0.08
FeO (wt.%)	14.87	14.97	14.43	15.01	14.58	14.83	14.97	15.68	14.50	14.40
MnO (wt.%)	0.36	0.43	0.35	0.31	0.33	0.39	0.45	0.38	0.31	0.27
MgO (wt.%)	12.99	12.57	13.20	12.61	13.21	12.83	12.57	12.27	12.86	13.12
CaO (wt.%)	11.05	11.04	10.99	10.78	10.98	11.09	10.88	10.85	11.05	11.06
Na_2O (wt.%)	1.91	1.94	1.92	2.03	1.95	2.39	1.90	2.05	1.95	1.91
K_2O (wt.%)	0.28	0.31	0.29	0.34	0.29	0.29	0.29	0.33	0.29	0.29
F (wt.%)	0.00	0.00	0.00	0.00	0.00	0.00	0.00	0.00	0.00	0.00
Cl (wt.%)	0.05	0.08	0.08	0.13	0.10	0.06	0.09	0.10	0.08	0.10
Physical-chemical conditions (Ridolfi et al., 2010)										
T (°C)	894.37	913.93	902.19	917.23	900.80	921.32	899.20	916.15	909.35	905.81
uncertanty (σest)	22.00	22.00	22.00	22.00	22.00	22.00	22.00	22.00	22.00	22.00
P (MPa)	268.51	333.27	294.01	352.07	284.97	322.82	288.41	350.13	308.50	299.00
uncertanty (Max error)	67.13	83.32	73.50	88.02	71.24	35.51	72.10	87.53	77.13	74.75
oceanic depth (km)	9.47	11.76	10.37	12.42	10.05	11.39	10.18	12.35	10.89	10.55
continental depth (km)	10.14	12.59	11.10	13.30	10.76	12.19	10.89	13.22	11.65	11.29
ΔNNO	1.06	0.90	1.15	0.93	1.13	0.87	0.98	0.84	0.99	1.08
logfO2	-10.90	-10.69	-10.66	-10.59	-10.71	-10.60	-10.88	-10.70	-10.68	-10.66
uncertanty (σest)	0.40	0.40	0.40	0.40	0.40	0.40	0.40	0.40	0.40	0.40
H2Omelt (wt.%)	7.07	7.62	7.27	7.53	7.09	7.00	7.29	7.60	7.36	7.26
uncertanty*	1.06	1.14	1.09	1.13	1.06	1.05	1.09	1.14	1.10	1.09
Physical conditions (Anderson & Smith, 1995)										
P (MPa)	1275.06	1295.21	1294.88	1311.43	1282.86	1223.88	1272.12	1315.91	1264.97	1276.09
uncertanty (Max error)	2.54	3.15	2.78	3.32	2.69	1.34	2.72	3.31	2.91	2.82
oceanic depth (km)	44.99	45.70	45.69	46.27	45.26	43.18	44.89	46.43	44.63	45.03
uncertanty (Max error)	2.12	2.12	2.12	2.12	2.12	2.12	2.12	2.12	2.12	2.12
continental depth (km)	48.16	48.92	48.90	49.53	48.45	46.22	48.04	49.70	47.77	48.19
uncertanty (Max error)	2.27	2.27	2.27	2.27	2.27	2.27	2.27	2.27	2.27	2.27

Table 12 (continued). Representative hornblende composition and thermobarometric calculations for the meta-igneous xenoliths within the samples of the Turakina mass-flow deposit.

Sample	MAN-OH4	MAN-OH4	MAN-OH4	MAN-OH4
Label	**hbl3_rim**	**hbl3_core**	**hbl4_rim**	**hbl4_core**
SiO_2 (wt.%)	43.25	41.79	43.52	42.85
TiO_2 (wt.%)	1.35	1.35	1.26	1.16
Al_2O_3 (wt.%)	11.07	13.03	10.73	11.91
Cr_2O_3 (wt.%)	0.17	0.15	0.06	0.18
FeO (wt.%)	14.94	14.20	14.59	14.82
MnO (wt.%)	0.36	0.26	0.42	0.40
MgO (wt.%)	12.74	12.82	13.02	12.74
CaO (wt.%)	10.99	10.98	11.02	10.97
Na_2O (wt.%)	1.85	2.12	1.86	1.93
K_2O (wt.%)	0.32	0.34	0.28	0.32
F (wt.%)	0.00	0.00	0.00	0.00
Cl (wt.%)	0.09	0.09	0.07	0.07
Physical-chemical conditions (Ridolfi et al., 2010)				
T (°C)	902.37	953.56	896.05	919.61
uncertanty (σest)	22.00	22.00	22.00	22.00
P (MPa)	295.25	475.60	272.27	359.14
uncertanty (Max error)	73.81	118.90	68.07	89.78
oceanic depth (km)	10.42	16.78	9.61	12.67
continental depth (km)	11.15	17.96	10.28	13.56
ΔNNO	0.97	0.89	1.08	0.98
logfO2	-10.83	-9.99	-10.84	-10.50
uncertanty (σest)	0.40	0.40	0.40	0.40
H2Omelt (wt.%)	7.28	8.09	7.13	7.78
uncertanty*	1.09	1.21	1.07	1.17
Physical conditions (Anderson & Smith, 1995)				
P (MPa)	1288.70	1254.86	1268.31	1319.37
uncertanty (Max error)	2.79	4.49	2.57	3.39
oceanic depth (km)	45.47	44.28	44.75	46.55
uncertanty (Max error)	2.12	2.12	2.12	2.12
continental depth (km)	48.67	47.39	47.90	49.83
uncertanty (Max error)	2.27	2.27	2.27	2.27

the geochemical compositions of the mass-flow deposits show a strong age and geochemical correlation with the 160 - 119 ka Wahianoa cone-building formation on Mt. Ruapehu (Gamble et al., 2003) (Fig. 31). A few samples overlap with the Te Herenga Formation composition, but the latter is now exposed only on the western and northern sectors of the Ruapehu edifice (Hackett & Houghton, 1989) (Fig. 3) and thus may not be representative of the entire eruptive period. This suggests that the multi-stage, polybaric magmatic mixing system postulated by Price et al. (2012) for Ruapehu was already established during the Te Herenga cone-building episode, with primitive magmas from the mantle feeding into and stalling within sill- and dyke-like storage systems in the middle and upper crust. These magma batches assimilated meta-igneous and meta-sedimentary crustal material and evolved independently by fractional crystallization. Petrographic textural evidence of magma mixing is absent from the clasts sampled from the Mataroa, Lower Whangaehu, and Piriaka Formations. However, results from applying the FC-AFC-FCA and mixing modeler of Ersoy and Helvaci (2010) indicate magma mixing must have been significant (Fig. 35). The partially fused autoliths in basaltic andesites and andesites of the Piriaka Formation may also be taken as evidence for replenishment of the magmatic storage system by hot, mantle-derived melts. Several large-volume flank-collapse-derived debris avalanches occurred at this time and the Te Herenga cone-building episode may have

clasts in the Turakina deposit contain two contrasting types of groundmass, indicating magma mingling (Fig. 29E). Mixing and mingling of magmas prior to eruption is also supported by the major and trace element variations observed. The trace element behaviour of the Turakina samples contrasts with the younger rock suites (Fig. 34). Despite the comparatively high SiO_2 contents, concentrations of K, Rb and Zr are among the lowest determined within the Ruapehu mass-flow suite (Fig. 31). Neither Rayleigh fractionation nor crustal assimilation models can adequately explain this geochemical signature. Major rhyolitic caldera unrest occurred in the Taupo Volcanic Zone (TVZ) during the same period as the Turakina cone-building formation, producing numerous ignimbrites (Houghton et al., 1995), including the Whakamaru ignimbrite, which originated north of Lake Taupo c. 360 - 340 ka ago and exceeds a volume of 1000 km^3 (Houghton et al., 1995; Brown et al., 1998). The regional thermal conditions required to generate these large-scale silicic magmatic systems might have also affected the lithosphere beneath Mt. Ruapehu, causing more extensive crustal melting and/or assimilation and resulting in the elevated silica-content of the Turakina andesites. The Turakina suite has small phenocrysts (≤0.4 mm), which may indicate a rapid magma ascent rate. The variable major and trace element concentrations of the Turakina samples suggest autonomous differentiation of mantle-derived melts within small-scale crustal storage systems prior to infusion of new magma and eventual eruption (c.f., Price et al., 2005; 2007; 2012).

The data for the Turakina mass-flow deposit can be used to show how the early Mt. Ruapehu magma system developed. The meta-igneous xenoliths are amphibole-bearing and a number of the lava clasts contain ≤2 mm long pargasite xenocrysts. Amphibole is extremely rare in the Ruapehu lava flows (Graham & Hackett, 1987; Palmer & Neall, 1989; Price et al., 2012). Hornblende is also rare within most of the Tongariro Volcanic Centre (TgVC), where it is limited to a lava flow in the Tama Lakes area and another on the Maungakatote satellite cone (Fig. 2) (Cole et al., 1983).

The amphibole-bearing xenoliths within the Turakina samples indicate crustal depths between 49.7 ± 2.27 km and 43.77 ± 2.27 km below Ruapehu, slightly higher than the 40 km estimated for crustal thickness by Villamor and Berryman (2006a) and Salmon et al. (2011). Moreover, the xenoliths confirm previous suggestions for an oceanic substrate underlying the North Island meta-greywacke basement (e.g., Graham et al., 1990; Price et al., 2005; 2012) and that inception of Ruapehu volcanism was preceded by underplating of the crust by mantle-derived melts c. 500 ka ago (e.g., Stern et al., 2010; Price et al., 2012). The magmas had high water contents (6.5 - 8.1 wt.% H_2O) (Table 11), more similar to the cooler Taranaki volcanic system in the western North Island (e.g., Price et al., 1999b; Turner et al., 2008). The geothermobarometer of Riodolfi et al. (2010) indicates that amphibole was stable in the Ruapehu melt until it reached depths between 18.0 ± 1.2 km and 10.2 ± 1.0 km. Davidson et al. (2007) suggests that mid- to deep-crust amphibole fractionation is very common at arc volcanoes even in cases where amphibole phenocrysts are absent within the eruptives. In the case of the Mt. Ruapehu mass-flow samples, trace element ratios of Dy/Yb and La/Yb indicate that "cryptic amphibole fractionation" (e.g., Davidson et al., 2007) did not play a major role in the magma genesis of the stratovolcano.

6.5.2 The Te Herenga eruptive epoch (250 - 180 ka)

Dated andesite lava clasts within the Mataroa, Lower Whangaehu and Piriaka Formations indicate formation during the Te Herenga cone-building episode (Chapter 5). Nonetheless,

been augmented by, or driven by, the same thermal and tectonic conditions that caused major caldera unrest in the TVZ (Houghton et al., 1995). Decompression of the magmatic system may have also been due to unloading of Ruapehu's flanks during these collapse events.

The basalts and andesites of the mass-flow suites contain amphibole-free granulitic xenoliths similar to those found in Ruapehu lava flows and corresponding to basement meta-greywacke from the Waipapa and/or Torlesse terranes. This shift to amphibole free, significantly drier melts (0.7 - 3.6 wt.% H_2O; Price et al., 2012) may indicate an intensifying heat flux from the mantle wedge over time, possibly associated with southward propagation of the TVZ (e.g., Stern, 1987). Increasing heat flow would eventually eliminate amphibole from the lower crust. A consequence would have been the shift of the main magma storage level of Mt. Ruapehu upwards in the crust, which is consistent with the present day dyke-like storage systems interpreted to occur at ≤10 km beneath Mt. Ruapehu (Miller & Savage, 2001; Gerst & Savage, 2004).

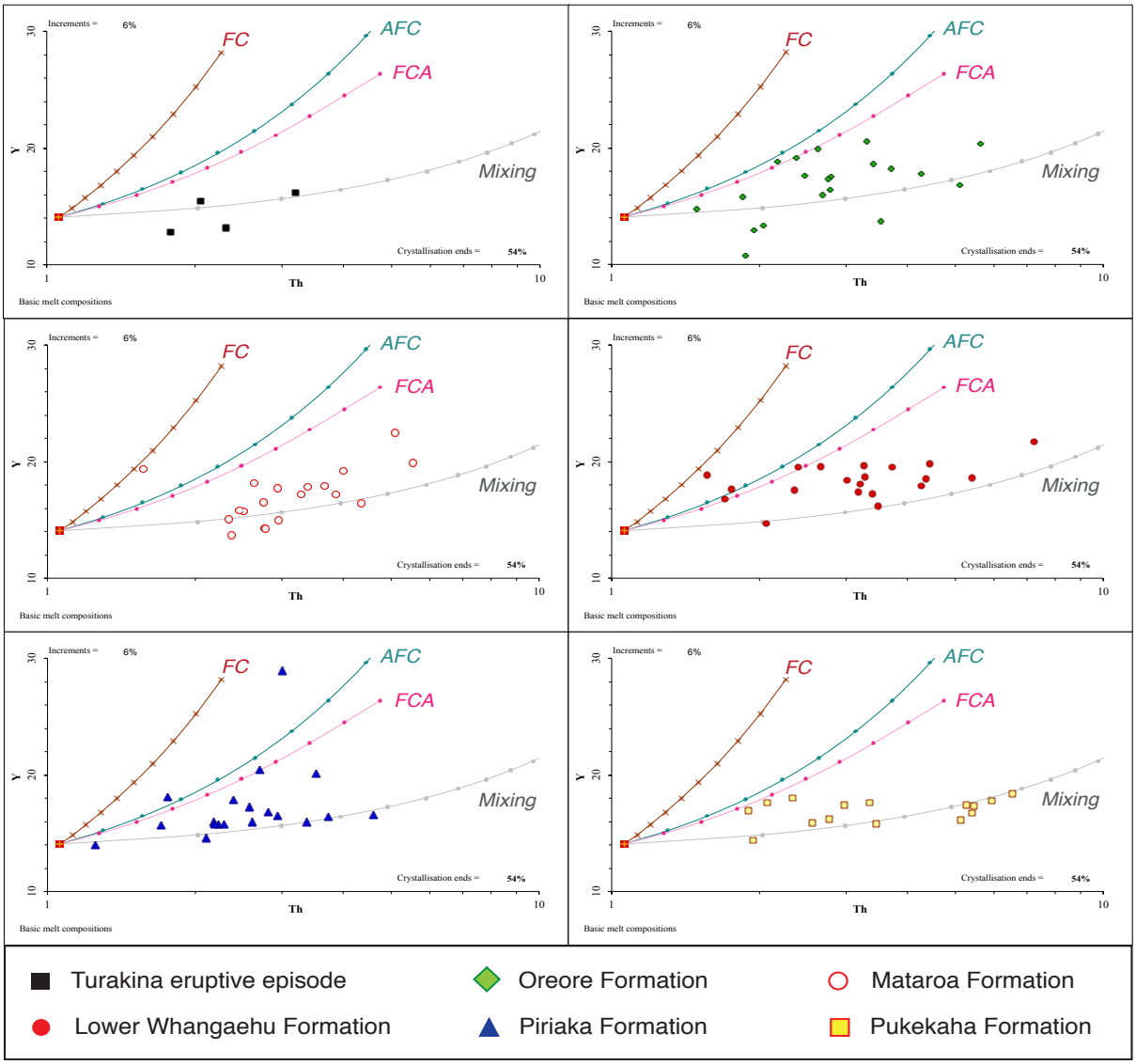

Figure 35. Model of the dominant magma modification processes affecting the Mt. Ruapehu melt. FC-AFC-FCA and mixing modeler after Ersoy and Helvaci (2010). The relative ratio of assimilated material to crystallized material (r) and the "increments" value reflect the Ruapehu melts to be derived from primitive mantle-derived melts subjected to 30% crystal fractionation and 6% crustal assimilation (Graham & Hackett, 1987).

6.5.3 The Oreore eruptive epoch (180 - 160 ka)

Geochemically, the Oreore Formation is the most primitive (SiO_2 ≤55 wt.%) of all the mass-flow sample suites and shows a compositional overlap with the lava flows of the Te Herenga cone-building phase on Mt. Ruapehu (Fig. 31), dated at 250 - 180 ka (Gamble et al., 2003). The geochemistry of the clasts of the Oreore Formation is consistent with the arrival of new primitive, mantle-derived magma into the storage system. The occurrence of two distinct types of groundmass within the mass flow clast samples indicates that magma mixing may have been a factor in the onset of this episode. Two samples (KL7 and OH4; Table 10) have the same petrological characteristics as the samples from the Turakina debris flow and are likely to represent an older part of the proto-Ruapehu cone that is either now buried or has collapsed away.

6.5.4 The Waimarino eruptive epoch (100 - 55 ka)

Dated andesite clasts within the Pukekaha Formation indicate eruption ages ranging between 65.0 ± 10.8 ka and 50.4 ± 10.5 ka (Chapter 5). Their chemical composition overlaps closely with the older Wahianoa cone-building lavas on Mt. Ruapehu (160 - 119 ka; Gamble et al., 2003). The main petrologic difference is that the andesites from the Pukekaha mass-flow deposits have two different groundmass types, showing mingling of magmas. These mingling features, along with the fact that the stratigraphically oldest deposits of the Pukekaha Formation have the highest concentrations of Rb, K, Ba and Zr for any samples with similar silica content, are indications that this period was characterized by vigorous magma recharge and it is, therefore, likely to represent a new cone-building phase.

6.6 Conclusions

Reconstructing the complete magmatic history of an active arc stratovolcano or composite cone is challenging, since older deposits are generally buried by younger volcaniclastic material and lavas on the edifice, or much of the proto-edifice has collapsed and been eroded away. Careful sampling of mass-flow deposits provides the opportunity to expand and extend the magmatic history and thereby gain new insights into the full activity of a volcano and also the earliest stages of development of the magmatic system. This approach has demonstrated how large-volume, landscape-modifying mass-flow deposits on the distal Ruapehu ring plain can be used to extend its eruptive history by over 90 ka to an onset age of >340 ka. The geochemistry of these samples also indicates that, from the earliest stages, the Ruapehu magmatic system was characterised by the storage and evolution of mantle-derived primitive magmas in a plexus of small-scale storage systems in the mid- to upper crust where magmas evolved along separate polybaric pathways. Magma mingling was common in the earlier history of the stratovolcano and could be indicative of the triggering of major phases of eruptive activity associated with specific individual mass flows and episodes of accelerated cone growth.

Furthermore, with the dating possible in distal large-scale mass-flow deposits, finer chronostratigraphic resolution provides a framework in which the details of eruption behaviour, cone growth and magma-system development can be better interpreted. Another two previously unknown eruptive epochs (the Oreore and Waimarino) have been identified, showing that new

cycles of magmatism occurred following the Te Herenga (250 - 180 ka; Gamble et al., 2003) and Wahianoa (160 - 119 ka; Gamble et al., 2003) cone-building episodes, respectively.

Moreover, by extending petrological and geochemical investigations into distal mass-flow deposit clasts, a new xenolith composition from the early magma system has been identified. Unusually for modern Ruapehu, these contain amphibole and show that the earliest magmas from this juvenile magmatic system were derived from >40 km depth and interacted with a relatively young magmatic underplate that developed 486.5 ± 37.6 ka ago. Amphibole-bearing gabbro has frequently been observed within igneous rock suites of other arc terranes (e.g., Adak; Conrad & Kay, 1984; Lesser Antilles; Arculus & Wills, 1980; Taranaki; Gruender et al., 2010; Santorini; Andújar et al., in review) and is thought to indicate the presence of mid- to lower crustal plutons. Fractionation and accumulation of amphibole within the deep crust has also been argued to trap water from mantle-derived melts and simultaneously generate intracrustal magmas and fluids (Davidson et al., 2007) within the arc lithosphere. In the case of Mt. Ruapehu, the rarity of amphibole in eruptives of the last ≤250 ka indicates a progressive increase in heat flux, raising source area temperatures above the amphibole stability field and accompanying the shifting of magma storage from the lower crust to mid- and/or upper crustal levels.

This example from Mt. Ruapehu shows that the geochemical examination of distal mass-flow deposits is an effective tool for understanding a more complete magmatic evolution of stratovolcanoes, as well as for providing information about the changes that occur in the basement underlying them. In addition, understanding the link between cone-building and collapse phases of the volcano, in relation to features of its magmatic system helps to improve our understanding of stratovolcano stability and growth/collapse cycles.

CHAPTER 7: LANDSCAPE DEVELOPMENT AND CLIMATE INFLUENCE ON EDIFICE STABILITY AT MOUNT RUAPEHU, NEW ZEALAND

7.1 Introduction

Aggradational fluvial terraces along river valleys are used to determine approximate regional tectonic uplift rates (e.g., Personius, 1995; Burbank et al., 1996; Li et al., 1997; Pazzaglia & Brandon, 2001). Previous studies mapped well-preserved Quaternary aggradational fluvial terraces throughout many parts of the eastern and central North Island of New Zealand, in part to calculate approximate inland uplift rates (Vella et al., 1988; Personius, 1995; Burbank et al., 1996; Li et al., 1997; Berryman et al., 2000; Pazzaglia & Brandon, 2001; Litchfield, 2003; Litchfield & Berryman, 2005; 2006). The construction of these terraces is dominantly climate controlled. They were formed during cold stages when catchment erosion and, hence, sediment supply into the river valleys was high (Milne, 1973a; Yoshikawa et al., 1981; Porter et al., 1992; Sugai, 1993; Fuller et al., 1998; Bridgeland, 2000; Litchfield & Berryman, 2005; 2006). Minimum depositional ages of the seven aggradational river terraces identified in the North Island of New Zealand were obtained by dating of overlying loess and tephra layers (Milne, 1973; Pillans, 1994; Litchfield & Berryman, 2005), and include:

the Ohakea Terrace (T1; 10 - 18 ky BP),
the Rata Terrace (T2; 30 - 50 ky BP),
the Porewa Terrace (T3; 70 - 80 ky BP),
the Greatford Terrace (T4; 110 - 120 ky),
the Marton Terrace (T5; 140 - 170 ky),
the Burnand Terrace (T6; 240 - 280 ky),
the Aldworth Terrace (T7; 340 - 350 ky), and
the Waituna Terrace (T8; 360 - 370 ky).

All ages were revised by Pillans (1994) and outlined in Table 13.

Mapping of aggradational fluvial terraces on the Ruapehu ring plain in relation to this climatic-geomorphic sequence had not been carried out before, but climate-relationships with laharic aggradation had been previously hinted at (Cronin et al., 1996).

Aggradational terraces made up of volcanic mass-flow deposits related to initial large-scale flank failures of Mt. Ruapehu, were identified and dated along six major river valleys on the distal southeastern to northwestern Ruapehu ring plain (Tost et al., 2014; Chapter 5). Large-scale mass-wasting events of ice-capped composite cones are often related to rapid deglaciation in temperate parts of the world (e.g., Alloway et al., 1986; Capra, 2006; Deemingl et al., 2012; Roverato et al., 2011; Capra et al., 2013). The loss of glaciers from heavily glaciated volcanoes may lead to eustatic uplift as well as the loss of slope-buttressing (Capra, 2006). Rapid glacier retreat is followed by enhanced erosion and stream discharge as well as internal fluid circulation, which, in association with increasing humidity and precipitation, can cause destabilisation of steep volcanic flanks. Climate change was not suggested as a definitive trigger mechanism for flank failures at Mt. Ruapehu, but the timing of major debris avalanches indicates at least a coincidental relationship (c.f., Tost et al., 2014; Chapter 5).

Volcanic cone collapse results in debris avalanches often exceeding several km^3 in volume. Deposition from these rapidly alters the surrounding volcanic landscape through valley filling, river damming and drainage re-direction (Crandell et al., 1984; Siebert, 1984; Procter et al., 2009; Zernack et al., 2012; Tost et al., 2015). The deposits are also rapidly modified and reshaped, producing subsequent very high annual sediment remobilisation fluxes, e.g., 10^3 to 10^6 Mg/km following the Mt. St. Helens (USA) collapse (e.g., Miliman & Syvitski, 1992; Mercado et al., 1996; Major et al., 2000).

The mass-flow deposits from Mt. Ruapehu form distinctive aggradational terraces on the highest topographic elevations along several river valleys and thus offer the potential for determination of post-emplacement regional uplift rates. The aims of this chapter were, hence, to i) identify and correlate the volcanic terraces in relation to any climate-related aggradational fluvial terraces along major river catchments dissecting the southeastern to northwestern Ruapehu ring plain, ii) calculate approximate uplift rates in the medial to distal reaches (20 - 50 km) of each river catchment, and iii) to discuss the possible relationship of climate change and major caldera unrest in the Taupo Volcanic Zone (TVZ) to mass wasting and river aggradation processes in a volcanic region. The massive and widespread remobilisation of sediment caused by flank collapse and large-scale syn-eruptive mass wasting may cause environmental and socioeconomic hazards that may exceed those of the triggering volcanic activity (e.g., Mercado et al., 1996). These must thus be a serious consideration for worst-case volcanic hazard assessment scenarios at Mt. Ruapehu.

7.1.1 Geological Setting

Mt. Ruapehu is a >340,000-year old stratovolcano, located at the southwestern boundary of the TVZ, which results from oblique subduction (1.27°/Ma) of the oceanic Pacific Plate beneath the continental Australian Plate (Graham et al., 1995; Wilson et al., 1995). The TVZ is the dominant focus of late-Pliocene to Quaternary volcanic activity in New Zealand (Graham & Hackett, 1987; Wilson et al., 1995) and one of the most productive magmatic systems on Earth (e.g., Wilson et al., 1995; Price et al., 2005). The nature of the TVZ basement is unclear and cannot be correlated with any particular lithology, but pre-volcanic marine sediments (greywacke), largely of Mesozoic age, crop out at the surface in the axial ranges east and west of the TVZ (Bibby et al., 1995; Wilson et al., 1995).

Mt. Ruapehu is sited within an active graben and the landscape surrounding the composite massif forms a vast aggradational ring plain that comprises tephra, pyroclastic-flow deposits, as well as laharic and fluvial deposits (e.g., Cole et al., 1986; Hackett & Houghton, 1989; Donoghue et al., 1995; Graham et al., 1995), which extent up to 100 km from the volcano (Tost et al., 2014; 2015). The distal side of the Ruapehu ring-plain area is generally downthrown due to ongoing normal and strike-slip faulting, which produces crosscutting geometries with marginal rift-boundary faults (Villamor & Berryman, 2006a; 2006b). Field work for this study was carried out along six major river catchments that radiate from and dissect the Mt. Ruapehu and Mt. Tongariro ring plains (Fig. 36). These are, from southeast to northwest: the Hautapu River, the Turakina River, the Mangawhero River, the Manganuioteao River, the Whakapapa River, and the Whanganui River. The latter four river systems are currently sourced from Mt. Ruapehu and/or Mt. Tongariro, whereas the Hautapu and Turakina Rivers are cut off from the volcano and originate from wetlands on the proximal to medial southern and southeastern Ruapehu ring plain

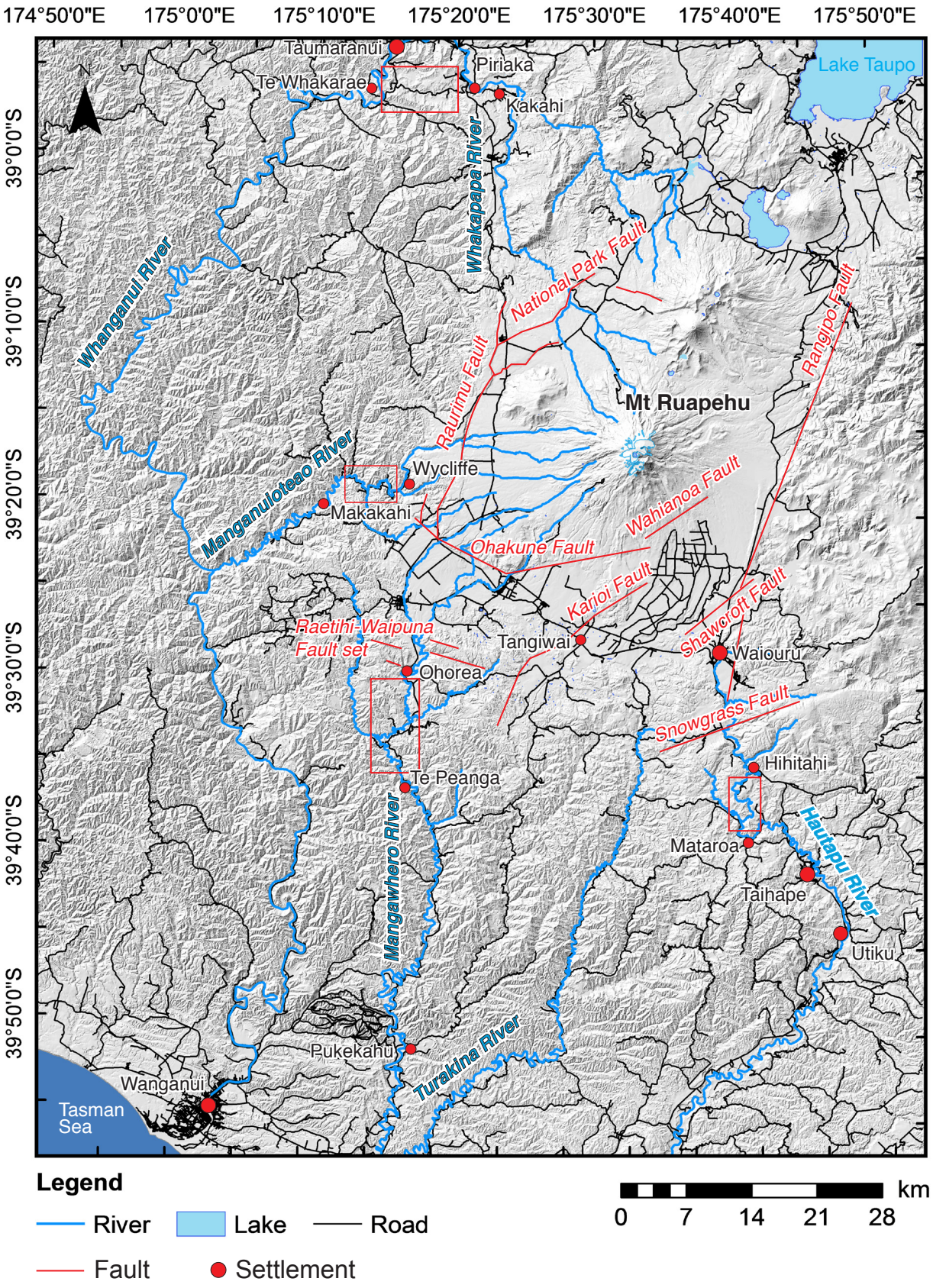

Figure 36. Digital elevation model of the Ruapehu ring plain outlining the river systems studied, as well as the areas of volcanic and non-volcanic aggradational fluvial terrace identification (red rectangles). On the proximal and medial Ruapehu ring plain numerous strike-slip faults were mapped and identified by Villamor and Berryman (2006a; 2006b).

(Fig. 36) (Rogers, 1993). The river catchments generally have a northeast to north-northeast trend, similar to the main structural orientation of the TVZ, although regional faulting (Villamor & Berryman, 2006a; 2006b) occasionally deflects their routes towards the west or northwest. Mapping and identification of non-volcanic aggradational fluvial terraces was limited to the medial to distal reaches (20 - 50 km) of four river valleys (Hautapu River, Mangawhero River, Manganuioteao River, and Whanganui River) where terrace straths are well preserved.

7.2 Methods

The terrace geographic distribution was mapped using GPS measurements to obtain accurate heights of terrace remnants. Extrapolation of the individual terrace surfaces downstream was made at 1:50,000 scale. Coverbed sequences were examined for dated loess and rhyolitic tephra layers to estimate terrace emplacement ages (Fig. 37). Coverbeds were correlated to the findings of previous studies in the Rangitikei River valley (Milne, 1973a; 1973b; Pillans, 1994). Andesitic lava clasts within the volcaniclastic terraces were dated (Chapter 5), and used to estimate maximum deposition ages, and compared to the ages of major caldera unrest in the TVZ (Table 13).

Approximate regional uplift rates were obtained following the method of Berryman et al. (2000) and Litchfield and Berryman (2006), assuming that each non-volcanic aggradational terrace was related to cold climates, and downcutting of the river is a warm-climate phenomenon. This assumption is based on the climate-sedimentation model proposed by Suggate (1965) and Eden (1989) where a reduction in vegetation cover during cold climates increases the erosion in the headwaters of the river systems, filling the valleys downstream. During interglacial periods, rainfall increases and forest cover re-establishes (McGlone et al., 1984), enhancing the stream discharge and, hence, the gravel transport through the river system (Litchfield & Berryman, 2006). The uplift-calculation model assumes constant river levels during cold stages and interglacial periods and similar aggradation altitudes during the cold periods, allowing estimation of rock-uplift rates by measuring the altitude difference between the individual aggradational terraces of known age (Berryman et al., 2000; Litchfield & Berryman, 2006).

7.3 Results

7.3.1 Generalised geology of the Ruapehu ring plain drainage systems

The systems studied here are generally steep gradient bedrock rivers, which flow within gorges for at least some of their length. Their bedrock comprises Mesozoic greywacke, Tertiary sedimentary rocks, and Quaternary volcaniclastic sediments. Exposures along their river catchments also comprise rocks and sediments, which range in age from Mesozoic to Recent and can be divided into three main suites. Mesozoic greywacke is solely exposed in the medial reaches (20 - 35 km) of the Whanganui River system (including Whakapapa River). Most of the aggradational fluvial terraces (volcanic and non-volcanic) in the medial to distal reaches (20 - 90 km) of the other river catchments are developed on late-Pliocene marine sandstones, concretionary siltstones, and mudstones (Fleming, 1953; Ker, 1970; Hodgson, 1993; Ogle et al., 2000; Tost et al., 2015). The river valleys in these materials are deeply incised, forming steep

slopes, with common gully erosion and slumping features. The third unit comprises Quaternary volcaniclastic sediments, consisting of tephra, ignimbrites, and laharic as well as fluvial deposits (Te Punga, 1952; Hodgson, 1993; Lecointre et al., 1998; 2004; Tost et al., 2014; 2015). In some areas, several metres of primary and reworked sequences of rhyolitic ignimbrites, andesitic mass-flow deposits, and tephra mantle the non-volcanic aggradational fluvial terraces.

7.3.2 Non-volcanic aggradational terrace sequences

Up to four non-volcanic fluvial aggradational terraces, formed subsequent to Mt. Ruapehu debris-avalanche emplacement, were identified and mapped in the medial to distal reaches (20 - 50 km) of the Hautapu, Mangawhero, Manganuioteao and Whanganui River valleys (Fig. 36). Only weak evidence for climate-aggradation fluvial terraces was found along the Turakina and Whakapapa River. The latter was strongly influenced by ongoing lahars from Mt. Ruapehu and mass-flow deposits generally buried any non-volcanic aggradational deposits. Furthermore river gradients are extremely steep in the proximity of the stratovolcano resulting in deep v-shaped bedrock valleys, which poorly preserve fluvial terraces. Exposures of mass-flow

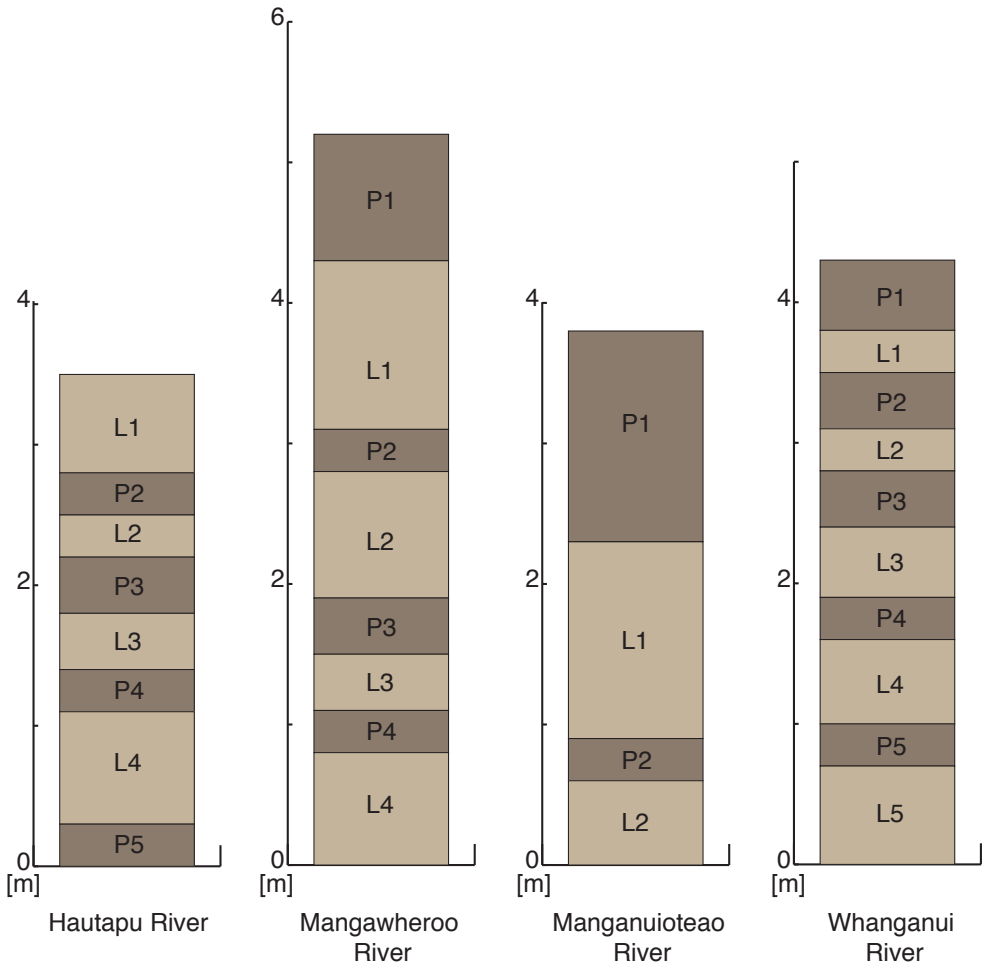

Figure 37. The coverbed sequences identified to overly the individual mass-flow formations within each river valley. P = Paleosol; Loess stratigraphy corresponds to the nomenclature from Milne, 1973a.

deposits and dated rhyolitic tephra layers along the Turakina River are limited to the very distal reaches of the river system (c. 90 km on linear distance), which is strongly influenced by aggradational marine terrace formation, due to climate-controlled base-level variations.
The non-volcanic fluvial aggradational terraces are dominantly preserved upon the sandstone/mudstone-dominated Tertiary substrate, and the youngest terrace related to the Last Glacial Maximum (LGM) forms large coalescing alluvial fans in the lower parts of the valley. The terrace remnants are elevated between 400 m (Hautapu River) and 60 m (Manganuioteao River) above the present river levels and their stratigraphic units include: 1) both greywacke and mudstone/sandstone gravel with intercalated planar- to cross-bedded silt and sand, which reflect energetic fluvial systems; 2) massive regional tabular silt deposits, interpreted as loess, with paleosols developed in their upper part; and 3) distinctive rhyolitic tephra units that extensively mantle the fluvial terrace cover sequences. Along the Manganuioteao River, an extremely steep and narrow river catchment originating on the western slopes of Mt. Ruapehu, terraces are less continuous and only form small remnants up to 60 m above the present river level. In all river catchments studied, andesite lava boulders (≤5 m in diameter) remain scattered on top of the non-volcanic aggradational terraces throughout the landscape, outlining the original areas of mass-flow deposit emplacement or where large clasts have fallen out of exposures of the debris flow deposits higher on the valley walls.

7.3.3 Volcanic aggradational terrace sequences

The dated deposits of the Mt. Ruapehu ring-plain volcaniclastic record were compared to the known Quaternary regional glacial and interstadial framework and landscape units (Table 13) (Pillans, 1983; Shackleton et al., 1990; Pillans, 1994). The oldest terraces in the medial to distal reaches (20 - 90 km) of the studied river valleys are generally made up of channelized long-runout mass-flow deposits related to large-scale flank failures and/or eruptive activity of Mt. Ruapehu (Tost et al., 2014; Chapter 5). The volcaniclastic deposits comprise 10 to 40-m thick sequences of debris-avalanche deposits (Keigler et al., 2011; Tost et al., 2014), overlain or underlain by debris-flow deposits and hyperconcentrated-flow deposits (Keigler et al., 2011; Tost et al., 2015; Chapter 5). The volcaniclastic sediments are generally poorly sorted and massive, with large clasts (≤5 m) supported in a sand-silt matrix (Keigler et al., 2011, Tost et al., 2014; 2015). The debris-avalanche units contain angular blocks (≤5 m) and poorly- to well-rounded clasts of andesitic lava (66 - 90 vol.%), along with hydrothermally altered clasts (≤5 vol.%), entrained river gravel (≤10 vol.%), and rip-ups of late-Pliocene bedrock (≤15 vol.%). The oldest distal volcanic deposits are from the c. 340 - 310 ka Turakina eruptive episode (Chapter 5). A very long runout debris-flow deposit from this eruptive period is exposed c. 1.5 km northwest of Turakina, 90 km south of Mt. Ruapehu (Fig. 22), emplaced on the Burnand (340 ka; Pillans, 1983) and cut by the Brunswick aggradational marine terraces (309 ka; Pillans, 1983) (Table 13). The Turakina River, south of Mt. Ruapehu, is now cut off from Mt. Ruapehu and currently rises from wetlands 4.5 km southwest of Tangiwai (Fig. 36). The second oldest mass-flow sequence (230 - 125 ka; Chapter 5) is exposed along the Hautapu River, which is also cut off from the proximal Ruapehu ring plain, and rises from wetlands southwest of Waiouru (Fig. 36). The c. 10-m thick volcaniclastic deposits along the Hautapu form a distinct terrace at 700 m a.s.l. between Hihitahi and Mataroa (Fig. 36; 38) and are overlain by four loess and soil horizons indicating cessation of deposition before 125 ka (Fig. 37) (Tost et al., 2015). In the Mangawhero River

Table 13. Overview of climate related marine- and fluvial aggradational terrace formation in relation to the periods of Ruapehu mass-flow emplacement (Chapter 5), and major caldera unrest in the TVZ.

South Taranaki-Wanganui marine terraces*	Rangitikei River terraces**	Rhyolite tephra	Associated ignimbrite******	Associated caldera eruptions******	Ruapehu mass-flow deposits*******
		Taupo (1.7 ka)***	Taupo (1.8 ka)	Taupo	
	Ohakea (10-18 ka)				
		Kawakawa (27.1 ka)***	Oruanui (22.6 ka)	Taupo	
	Rata (30-50 ka)				
Rakaupiko (60 ka)					Pukekaha Formation
		Rotoehu (61 ka)****	Rotoiti (65 ka)	Okataina	
	Porewa (70-80 ka)				
Hauriri (81 ka)					
	Greatford (110-120 ka)				Mataroa and Pukekaha Formations
Rapanui (120 ka)					
	Marton (140-170 ka)				Oreore and Piriaka Formations
Ngarino (211 ka)					Piriaka and Mataroa Formations
	Burnand (240-280 ka)				
Brunswick (309 ka)		Fordell Ash (ca. 310 ka)*****			
		Upper Griffin Road	Kaingaroa (230 ka)	Reporoa	
		Middle Griffin Road	Matahina (280 ka)	Okataina	
		Lower Griffin Road	Whakamaru (320 ka)		Turakina eruptive episode
Braemore (337 ka)	Aldworth (340-350 ka)				
		Rangitawa Pumice (370 ka)*		Whakamaru	

*after Pillans, 1983
**after Pillans, 1994
***after Lowe et al., 2007
****after Wilson et al., 1995
*****after Bussel & Pillans, 1992
******after Houghton et al., 1995
*******after Chapter 5

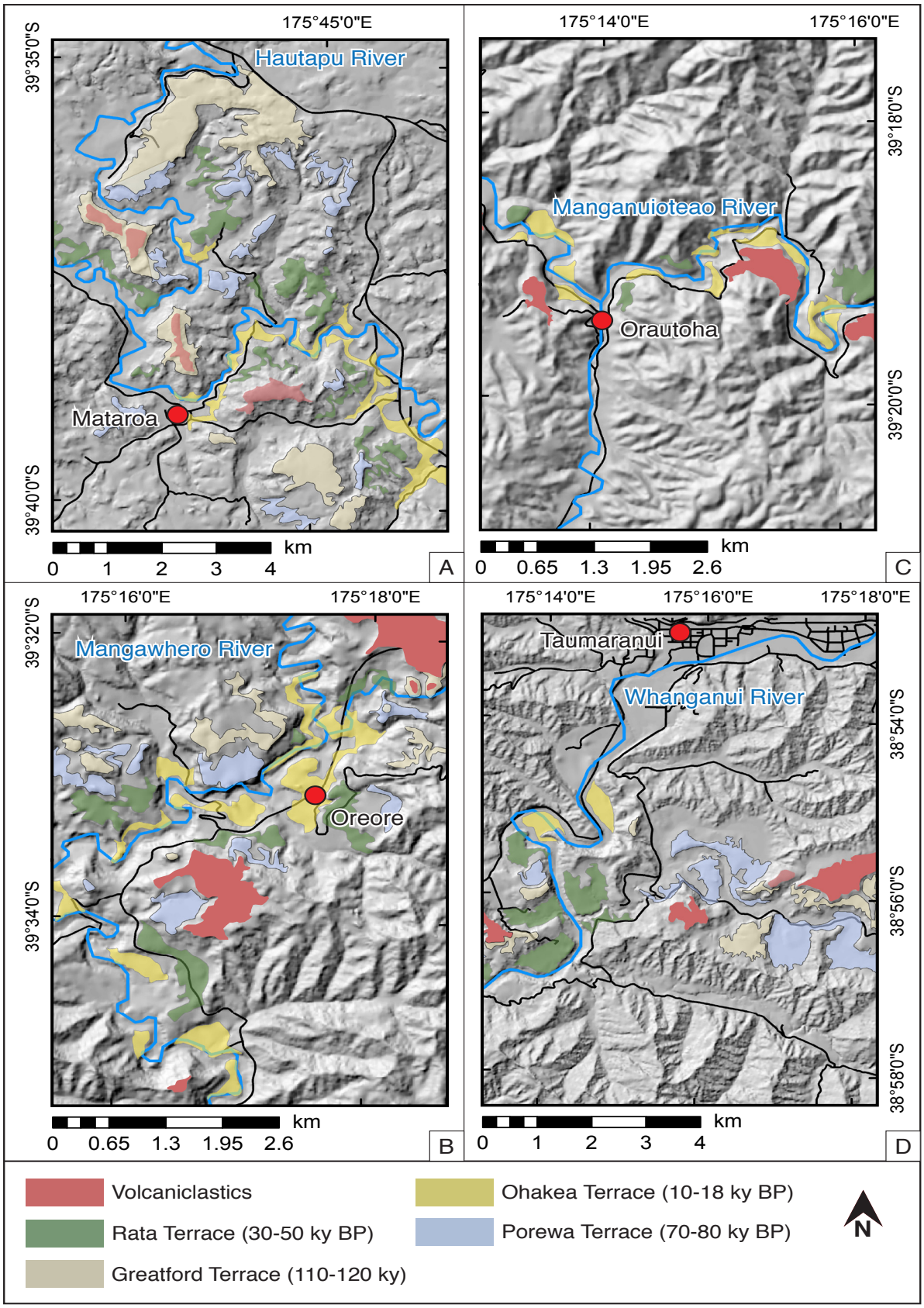

Figure 38. Digital elevation model of the aggradational fluvial terraces identified along four major river systems of the Ruapehu ring plain. Along all river valleys, sequences of mass-flow deposits, sourced from the stratovolcano, form a distinct aggradational terrace at the highest elevation of the valley margins. The extremely high sediment flux generally resulted in blockage of the original river path. Subsequently, up to four non-volcanic fluvial aggradational terraces are exposed on lower altitudes.

catchment, volcanic deposits of >25 m thick relating to the Oreore cone-building episode (180 - 160 ka; Chapter 5) form a distinct regional plateau between Ohorea and Te Peanga >460 m a.s.l. (Fig. 36; 38). The present Mangawhero River drains the southern slopes of Mt. Ruapehu, made up of 15 - 55 ka lava and volcaniclastic sequences of the Mangawhero cone-building episode (Hackett & Houghton, 1989; Gamble et al., 2003). In the Whanganui River, a >40-m thick stack of volcaniclastic deposits forms a major high terrace along the Whakapapa River tributary as well as a distinct east-west elongated plateau (>300 m a.s.l.) between Kakahi and Te Whakarae (Fig. 36; 38), marking the river's former course >150 ka ago (Chapter 5). The Manganuioteao River west of Mt. Ruapehu has experienced little course variation, with the oldest volcaniclastic unit emplacement forming a distinctive plateau on the highest topographic elevations of the valley margins (>410 m a.s.l.) between Wycliffe and c. 6 km southwest of Makakahi, overlain by two loess and two soil horizons (Figs. 36 - 38).

7.3.4 Approximate rates of uplift

Andesite lava boulders within the volcanic mass-flow deposit terraces were dated (Chapter 5), and overlying coverbed sequences were used to define when deposition of these sequences ceased (Table 13). The volcanic deposits form distinctive plateaus on the highest elevations along the river valley margins and enable accurate identification of the subsequent, lower fluvial aggradational terraces, formed during cold stages. Applying the method of Berryman et al. (2000), we assume that aggradation within the river valleys during each cold stage reached a similar altitude, and, hence, the elevation difference in relation to depositional age equals the rock uplift rate between the aggradation events. This method is appropriate because the non-volcanic aggradational fluvial terraces are generally of similar thickness (e.g., Litchfield & Berryman, 2005). In order to calculate approximate regional rock-uplift rates, the elevation difference between the aggradational terraces identified is divided by the age difference (from Pillans, 1994). This excludes the fluvial aggradational terrace formed during the LGM, since the present river level couldn't be accurately determined. We assume an uncertainty of ±15 m (based on potential altitude uncertainties on a 1:50,000 scale) for the elevation error subsequent to aggradational terrace abandonment. The error for the individual uplift rates is hence:

$$\left(\% \frac{30}{height\ difference}\right) * uplift\ rate$$

The results for the approximate rates of uplift within each river catchment are outlined in Table 14. The uplift rates calculated here, lie within the range of previously estimated inland rates (e.g., Pillans, 1986; Berryman et al., 2000; Pulford & Stern, 2004; Litchfield & Berryman, 2006). Most of the non-volcanic fluvial aggradational terraces along the Ruapehu river systems are regionally uplifted by c. 2 ± 0.5 mm yr^{-1}, and it appears that uplift values increased since the Ratan aged cold period, 50 ka ago (Table 14). The lowest uplift values correspond to the time interval of volcaniclastic mass-flow emplacement within the river catchments.

7.4 Discussion

This study focused on the medial to distal reaches (20 - 90 km) of six major river systems, which flow from the Ruapehu and Tongariro ring plains (Fig. 36). Of these, four experienced

significant alteration of pathways following rapid and substantial mass-flow aggradation. Subsequent incision of the river systems into the underlying Tertiary mudstone and sandstone basement, accompanied by river-bed aggradation during cold stages resulted in the formation of up to five non-volcanic fluvial-gravel terraces (Fig. 38). Approximate uplift rates calculated between individual straths are similar for all river valleys studied at 2.0 ± 1.5 mm yr^{-1} (Table 14). Higher values (3.3 ± 1.3 mm yr^{-1} to 5 ± 1.25 mm yr^{-1}) occurred in the period following Oxygen Isotope Stage 2 (30 - 50 ka; Shackleton et al., 1990; Pillans, 1994), potentially caused by an oscillating climate that did not reach full glacial conditions (c.f., McGlone et al., 1984; Berryman, 1992), and/or increased regional tectonic activity. The higher values could also be related to sediment 'exhaustion' of the river system, and/or a catchment floor that, as a result of long-term river incision, becomes gradually narrower. Both causes would strongly contribute to enhanced downcutting rates of the river systems. Significantly lower uplift rates are calculated for periods after rapid volcaniclastic ring-plain aggradation (0.167 ± 0.250 mm yr^{-1} to 0.571 ± 0.214 mm yr^{-1}; Table 14). The actual uplift rates during these time intervals were most likely similar to these calculated for the time intervals between non-volcanic aggradational terrace formations, but enhanced sediment flux due to rapid mass-flow emplacement might have caused an offset in the uplift-rate values.

7.4.1 Catchment change in Ruapehu river systems following large-scale debris-avalanche deposition

7.4.1.1 The Turakina River

The Turakina River, no longer drains the southern slopes of Mt. Ruapehu (as described above), yet it contains a volcanic debris-flow deposit from the volcano (Chapter 6). This unit, between 340 - 310 ka, is the earliest evidence for volcanism at Mt. Ruapehu and the proto-Turakina River was c. 1.5 km west of the present course in its most distal reaches and obviously connected to the volcanic system (Fig. 22). There are no subsequent volcaniclastic deposits along the present river valley, which may reflect blockage and subsequent diversion of the proto-Turakina river course by proximal debris-avalanche deposits.

7.4.1.2 The Hautapu River (Tost et al., 2015)

At present, the Hautapu River is cut off from the proximal Ruapehu ring plain, (Fig. 36). The oldest mass-flow deposit in the catchment is a major debris-avalanche deposit, but this did not block the catchment, with further pumice rich lahars spilling into the proto-Hautapu River catchment until 125 ka at the latest (Tost et al., 2015). This coincided with the incision of the Whangaehu River into the proximal Ruapehu ring plain and capture of the volcanic runoff. The stream capture was augmented by ongoing movement along the Karioi Fault, forming a depression hosting the Whangaehu River (Tost et al., 2015), which is the major route for current syn- or post-eruptive lahars (Cronin et al., 1996; Cronin et al., 1997; Manville et al., 1998; Cole et al., 2009; Lube et al., 2012). Subsequent faulting along the Shawcroft/Rangipo Fault intersection and deepening of the graben enclosing Mt. Ruapehu has made it unlikely that future lahars (apart from catastrophic flank failures) will enter the Hautapu catchment. The ensuing reduced sediment supply into the river has led to deep incision of the Hautapu River into the late-Pliocene Taihape Mudstone during warm climate periods, with non-volcanic gravel deposition during cold stages. Simultaneous and constant uplift (c. 2.0 ± 0.5 mm yr^{-1} to

Table 14. Surface altitudes and approximate uplift rates of the aggradational fluvial terraces mapped and identified on the medial to distal Ruapehu ring plain.

River catchment	Elevation mass-flow deposits (m a.s.l.)	Age mass-flow deposits (ka)*	Elevation non-volcanic terraces (m a.s.l.)	Age non-volcanic terraces (ka)**	Approximate rock uplift (mm/yr)***	Error rock uplift rate (mm/yr)***
Hautapu River	700-710	230-180 ka			0.167	0.250
			600-660	110-120	2	0.5
			560-600	70-80	2	0.75
			520-560	30-50	3.333	1.25
			<520	10-18	N/A	
Mangawhero River	460-480	180-160			N/A	
			440-480	140-170	N/A	
			400-440	110-120	1.333	0.500
			360-400	70-80	2	0.750
			320-360	30-50	3.333	1.250
			<320	10-18	N/A	
Manganuioteao River	410-420	50-80			0.333	0.500
			320-380	30-50	5	1.250
			<320	10-18	N/A	
Whanganui River	300-340	250-180			0.571	0.214
			280-300	140-170	2	1.500
			240-280	110-120	1.333	0.500
			200-240	70-80	2	0.750
			160-200	30-50	3.333	1.250
			<160	10-18	N/A	

*ages after Chapter 5
**ages after Pillans (1994)
***calculated after Berryman et al. (2000)

3.33 ± 1.25 mm yr^{-1}; Table 14) has strongly elevated the cool-climate aggradational surfaces and the oldest volcaniclastic sequence (the Mataroa Formation) forms a distinct plateau at the highest valley margins (Fig. 38).

7.4.1.3 The Mangawhero River

The present Mangawhero River rises from the southern slopes of Mt. Ruapehu. This slope is made up of lava and volcaniclastic sequences dated as part of the 15 - 55 ka Mangawhero cone-building episode (Hackett & Houghton, 1989; Gamble et al., 2003). The onset of volcanic deposits exposed along the more distal Mangawhero River catchment, are much older, relating to the Oreore cone-building episode (180 - 160 ka; Chapter 5). Prior to emplacement of the Oreore Formation, the Mangawhero River appears to have drained a proto-Ruapehu edifice made up of Te Herenga Formation-aged lavas and pyroclastics (250 - 180 ka; Gamble et al., 2003). The volcaniclastic exposures on the distal Ruapehu ring plain show that the medial to distal Mangawhero River valley has generally been in a stable position since 180 - 160 ka ago (Fig. 22), probably related to the pattern of active regional faulting. Villamor and Berryman (2006a) identified numerous strike-slip faults on the southwestern proximal and distal Ruapehu ring plain, which form a natural depression that hosts the present Mangawhero River (Fig. 36). The subsequent stratigraphy exposed along the Mangawhero River suggests that the river system preferentially cut down into the softer Miocene substrate sediment, offsetting the valley westward of the volcaniclastic units. Simultaneous constant regional uplift (c. 1.33 ± 0.5 mm yr^{-1} to 3.33 ± 1.25 mm yr^{-1}; Table 14) has elevated the volcaniclastic surfaces of the Oreore Formation forming a distinctive plateau on the highest valley margins (>460 m a.s.l.). Subsequent fluvial processes were not energetic enough to move large andesitic boulders from otherwise eroded areas of debris-avalanche deposition, and these remain scattered on top of up to four non-volcanic aggradational terraces between Ohorea to Pukekahu (Fig. 36). Subsequently, volcanic hyperconcentrated flows spilled into the Mangawhero River via the Makotuku River c. 50 - 80 kyr ago (Chapter 5), and have been deposited within the cold-climate gravel aggradational surface at lower altitudes (the T2 aggradational terrace, c.f., Milne, 1973). During the Mangawhero cone-building episode (15 - 55 ka; Gamble et al., 2003), the Makotuku River became cut-off from the proximal Ruapehu ring plain, with these younger mass flows travelling down a channel similar to the current Mangawhero River drainage system.

7.4.1.4 The Whakapapa and Whanganui River systems

A >40 m thick stack of volcaniclastic deposits of the Piriaka Formation forms a distinct east-west elongated plateau between Piriaka and Te Whakarae (Fig. 38), marking the route of a proto-Whanganui River catchment established >150 ka. The thickness of the Piriaka Formation suggests that this route was used by mass flows for thousands of years before cut-off occurred and the river incised its present route, passing the town of Taumaranui (Fig. 36). The exact time of cut-off is unclear, because coverbed sequences are missing and $^{40}Ar/^{39}Ar$-dates were only obtained from diamicton deposit exposed at the lower half of the sequence (Chapter 5). Constant regional uplift (c. 1.33 ± 0.5 mm yr^{-1} to 3.33 ± 1.25 mm yr^{-1}; Table 14) has resulted in an inverted stratigraphy, with the Piriaka Formation forming a distinctive plateau on the highest topographic elevation between Kakahi and Te Whakarae (>300 m a.s.l.). The same high-level terrace can be traced upstream along the Whakapapa River valley and volcanic mass-flow deposits exposed at Kakahi also belong to the Piriaka Formation. The deposition pattern indicates that in its

middle reaches the route of the Whakapapa River was constant over the last c. 150 ka. In the headwaters of the Whakapapa River, however, on the northwestern proximal Ruapehu ring plain, only volcaniclastics <9.6 ka are exposed within its deep catchment, suggesting this topography was created by the Murimotu debris avalanche c. 9.5 ka go (Palmer & Neall, 1989) and the subsequent Whakapapa cone-building Formation lavas (<15 ka; Gamble et al., 2003). Prior to this period, the Whakapapa River likely originated from another part of northern Ruapehu.

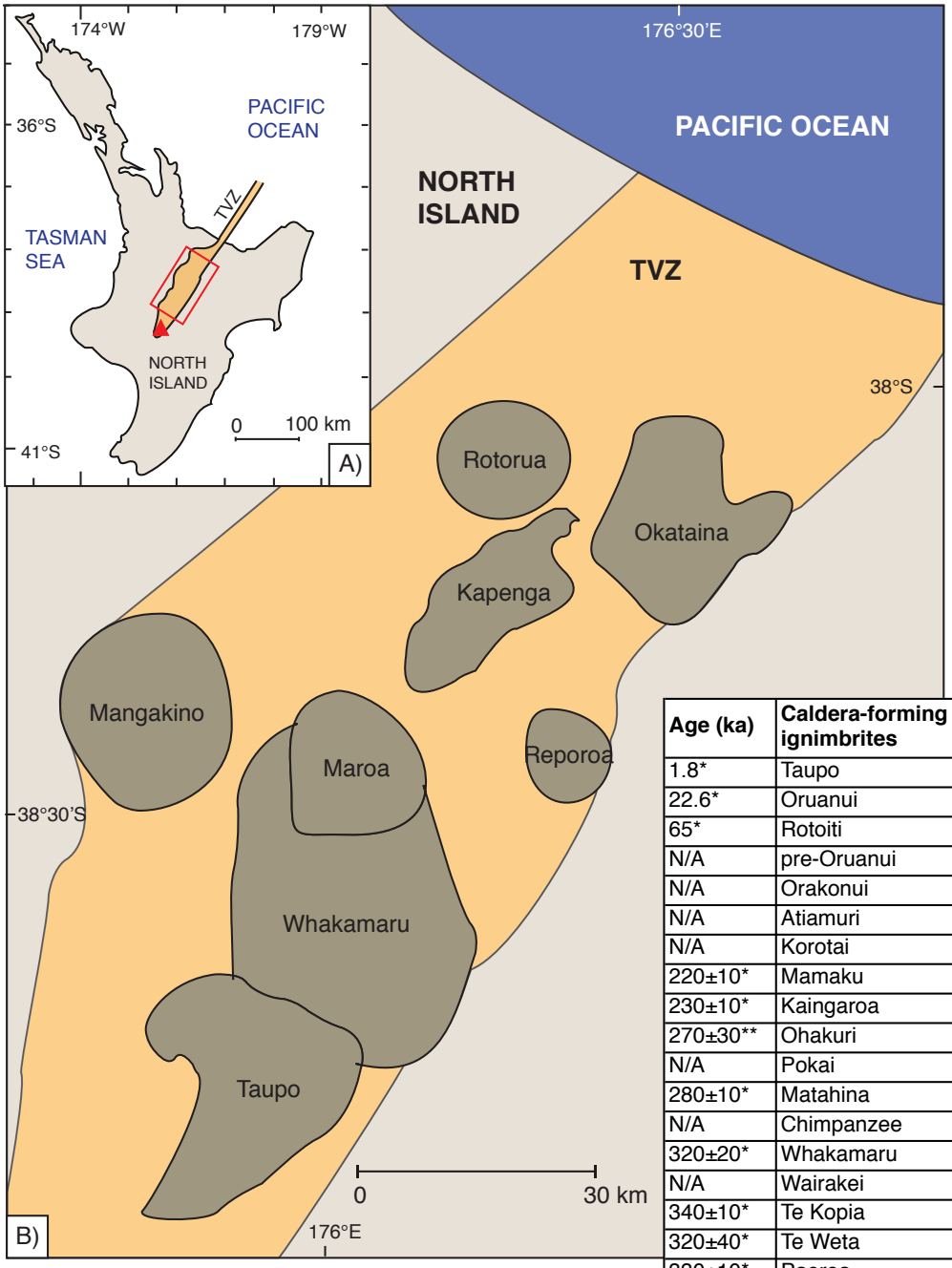

Age (ka)	Caldera-forming ignimbrites	Associated caldera centers
1.8*	Taupo	Taupo
22.6*	Oruanui	Taupo
65*	Rotoiti	Okataina
N/A	pre-Oruanui	Taupo
N/A	Orakonui	Maroa
N/A	Atiamuri	Maroa
N/A	Korotai	Maroa
220±10*	Mamaku	Rotorua
230±10*	Kaingaroa	Reporoa
270±30**	Ohakuri	Kapenga
N/A	Pokai	Kapenga
280±10*	Matahina	Okataina
N/A	Chimpanzee	Kapenga
320±20*	Whakamaru	Whakamaru
N/A	Wairakei	Whakamaru
340±10*	Te Kopia	Whakamaru
320±40*	Te Weta	Whakamaru
330±10*	Paeroa	Whakamaru
320±30*	Manunui	Whakamaru
360±30**	Rangitaiki	Whakamaru
340±10*	Te Whaiti	Whakamaru

Figure 39. Rhyolitic caldera formation in the TVZ. (A) The TVZ (yellow field) is a c. northeast-trending magmatic system divided into three individual magmatic zones, based on the chemical composition of the volcaniclastics. Rhyolitic volcanism is limited to the central part of the TVZ (red rectangle). (B) Localities of the major rhyolitic calderas in the central TVZ that erupted large amounts of volcaniclastic material over the last 340 ± 10 ka (Table), which was likely associated with enhanced regional tectonic activity.

7.4.1.5 The Manganuioteao River

The only river system with little path variation is the Manganuioteao River west of Mt. Ruapehu. This is most likely due to tectonic movement along the Waimarino Fault (Lecointre et al., 1998), which guides the river's course (Fig. 36). The deep gorge of the Manganuioteao River catchment exposes >95 vol.% volcaniclastics (Chapter 5). Reduced sediment supply into the river catchment during periods of eruptive quiescence led to deep incision of the Manganuioteao River into volcaniclastic deposits and the underlying late-Pliocene silt- and sandstones. Ongoing uplift (c. 0.33 ± 0.5 mm yr^{-1} to 5 ± 1.25 mm yr^{-1}; Table 14) has elevated the mass-flow surfaces to form aggradational terraces and thus an inverted stratigraphy, with the oldest part of the Pukekaha Formation forming a distinctive plateau on the highest topographic elevations of the valley margins (>60 m above the river floor). The significantly elevated uplift rate calculated for the Manganuioteao River <50 ka ago, might be related to enhanced incision of the steep gradient river into the comparatively soft underlying Tertiary silt- and sandstone bedrock and/or enhanced regional tectonic activity in the medial reaches of the Ruapehu ring plain (Fig. 36). The river system was not energetic enough to remove large andesitic boulders (≥2 m) from the original areas of debris-avalanche deposit emplacement, hence these remain scattered on top of the non-volcanic aggradational terraces throughout the landscape from Wycliffe to c. 6 km southwest of Makakahi (Fig. 38).

7.4.2 Climate change and major caldera unrest as potential trigger for Mount Ruapehu flank failures and long-runout mass flows

The volcanic aggradational terraces studied comprise debris-avalanche deposits, related to major flank failures of Mt. Ruapehu. As the formation of non-volcanic fill terraces, also rapid ring-plain aggradation due to major failures of steep volcanic flanks could be triggered or pre-conditioned by major climate changes, and/or major rhyolitic caldera unrest of large silicic magma systems, as the TVZ (Fig. 39).

The oldest volcaniclastic deposits include a debris-flow deposit from the c. 340 - 280 ka Turakina eruptive episode, exposed c. 1.5 km northwest of Turakina (Fig. 22) between the Burnand (340 ka; Pillans, 1983) and the Brunswick aggradational marine terraces (309 ka; Pillans, 1983), which correlate to Oxygen Isotope Stage 9b and 9a, respectively (Table 13) (Shackleton et al., 1990). Additionally, loess deposition within the Rangitikei aggradational river terraces hints to a cold period on New Zealand's mainland 340 - 350 ka ago (Pillans, 1994). This places the timing of the Turakina-related mass-wasting event at the interface between the cold climate of the Aldworth cold period and its preceding interstadial (Fig. 40). During the glacial/stadial climate, enhanced growth of glaciers likely occurred in the alpine region of the TgVC, covering the volcanic flanks as well as most of the proximal ring plain >1,100 m a.s.l. (McArthur & Shepherd, 1990). A gradual increase in temperature from 340 to 310 ka may have resulted in rapid melting of snow and ice, reducing any ice-armouring effect and increasing pore-water circulation within the cone, which would have enhanced alteration and ultimately weakened the volcanic edifice. Houghton et al. (1995) noted that major caldera unrest occurred in the TVZ 340 - 280 ka ago, and resulted in emplacement of the Te Kopia (340 ± 10 ka), Wairakei (age unknown), Whakamaru (320 ± 20 ka), Chimpanzee (age unknown), and Matahina ignimbrites (280 ± 10 ka), each erupting and fragmenting between 30 - 1000 km^3 of rhyolitic volcaniclastics (Fig. 39). These large-scale eruptions were likely accompanied by intensive tectonic activity within the TVZ, and

hence, also the TgVC. The enhanced regional seismicity in the TVZ, could have triggered or contributed to the explosive activity and potential destabilisation of Mt. Ruapehu (Chapter 5).

The debris avalanches within the Mataroa and Lower Whangaehu Formations (Keigler et al., 2011; Tost et al., 2015), south of Mt. Ruapehu, hint to a second major destructive episode of Mt. Ruapehu <230 - 240 ka ago (Chapter 5), coinciding with the shift from Oxygen Isotope Stage 8 (240 - 280 ka; Shackleton et al., 1990 ; Pillans, 1994) to a warmer and more humid interstadial climate (Table 13; Fig. 40). This shift to a milder climate engendered rapid glacier unloading on

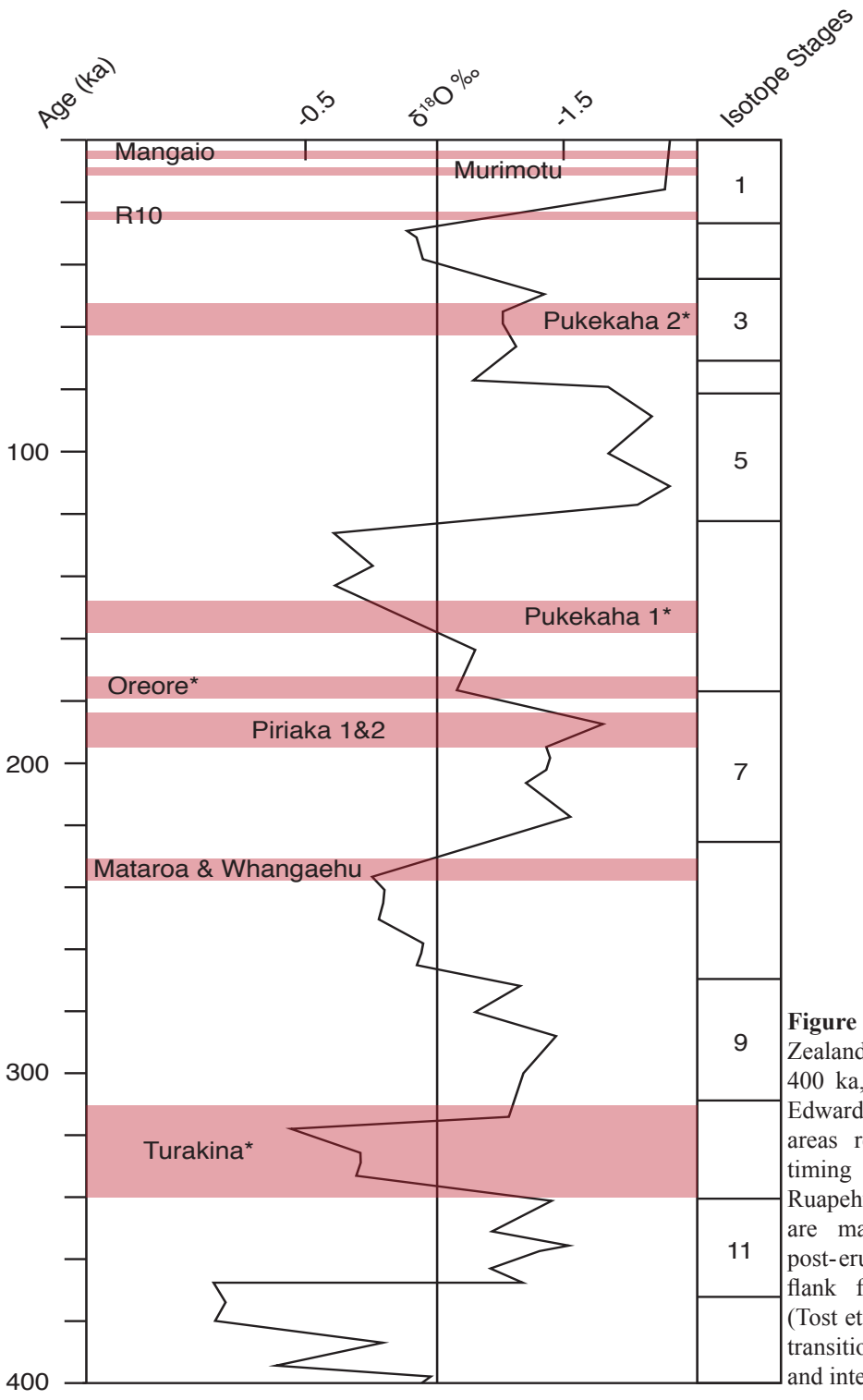

Figure 40. Development of New Zealand's climate over the last 400 ka, modified after Beau and Edwards (1983). The red-shaded areas represent the approximate timing of flank failures at Mt Ruapehu. Syn-eruptive events are marked (*). Most of the post-eruptive large-scale (>1 km^3) flank failures of Mt. Ruapehu (Tost et al., 2014) occurred during transitions between cold stages and interstadial climates.

the stratovolcano, and likely increased the pore water circulation in the cone.
Major caldera unrest in the TVZ occurred between c. 270 - 220 ka ago, emplacing the Ohakuri (270 ± 30 ka; Kohn, GNS-files, unpublished fission track ages), Kaingaroa (230 ± 10 ka; Houghton et al., 1995), and Mamaku ignimbrites (220 ± 10 ka; Houghton et al., 1995) (Fig. 39). This period of large-scale (30 - 100 km^3; Houghton et al., 1995) rhyolitic activity likely caused enhanced seismicity within the TVZ, potentially contributing to the destabilisation of the southeastern Mt. Ruapehu flank.

During Oxygen Isotope Stage 6 (140 - 170 ka; Shackleton et al., 1990; Pillans, 1994), glaciers likely re-grew on the volcanic edifice. At the same time, ascent of magma into the cone likely led to failure of its southern flank, and formation of the basal debris-avalanche deposit within the Oreore Formation (Table 13; Chapter 5). This deposit contains 10 - 15 vol.% pumice as well heat-fractured andesitic lava and bombs, indicating hot pyroclastics were deposited on the glaciated and snow-covered slopes of Mt. Ruapehu (Chapter 5). The debris avalanche was followed by many lahars, into the Mangawhero, Manganuioteao, as well as the Whanganui River catchments, likely associated with pyroclastic flows and falls remobilised from snow and ice.

Following the Porewa cold stage, there was a 20 ka-long period of warmer interstadial climate (Fig. 40) (Pillans, 1994), again leading to a rapid retreat of the glaciers on Mt. Ruapehu. The edifice unloading may have led to eruption, with a syn-eruptive debris avalanche represented by the basal diamicton deposit in the Pukekaha Formation (Chapter 5).
Major caldera unrest in the TVZ also occurred during this period, resulting in emplacement of the Rotoiti ignimbrite (Fig. 39) (65 ka; Murphy & Seward, 1981). Enhanced seismic activity related to this large-scale rhyolitic eruption might have contributed to the ascent of melt, and subsequent edifice failure of Mt. Ruapehu.

During the early part of the last 50 ka, major sub-plinian eruptions led to multiple pumice-rich lahars in the northeastern Ruapehu ring plain (Cronin et al., 1996). This was followed by similar deposition in the southeastern ring plain (Hodgson, 1993). The largest known flank failure during this time was the ~9.5 ka Murimotu debris avalanche (Palmer & Neall, 1989). This was interpreted to have been triggered by intrusion of a dacitic cryptodome (Palmer & Neall, 1989; McClelland & Erwin 2003). Its timing was considerably delayed from the known rapid warming at the end of the last glacial, at around 15 ka B.P. (McGlone et al., 1984).

A smaller flank failure led to deposition of the Mangaio Formation (4.6 ka; Donoghue & Neall, 2001), during the warmest period of the mid-Holocene. This deposit is distinguished by its very high clay content and dominantly hydrothermally altered clast assemblage. The high humidity and lack of glacial cover led to extreme fluid circulation and hydrothermal alteration in part of the edifice, leading to the Mangaio collapse.

7.5 Conclusions

In total, five aggradational fluvial terraces were identified and mapped along the medial reaches of four major river catchments dissecting the Ruapehu ring plain. Geomorphic identification and

mapping of fluvial aggradational terraces along river catchments provide insights into long-term processes of climate-controlled landscape change. These terraces dominantly formed during cold climates characterized by enhanced sediment supply into the river catchments (e.g., Milne, 1973a; Yoshikawa et al., 1981; Porter et al., 1992; Sugai, 1993; Fuller et al., 1998; Bridgeland, 2000; Litchfield & Berryman, 2005; 2006). Approximate regional inland uplift rates of 1.33 ± 0.5 mm yr^{-1} to 5 ± 1.25 mm yr^{-1} were obtained using altitude-difference measurements between aggradational surface straths, which correspond well with values obtained for other river catchments on the eastern and central North Island of New Zealand (e.g., Pillans, 1986; Berryman et al., 2000; Pulford & Stern, 2004; Litchfield & Berryman, 2006).
Climate change was likely a significant contributor to large-scale flank failures of Mt. Ruapehu, producing debris avalanches that filled river valleys. Later downcutting formed terraces from these deposits, normally the highest terrace/surface in each of the valleys studied. Understanding the interplay between edifice stability and climate factors such as significant changes in temperature, capping/supporting ice cover and precipitation rate, is essential in order to improve our time-varying hazard forecasting at Ruapehu volcano. The cone-collapse events occurred during both glacial and interstadial climates. New stratigraphy, coupled with $^{40}Ar/^{39}Ar$-dating of clasts within debris-avalanche deposits, suggest that collapse followed by heightened volcanism was more common in warming periods interface between a cold and a warming climate. Four individual collapse events have occurred during these climatic conditions: the Turakina cone-building episode, the Mataroa Formation, the Lower Whangaehu Formation, and the Murimotu Formation. Rapid loss of ice from the volcano slopes in the transition out of cold climates leads not only to a reduction in flank support, but it is also coupled with greater fluid input and deep circulation in the volcano (e.g., Capra, 2006; Capra et al., 2013).
Flank failures and debris avalanches from Mt. Ruapehu during interstadial climates appear (Mangawhero Formation, Murimotu Formation, Mangaio Formation) to be dominantly associated with magmatic intrusion and syn-collapse sub-plinian explosive eruptions similar to the 1981 eruption of Mt. St Helens (e.g., Voight, 1981).

The almost instantaneous deposition of vast amounts of volcaniclastic material on the Ruapehu ring plain, due to debris-avalanche formation, resulted in partial or complete subsequent re-adjustment of the drainage systems studied. The greatest landscape changes can be observed along the river catchments of the Hautapu, Turakina, Mangawhero, Whakapapa, and Whanganui Rivers. Periods of rapid ring-plain aggradation resulted in deposition of voluminous volcaniclastic sediments in the river valleys, in parts infilling and blocking initial river pathways. Subsequent and ongoing uplift (c. 1.33 ± 0.5 mm yr^{-1} to 5 ± 1.25 mm yr^{-1}) accompanied by regional tectonic faulting (Villamor & Berryman 2006a; 2006b) has resulted in an inverted stratigraphy, with the volcaniclastic surfaces forming distinct plateaus on the highest topographic elevation adjacent to the individual river catchments. During cold climates, enhanced erosion in the alpine regions of the TgVC resulted in increased sediment supply into the Ruapehu river systems, forming up to four non-volcanic aggradational terraces within their valleys, with the youngest (10 - 18 ka; Pillans, 1994) exposed at the valley floor and the oldest (140 - 170 ka; Pillans, 1994) beneath the mass-flow deposits.

CHAPTER 8: SYNOPSIS AND FUTURE OUTLOOK

8.1 Approach and findings of this study

Mt. Ruapehu is among the most active stratovolcanoes in New Zealand. Over its recent history, the volcano has been characterized by small-scaled eruptions (~0.05 km^3 magma batches; Price et al., 2012), including near-source surges (e.g., Kilgour et al., 2010; Christenson et al., 2010), wider-scale tephra falls (Cronin et al., 2003) and long-runout lahars generated both during and between eruptions (e.g., Cronin & Neall, 1997). Pre-historic eruption episodes from Ruapehu included far larger sub-plinian examples (Pardo et al., 2014). Further, valley sequences radiating from the edifice contain many large-volume mass-flow deposits that were emplaced throughout the history of the composite cone (e.g., Park, 1910a; Te Punga, 1952; Grindley, 1960; Hodgson, 1993; Parish, 1994; Cronin et al., 1996a; Lecointre et al., 2004; Keigler et al., 2011).

A composite record of Mt. Ruapehu and its surrounds has been established spanning the last c. 50 ka (Hackett & Houghton, 1989; Palmer, 1991; Cronin et al., 1996a; Cronin & Neall, 1997; Lecointre et al., 1998; Gamble et al., 1999; Waight et al., 1999; Donoghue & Neall, 2001; Pardo et al., 2012). The older eruptive history was, however, only known from a few isolated studies in single localities. The results of this study provided new, more comprehensive knowledge of the older part of the geological record, helping to elucidate the nature and frequency of Mt. Ruapehu's entire record of volcanic activity. In the context of rapid aggradation in proximal areas, long-runout mass-flow deposits are one of the few ways in which the older record of such stratovolcanoes can be reconstructed. Knowing the full history of eruptive activity from this volcano over its entire lifespan enables a more robust evaluation of future hazards and eruptive behaviour. The diamictons studied here showed a much wider range in volume and deposit style in the ancient volcanic history of Ruapehu, and were used to date and interpret i) cone collapses, ii) voluminous mass-flow mechanisms, iii) styles and magnitudes of volcanism, iv) magmatic evolution, v) climate interaction, and vi) landscape response to rapid volcaniclastic ring-plain aggradation.

In the first part of this study, the Mataroa Formation along the Hautapu River southeast of Mt. Ruapehu was revealed to represent deposits from one of the largest known collapse events of the stratovolcano's history, occurring c. 230 - 180 ka, followed by c. 50 ka of vigorous regrowth that produced numerous large-scale (VEI ≥4) pyroclastic eruptions and pumice-rich lahars. Destabilisation of the southeastern volcanic flank (formed <230 ka ago during the Te Herenga cone-building episode) produced a 2 - 3 km^3 debris avalanche that spilled into the Hautapu valley, inundating >260 km^2. Confinement and elevated pore pressures transformed the collapsed mass into a cohesive debris flow and enhanced its mobility (Tost et al., 2014). Following the collapse, rapid decompression of the unloaded magmatic system triggered sub-plinian to plinian eruptions accompanied by long-runout syn-eruptive lahars. The volcaniclastic deposition within the proto-Hautapu River catchment filled its valley and was eventually followed by complete truncation of it from the volcano source (aided by regional faulting) c. 125 ka ago. Starved of its sediment supply, the river deeply incised into the eastern margins of the volcaniclastic deposits, and the underlying Pliocene mudstones. Constant uplift and climatic-induced aggradation-degradation cycles ultimately formed a topographically

reversed terraced landscape with the Mataroa Formation exposed as a distinctive plateau on the highest topographic elevation within the Hautapu River valley (Tost et al., 2015).

This volcanic incursion into the Hautapu valley was repeated in many other catchments, with a debris-avalanche deposit of similar age and lithology found within the Whangaehu River immediately westward. Broadly common ages (within possible errors of evaluation), and similar chemistry and characteristics of deposits in both these catchments, indicate that the two units are related to the same collapse event, which would certainly be the largest known from the volcano. Even if not related, both these events represent flank collapses of significant enough magnitudes to affect the magma system below Mt. Ruapehu, leading to rejuvenated volcanism (as seen in the associated large-scale pumice-rich lahars). Thus it could be expected that major collapses from volcanoes such as Mt. Ruapehu, would be followed by a burst of violent explosive eruptions. In addition, the landscape surrounding such volcanoes may be permanently altered by the large-scale deposition of mass-flow deposits, which may alter river pathways for tens of thousands of years (e.g., Procter et al., 2009).

As a further major outcome of this study, debris-avalanche deposits were also mapped within the Mangawhero, Manganuioteao, Whakapapa and Whanganui River catchments to the south, west and northwest of the volcano. These deposits evidence a series of debris avalanches of between 1.3 and 3 km^3 from Mt. Ruapehu. These have collectively inundated an area of >1,200 km^2 (Tost et al., 2014). All of the Ruapehu debris-avalanche deposits show very poor sorting, a matrix of clay to sand that supports large clasts that include: subrounded boulders up to 5 m in diameter, jig-saw fractured clasts, deformed clasts, domains of similar lithologies, fragments of clastic material, and deformed rip-up clasts of late-Pliocene marine sediments. A key in understanding the emplacement of these deposits lies in the highly dissected landscape surrounding the stratovolcano, which channels voluminous mass flows into deep gorges. Here, loading of water-saturated substrates may form a basal shear zone, lubricating the mass flows and leading to very long runouts (Tost et al., 2014). Comparison to other debris-avalanche deposits worldwide demonstrates that extremely long-runout landslides are common in settings with rugged topographies and especially deep valleys. The runouts of these channelised flows are 2 - 3 times greater than those of unconfined subaerial volcanic landslides of similar volume (Tost et al., 2014). This shows that identification of the geomorphic conditions that enhance runouts of potential future debris avalanches is critical for accurately defining mass-flow hazards at stratovolcanoes, especially in humid tropical and temperate climates.

8.2 Reconstruction of the eruptive history of Mount Ruapehu

Although not a traditional target for chronological studies, lava clasts within debris-avalanche deposits may be highly useful for $^{40}Ar/^{39}Ar$-dating of longer-term and more complete records of stratovolcanoes. By integrating these lava-formation ages with deposition ages from stratigraphic, geomorphic and lithological characteristics of the mass-flow deposits that host them, cone growth and destruction stages of the volcano can be reconstructed. At Ruapehu, this has provided a new record showing repeated growth and collapse cycles at the volcano.

The results of this study have extended the known age of Mt. Ruapehu, with the earliest known

eruptives within the Turakina episode from >340 to 280 ka ago. The lithology of these deposits is consistent with lahars re-depositing pumice produced during large-scale plinian eruptions at Mt. Ruapehu. A syn-eruptive large-scale collapse of the southern flank of proto-Mt. Ruapehu produced a voluminous mass flow into the Turakina River catchment with deposits found c. 90 km south of the volcano. This eruption period also coincided with large-scale caldera volcanism in the Taupo Volcanic Zone (Houghton et al., 1995).

The next phase of cone growth at Mt. Ruapehu was the Te Herenga cone-building episode (250 - 180 ka; Gamble et al., 2003). This phase produced voluminous lavas and probably pyroclastic deposits to build a very unstable cone. During this period, up to four separate major flank collapses occurred, producing debris-avalanche deposits into the Hautapu, Whangaehu, Whakapapa and Whanganui River catchments. The deposit lithologies suggest that all of these failures occurred after weakening of the edifice due to hydrothermal alteration, potentially accentuated by magmatic unrest. The collapses occurred toward the end of the penultimate glaciation and onset of the last Interglacial. This implies that the loss of glacial ice cover on the volcano may have led to rapid unloading and saturation of the edifice, exacerbating the potential for collapse. Following the flank collapses, rapid unloading of the magmatic system resulted in decompression and rejuvenated explosive pumice-producing sub-plinian and plinian eruptions. The products of these were subsequently remobilised into numerous syn-eruptive lahars, which spilled into the four river catchments. After the bursts of pumice-rich lahars, lower-energy fluvial processes resumed in the affected catchments, leading to downcutting and narrow valley forms.

The next major growth phase of Ruapehu was the Oreore cone-building episode between c. 180 - 160 ka ago. This began with a large syn-eruptive collapse from the southern volcano flank, coupled with a plinian/sub-plinian eruption. Fresh pumice and chilled pyroclastic clasts were incorporated into the resulting debris-avalanche deposit, as well as within numerous syn-eruptive lahars that spilled into the proto-Mangawhero River valley.

The Oreore episode was soon followed by the start of the Wahianoa cone-building episode, recognised by extensive lava flows on the volcanic flanks (dated between 160 - 119 ka; Gamble et al., 2003), as well as a debris-avalanche deposit exposed along the Manganuioteao River. The lithology of the debris-avalanche deposit included common pyroclastic material and fragile cooling-fractured blocks, indicating a syn-eruptive flank collapse.

The next major deposition interval, termed the Waimarino cone-building episode (c. 100 - 55 ka), began with lahars associated with remobilised pyroclastic deposits that spilled into the Upper Waikato River from >80 - 65 ka, with later units being more polylithologic and likely inter-eruptive (Cronin et al., 1996a). Laharic units of similar age were deposited into the Whakapapa River (Neall, 1993; this study), the Waimarino, Manganuioteao and the Mangaturuturu Rivers (Grindley, 1960; Hay, 1967; Lecointre et al., 1998). Numerous large sub-plinian to plinian eruptions occurred regularly from 65 - 55 ka, with tephras deposited to the east (Cronin et al., 1996a), coinciding with collapse of the western flank of Mt. Ruapehu to produce a debris avalanche into the Manganuioteao River catchment. This was followed by numerous syn-eruptive lahars, which spilled into most western Ruapehu catchments.

This study provided new insights into the eruptive activity of Mt. Ruapehu prior to 50 ka and shows that major flank collapses occurred both with, and in the absence of, large volcanic eruptions. The growth of the volcano appears to be highly episodic, with vigorous regrowth phases commonly following major flank collapses and interspersed by quiescence/low-level periods of activity. The current volcanic behaviour is dominated by small-scaled eruptions

(VEI 1 - 3), but with a large unstable edifice and ongoing hydrothermal alteration, this situation could rapidly change. Hence, for hazard assessment, it is essential to consider the full-range hazards that can occur in potential new episodes of cone growth and collapse at Mt. Ruapehu.

8.3 Petrological and geochemical implications of this study

Previous petrological and geochemical studies on Mt. Ruapehu were limited to the lava-flow sequences exposed on the volcanic edifice (e.g., Cole, 1983; Graham & Hackett, 1987; Hackett & Houghton, 1989; Price et al., 1999; Gamble et al., 2003, Price et al., 2012). This means that most sampling was dominantly from similar (most recent) episodes of volcanism. Older volcanic periods, such as the Te Herenga cone-building episode (250 - 180 ka; Gamble et al., 2003), are found as eroded remnants, exposed on a single small sector of the volcanic edifice (Hackett & Houghton, 1989), and thus may not be representative of the entire eruptive period. Adding petrological and compositional data from lava clasts within the mapped and dated mass-flow deposits studied here provided new insights into some of the missing periods of magmatic system evolution on the volcano.

This study has pushed back the estimate of the oldest Ruapehu volcanism, by finding distinctive Ruapehu major- and trace-element compositions from clasts within a long-runout debris-flow deposit exposed at Turakina, 90 km south of the volcano. This deposit, bracketed by marine terrace sequences (Pillans, 1983), was deposited 310 - 340 ka ago. Pargasite-bearing autoliths within these units were dated at 486.5 ± 37.6 ka, which shows that Ruapehu's deeper magmatic system is even older, and indicates that the earliest "Turakina" magmas were more hydrous than subsequent lavas and derived from >40 km depths. The autoliths are absent from all younger units studied. This shows that hydrous magmas were only short lived, and as the heat flux rose to present-day levels, the system became dryer and moved outside the amphibole-stability field. This was coupled with the shifting of Ruapehu's magma-storage system from the lower crust to mid- and/or upper crustal levels. The whole-rock composition of the Turakina mass-flow lava samples shows that the magmas associated with this early eruptive episode were derived from a magmatic system similar to that seen in Recent lavas. Thus, a system had developed where primitive magmas accumulated within multiple, small-scaled pockets and evolved along separate polybaric pathways.

Previous studies concluded that the modern magma-storage system was first established during the Wahianoa cone-building episode (160 - 119 ka; Gamble et al., 2003), because the earlier Te Herenga lavas on the edifice are of more primitive origin (Price et al., 2012). The lava clasts of Te Herenga age sampled from debris-avalanche deposits, however, span a wider geochemical array, including more evolved compositions. With the broader sampling insights from the ring-plain sequences, it was found here that the most primitive lavas seen from Mt. Ruapehu are generally in Oreore Formation deposits, indicating a major phase of primitive magma replenishment at Mt. Ruapehu around 180 - 160 ka ago. Textural evidence for magma mingling is observed for all Ruapehu samples, which likely reflects a common trigger mechanism of major eruptive episodes, especially those associated with accelerated eruptions occurring after a major cone collapse and magma-system unroofing.

8.4 Debris-avalanche hazards

This study has identified seven debris-avalanche deposits on the proximal and distal ring plain related to individual flank failures of Mt. Ruapehu. Five of these have never been described before and only one of them had been identified as a debris avalanche (Keigler et al., 2011). $^{40}Ar/^{39}Ar$-dating of lava clasts within each deposit does not indicate a clear collapse frequency, but from reconstruction of the stratovolcano, it seems that it takes c. 60 - 90 ka until major flank failure occurs. Volcanic debris-avalanches are among the largest and most violent processes known from stratovolcanoes (Ui, 1983; Siebert, 1984; Glicken, 1991; Palmer, 1991), and can be triggered by magma intrusion, spreading of large growing edifices on soft sedimentary substrates, major tectonism, deep hydrothermal alteration, and also rapid deglaciation of ice-capped composite cones during major climate changes (e.g., Siebert, 1984; Alloway et al., 1986; McGuire, 1996; Capra, 2006; Deemingl et al., 2012; Roverato et al., 2011; Zernack et al., 2012; Capra et al., 2013). Examining the timing of major climate change in relation to flank failures of Mt. Ruapehu reveals several coincidences. Glacial-eustatic changes and landscape responses in New Zealand during Late Quaternary climates are well known (Pillans, 1983; 1994). The Turakina, Mataroa, Lower Whangaehu, and Piriaka collapses from Mt. Ruapehu occurred during transitions between glacial and interstadial climates. At these times, the loss of slope stability induced by rapid glacier retreat, and increased water availability and deep circulation, destabilises steep and hydrothermally altered volcanic flanks. In addition, the Oreore and Pukekaha events show clear evidence for being syn-eruptive collapses with juvenile lithologies throughout the deposits. Magmatic intrusion/eruption-triggered collapses took place during glacial, as well as interstadial, climates.

The temperate and humid climate of Mt. Ruapehu, accompanied by seasonal glacier retreat, amplifies pore-water circulation through Mt. Ruapehu's loose and hydrothermally altered volcaniclastics, and could potentially trigger small-scaled post-eruptive collapses without warning, such as that represented by the ~4500 yrs B.P. Mangaio Formation (Donoghue & Neall, 2001).

8.5 Post-collapse geomorphic impacts of volcanic debris avalanches

Partial cone collapses may dramatically alter the geomorphology of areas tens to 100 km away from the volcano by filling valleys with debris-avalanche deposits, damming rivers, and/or completely truncating and reshaping previous drainage systems (e.g., Crandell et al., 1984; Siebert, 1984; Procter et al., 2009; Zernack et al., 2012). Long-runout debris avalanches occurred within seven major river catchments around Mt. Ruapehu. Six of these river systems show clear indications for major alteration of their stream path as a consequence of mass-flow aggradation. The Hautapu and Turakina River systems are currently completely truncated from the volcano. Ongoing regional strike-slip faulting on the proximal and distal Ruapehu ring plain exacerbated this (Villamor & Berryman, 2006b), but the initial changes were wrought by extremely high sediment fluxes into the drainage systems due to sudden mass-flow emplacement. After a cone-collapse event, a rejuvenation of highly vigorous explosive volcanism often began at Mt. Ruapehu. This also produced large-scale mass-wasting events in the form of numerous post- and syn-eruptive lahars, contributing to the valley fills.

In the central North Island of New Zealand, constant uplift (c. 1.33 - 5 mm yr^{-1}) led to rapid river entrenchment into volcaniclastic aggradational deposits, especially during periods of reduced sediment supply. Thus over time, mass flow aggradational surfaces were elevated high above the active river channel to form distinctive plateaus. Coupled with the relative hardness of volcaniclastic deposits, compared to the weak Miocene-Pliocene mudstones in this area, the highest topographic elevations of each catchment are typically formed in volcanic mass-flow deposits. After major debris-avalanche deposits, even if fluvial erosion has removed the bulk of the materials, the power of the normal fluvial processes was not enough to remove the largest andesitic boulders, leaving them stranded and scattered on top of younger river terraces throughout the area. The volcanic collapses of Mt. Ruapehu have thus had long-lived impacts on the surrounding landscape. This indicates that future collapse events will also significantly alter drainage systems for thousands of years. Such landscape response could cause severe environmental and socioeconomic impacts that could well exceed those of associated explosive volcanic eruptions (e.g., Mercado et al., 1996) and thus should be considered for future long-term hazard mitigation planning.

CHAPTER 9: CONCLUSIONS

Eruptions of stratovolcanoes are among the most hazardous natural phenomena known to humankind. The products of explosive eruptions, including pyroclastic flows and widespread falls, affect broad areas and may also induce global climate impacts. Hydrological responses to pyroclastic eruptions may also be considerable in tropical and temperate areas where rainfall or ice/snow interaction produces lahars that run out many tens to a few hundred km from volcanic slopes (e.g., Mothes, 1992; Rodolfo, 2000; Lecointre et al., 2004; Doyle et al., 2009).

Further to eruption related hazards, the steep and unstable nature of stratovolcanoes poses an inherent major regional hazard. These large edifices grow rapidly, at times on weak sedimentary substrates, and involve a mixture of solid (lava) and fragmental (pyroclastic and volcano-sedimentary) material, buttressed in some cases by ice and glaciers. Spreading of a growing volcanic load on a weak substrate, increasing height and steepness of cones, loss of buttressing ice, internal fluid circulation and hydrothermal alteration, as well as intrusions of new magma into an edifice, all promote its potential failure. When a catastrophic sudden failure or collapse of complete edifice flanks occurs, it generates a debris avalanche. These rapidly moving “dry” mass flows are driven by the huge potential energy of the large volume and may travel tens to up to hundreds of km from the volcano, destroying everything in their paths. Further, such landslides, which typically involve 1 - 10 km^3 of material, may permanently change the surrounding landscape and fill valleys, block rivers and prograde coastal areas (Siebert, 1984; McGuire, 1996; Zernack et al., 2012; Tost et al., 2015).

The combined record of mass-flow deposits from debris avalanches, as well as syn- and intra-eruptive lahars, may be found in river valleys and overlapping fans many tens to hundreds of km around the source volcano. These distal volcaniclastic deposits can be preserved in the landscape over long periods of geological time and may constitute the only remnants of older eruptive records of a long-lived stratovolcano, where proximal lavas and pyroclastics are buried on, or eroded from, the volcanic edifice (Zernack et al., 2011). In this way, studying the record of mass-flow deposits will help to more robustly evaluate the potential future hazards and eruptive behaviour of a stratovolcano, and provide a more complete understanding of the evolution of its magmatic system.

9.1 Fulfilment of study objectives

The objectives of this study, as outlined in Chapter 1, began with contributing to the known geological, petrological, and geochemical record of Mt. Ruapehu. To this end a full stratigraphic record of volcaniclastic deposits exposed within the Hautapu, Turakina, Mangawhero, Manganuioteao, Whakapapa and Whanganui River valleys was constructed and is presented in Chapter 5. This was combined with $^{40}Ar/^{39}Ar$-dating of lava samples and cover-bed sequences to reveal that the eruptive activity of Mt. Ruapehu has spanned ≥340,000 years, at least 40 ka older than previously thought (Gamble et al., 1993). Three hitherto unknown cone-building episodes of the volcano (Turakina, Oreore, Waimarino) were identified based on the lithology and stratigraphy of the dated distal mass-flow deposits. Large-scale plinian to sub-plinian eruptions of the stratovolcano were commonly associated with pyroclastic density currents,

syn-eruptive flank collapses, and long-runout mass flows. At Mt. Ruapehu cone collapse and regrowth cycles appear broadly coincident with periods of enhanced caldera volcanism in the TVZ (Houghton et al., 1995), as well as transitions from glacial periods into interglacial climates (Chapter 7).

Geochemical and petrological studies of selected samples from the mass-flow deposits were compared to the known and dated lava-flow sequences exposed on the Mt. Ruapehu edifice (e.g., Hackett & Houghton, 1989; Waight et al., 1999; Gamble et al., 2003). In Chapter 6 these data were used to understand magmatic compositional change and development during three previously unknown cone-building episodes. The examination of these lava samples also shows that the multi-stage plumbing model, proposed for the Ruapehu melts in the latest 180 ka of volcanism, was already well established by 340 ka ago. Magma mixing appears to have been common during all cone-building episodes and may have been a common trigger of major eruptions, syn-eruptive collapses, and volcanic cone re-growth.

Debris-avalanche deposits from up to four edifice failures have been previously recognized at Mt. Ruapehu (Palmer & Neall, 1989; Donoghue & Neall, 2001; Keigler et al., 2011). Within this study, a further six debris-avalanche deposits related to major flank failures of Mt. Ruapehu were identified and mapped between the southwestern to northwestern distal ring plain, revealing that the frequency of these catastrophic hazard processes is much higher than previously thought. The voluminous landslides (between 1.3 and 3 km^3) were confined to the valleys of deeply incised river systems, which optimised their runouts leading to deposition up to 100 km from source, inundating a combined area of >1,200 km^2. Decompression of the magmatic system due to rapid unloading following collapse commonly triggered subsequent vulcanian to sub-plinian eruptions, which produced syn-eruptive mass flows that also spilled into multiple river catchments.

The rapid and voluminous edifice collapse was followed by remobilisation of debris from the collapse scarp and/or the mass-flow deposits, leading to aggrading volcanic conglomerates alongside and on the margins of the undulating debris-avalanche deposit topography. Subsequent syn- and post-eruptive lahars emplaced tabular deposits that smoothed the irregular debris-avalanche surface. Regional strike-slip faulting (Villamor & Berryman, 2006a; 2006b) resulted in the river systems being re-established along similar routes as the previous drainage pathways. Subsequent and ongoing uplift (c. 1.33 ± 0.5 mm yr^{-1} to 5 ± 1.25 mm yr^{-1}) elevated the aggradational volcaniclastic surfaces, which due to their relative resistance to erosion in comparison to the surrounding Tertiary mudstones, led to development of distinct plateaus at the tops of the valley margins (e.g., Tost et al., 2015).

9.2 Unanticipated findings

9.2.1 Igneous basement identification

Clasts sampled from the Turakina mass-flow deposit comprise unusual amphibole-bearing xenoliths, which reflect a hitherto unknown basement type underlying the Ruapehu massif at >40 km depth, and indicate that the magmas associated with the Turakina cone-building episode were much more hydrous than those observed in lavas on the current edifice. Furthermore, the xenoliths confirm that the inception of Ruapehu's volcanism was preceded by magmatic crustal underplating (e.g., Graham et al., 1990; Price et al., 2005; Stern et al., 2010; Price et al.,

2012). High-precision dating of the pargasites suggests that the deeper magmatic system of the stratovolcano was probably established by 486.5 ± 37.6 ka ago. These xenoliths are absent within the Ruapehu lavas formed ≤250 ka ago, which indicates a shift of the stratovolcano's magma-storage system from the lower crust to mid- and/or upper crustal levels. This change likely results from a progressively increasing heat flux to the high present day values where amphibole is no longer stable.

9.2.2 Transport and emplacement mechanisms of channelized debris avalanches (Tost et al., 2014)

Mapping of the debris-avalanche deposits studied revealed both an extraordinarily long runout, and that the flows were channelled down deep river valleys radiating from the Ruapehu ring plain. The sedimentological characteristics of the deposits show a range of dry debris-avalanche characteristics (jig-saw fractured clasts, domains of similar lithologies) along with unusual features, such as ripped-up basement mudstone, rounded lava boulders and fluvial gravels. It was concluded that the channelization of the flowing debris avalanches led to enhanced basal and marginal erosion, which resulted in entrainment of water-saturated substrate and concentration of fluids at the base of flows. As a consequence, a basal lubrication zone developed, which reduced the basal friction of the flows, and led to mobilisation and significantly enhanced runouts (up to 100 km from the volcano).
Comparison of these Ruapehu examples with debris-avalanche deposits worldwide indicates that extremely long-runout mass flows dominantly occur in humid tropical and temperate settings, where deep river valleys channelize collapsing masses and cause liquefaction at their base. The runout of such confined debris avalanches is generally 2 - 3 times longer than for unconfined, spreading flows of similar volume.

9.2.3 Climate interaction as a potential trigger for flank collapses at Mt. Ruapehu

Comparison of dated debris-avalanche deposits to known glacial and interglacial cycles and the associated landforms (Pillans, 1983; 1994) indicates that large-scale debris avalanches from Mt. Ruapehu occurred commonly at the shift from glacial to interstadial climates. Destabilisation of the steep and hydrothermally altered volcanic flanks was likely exacerbated by rapid unloading during deglaciation of the ice-capped composite cone. Syn-eruptive collapse can occur anytime and is most likely caused by swelling of the edifice by magma intrusion and enhanced seismicity.

9.3 Potential future work

During this research a number of additional areas of investigation were uncovered, which are listed below:

A) Investigate the physical and textural properties of the tephra exposed within the Pukekaha Formation, in order to elucidate the column height and eruption properties of these events in the earlier part of the Mt. Ruapehu eruption record.

B) Studies of textures within the pumice lapilli of the mass-flow deposits in order to gain insights

into the volatile-content of the melt and explosivity of the oldest eruptions from Mt. Ruapehu.

C) Detailed studies of mass-flow lithologies to gain a clearer understanding of characteristic features that define syn- and post-eruptive lahars.

D) Geochemical analyses of hyaline groundmasses from lava-flow sequences on the cone, as well as pumice lapilli within the distal mass-flow deposits, could provide deeper insights into the magmatic evolution of Mt. Ruapehu.

E) Offshore drilling close to river estuaries in the main catchments that guide lahars could provide more detailed knowledge regarding Ruapehu's (and Tongariro's) eruptive history >340 ka.

F) Further high-precision dating of mass-flow units (including the Turakina debris flow), in order to establish a more detailed stratigraphic framework for large-scale eruptions (VEI ≥4) and collapse events of Mt. Ruapehu.

G) Investigate the occurrence of hornblende-bearing xenoliths throughout the TVZ, in order to gain a clearer understanding of the properties of the deep magmatic system, as well as the nature and extent of the basement-type.

H) Investigate the nature of the fluvial terraces, especially regarding the relationship between climate snd sediment supply coupled with regional uplift and low offshore gradient.

CHAPTER 10: REFERENCES

Acocella, V., Spinks, K., Cole, J., & Nicol, A. (2002). Oblique back-arc rifting of the Taupo Volcanic Zone, New Zealand. Tectonics, 22(2), 1045.

Adams, C. J., Barley, M. E., Maas, R., & Doyle, M. G. (2002). Provenance of Permian-Triassic volcaniclastic sedimentary terranes in New Zealand: evidence from their radiogenic isotope characteristics and detrital mineral age patterns. New Zealand Journal of Geology and Geophysics, 45(2), 221-242.

Adams, C. J., Campbell, H. J., & Griffin, W. L. (2007). Provenance comparisons of Permian to Jurassic tectonostratigraphic terranes in New Zealand: perspectives from detrital zircon age patterns. Geological Magazine, 144(04), 701-729.

Alloway, B. D., Neall, V. E., & Vucetich, C. G. (1986). Another prehistoric debris avalanche deposit recognized from ancestral Egmont volcano. International Volcanological Congress, New Zealand 2.

Alloway, B., McComb, P., Neall, V., Vucetich, C., Gibb, J., Sherburn, S., & Stirling, M. (2005). Stratigraphy, age, and correlation of voluminous debris-avalanche events from an ancestral Egmont Volcano: Implications for coastal plain construction and regional hazard assessment. Journal of the Royal Society of New Zealand 35(1-2), 229-267.

Anderson, J. L., & Smith, D. R. (1995). The effects of temperature and $f0_2$ on the Al-in-hornblende barometer. American Mineralogist, 80, 549-559.

Andújar, J., Scaillet, B., Pichavant, M., & Druitt, T. H. (in review). Differentiation Conditions of a Basaltic Magma from Santorini, and its Bearing on the Production of Andesite in Arc Settings. Submitted to Journal of Petrology.

Arculus, R. J., & Wills, K. J. (1980). The petrology of plutonic blocks and inclusions from the Lesser Antilles island arc. Journal of Petrology, 21(4), 743-799.

Arculus R. J. & Powell, R. (1986). Source component mixing in regions of arc magma generation. Journal of Geophysical Research 91, 5913-5926.

Arguden, A. T., & Rodolfo, K. S. (1990). Sedimentologic and dynamic differences between hot and cold laharic debris flows of Mayon Volcano, Philippines. Geological Society of America Bulletin, 102(7), 865-876.

Begét, J. E., & Kienle, J. (1992). Cyclic formation of debris avalanches at Mt Augustine Volcano. Nature, 356, 701-704.

Berger, G. W., Pillans, B. J., & Palmer, A. S. (1992). Dating loess up to 800 ka by thermoluminescence. Geology, 20(5), 403-406.

Berryman, K. (1992). A stratigraphic age of Rotoehu Ash and late Pleistocene climate interpretation based on marine terrace chronology, Mahia Peninsula, North Island, New Zealand. New Zealand journal of geology and geophysics, 35(1), 1-7.

Berryman, K., Marden, M., Eden, D., Mazengarb, C., Ota, Y., & Moriya, I. (2000). Tectonic and paleoclimatic significance of Quaternary river terraces of the Waipaoa River, east coast, North Island, New Zealand. New Zealand Journal of Geology and Geophysics, 43(2), 229-245.

Bertolani, M., & Loschi-Ghittoni, A. G. (1986). Clay materials from the Central Valley of Costa Rica and their possible ceramic uses. Applied Clay Science, 1(3), 239-254.

Beu, A. G., & Edwards, A. R. (1984). New Zealand Pleistocene and late Pliocene glacio-eustatic cycles. Palaeogeography, Palaeoclimatology, Palaeoecology, 46(1), 119-142.

Beverage, J. P., & Culbertson, J. K. (1964). Hyperconcentrations of suspended sediment. Journal of the Hydraulics Division, American Society of Civil Engineers, 90, pp. 117-126.

Bibby, H. M., Caldwell, T. G., Davey, F. J., & Webb, T. H. (1995). Geophysical evidence on the structure of the Taupo Volcanic Zone and its hydrothermal circulation. Journal of Volcanology and Geothermal Research, 68(1), 29-58.

Blong, R. J. (1984). Volcanic hazards. A sourcebook on the effects of eruptions.

Bridgland, D. R. (2000). River terrace systems in north-west Europe: an archive of environmental change, uplift and early human occupation. Quaternary Science Reviews, 19(13), 1293-1303.

Briffa, K. R., Jones, P. D., Schweingruber, F. H., & Osborn, T. J. (1998). Influence of volcanic eruptions on Northern Hemisphere summer temperature over the past 600 years. Nature, 393(6684), 450-455.

Brown, S. J. A., Wilson, C. J. N., Cole, J. W., & Wooden, J. (1998). The Whakamaru group ignimbrites, Taupo Volcanic Zone, New Zealand: evidence for reverse tapping of a zoned silicic magmatic system. Journal of Volcanology and Geothermal Research, 84(1), 1-37.

Burbank, D. W., Leland, J., Fielding, E., Anderson, R. S., Brozovic, N., Reid, M. R., & Duncan, C. (1996). Bedrock incision, rock uplift and threshold hillslopes in the northwestern Himalayas, Nature, 379, 505–510.

Bussell, M. R., & Pillans, B. (1992). Vegetational and climatic history during oxygen isotope stage 9, Wanganui district, New Zealand, and correlation of the Fordell Ash. Journal of the Royal Society of New Zealand, 22(1), 41-60.

Cameron, E., Gamble, J., Price, R., Smith, I., McIntosh, W., & Gardner, M. (2010). The petrology, geochronology and geochemistry of Hauhungatahi volcano, SW Taupo Volcanic Zone. Journal of Volcanology and Geothermal Research, 190(1), 179-191.

Campbell, C. S. (1989). Self-lubrication for long runout landslides. The Journal of Geology, 653-665.

Campbell, I. B. (1973). Recent aggradation in Whangaehu valley, central North Island, New Zealand. New Zealand Journal of Geology and Geophysics, 16(3), 643-649.

Cao, R., & Qian, S. (1990). Sediment transport characteristics of hyperconcentrated flow with suspended load. Hydraulics/Hydrology of Arid Lands (H²AL), 657-662.

Capra, L. (2006). Abrupt climatic changes as triggering mechanisms of massive volcanic collapses. Journal of Volcanology and Geothermal Research, 155(3), 329-333.

Capra, L., Bernal, J. P., Carrasco-Núñez, G., & Roverato, M. (2013). Climatic fluctuations as a significant contributing factor for volcanic collapses. Evidence from Mexico during the Late Pleistocene. Global and Planetary Change, 100, 194-203.

Carrasco-Nuñez, G., Díaz-Castellón, R., Siebert, L., Hubbard, B., Sheridan, M. F., & Rodríguez, S. R. (2006). Multiple edifice-collapse events in the Eastern Mexican Volcanic Belt: The role of sloping substrate and implications for hazard assessment. Journal of Volcanology and Geothermal Research, 158, 151-176.

Cashman, K. V., Deligne, N. I., Gannett, M. W., Grant, G. E., & Jefferson, A. (2009). Fire and water: Volcanology, geomorphology, and hydrogeology of the Cascade Range, central Oregon. Field Guides, 15, 539-582.

Chinn, T. J. (2001). Distribution of the glacial water resources of New Zealand. Journal of Hydrology (New Zealand), 40(2), 139-187.

Christenson, B. W., & Wood, C. P. (1993). Evolution of a vent-hosted hydrothermal system

beneath Ruapehu Crater Lake, New Zealand. Bulletin of Volcanology, 55(8), 547-565.

Christenson, B. W., Reyes, A. G., Young, R., Moebis, A., Sherburn, S., Cole-Baker, J., & Britten, K. (2010). Cyclic processes and factors leading to phreatic eruption events: Insights from the 25 September 2007 eruption through Ruapehu Crater Lake, New Zealand. Journal of Volcanology and Geothermal Research, 191(1), 15-32.

Christiansen, R. L. & Peterson, D. W. (1981). The 1980 eruptions of Mount St. Helens. US Deptartment of the Interior, US Geological Survey, Washington, (1250), 17.

Cioni, R., Marianelli, P., Santacroce, R., & Sbrana, A. (2000). Plinian and subplinian eruptions. In: Houghton, B., Rymer, H., Stix, J., McNutt, S., & Sigurdsson, H. (eds.), Encyclopedia of Volcanoes. Academic Press, San Diego, 477-494.

Clark, R. H. (1960). Andesite lavas of the North Island, New Zealand. Department of Geology, Victoria University, Wellington, New Zealand, 123-131.

Coates, D. R. (1977). Landslide perspectives. Reviews in Engineering Geology 3, 3-28.

Coats, R. R. (1950). Volcanic activity in the Aleutian arc. US Government Printing Office, 35-49.

Cole, J. W. (1978). Andesites of the Tongariro Volcanic Centre, North Island, New Zealand. Journal of Volcanology and Geothermal Research, 3(1), 121-153.

Cole, J. W. (1982). Tonga-Kermadec-New Zealand. Andesites; Orogenic Andesites and Related Rocks. Chichester: John Wiley, 245-258.

Cole, J. W., Cashman, K. V., & Rankin, P. C. (1983). Rare-earth element geochemistry and the origin of andesites and basalts of the Taupo Volcanic Zone, New Zealand. Chemical Geology, 38(3), 255-274.

Cole, J. W., Graham, I. J., Hackett, W. R., & Houghton, B. F. (1986). Volcanology and petrology of the Quaternary composite volcanoes of Tongariro volcanic centre, Taupo volcanic zone. Royal Society of New Zealand Bulletin, 23, 224-250.

Cole, S. E., Cronin, S. J., Sherburn, S., & Manville, V. (2009). Seismic signals of snow-slurry lahars in motion: 25 September 2007, Mt Ruapehu, New Zealand. Geophysical Research Letters, 36(9).

Collins, G. S., & Melosh, H. J. (2003). Acoustic fluidization and the extraordinary mobility of sturzstroms. Journal of Geophysical Research 108(B10), 2473.

Conrad, W. K., & Kay, R. W. (1984). Ultramafic and mafic inclusions from Adak Island: crystallization history, and implications for the nature of primary magmas and crustal evolution in the Aleutian Arc. Journal of Petrology, 25(1), 88-125.

Costa, J. E. (1984). Physical geomorphology of debris flows. In: Developments and Applications of Geomorphology. Springer Berlin Heidelberg, 268-317.

Coussot, P. (1995). Structural similarity and transition from Newtonian to non-Newtonian behavior for clay-water suspensions. Physical Review Letters, 74(20), 3971.

Coussot, P., & Piau, J. M. (1994). On the behavior of fine mud suspensions. Rheologica Acta, 33(3), 175-184.

Crandell, D. R., & Mullineaux, D. R. (1973). Pine Creek volcanic assemblage at Mount St. Helens, Washington. U.S. Geological Survey Bulletin 1383-A, 23 p.

Crandell, D. R., Miller, C. D., Glicken, H. X., Christiansen, R. L., & Newhall, C. G. (1984). Catastrophic debris avalanche from ancestral Mount Shasta volcano, California. Geology, 12(3), 143-146.

Cronin, S. J. (1996). Late quarternary volcanic stratigraphy within a portion of the northeastern Tongariro volcanic centre. PhD thesis, Massey University, Palmerston North, New Zealand.

Cronin, S. J. (2013). Stratovolcanoes. In: Bobrowsky, P. (ed.) Encyclopedia of Natural Hazards, Springer, 941-947.

Cronin, S. J., & Neall V. E. (1997). A late Quaternary stratigraphic framework for the northeastern Ruapehu and eastern Tongariro ring plains, New Zealand. New Zealand Journal of Geology and Geophysics, 40(2), 185-197.

Cronin, S. J., Neall, V. E., & Palmer, A. S. (1996a). Geological history of the north-eastern ring plain of Ruapehu volcano, New Zealand. Quaternary International, 34, 21-28.

Cronin, S. J., Neall, V. E., Lecointre, J. A., & Palmer, A. S. (1996b). Unusual "snow slurry" lahars from Ruapehu volcano, New Zealand, September 1995. Geology, 24(12), 1107-1110.

Cronin, S. J., Hodgson, K. A., Neall, V. E., Palmer, A. S., & Lecointre, J. A. (1997a). 1995 Ruapehu lahars in relation to the late Holocene lahars of Whangaehu River, New Zealand. New Zealand Journal of Geology and Geophysics, 40(4), 507-520.

Cronin, S. J., Neall, V. E., Lecointre, J. A., & Palmer, A. S. (1997b). Changes in Whangaehu River lahar characteristics during the 1995 eruption sequence, Ruapehu volcano, New Zealand. Journal of Volcanology and Geothermal Research, 76(1), 47-61.

Cronin, S. J., Neall, V. E., Lecointre, J. A., & Palmer, A. S. (1999). Dynamic intercations between lahars and stream flows: A case study from Ruapehu Volcano, New Zealand. Geological Society of America Bulletin, 111, 28-38.

Cronin, S. J., Lecointre, J. A., Palmer, A. S., & Neall, V. E. (2000). Transformation, internal stratification, and depositional processes within a channelised, multi-peaked lahar flow. New Zealand Journal of Geology and Geophysics, 43(1), 117-128.

Cronin, S. J., Neall, V. E., Lecointre, J. A., Hedley, M. J., & Loganathan, P. (2003). Environmental hazards of fluoride in volcanic ash: a case study from Ruapehu volcano, New Zealand. Journal of Volcanology and Geothermal Research, 121(3), 271-291.

Dade, W. B., & Huppert, H. E. (1998). Long-runout rockfalls. Geology, 26(9), 803-806.

Darby, D. J., & Williams, R. O. (1991). A new geodetic estimate of deformation in the Central Volcanic Region of the North Island, New Zealand. New Zealand Journal of Geology and Geophysics, 34, 127-136.

Davidson, J., Turner, S., Handley, H., Macpherson, C., & Dosseto, A. (2007). Amphibole "sponge" in arc crust?. Geology, 35(9), 787-790.

Davies, T. R. (1982). Spreading of rock avalanche debris by mechanical fluidization. Rock Mechanics, 15(1), 9-24.

Davies, T. R., & McSaveney, M. J. (1999). Runout of dry granular avalanches. Canadian Geotechnical Journal, 36(2), 313-320.

Davies, T. R., & McSaveney, M. J. (2012). Mobility of long-runout rock avalanches. In: Landslides, Types, Mechanisms and Modelling. Clague, J. J., & Stead, D. (eds). Cambridge University Press, 50-58.

Davies, T. R., McSaveney, M. J., & Hodgson, K. A. (1999). A fragmentation-spreading model for long-runout rock avalanches. Canadian Geotechnical Journal, 36(6), 1096-1110.

De Silva, S. L., & Zielinski, G. A. (1998). Global influence of the AD 1600 eruption of Huaynaputina, Peru. Nature, 393(6684), 455-458.

Deely, J. M., & Shephard, D. S. (1996). Whangaehu River, New Zealand: geochemistry of a river discharging from an active crater lake. Applied Geochemistry, 11, 447-460.

Deemingl, K., McGuire, B., & Harrop, P. (2012). Climate change and collapsing volcanoes: evidence from Mount Etna, Sicily. Climate Forcing of Geological Hazards, 56-77.

Dinehart, R. L. (1999). Correlative velocity fluctuations over a gravel river bed. Water Resources Research, 35(2), 569-582.

Donoghue, S. L. (1991). Late Quaternary volcanic stratigraphy of the southeastern sector of the Mount Ruapehu ring plain. PhD thesis, Palmerston North, Massey University, New Zealand.

Donoghue, S. L., & Neall, V. E. (2001). Late Quaternary constructional history of the southeastern Ruapehu ring plain, New Zealand. New Zealand Journal of Geology and Geophysics, 44(3), 439-466.

Donoghue, S. L., Gamble, J. A., Palmer, A. S., & Stewart, R. B. (1995). Magma mingling in an andesite pyroclastic flow of the Pourahu Member, Ruapehu volcano, New Zealand. Journal of Volcanology and Geothermal Research, 68(1), 177-191.

Doyle, E. E., Cronin, S. J., Cole, S. E., & Thouret, J-C. (2009). The challenge of incorporating temporal and spatial changes into numerical models of lahars. In: Anderssen, R. S., Braddock, R. D., & Newham, L. T. H. (eds.), Proceedings of the 18th World IMACS Congress and MODSIM09 International Congress on Modelling and Simulation: Modelling and Simulation Society of Australia and New Zealand and International Association for Mathematics and Computers in Simulation, Cairns, Australia, July 2009, 2665-2671.

Dungan, M. A., Wulff, A. & Thompson, R. (2001). Eruptive stratigraphy of the Tatara-San Pedro Complex, 36oS, southern volcanic zone, Chilean Andes: reconstruction method and implications for magma evolution at long-lived arc volcanic centers. Journal of Petrology, 42, 555-626.

Eden, D. N. (1989). River terraces and their loessial cover beds, Awatere River valley, South Island, New Zealand. New Zealand Journal of Geology and Geophysics, 32, 487–497.

Eggins, S. M., Rudnick, R. L., & McDonough, W. F. (1998). The composition of peridotites and their minerals: a laser-ablation ICP–MS study. Earth and Planetary Science Letters, 154(1), 53-71.

Ersoy, Y., & Helvacı, C. (2010). FC–AFC–FCA and mixing modeler: A Microsoft® Excel© spreadsheet program for modeling geochemical differentiation of magma by crystal fractionation, crustal assimilation and mixing. Computers & Geosciences, 36(3), 383-390.

Ewart, A., & Stipp, J. J. (1968). Petrogenesis of the volcanic rocks of the Central North Island, New Zealand, as indicated by a study of Sr87Sr86 ratios, and Sr, Rb, K, U and Th abundances. Geochimica et Cosmochimica Acta, 32(7), 699-736.

Feldmeyer, A. E., Jones, B. C., Firth, C. W., & Knight, F. (1943). Geology of the Palmerston North-Wanganui Basin “west side”, North Island, New Zealand. New Zealand Geological Survey Petroleum Report Series 171.

Fleming, C. A. (1953). The Geology of the Wanganui Subdivision. New Zealand Geological Survey Bulletin, 52, 362.

Francis, P. W., Gardeweg, M., Ramirez, C. F., & Rothery, D. A. (1985). Catastrophic debris avalanche deposit of Socompa volcano, northern Chile. Geology, 13(9), 600-603.

Fuller, I. C., Macklin, M. G., Lewin, J., Passmore, D. G., & Wintle, A. G. (1998). River response to high-frequency climate oscillations in southern Europe over the past 200 ky. Geology, 26(3), 275-278.

Gamble, J. A., Smith, I. E. M., McCulloch, M. T., Graham, I. J., & Kokelaar, B. P. (1993). The geochemistry and petrogenesis of basalts from the Taupo Volcanic Zone and Kermadec Island Arc, SW Pacific. Journal of Volcanology and Geothermal Research, 54(3), 265-290.

Gamble, J. A., Wood, C. P., Price, R. C., Smith, I. E. M., Stewart, R. B., & Waight, T. (1999). A

fifty year perspective of magmatic evolution on Ruapehu Volcano, New Zealand: verification of open system behaviour in an arc volcano. Earth and Planetary Science Letters, 170(3), 301-314.

Gamble, J. A., Price, R. C., Smith, I. E. M., McIntosh, W. C., & Dunbar, N. W. (2003). $^{40}Ar/^{39}Ar$ geochronology of magmatic activity, magma flux and hazards and Ruapehu Volcano, Taupo Volcanic Zone, New Zealand. Journal of Volcanology and Geothermal Research, 120, 271-287.

Gaylord, D. R., & Neall, V. E. (2012). Subedifice collapse of an andesitic stratovolcano: The Maitahi Formation, Taranaki Peninsula, New Zealand. Geological Society of America Bulletin, 124, 181-199.

Gerst, A., & Savage, M. K. (2004). Seismic anisotropy beneath Ruapehu volcano: A possible eruption forecasting tool. Science, 306(5701), 1543-1547.

Glicken, H. (1982). Criteria for identification of large volcanic debris avalanches (abstr). Eos, Transactions of the American Geophysical Union, 63, 1141.

Glicken, H. (1991). Sedimentary architecture of large volcanic debris-avalanches. In: Fisher, R. V., & Smith, G. A., (eds.) Sedimentation in volcanic settings: SEPM Special Publications, 45, 99-106.

Glicken, H., Siebert, L., & Beget, J. E. (1995). The 1883 and late-prehistoric eruptions of Augustine volcano, Alaska. Journal of Volcanology and Geothermal Research, 66(1), 367-395.

Graham, I. J. (1987). Petrography and origin of metasedimentary xenoliths in lavas from Tongariro Volcanic Centre. New Zealand Journal of Geology and Geophysics, 30, 139-157.

Graham, I. J., & Hackett, W. R. (1987). Petrology of calc-alkaline lavas from Ruapehu volcano and related vents, Taupo Volcanic Zone, New Zealand. Journal of Petrology, 28(3), 531-567.

Graham, I. J., Blattner, P. & McCulloch, M. T. (1990). Meta-igneous granulite xenoliths from Mt. Ruapehu, New Zealand: fragments of altered oceanic crust? Contributions to Mineralogy and Petrology, 105, 650-661.

Graham, I. J., Cole, J. W., Briggs, R. M., Gamble, J. A., & Smith, I. E. M. (1995). Petrology and petrogenesis of volcanic rocks from the Taupo Volcanic Zone: a review. Journal of Volcanology and Geothermal Research, 68(1), 59-87.

Green, D. H., & Hibberson, W. (1969). Experimental duplication of conditions of precipitation of high pressure phenocrysts in basaltic magma. Physical Earth Planetary Interiors, 3, 247-254.

Greenaway, R. (1998). The Restless Land: Stories of Tongariro National Park. Tongariro/Taupo Conservancy, Department of Conservation and Tongariro Natural History Society.

Grindley, G. W. (1960). Sheet 8—Taupo. Geological map of New Zealand 1:250 000. Department of Scientific and Industrial Research, Wellington, New Zealand.

Grindley, G. W., & Hull, A. G. (1986). Historical Taupo earthquakes and earth deformation. Royal Society of New Zealand Bulletin, 24, 173-186.

Hackett, W. R., & Houghton, B. F. (1989). A facies model for a Quaternary andesitic composite volcano: Ruapehu, New Zealand. Bulletin of Volcanology, 51(1), 51-68.

Harlen, L. (1999). From ‘useless’ Lands to World Heritage: A History of Tourism in Tongariro National Park. McS-thesis, Massey University, Palmerston North, New Zealand.

Hawkesworth, C. J., Gallagher, K., Hergt, J. M., & McDermott, F. (1993). Mantle and slab contribution in arc magmas. Annual Review of Earth and Planetary Sciences, 21, 175-204.

Hay, R. F. (1967). Sheet 7 – Taranaki. Geological Map of New Zealand 1:250 000, New Zealand

Geological Survey, Wellington.

Hayashi, J. N., & Self, S. (1992). A comparison of pyroclastic flow and debris avalanche mobility. Journal of Geophysical Research, 97(B6), 9063-9071.

Heilprin, A. (1903). Mont Pelee and the tragedy of Martinique. Study of the great catastrophes of 1902. Lippincott.

Hildreth, W., & Lanphere, M. A. (1994). Potassium-argon geochronology of a basalt-andesite-dacite arc system: The Mount Adams volcanic field, Cascade Range of southern Washington. Geological Society of America Bulletin, 106(11), 1413-1429.

Hobden, B. J., Houghton, B. F., Lanphere, M. A., & Nairn, I. A. (1996). Growth of the Tongariro volcanic complex: New evidence from K-Ar age determinations. New Zealand Journal of Geology and Geophysics, 39, 151-154.

Hobden, B. J. (1997). Modelling magmatic trends in time and space: eruptive and magmatic history of Tongariro volcanic complex. Unpublished PhD thesis, University of Canterbury, New Zealand.

Hobden, B. J., Houghton, B. F., Davidson, J. P., & Weaver, S. D. (1999). Small and short-lived magma batches at composite volcanoes: time windows at Tongariro volcano, New Zealand. Journal of the Geological Society, 156(5), 865-868.

Hobden, B. J., Houghton, B. F. & Nairn, I. A. (2002). Growth of a young, frequently active cone: Ngauruhoe Volcano, New Zealand. Bulletin of Volcanology, 64, 392-409.

Hochstein, M. P. (1995). Crustal heat transfer in the Taupo Volcanic Zone (New Zealand): comparison with other volcanic arcs and explanatory heat source models. Journal of Volcanology and Geothermal Research, 68(1), 117-151.

Hodgson, K. A. (1993). Late Quaternary Lahars from Mount Ruapehu in the Whangaehu River Valley, North Island, New Zealand. PhD thesis, Massey University, Palmerston North, New Zealand. 2 vol., 356 and 112 pp, maps.

Hodgson, K. A., & Neall, V. E. (1993). Ruapehu lahars in the Wanganui District. Final report to the Department of Conservation, 71 p.

Houghton, B. F., Latter, J. H., & Hackett, W. R. (1987). Volcanic hazard assessment for Ruapehu composite volcano, Taupo volcanic zone, New Zealand. Bulletin of Volcanology, 49(6), 737-751.

Houghton, B. F., Wilson, C. J. N., McWilliams, M. O., Lanphere, M. A., Weaver, S. D., Briggs, R. M., & Pringle, M. S. (1995). Chronology and dynamics of a large silicic magmatic system: central Taupo Volcanic Zone, New Zealand. Geology, 23(1), 13-16.

Hsü, K. J. (1975). Catastrophic debris streams (sturzstroms) generated by rockfalls. Geological Society of America Bulletin, 86(1). 129-140.

Hungr, O., & Evans, S. G. (2004). Entrainment of debris in rock avalanches: An analysis of a long run-out mechanism. Geological Society of America Bulletin, 116(9-10), 1240-1252.

Hungr, O., Mc Dougall, S., & Bovis, M. (2005). Entrainment of material by debris flows. In: Jokob, M., Hungr, O. (eds.), Debris Flow Hazards and Related Phenomena. Springer-Verlag, 136-157.

Hyde, J. H. (1975). Upper Pleistocene pyroclastic-flow deposits and lahars south of Mount St. Helens volcano, Washington. U.S. Geological Survey Bulletin 1383-B, 20 p.

Iverson, R. M. (1997). The physics of debris flows. Reviews of Geophysics, 35(3), 245-296.

Iverson, R. M. (2012). Elementary theory of bed-sediment entrainment by debris flows and avalanches. Journal of Geophysical Research, 117(F3).

Iverson, R. M., Reid, M. E., Logan, M., LaHusen, R. G., Godt, J. W., & Griswold, J. P. (2010). Positive feedback and momentum growth during debris-flow entrainment of wet bed sediment. Nature Geoscience, 4(2), 116-121.

Janda, R. J., Scott, K. M., Nolan, K. M., & Martinson, H. A. (1981). Lahar movement, effects, and deposits. U.S. Geological Survey Professional Paper, 1250, 461-478.

Johnson, J. (2014). Tongariro Northern Circuit – Great Walk Season 2013-2014. Department of Conservation unpublished Annual Report, 19.

Johnston, D. M., Houghton, B. F., Neall, V. E., Ronan, K. R., & Paton, D. (2000). Impacts of the 1945 and 1995–1996 Ruapehu eruptions, New Zealand: an example of increasing societal vulnerability. Geological Society of America Bulletin, 112(5), 720-726.

Kamp, P. J., Vonk, A. J., Bland, K. J., Hansen, R. J., Hendy, A. J., McIntyre, A. P., & Nelson, C. S. (2004). Neogene stratigraphic architecture and tectonic evolution of Wanganui, King Country, and eastern Taranaki Basins, New Zealand. New Zealand Journal of Geology and Geophysics, 47(4), 625-644.

Keigler, R., Thouret, J. C., Hodgson, K. A., Neall, V. E., Lecointre, J. A., Procter, J. N., & Cronin, S. J. (2011). The Whangaehu Formation: Debris-avalanche and lahar deposits from ancestral Ruapehu volcano, New Zealand. Geomorphology, 133(1), 57-79.

Keleman, P. B., Hanghoj, K. & Greene, A. R. (2005). One view of the geochemistry of subduction-related magmatic arcs, with an emphasis on primitive andesite and lower crust. In: Rudnick, R. L. (ed.) The crust. Treatise on Geochemistry 3. Oxford: Elsevier Pergamon, 593-659.

Kelfoun, K., & Druitt, T. H. (2005). Numerical modeling of the emplacement of Socompa rock avalanche, Chile. Journal of Geophysical Research, 110(B12).

Kent, P. E. (1966). The transport mechanism in catastrophic rock falls. The Journal of Geology, 79-83.

Ker, D. S. (1970). Renewed movement on a slump at Utiku. New Zealand Journal of Geology and Geophysics, 13(4), 996-1017.

Ker, D. S., (1991). Provisional geological map of 1:50 000 sheet T21AC (Hautapu). New Zealand Geological Survey Report G144.

Kershaw, C. (1989). The geology of the area around Kaimatira Bluff, Wanganui, New Zealand. B.Sc. (Hons) thesis, Victoria University of Wellington, New Zealand.

Kilgour, G., Manville, V., Pasqua, F. D., Graettinger, A., Hodgson, K. A., & Jolly, G. E. (2010). The 25 September 2007 eruption of Mount Ruapehu, New Zealand: directed ballistics, surtseyan jets, and ice-slurry lahars. Journal of Volcanology and Geothermal Research, 191(1), 1-14.

Kohn, B. P., Pillans, B., & McGlone, M. S. (1992). Zircon fission track age for middle Pleistocene Rangitawa Tephra, New Zealand: stratigraphic and paleoclimatic significance. Palaeogeography, palaeoclimatology, palaeoecology, 95(1), 73-94.

Koppers, A. A. (2002). ArArCALC—software for $^{40}Ar/^{39}Ar$ age calculations. Computers & Geosciences, 28(5), 605-619.

Kostaschuk, R., Terry, J., & Raj, R. (2003). Suspended sediment transport during tropical-cyclone floods in Fiji. Hydrological processes, 17(6), 1149-1164.

Laronne, J. B., Reid, I., Yitshak, Y., & Frostick, L. E. (1994). The non-layering of gravel streambeds under ephemeral flood regimes. Journal of Hydrology, 159(1), 353-363.

Leake, B. E., Woolley, A. R., Arps, G. E. S., Birch, W. D., Gilbert, M. G., Grice, J. D., Hawthorne, F. G., Kato, A., Kisch, H. J., Krivovichev, V. G., Linthout, K., Laird, J., Mandarino, J. A., Maresch, W. V., Nickel, E. H., Rock, N. M. S., Schumacher, J. G., Smith, D. C., Stephenson,

N. C. N., Ungaretti, L., Whittaker, E. J. W. & Guo, Y. Z. (1997). Nomenclature of amphiboles, report of the Subcommitee on amphiboles of the International Mineralogical Association Commission on new minerals and mineral names. American Mineralogist 82, 1019-1037.

LeBas, M. J., Lemaitre, R. W., Streckeisen, A., & Zanetting, B. (1986). A chemical classification of volcanic rocks based on the total alkali-silica diagram. Journal of Petrology, 27, 745-750.

Lecointre, J. A., Neall, V. E., & Palmer, A. S. (1998). Quaternary lahar stratigraphy of the western Ruapehu ring plain, New Zealand. New Zealand Journal of Geology and Geophysics, 41(3), 225-245.

Lecointre, J., Hodgson, K., Neall, V., & Cronin, S. (2004). Lahar-triggering mechanisms and hazard at Ruapehu volcano, New Zealand. Natural Hazards, 31(1), 85-109.

Legros, F. (2002). The mobility of long-runout landslides. Engineering Geology, 63(3), 301-331.

LeMaitre, R. W. (1989). A classification of igneous rocks and glossary of terms. Blackwell, Oxford. 193 pp.

Li, J. J., Fang, X. M., Van der Voo, R., Zhu, J. J., Niocaill, C. M., Ono, Y., ... & Wang, J. M. (1997). Magnetostratigraphic dating of river terraces: Rapid and intermittent incision by the Yellow River of the northeastern margin of the Tibetan Plateau during the Quaternary. Journal of Geophysical Research: Solid Earth (1978–2012), 102(B5), 10121-10132.

Lindsley, D. H. (1983). Pyroxene thermometry. American Mineralogist, 68(5-6), 477-493.

Lipman, P. W., & Mullineaux, D. R. (eds.), (1981). The 1980 eruptions of Mount St. Helens, US Deptartment of the Interior, US Geological Survey, Washington, 1250.

Litchfield, N. (2003). Maps, stratigraphic logs and age control data for river terraces in the eastern North Island, Rep. 2003/31, Institute of Geology and Nuclear Sciences, Lower Hutt, New Zealand.

Litchfield, N. J., & Berryman, K. R. (2005). Correlation of fluvial terraces within the Hikurangi Margin, New Zealand: implications for climate and baselevel controls. Geomorphology, 68(3), 291-313.

Litchfield, N., & Berryman, K. (2006). Relations between postglacial fluvial incision rates and uplift rates in the North Island, New Zealand. Journal of Geophysical Research: Earth Surface (2003–2012), 111(F2).

Lowe, D. J., Shane, P. A., Alloway, B. V., & Newnham, R. M. (2008). Fingerprints and age models for widespread New Zealand tephra marker beds erupted since 30,000 years ago: a framework for NZ-INTIMATE. Quaternary Science Reviews, 27(1), 95-126.

Lube, G., Cronin, S. J., & Procter, J. N. (2009). Explaining the extreme mobility of volcanic ice-slurry flows, Ruapehu volcano, New Zealand. Geology, 37(1), 15-18.

Lube, G., Cronin, S. J., Manville, V., Procter, J. N., Cole, S. E., & Freundt, A. (2012). Energy growth in laharic mass flows. Geology, 40(5), 475-478.

Maizels, J. (1989). Sedimentology, paleoflow dynamics and flood history of jokulhlaup deposits: paleohydrology of Holocene sediment sequences in southern Iceland sandur deposits. Journal of Sedimentary Research, 59(2).

Major, J. J., & Newhall, C. G. (1989). Snow and ice perturbation during historical volcanic eruptions and the formation of lahars and floods. Bulletin of Volcanology, 52(1), 1-27.

Major, J. J., Janda, R. J., & Daag, A. S. (1996). Watershed disturbance and lahars on the east side of Mount Pinatubo during the mid-June 1991 eruptions. In: Newhall, C.G., and Punonbayan, R.S. (eds.), Fire and mud: Eruptions and lahars of Mount Pinatubo, Philippines: Quezon City, Philippine Institute of Volcanology and Seismology, and Seattle, University of

Washington Press, 895-919.

Major, J. J., Pierson, T. C., Dinehart, R. L., & Costa, J. E. (2000). Sediment yield following severe volcanic disturbance—a two-decade perspective from Mount St. Helens. Geology, 28(9), 819-822.

Manville, V., Hodgson, K. A., & White, J. D. L. (1998). Rheological properties of a remobilised-tephra lahar associated with the 1995 eruptions of Ruapehu volcano, New Zealand. New Zealand Journal of Geology and Geophysics, 41(2), 157-164.

Manville, V., & Wilson, C. J. (2004). The 26.5 ka Oruanui eruption, New Zealand: A review of the roles of volcanism and climate in the post-eruptive sedimentary response. New Zealand Journal of Geology and Geophysics, 47(3), 525-547.

Martin, J. E. (1991). People, Power and Power Stations: Electric Power Generation in New Zealand 1880-1990. Wellington: Bridget Williams Books Ltd and Electricity Corporation of New Zealand. pp. 316.

Martin, A. P., Cooper, A. F. & Price, R. C. (2013). Petrogenesis of Cenozoic, alkalic volcanic lineages at Mount Morning, West Antarctica and their entrained lithospheric mantle xenoliths: lithospheric versus asthenospheric mantle sources. Geochimica et Cosmochimica Acta 122, 127-152.

McArthur, J. L., & Shepherd, M. J. (1990). Late Quaternary glaciation of Mt Ruapehu, North Island, New Zealand. Journal of the Royal Society of New Zealand, 20(3), 287-296.

McClelland, E., & Erwin, P. S. (2003). Was a dacite dome implicated in the 9,500 B.P. collapse of Mt Ruapehu? A palaeomagnetic investigation. Bulletin of Volcanology, 65, 294-305.

McCormick, M. P., Thomason, L. W., & Trepte, C. R. (1995). Atmospheric effects of the Mt Pinatubo eruption. Nature, 373(6513), 399-404.

McCulloch, M. T., & Gamble, J. A. (1991). Geochemical and geodynamical constraints on subduction zone magmatism. Earth and Planetary Science Letters, 102(3), 358-374.

McDougall, S., & Hungr, O. (2005). Dynamic modelling of entrainment in rapid landslides. Canadian Geotechnical Journal, 42(5), 1437-1448.

McGlone, M. S., Howorth, R. & Pullar, W. A. (1984). Late Pleistocene stratigraphy, vegetation and climate of the Bay of Plenty and Gisborne regions, New Zealand. New Zealand Journal of Geology and Geophysics, 27, 327-350.

McGuire, W. J. (1996). Volcano instability: a review of contemporary themes. Geological Society, London, Special Publications, 110(1), 1-23.

Mercado, R. A., Bertram, J., Lacsamana, T., and Pineda, G. L. (1996). Socioeconomic impacts of the Mount Pinatubo eruption. In: Newhall, C. G., and Punonbayan, R. S. (eds.), Fire and mud: Eruptions and lahars of Mount Pinatubo, Philippines: Quezon City, Philippine Institute of Volcanology and Seismology, and Seattle, University of Washington Press, 1063-1070.

Michaelis, F. B. (1983). Effect of Turoa oil spill on aquatic insects in the Mangawhero river system. New Zealand Entomologist, 7(4), 447-455.

Miller, V., & Savage, M. (2001). Changes in seismic anisotropy after volcanic eruptions: evidence from Mt. Ruapehu. Science, 293(5538), 2231-2233.

Milliman, J. D., & Syvitski, J. P. (1992). Geomorphic/tectonic control of sediment discharge to the ocean: the importance of small mountainous rivers. The Journal of Geology, 525-544.

Milne, J. D. G. (1973a). Map and sections of river terraces in the Rangitikei Basin. New Zealand Soil Survey Report 4 North Island, New Zealand (Four sheets).

Milne, J. D. G. (1973b). Mount Curl Tephra, a 230000-year-old implications for quaternary

chronology marker bed in New Zealand, and its. New Zealand Journal of Geology and Geophysics, 16(3), 519-532.

Mimura, K., Kawachi, S., Fijimoto, U., Taneichi, M., Hyuga, T., Ichikawa, S., & Kolzumi, M. (1982). Debris avalanche hills and their natural remnant magnetization – Nirasaki debris avalanche, central Japan. Journal of the Geological Society of Japan, 88, 653-663.

Mortimer, N., Tulloch, A. J., & Ireland, T. R. (1997). Basement geology of Taranaki and Wanganui Basins, New Zealand. New Zealand Journal of Geology and Geophysics, 40(2), 223-236.

Mothes, P. A. (1992). Lahars of Cotopaxi Volcano, Ecuador: hazard and risk evaluation. In: Geohazards, Springer Netherlands, 53-63.

Mothes, P. A., Hall, M. L., & Janda, R. J. (1998). The enormous Chillos Valley Lahar: an ash-flow-generated debris flow from Cotopaxi Volcano, Ecuador. Bulletin of Volcanology, 59(4), 233-244.

Mullineaux, D. R., & Crandell, D. R. (1962). Recent lahars from Mount St. Helens, Washington. Geological Society of America Bulletin, 73(7), 855-870.

Murphy, R. P., & Seward, D. (1981). Stratigraphy, lithology, paleomagnetism, and fission track ages of some ignimbrite formations in the Matahana Basin, New Zealand. New Zealand Journal of Geology and Geophysics, 24(3), 325-331.

Nairn, I. A., & Beanland. S. (1989). Geological setting of the 1987 Edgecumbe earthquake, New Zealand. New Zealand Journal of Geology and Geophysics, 32(1), 1-13.

Nairn, I. A., Wood, C. P., & Hewson, C. A. Y. (1979). Phreatic eruptions of Ruapehu: April 1975. New Zealand Journal of Geology and Geophysics, 22(2), 155-170.

Naish, T., & Kamp, P. J. (1997). Sequence stratigraphy of sixth-order (41 ky) Pliocene–Pleistocene cyclothems, Wanganui Basin, New Zealand: a case for the regressive systems tract. Geological Society of America Bulletin, 109(8), 978-999.

Nakagawa, M., Wada, K., Thordarson, T., Wood, C. P., & Gamble, J. A. (1999). Petrological investigation of the 1995 and 1996 eruptions of Ruapehu volcano, New Zealand: formation of discrete and small magma pockets and their intermittent discharge. Bulletin of Volcanology, 61, 15-31.

Nakagawa, M., Wada, K., & Wood, C. P. (2002). Mixed magmas, mush chambers and eruption triggers: evidence from zoned clinopyroxene phenocrysts in andesitic scoria from the 1995 eruptions of Ruapehu volcano, New Zealand. Journal of Petrology, 43(12), 2279-2303.

Neall, V. E. (1993). A volcanic hazards analysis of three zones in the Manawatu-Wanganui region. Report to Manawatu-Wanganui Regional Council and Ministry and Civil Defense, 17p. + map.

New Zealand Meteorological Service (1973). Rainfall normals for New Zealand 1941-1970. New Zealand Meteorological Service Miscellaneous Publication, 145.

Newhall, C. G., & Self, S. (1982). The Volcanic Explosivity Index (VEI) an estimate of explosive magnitude for historical volcanism. Journal of Geophysical Research: Oceans (1978–2012), 87(C2), 1231-1238.

Nicoletti, P. G., & Sorriso-Valvo, M. (1991). Geomorphic controls of the shape and mobility of rock avalanches. Geological Society of America Bulletin, 103(10), 1365-1373.

Nockolds, S. R., & Allen, R. (1954). The geochemistry of some igneous rock series: Part II. Geochimica et Cosmochimica Acta, 5(6), 245-285.

Norrish, K., & Hutton, J. T. (1969). An accurate X-ray spectrographic method for the analysis of a wide range of geological samples. Geochimica et Cosmochimica Acta, 33(4), 431-453.

O'Shea, B. E. (1954). Ruapehu and the Tangiwai disaster. New Zealand Journal of Science and Technology B, 36, 174-189.

O'Connor J. E., Hardison J. H., & Costa J. E. (2001). Debris flows from failures of Neoglacial-Age Moraine dams in the Three Sisters and Mount Jefferson Wilderness Areas, Oregon. U.S. Geological Survey Professional Paper 1606, ISSN 1044–9612.

Odell, N. E. (1955). Mount Ruapehu, New Zealand: Obserations on its Crater Lake and Glaciers. Journal of Glaciology, 2(18), 601-607.

Ogle, C. C., La Cock, G. D., Arnold, G., & Mickleson, N. (2000). Impact of an exotic vine Clematis vitalba (F. Ranunculaceae) and of control measures on plant biodiversity in indigenous forest, Taihape, New Zealand. Austral Ecology, 25(5), 539-551.

Oppenheimer, C. (2003). Climatic, environmental and human consequences of the largest known historic eruption: Tambora volcano (Indonesia) 1815. Progress in Physical Geography, 27(2), 230-259.

Palmer, B. A. (1991). Holocene lahar deposits in the Whakapapa catchment, northwestern ring plain, Ruapehu volcano (North Island, New Zealand). New Zealand Journal of Geology and Geophysics, 34(2), 177-190.

Palmer, B. A., & Neall, V. E. (1989). The Murimotu Formation—9500 year old deposits of a debris avalanche and associated lahars, Mount Ruapehu, North Island, New Zealand. New Zealand Journal of Geology and Geophysics, 32(4), 477-486.

Palmer, B. A., Alloway, B. V., & Neall, V. E. (1991). Volcanic debris-avalanche deposits in New Zealand - lithofacies organization in unconfined, wet-avalanche flows. Sedimentation in volcanic settings. SEPM Special Publications, 45, 89-98.

Pardo, N., Cronin, S. J., Palmer, A. S., & Németh, K. (2012). Reconstructing the largest explosive eruptions of Mt. Ruapehu, New Zealand: lithostratigraphic tools to understand subplinian–plinian eruptions at andesitic volcanoes. Bulletin of Volcanology, 74(3), 617-640.

Pardo, N., Cronin, S. J., Wright, H. M., Schipper, C. I., Smith, I., & Stewart, B. (2014). Pyroclast textural variation as an indicator of eruption column steadiness in andesitic Plinian eruptions at Mt. Ruapehu. Bulletin of Volcanology, 76(5), 1-19.

Parish, A. (1994). Petrology and Provenance of the O'Leary Conglomerate, North East Wanganui, New Zealand. B.Sc (Hons) thesis, Victoria University of Wellington, New Zealand.

Park, J. (1910a). The Geology of New Zealand. Whitecombe & Tombs (Ltd.), Wellington, 194-195.

Park, J. (1910b). On the Glacial Till in Hautapu Valley, Rangitikei, Wellington. Transactions of the New Zealand Institute, 42, 580-584.

Pazzaglia, F. J., & Brandon, M. T. (2001). A fluvial record of long-term steady-state uplift and erosion across the Cascadia Forearc High, western Washington State, American Journal of Science, 301, 385–431.

Personius, S. F. (1995). Late Quaternary stream incision and uplift in the forearc of the Cascadia subduction zone, western Oregon, Journal of Geophysical Research, 100(B10), 20,193–20, 210.

Pierson, T. C. (1986). Flow behavior of channelized debris flows, Mount St. Helens, Washington. Hillslope processes, 269-296.

Pierson, T. C. (2005). Hyperconcentrated flow—transitional process between water flow and debris flow. In: Debris-flow hazards and related phenomena, Springer Berlin Heidelberg, 159-202.

Pierson, T. C., & Scott, K. M. (1985). Downstream dilution of a lahar: transition from debris flow to hyperconcentrated streamflow. Water Resources Research, 21(10), 1511-1524.

Pierson, T. C., Janda, R. J., Umbal, J. V., & Daag, A. S. (1992). Immediate and long-term hazards from lahars and excess sedimentation in rivers draining Mt. Pinatubo, Philippines. US Department of the Interior, US Geological Survey, 183-203.

Pierson, T. C., Daag, A. S., Delos Reyes, P. J., Regalado, M. T. M., Solidum, R. U., & Tubianosa, B. S. (1996). Flow and deposition of posteruption hot lahars on the east side of Mount Pinatubo, July–October 1991. In: Newhall, C.G., and Punonbayan, R.S. (eds.), Fire and mud: Eruptions and lahars of Mount Pinatubo, Philippines: Quezon City, Philippine Institute of Volcanology and Seismology, and Seattle, University of Washington Press, 921-950.

Pillans, B. (1983). Upper Quaternary marine terrace chronology and deformation, south Taranaki, New Zealand. Geology, 11(5), 292-297.

Pillans, B. (1986). A late Quaternary uplift map for the North Island, New Zealand. The Royal Society of New Zealand Bulletin, 24, 409–417.

Pillans, B. (1994). Direct marine-terrestrial correlations, Wanganui Basin, New Zealand: the last 1 million years. Quaternary Science Reviews, 13(3), 189-200.

Pillans, B., Holgate, G., & McGlone, M. (1988). Climate and sea level during oxygen isotope stage 7b: on-land evidence from New Zealand. Quaternary Research, 29(2), 176-185.

Porter, S. C., Zhisheng, A., & Hongbo, Z. (1992). Cyclic Quaternary alluviation and terracing in a nonglaciated drainage basin on the north flank of the Qinling Shan, central China. Quaternary Research, 38(2), 157-169.

Price, R. C., Waight, T. E., Chapman, J. R., Beyer, E. E., Smith, I. E. M. & Stewart R. B. (1997). The geochemical evolution of arc magmas in a continental setting: evidence from detailed chemo-stratigraphy at Ruapehu, New Zealand. State of the arc '97, Island arc magma genesis workshop, Adelaide, Australia, 1997. Abstract Geological Society of Australia 45, 115-117.

Price, R. C., Stewart, R. B., Woodhead, J. D., & Smith, I. E. M. (1999). Petrogenesis of high-K arc magmas: evidence from Egmont volcano, North Island, New Zealand. Journal of Petrology, 40(1), 167-197.

Price, R. C., Gamble, J. A., Smith, I. E., Stewart, R. B., Eggins, S., & Wright, I. C. (2005). An integrated model for the temporal evolution of andesites and rhyolites and crustal development in New Zealand's North Island. Journal of Volcanology and Geothermal Research, 140(1), 1-24.

Price, R. C., George, R., Gamble, J. A., Turner, S., Smith, I. E., Cook, C., Hobden, B., & Dosseto, A. (2007). U–Th–Ra fractionation during crustal-level andesite formation at Ruapehu volcano, New Zealand. Chemical Geology, 244(3), 437-451.

Price, R. C., Gamble, J. A., Smith, I. E. M, Maas, R., Waight, T., Stewart, R. B., & Woodhead, J. (2012). The anatomy of an andesite volcano: A time-stratigraphic study of andesite petrogenesis and crustal evolution at Ruapehu volcano, New Zealand: Journal of Petrology 53, 2139-2189.

Procter, J. N., Cronin, S. J., & Zernack, A. V. (2009). Landscape and sedimentary response to catastrophic debris avalanches, western Taranaki, New Zealand. Sedimentary Geology, 220(3), 271-287.

Pudasaini, S. P., & Miller, S. A. (2013). The hypermobility of huge landslides and avalanches. Engineering Geology, 157, 124-132.

Pulford, A., & Stern, T. (2004). Pliocene exhumation and landscape evolution of central North

Island, New Zealand: The role of the upper mantle. Journal of Geophysical Research, 109(F1), F01016.

Ridolfi, F., Renzulli, A. & Puerini, M. (2010). Stability and chemical equilibrium of amphibole in calc-alkaline magmas: an overview, new thermobarometric formulations and application to subduction-related volcanoes. Contributions to Mineralogy and Petrology, 160, 45-66.

Robinson, R., Smith, E. G., & Latter, J. H. (1981). Seismic studies of the crust under the hydrothermal areas of the Taupo Volcanic Zone, New Zealand. Journal of Volcanology and Geothermal Research, 9(2), 253-267.

Rodolfo, K. S. (2000). The hazard from lahars and jökulhlaups. In: Houghton, B., Rymer, H., Stix, J., McNutt, S., & Sigurdsson, H. (eds.), Encyclopedia of Volcanoes. Academic Press, San Diego, 973-995.

Rodolfo, K. S., & Arguden, A. T. (1991). Rain–lahar generation and sediment-delivery systems at Mayon Volcano, Phillipines. In: Fisher, R. V., Smith, G. A. (Eds.), Sedimentation in Volcanic Settings, 45. SEPM Special Publication, 71-87.

Rodolfo, K. S., Umbal, J. V., Alonso, R. A., Remotigue, C. T., Paladio-Melosantos, M. L., Salvador, J. H., ... & Miller, Y. (1996). Two years of lahars on the western flank of Mount Pinatubo: Initiation, flow processes, deposits, and attendant geomorphic and hydraulic changes. In: Newhall, C.G., and Punonbayan, R.S. (eds.), Fire and mud: Eruptions and lahars of Mount Pinatubo, Philippines: Quezon City, Philippine Institute of Volcanology and Seismology, and Seattle, University of Washington Press, 989-1013.

Rogers, G. M. (1993). Moawhango Ecological Region. Survey report no. 17 for the Protected Natural Areas Programme. New Zealand Protected Natural Areas Programme, Department of Conservation, Wanganui. 103 p.

Roser, B. P., & Korsch, R. J. (1999). Geochemical characterization, evolution and source of a Mesozoic accretionary wedge: the Torlesse terrane, New Zealand. Geological Magazine, 136(05), 493-512.

Roser, B., Kimura, J-I., & Sifeta, K. (2003). Tantalum and niobium contamination from tungsten carbide ring mills: much ado about nothing. Geoscience Report Shimane University 22, 107-110.

Roverato, M., Capra, L., Sulpizio, R., & Norini, G. (2011). Stratigraphic reconstruction of two debris avalanche deposits at Colima Volcano (Mexico): Insights into pre-failure conditions and climate influence. Journal of Volcanology and Geothermal Research, 207(1), 33-46.

Roverato, M., Cronin, S., Procter, J., & Capra, L. (2015). Textural features as indicators of debris avalanche transport and emplacement, Taranaki volcano. Geological Society of America Bulletin, 127(1-2), 3-18.

Rowland, J. V., Wilson, C. J. N., & Gravley, D. M. (2010). Spatial and temporal variations in magma-assisted rifting, Taupo Volcanic Zone, New Zealand. Journal of Volcanology and Geothermal Research 190, 89-108.

Rudnick, R. L. & Gao, S. (2005). Composition of the continental crust. In: Rudnick, R. L. (ed.) The crust. Treatise in Geochemistry 3. Oxford: Elsevier-Pergamon, 1-64.

Rundle, S. (2008). Results of the 2008 Whanganui Journey Visitor Survey. Unpublished Report, National Office, Department of Conservation, 63 p.

Salmon, M. L., Stern, T. A., & Savage, M. K. (2011). A major step in the continental Moho and its geodynamic consequences: the Taranaki–Ruapehu line, New Zealand. Geophysical Journal International, 186(1), 32-44.

Sassa, K. (1988). Motion of Landslides and Debris Flows: Prediction of Hazard Area. Report for Grant-in-aid for Scientific Research by Japanese Ministry on Education, Science and Culture (project No. 61480062). Disaster Prevention Research Institute.

Sassa, K., Fukuoka, H., Wang, G., & Ishikawa, N. (2004). Undrained dynamic-loading ring-shear apparatus and its application to landslide dynamics. Landslides, 1(1), 7-19.

Scheidegger, A. E. (1973). On the prediction of the reach and velocity of catastrophic landslides. Rock Mechanics, 5(4), 231-236.

Scott, K. M. (1988). Origins, behavior, and sedimentology of lahars and lahar-runout flows in the Toutle-Cowlitz River system. U.S. Geological Survey Professional Paper 1447-A, 74 pp.

Scott, K. M., Vallance, J. W., & Pringle, P. T. (1995). Sedimentology, behaviour, and hazards of debris flows at Mount Rainier, Washington. Washington: US Government Printing Office.

Shackleton, N. J., Berger, A., & Peltier, W. R. (1990). An alternative astronomical calibration of the lower Pleistocene timescale based on ODP Site 677. Transactions of the Royal Society of Edinburgh: Earth Sciences, 81(04), 251-261.

Siebert, L. (1984). Large volcanic debris avalanches: characteristics of source areas, deposits, and associated eruptions. Journal of Volcanology and Geothermal Research, 22(3), 163-197.

Singer, B. S., Thompson, R. A., Dungan, M. A., Feeley, T. C., Nelson, S. T., Pickens, J. C., ... & Metzger, J. (1997). Volcanism and erosion during the past 930 ky at the Tatara–San Pedro complex, Chilean Andes. Geological Society of America Bulletin, 109(2), 127-142.

Sissons, B. A. (1979). The horizontal kinematics of the North Island of New Zealand. PhD thesis, Victoria University of Wellington, New Zealand.

Smith, G. A. (1986). Coarse-grained nonmarine volcaniclastic sediment: terminology and depositional process. Geological Society of America Bulletin, 97(1), 1-10.

Smith, G. A., Grubensky, M. J., & Geissman, J. W. (1999). Nature and origin of cone-forming volcanic breccias in the Te Herenga Formation, Ruapehu, New Zealand. Bulletin of Volcanology, 61(1-2), 64-82.

Steiner, A. (1958). Petrogenetic implications of the 1954 Ngauruhoe lava and its xenoliths. New Zealand Journal of Geology and Geophysics, 1(2), 325-363.

Stern, T. A. (1987). Asymmetric back-arc spreading, heat flux and structure associated with the Central Volcanic Region of New Zealand. Earth and Planetary Science Letters, 85(1), 265-276.

Stern, T. A., & Davey, F. J. (1987). A seismic investigation of the crustal and upper mantle structure within the Central Volcanic Region of New Zealand. New Zealand Journal of Geology and Geophysics, 30(3), 217-231.

Stern, T., Stratford, W., Seward, A., Henderson, M., Savage, M., Smith, E., Benson, A., Greve, S., & Salmon, M. (2010). Crust–mantle structure of the central North Island, New Zealand, based on seismological observations. Journal of Volcanology and Geothermal Research, 190(1), 58-74.

Stipp, J. J. (1968). The geochronology and petrogenesis of the Cenozoic volcanics of the North Island, New Zealand. Unpublished PhD thesis, Australian National University, Canberra, ACT, Australia.

Stoopes, G. R., & Sheridan, M. F. (1992). Giant debris avalanches from the Colima Volcanic Complex, Mexico: Implications for long-runout landslides (>100 km) and hazard assessment. Geology, 20(4), 299-302.

Stratford, W. R., & Stern, T. A. (2006). Crust and upper mantle structure of continental backarc: central North Island, New Zealand. Geophysical Journal International, 166, 469-484.

Sugai, T. (1993). River terrace development by concurrent fluvial processes and climatic changes. Geomorphology, 6(3), 243-252.

Suggate, R. P. (1965). Late Pleistocene geology of the northern part of the South Island, New Zealand. New Zealand Geological Survey Bulletin, 77, 91.

Sun, S. S., & McDonough, W. (1989). Chemical and isotopic systematics of oceanic basalts: implications for mantle composition and processes. Geological Society, London, Special Publications, 42(1), 313-345.

Suryo, I., & Clarke, M. C. G. (1985). The occurrence and mitigation of volcanic hazards in Indonesia as exemplified at the Mount Merapi, Mount Kelut and Mount Galunggung volcanoes. Quarterly Journal of Engineering Geology and Hydrogeology, 18(1), 79-98.

Symons, G. J., Judd, J. W., Strachey, S. R., Wharton, W. J. L., Evans, F. J., Russell, F. A. R., ... & Whipple, G. M. (1888). The eruption of krakatoa: And subsequent phenomena. Trübner & Company.

Takarada, S., Ui, T., & Yamamoto, Y. (1999). Depositional features and transportation mechanism of valley-filling Iwasegawa and Kaida debris avalanches, Japan. Bulletin of Volcanology, 60(7), 508-522.

Tanaka, H., Kawamura, K., Nagao, K. & Houghton, B. F. (1997). K-Ar ages and palaeosecular variation of direction and intensity from Quaternary lava sequences in the Ruapehu volcano, New Zealand. Journal of Geomagnetism and Geoelectricity, 49, 587-599.

Tatsumi, Y. Hamilton, D. L. & Nesbitt, R. W. (1986). Chemical characteristics of fluid phase released from a subducted lithosphere and origin of arc magmas: Evidence from high-pressure experiments and natural rocks. Journal of Volcanology and Geothermal Research, 29, 293-309.

Te Punga, M. T. (1952). The geology of the Rangitikei Valley. New Zealand Geological Survey Memoir, 8, 46 pp.

Thompson, C. S. (1984). The weather and climate of the Tongariro region. New Zealand Meteorological Service Miscellaneous Publication, 115(14), 1-35.

Tibaldi, A. (2008). Contractional tectonics and magma paths in volcanoes. Journal of Volcanology and Geothermal Research, 176, 291-301.

Tibaldi, A., & Lagmay, A. M. F. (2006). Interaction between volcanoes and their basement. Journal of Volcanology and Geothermal Research, 158, 1-5.

Tibaldi, A., Mahar, A. F., Lagmay, A., & Ponomareva, V. V. (2005). Effects of basement structural and stratigraphic heritages on volcano behaviour and implications for human activities. Episodes, 28(3).

Tibaldi, A., Bistacchi, A., Pasquarè, F., & Vezzoli, L. (2007). Extensional tectonics and volcano lateral collapses: insights from Ollagüe volcano (Chile) and analogue modelling. TerraNova 18, 282-289.

Tost, M., Cronin, S. J., Procter, J. N. (2014). Transport and emplacement mechanisms of channelized long-runout debris avalanches, Ruapehu volcano, New Zealand. Bulletin of Volcanology, 76(12), 1-14.

Tost, M., Cronin, S. J., Procter, J. N., Smith, I. E. M., Neall, V. E., & Price, R. C. (2015). Impacts of catastrophic volcanic collapse on the erosion and morphology of a distal fluvial landscape: Hautapu River, Mount Ruapehu, New Zealand. Geological Society of America Bulletin,

B31010-1.

Tsuya, H. (1955). Geological and petrological studies of volcano Fuji, 5, Tokyo Daigaku Jishin Kenkyusho lho, 33, 341-382.

Turner, M. B., Cronin, S. J., Smith, I. E., Stewart, R. B., & Neall, V. E. (2008). Eruption episodes and magma recharge events in andesitic systems: Mt Taranaki, New Zealand. Journal of Volcanology and Geothermal Research, 177(4), 1063-1076.

Turner, M. B., Cronin, S. J., Bebbington, M. S., Smith, I. E., & Stewart, R. B. (2011). Relating magma composition to eruption variability at andesitic volcanoes: A case study from Mount Taranaki, New Zealand. Geological Society of America Bulletin, 123(9-10), 2005-2015.

Ui, T. (1983). Volcanic dry avalanche deposits—identification and comparison with nonvolcanic debris stream deposits. Journal of Volcanology and Geothermal Research, 18(1), 135-150.

Ui, T., Takarada, S., & Yoshimoto, M. (2000). Debris avalanches. In: Houghton, B., Rymer, H., Stix, J., McNutt, S., & Sigurdsson, H. (eds.), Encyclopedia of Volcanoes. Academic Press, San Diego, 617-626.

Ui, T., Kawachi, S., & Neall, V. E. (1986). Fragmentation of debris avalanche material during flowage—evidence from the Pungarehu Formation, Mount Egmont, New Zealand. Journal of Volcanology and Geothermal Research, 27(3), 255-264.

Ulate, C. A. & Corrales, M. F. (1996). Mudfloods related to the Irazu Volcano eruptions. Journal of the Hydraulics Division, Proceedings of the American Society of Civil Engineers, 92 (HY6), 117-129.

Vallance, J. W. (2000). Lahars. In: Encyclopedia of volcanoes. Sigurdsson, H., Houghton, B., Rymer, H., Stix J., & McNutt, S., (eds). Academic Press San Diego, 601-616.

Vallance, J. M., & Scott, K. (1997). The Osceola Mudflow from Mount Rainier: sedimentology and hazard implications of a huge clay-rich debris flow. Geological Society of American Bulletin, 109, 143-163.

van Gassen, W., & Cruden, D. M. (1989). Momentum transfer and friction in the debris of rock avalanches. Canadian Geotechnical Journal, 26(4), 623-628.

Vella, P., Kaewyana, W., & Vucetich, C. G. (1988). Late Quaternary terraces and their cover beds, north-western Wairarapa, New Zealand, and provisional correlations with oxygen isotope stages. Journal of the Royal Society of New Zealand, 18, 309-324.

Villamor, P. & Berryman, K. R. (2006a). Evolution of the southern termination of the Taupo Rift, New Zealand. New Zealand Journal of Geology and Geophysics 49, 23-37.

Villamor, P., & Berryman, K. R. (2006b). Late Quaternary geometry and kinematics of faults at the southern termination of the Taupo Volcanic Zone, New Zealand. New Zealand Journal of Geology and Geophysics, 49(1), 1-21.

Villamor, P., van Dissen, R., Alloway, B. V., Palmer, A. S., & Litchfield, N. (1997). The Rangipo fault, Taupo rift, New Zealand: An example of temporal slip-rate and single-event displacement variability in a volcanic environment. Geological Society of American Bulletin, 119, 529-547.

Voight, B. (1978). Rockslides and avalanches-1. Natural phenomena, Amsterdam Elsevier, 833 p.

Voight, B., & Sousa, J. (1994). Lessons from Ontake-san: a comparative analysis of debris avalanche dynamics. Engineering Geology, 38(3), 261-297.

Voight, B., Glicken, H., Janda, R. J., & Douglass, P. M. (1981). Catastrophic rockslide-avalanche of May 18. U.S. Geological Survey, Professional Paper, 1250, 347-377.

Voight, B., Janda, R. J., & Douglass, P. M. (1983). Nature and mechanics of the Mount St

Helens rockslide-avalanche of 18 May 1980. Geotechnique, 33(3), 243-273.

Waananen, A. O., Harris, D. D., Williams, R. C. (1970). Floods of December 1964 and January 1965 in the far western states. 2. Streamflow and sediment data. U.S. Geological Survey Water Supply Paper 1866-B, 861 p.

Wager, L. R., & Mitchell, R. L. (1951). The distribution of trace elements during strong fractionation of basic magma - a further study of the Skaergaard intrusion, East Greenland. Geochimica et Cosmochimica Acta, 1(3), 129-208.

Waight, T. E., Price, R. C., Stewart, R. B., Smith, I. E. M., & Gamble, J. (1999). Stratigraphy and geochemistry of the Turoa area, with implications for andesite petrogenesis at Mt Ruapehu, Taupo Volcanic Zone, New Zealand. New Zealand Journal of Geology and Geophysics, 42(4), 513-532.

Walcott, R. I. (1984). Reconstruction of the New Zealand region for the Neogene. Palaeogeography, Palaeoclimatology, Palaeoecology, 46, 217-231.

Walcott, R. I. (1987). Geodetic strain and the deformational history of the North Island of New Zealand during the late Cainozoic. Philosophical Transactions of the Royal Society of London. Series A, Mathematical and Physical Sciences, 321(1557), 163-181.

Weaver, B. L., & Tarney, J. (1984). Major and trace element composition of the continental lithosphere. Physics and Chemistry of the Earth, 15, 39-68.

Whipple, K. X., & Tucker, G. E. (2002), Implications of sediment-flux-dependent river incision models for landscape evolution, Journal of Geophysical Research, 107(B2), 2039.

Wilson, C. J. N., Houghton, B. F., Lanphere, M. A., & Weaver, S. D. (1992). A new radiometric age estimate for the Rotoehu Ash from Mayor Island volcano, New Zealand. New Zealand Journal of Geology and Geophysics, 35(3), 371-374.

Wilson, C. J. N., Houghton, B. F., McWilliams, M. O., Lanphere, M. A., Weaver, S. D., & Briggs, R. M. (1995). Volcanic and structural evolution of the Taupo Volcanic Zone, New Zealand: a review. Journal of Volcanology and Geothermal Research, 68, 1-28.

Wood, R., & Davy, B. (1994). The Hikurangi Plateau. Marine Geology, 118, 153-173.

Yoshikawa, T., Kaizuka, S., Ota, Y. (1981). The landforms of Japan. University of Tokyo Press, Tokyo.

Zernack, A. V., Procter, J. N., & Cronin, S. J. (2009). Sedimentary signatures of cyclic growth and destruction of stratovolcanoes: a case study from Mount Taranaki, New Zealand. Sedimentary Geology, 220(3), 288-305.

Zernack, A. V., Cronin, S. J., Neall, V. E., & Procter, J. N. (2011). A medial to distal volcaniclastic record of an andesite stratovolcano: detailed stratigraphy of the ring-plain succession of south-west Taranaki, New Zealand. International Journal of Earth Sciences, 100(8), 1937-1966.

Zernack, A. V., Cronin, S. J., Bebbington, M. S., Price, R. C., Smith, I. E., Stewart, R. B., & Procter, J. N. (2012). Forecasting catastrophic stratovolcano collapse: A model based on Mount Taranaki, New Zealand. Geology, 40(11), 983-986.

Appendix I. Physical parameters of the Ruapehu debris avalanches in relation to non-volcanic landslides, subaerial volcanic landslides (confined and unconfined), submarine landslides, block-and-ash flows, and pumice flows.

	V [km^3]	L_{max} [km]	H_{max} [km]	A [km^2]	H_{max}/L_{max}*	$A/V_{2/3}$**	L_{max}/H_{max}***	References
Other subaerial volcanic landslides (unconfined)								
Acatenango	5	41.0		210		71.82		e.g., Vallance et al. (1995)
Akagi	4	19.0	2.4		0.13		7.92	Hayashi & Self (1992)
Akagi (Nashigi)	6	23.5	2.4		0.10		9.79	Yoshida et al. (2012)
Antuco	15	30.0		200		32.88		Moreno (1991)
Asakusa	0.04	6.5	1.0		0.15		6.50	Hayashi & Self (1992)
Asama	2	20.0	1.8	90	0.09	56.70	11.11	Hayashi & Self (1992)
Augustine 1540	0.5			30		47.62		Siebert et al. (1995)
Augustine 1883	0.35	10.0	1.2		0.12		8.33	Beget & Kienle (1992)
Avachinsky	8	30.0		200		50.00		Melekestsev et al. (1992)
Bandai-san 1888	1.5	11.0	1.2	34	0.11	25.95	9.17	Hayashi & Self (1992)
Bezymianni 1956	0.8	18.0	2.4	30	0.13	34.81	7.50	Hayashi & Self (1992)
Callaqui	0.15	15.0	3.1		0.21		4.84	Hayashi & Self (1992)
Canlaon	13	33.0		400		72.35		Geronimo-Cantane (1997)
Chaos Crags	0.15	5.0	0.7	8	0.13	28.34	7.69	Hayashi & Self (1992)
Chimborazo	8.1	35.0	3.6		0.10		9.72	Hayashi & Self (1992)
Chokai	3.5	25.0	2.2		0.09		11.36	Hayashi & Self (1992)
Citlaltépetl (Jamapa)	25	75.0		350		40.94		Carrasco-Nuñez et al. (2006)
Citlaltépetl (Teteltzingo)	2.2	110.0		175		103.46		Carrasco-Nuñez et al. (2006)
Colima	12.5	40.0	4.0	900	0.10	167.10	10.00	Hayashi & Self (1992)
Colima (La Lumbre-Los Ganchos)	1.7	25.0		48	0.13	33.70		Cortés et al. (2010)
Colima (Paleofuego)	10	70.0		1550		333.94		Luhr & Prestegaard (1985)
Colima (San Marcos)	1.3	20.0		140		117.53		Roverato et al. (2011)
Drum	7	85.0		200		54.66		Richter et al. (1979)
Egmont (Pungarehu)	7.5	31.0	2.6	250	0.08	65.25	11.92	e.g., Palmer et al. (1991)
Egmont	5.8	39.0		500		154.89		Palmer et al. (1991)
Egmont (Opua)	0.35	27.0	2.5	120	0.09	241.62	10.80	Hayashi & Self (1992)
Fernandina	0.9			10		10.73		e.g., Rowland & Munro (1992)

Appendix I (continued). Physical parameters of the Ruapehu debris avalanches in relation to non-volcanic landslides, subaerial volcanic landslides (confined and unconfined), submarine landslides, block-and-ash flows, and pumice flows.

	V [km^3]	L_{max} [km]	H_{max} [km]	A [km^2]	H_{max}/L_{max}*	$A/V_{2/3}$**	L_{max}/H_{max}***	References
Other subaerial volcanic landslides (unconfined)								
Fuego	15	50.0		420		69.05		e.g., Vallance et al. (1995)
Fuji (Gotemba)	1.8	24.0	2.7		0.11		8.89	Yoshida et al. (2012)
Galunggung	2.9	25.0	1.9	175	0.08	86.05	13.16	Hayashi & Self (1992)
Galunggung	16	23.0		170		26.77		Bronto (1989)
Iizuna	5	17.0						Kawachi & Hayatsu (1994)
Iriga	1.5	11.0	1.1	65	0.10	49.60	10.48	Hayashi & Self (1992)
Iwaki	1.3	14.0	1.6		0.11	0.00	8.75	Hayashi & Self (1992)
Jocotitlán	2.8	12.0	1.2	80	0.11	40.27	10.43	Siebe et al. (1992)
Kharimkotan	0.5			20		31.75		e.g., Belousova (1996)
Komagatake	1.3			126		105.78		e.g., Yoshimoto et al. (2003)
Komagatake (Onuma)	0.25	11.5	1.0		0.09		11.50	Hayashi & Self (1992)
Kurohime	0.12	6.0	0.8		0.13		7.50	Hayashi & Self (1992)
Las Cumbres	60	120.0		1500		97.87		Carrasco-Nuñez et al. (2006)
Massif Central (Perrier)		35.0	0.2		0.13		205.88	Bernard et al. (2009)
Mawenzi	7.1	60.0	4.5	1150	0.08	311.31	13.33	e.g., Hayashi & Self (1992)
Meru	15	50.0	3.9	1400	0.08	230.18	12.82	Hayashi & Self (1992)
Monbacho	1	12.0	1.3	45	0.11	45.00	9.23	Hayashi & Self (1992)
Mombacho (El Crater)	1.75	12.4	1.5	49.5	0.12	34.09	8.27	Shea et al. (2008)
Mombacho (Las Isletas)	1.2	11.9	1.3	56.8	0.11	50.30	8.85	Shea et al. (2008)
Mt Iriga1	1.5	12.0	1.2	70	0.07	53.42	10.00	Paguican et al. (2012)
Mt Iriga2	2	16.0	1.2	70	0.10	44.10	13.33	Paguican et al. (2012)
Mt St Helens 1980	2.5	24.0	2.6	60	0.11	32.57	9.41	Hayashi & Self (1992)
Mt St Helens 20 000 BP	1	16.0	1.8		0.11		9.14	Siebert (1984)
Myoko (Sekikawa)	0.8	19.0	2.0		0.11		9.50	Hayashi & Self (1992)
Myoko (Taguchi)	0.23	8.0	1.4		0.11		5.71	Hayashi & Self (1992)
Nasu (Nashigi)	1	19.0	1.6		0.08		11.88	Yoshida et al. (2012)
Nevado de Toluca	0.52	8.0		22		34.02		Capra et al. (2012)

Appendix I (continued). Physical parameters of the Ruapehu debris avalanches in relation to non-volcanic landslides, subaerial volcanic landslides (confined and unconfined), submarine landslides, block-and-ash flows, and pumice flows.

	V [km^3]	L_{max} [km]	H_{max} [km]	A [km^2]	H_{max}/L_{max}*	$A/V_{2/3}$**	L_{max}/H_{max}***	References
Other subaerial volcanic landslides (unconfined)								
Oshima-Oshima	2.5			69		37.46		e.g., Satake & Kato (2001)
Ovalnaya Zimina	0.4	17.0	2.4		0.14		7.08	Hayashi & Self (1992)
Papandayan	0.14	11.0	1.5		0.14		7.33	Hayashi & Self (1992)
Parinacota	6	22.0		140	0.08	42.40		Clavero et al. (2002)
Pico de Orizaba	20	70.0		350		47.50		Carrasco-Nunez et al. (1997)
Planchon-Peteroa	10	78.0		370		79.71		e.g., Naeanjo et al. (1997)
Popa	0.8	11.0	1.2		0.11		9.17	Hayashi & Self (1992)
Popocatepetl	9	60.0		300		69.34		e.g., Siebe et al. (1995)
Popocatepetl	28	33.0	4.0		0.12		8.25	Hayashi & Self (1992)
Pouakai (Maitahi)	7.5	30.0		360		93.96		e.g., Gaylord & Neall (2012)
Raung	25	79.0		1045		122.22		e.g., Siebert et al. (1996)
Ritter Island	5			100		34.20		e.g., Silver et al. (2009)
Ruapehu (Murimotu)	0.2	13.0	1.6	23	0.12	67.25	8.13	Palmer & Neall (1989)
Santa Ana (Acajutla)	16	50.0		390	0.05	61.42		Siebert et al. (2004)
Shasta	26	50.0	3.6	450	0.07	51.27	14.08	Hayashi & Self (1992)
Shasta	46	49.0	3.6	675	0.07	52.58	13.80	Crandell (1989)
Shiribetsu (Rusutsu)	2	7.5	1.0		0.13		7.50	Yoshida et al. (2012)
Shiveluch 1964	1.5	12.0	2.0	98	0.17	74.79	6.00	Hayashi & Self (1992)
Shiveluch 10 000	35	35.0	4.0	350	0.11	32.71	8.75	Belousov et al. (1999)
Sierra Veluda	0.5	25.0	3.4		0.14		7.35	Hayashi & Self (1992)
Socompa	17	35.0	3.3	480	0.09	72.60	10.77	Hayashi & Self (1992)
Socompa	25.7	35.0	3.3	606	0.08	69.59	10.61	e.g., Wadge et al. (1995)
Soufrière	0.5	9.5	1.4	25	0.14	39.69	7.04	Siebert (1984)
Soufrière Hills 1997	0.005	4.5	1.0		0.22		4.50	Voight et al. (2002)
Tancitaro	18	73.0	3.6	1155	0.05	168.16	20.56	Morelli et al. (2010)
Tashirodake	0.1	12.4	0.7		0.06		17.71	Takarada et al. (1999)
Tata Sabaya	6	23.0		230	0.08	69.66		e.g., Godoy et al. (2012)

Appendix I (continued). Physical parameters of the Ruapehu debris avalanches in relation to non-volcanic landslides, subaerial volcanic landslides (confined and unconfined), submarine landslides, block-and-ash flows, and pumice flows.

	V [km^3]	L_{max} [km]	H_{max} [km]	A [km^2]	H_{max}/L_{max}*	$A/V_{2/3}$**	L_{max}/H_{max}***	References
Other subaerial volcanic landslides (unconfined)								
Tateshina	0.35	12.5	1.4		0.11		8.93	Hayashi & Self (1992)
Toluca	5	55.0		500		171.00		Macias et al. (1997)
Tongariro (Te Whaiau)	0.5	15.0	1?	40		63.50		Lecointre et al. (2001)
Unzen	0.34	6.5	0.9	12	0.13	24.63	7.65	Hayashi & Self (1992)
Usu	0.3	6.5	0.5		0.08		13.00	Hayashi & Self (1992)
Usu (Zenkoji)	1.5	6.5	1.0		0.15		6.50	Yoshida et al. (2012)
Vesuvius 1944	0.0002	0.6	0.6	0.022	0.90	6.93	1.11	Hazlett et al. (1991)
Vesuvius 1944	0.0009	0.9	0.5	0.113	0.54	12.12	1.86	Hazlett et al. (1991)
Vesuvius 1944	0.0006	0.5	0.3	0.099	0.57	14.75	1.75	Hazlett et al. (1991)
Vesuvius 1944	0.0008	1.0	0.5	0.126	0.49	14.71	2.04	Hazlett et al. (1991)
Vesuvius 1944	0.001	1.2	0.6	0.136	0.51	13.60	1.95	Hazlett et al. (1991)
Vesuvius 1944	0.0011	0.7	0.4	0.145	0.53	13.61	1.89	Hazlett et al. (1991)
Vesuvius 1944	0.0012	0.8	0.4	0.161	0.50	14.58	2.00	Hazlett et al. (1991)
Volcán de Colima	12	65.0		1600	0.09	305.26		Stoopes & Sheridan (1992)
Wrangell	12.6	70.0		840		155.13		Yehle & Nichols (1980)
Yatsugatake (Nirasaki)	9	32.0	2.4		0.08		13.33	Hayashi & Self (1992)
Yatsugatake (Otsukigawa)	0.27	12.5	1.4		0.11		8.93	Hayashi & Self (1992)
Other subaerial volcanic landslide (confined)								
Mageik	0.09	9.0	0.8	10	0.09	49.79	11.25	e.g., Hayashi & Self (1992)
Mount Rainier (Osceola)	3.8	70.0	4.9	547	0.04	224.63	14.29	Vallance & Scott (1997)
Nevado de Colima	33	120.0		2200	0.04	213.84		Stoopes & Sheridan (1992)
Ontake-san	0.0036	12.9	1.6		0.12		8.32	Voight & Sousa (1994)
Ontake (Iwasegawa)	0.1	12.4	0.7		0.06		17.71	Takarada et al. 1999
Ontake (Kaida)	0.3	46.0	2.5		0.05		18.40	Takarada et al. 1999
Peteroa	16	85.0	3.9		0.05		21.79	Hayashi & Self (1992)
Tashiro	0.55	8.8	0.7		0.08		12.57	Hayashi & Self (1992)

Appendix I (continued). Physical parameters of the Ruapehu debris avalanches in relation to non-volcanic landslides, subaerial volcanic landslides (confined and unconfined), submarine landslides, block-and-ash flows, and pumice flows.

	V [km^3]	L_{max} [km]	H_{max} [km]	A [km^2]	H_{max}/L_{max}*	$A/V_{2/3}$**	L_{max}/H_{max}***	References
Other subaerial volcanic landslide (confined)								
Tongariro (Te Maari)	0.0007	2.0	0.4		0.22		4.55	Procter et al. (2013)
Ruapehu landslides (this study)								
Ruapehu (Mataroa)	2.9	64.0	2.1	256	0.03	125.89	30.48	Tost et al. (in review); this study
Ruapehu (Pukekahu)	1.56	56.0	2.4	120	0.04	89.21	23.33	This study
Ruapehu (Oreore)	3	80.0	2.3	200	0.03	96.15	34.78	This study
Ruapehu (Piriak-A)	1.35	72.0	2.5	225	0.03	184.20	28.80	This study
Ruapehu (Piriaka-B)	1.4	75.0	2.5	260	0.03	207.76	30.00	This study
Ruapehu (Lower Whangaehu)	2.4	60.0	2.3	120	0.04	66.94	26.09	Tost et al. (in review); this study
Non-volcanic subaerial landslides								
Abimes de Myans	0.15			15		53.13		e.g., Griswold & Iverson (2008)
Am Saum	0.1			1		4.64		e.g., Griswold & Iverson (2008)
Biasca	0.015			1		16.44		e.g., Griswold & Iverson (2008)
Blackhawk	0.28	9.6	1.2		0.13		8.00	e.g., Legros (2002)
Bormio	0.18			4		12.55		e.g., Griswold & Iverson (2008)
Brione	0.016			0.7		11.02		e.g., Griswold & Iverson (2008)
Cal de la Madeleine	0.115			1.84		7.78		e.g., Griswold & Iverson (2008)
Cayley	0.005			0.6		20.52		e.g., Griswold & Iverson (2008)
Corno di Dosde	0.02	3.7	1.2		0.32		3.08	Hayashi & Self (1992)
Dejenstock	0.6			6.4		9.00		e.g., Griswold & Iverson (2008)
Deyen, Glarus	0.6	6.6	0.7		0.11		8.92	Hayashi & Self (1992)
Diablerets	0.05	5.5	1.9	2.2	0.34	16.21	2.89	e.g., Hayashi & Self (1992)
Disentis	0.015	2.1	0.7	0.8	0.36	13.15	2.84	e.g., Griswold & Iverson (2008)
Dobratsch	0.36			16		31.62		e.g., Griswold & Iverson (2008)
Dobratsch	0.17			8		26.07		e.g., Griswold & Iverson (2008)
Dobratsch	0.03			5		51.79		e.g., Griswold & Iverson (2008)

Appendix I (continued). Physical parameters of the Ruapehu debris avalanches in relation to non-volcanic landslides, subaerial volcanic landslides (confined and unconfined), submarine landslides, block-and-ash flows, and pumice flows.

	V [km^3]	L_{max} [km]	H_{max} [km]	A [km^2]	H_{max}/L_{max}*	$A/V_{2/3}$**	L_{max}/H_{max}***	References
Non-volcanic subaerial landslides								
Eibsee	0.4			11		20.26		e.g., Griswold & Iverson (2008)
Elm	0.01	2.3	0.7	0.58	0.31	12.50	3.24	e.g., Legros (2002)
Engelberg	2.75	7.4	1.6	9	0.22	4.59	4.63	e.g., Hayashi & Self (1992)
Felsberg	0.0001			0.1		46.42		e.g., Griswold & Iverson (2008)
Fernpass	1	15.6	1.4		0.09		11.14	Hayashi & Self (1992)
Fidaz	0.0004			0.2		36.84		e.g., Griswold & Iverson (2008)
Fionnay	0.004			0.4		15.87		e.g., Griswold & Iverson (2008)
Flims	12	15.6	2.0	51	0.13	9.73	7.80	e.g., Hayashi & Self (1992)
Frank	0.03	3.5	0.9	3	0.25	31.07	4.02	e.g., Griswold & Iverson (2008)
Glarnish	0.8	7.5	1.9	8.8	0.25	10.21	3.95	e.g., Hayashi & Self (1992)
Goldau	0.035	6.0	1.2	4	0.21	37.38	5.00	e.g., Hayashi & Self (1992)
Grand Clapier	0.016			0.41		6.46		e.g., Griswold & Iverson (2008)
Gros Ventre	0.038	3.4	0.6		0.17		6.07	Hayashi & Self (1992)
Haiming	0.0295			1.7		17.81		e.g., Griswold & Iverson (2008)
Haltenguet	0.0002			0.075		26.57		e.g., Griswold & Iverson (2008)
Haslensee	0.03			0.7		7.25		e.g., Griswold & Iverson (2008)
Hintersee	0.013			0.95		17.18		e.g., Griswold & Iverson (2008)
Hope	0.0473	3.0	1.2	2.65	0.38	20.26	2.61	e.g., Griswold & Iverson (2008)
Huascaran	0.013	16.0	2.4	6	0.22	108.52	6.67	e.g., Hayashi & Self (1992)
Huascaran	0.075	16.0	2.4	22.5	0.22	126.51	6.67	e.g., Hayashi & Self (1992)
Inyo Mountains	0.025			1.2		14.04		e.g., Griswold & Iverson (2008)
Kals	0.02			1		13.57		e.g., Griswold & Iverson (2008)
Kandeltal	0.14	9.9	1.9		0.19		5.21	Hayashi & Self (1992)
Kleines Rinderhorn	0.04			1		8.55		e.g., Griswold & Iverson (2008)
Kofels	2.1			12		7.32		e.g., Griswold & Iverson (2008)
Lac Lauvitel	0.068			1.6		9.60		e.g., Griswold & Iverson (2008)
Lago de Antrona	0.012			1		19.08		e.g., Griswold & Iverson (2008)

Appendix I (continued). Physical parameters of the Ruapehu debris avalanches in relation to non-volcanic landslides, subaerial volcanic landslides (confined and unconfined), submarine landslides, block-and-ash flows, and pumice flows.

	V [km^3]	L_{max} [km]	H_{max} [km]	A [km^2]	H_{max}/L_{max}*	$A/V_{2/3}$**	L_{max}/H_{max}***	References
Non-volcanic subaerial landslides								
Lago di Alleghe	0.02			0.5		6.79		e.g., Griswold & Iverson (2008)
Lago di Molveno	0.4			3.6		6.63		e.g., Griswold & Iverson (2008)
Lago di Poschiavo	0.165			1		3.32		e.g., Griswold & Iverson (2008)
Lago di Tovel	0.25			5.2		13.10		e.g., Griswold & Iverson (2008)
Lavini de Marco	0.15			3.5		12.40		e.g., Griswold & Iverson (2008)
Lofer	0.08			3.48		18.74		e.g., Griswold & Iverson (2008)
Ludiano	0.014			0.6		10.33		e.g., Griswold & Iverson (2008)
Madison Canyon	0.029	1.6	0.4	0.7	0.27	7.42	3.72	e.g., Hayashi & Self (1992)
Mallnitz	0.1			2.4		11.14		e.g., Griswold & Iverson (2008)
Marocche im Sarcatal	0.469			12		19.88		e.g., Griswold & Iverson (2008)
Marquartstein	0.05			2.3		16.95		e.g., Griswold & Iverson (2008)
Masiere di vedane	0.17			7		22.81		e.g., Griswold & Iverson (2008)
Melkode	0.007			0.72		19.68		e.g., Griswold & Iverson (2008)
Mombiel	0.0008	0.8	0.4		0.47		2.16	Hayashi & Self (1992)
Monte Avi	0.04			1		8.55		e.g., Griswold & Iverson (2008)
Monte Corno	0.017			0.7		10.59		e.g., Griswold & Iverson (2008)
Monte Spinale	0.55			11.6		17.28		e.g., Griswold & Iverson (2008)
Mordbichl	0.02			0.45		6.11		e.g., Griswold & Iverson (2008)
Mount Munday	0.01			2.2		47.40		e.g., Griswold & Iverson (2008)
Oberes Vallesinella	0.0085			0.88		21.13		e.g., Griswold & Iverson (2008)
Obernbergtal	0.0565			2.7		18.34		e.g., Griswold & Iverson (2008)
Obersee GL	0.12	5.0	1.8	2.5	0.36	10.28	2.78	e.g., Griswold & Iverson (2008)
Oberterzen	0.1			5		23.21		e.g., Griswold & Iverson (2008)
Oeschinensee	0.12			1.7		6.99		e.g., Griswold & Iverson (2008)
Parnir	2	6.2	1.5		0.24		4.13	Hayashi & Self (1992)
Parpan-Lenzerheide	0.4			8		14.74		e.g., Griswold & Iverson (2008)
Pletzachkogel	0.08			4		21.54		e.g., Griswold & Iverson (2008)

Appendix I (continued). Physical parameters of the Ruapehu debris avalanches in relation to non-volcanic landslides, subaerial volcanic landslides (confined and unconfined), submarine landslides, block-and-ash flows, and pumice flows.

	V [km^3]	L_{max} [km]	H_{max} [km]	A [km^2]	H_{max}/L_{max}*	$A/V_{2/3}$**	L_{max}/H_{max}***	References
Non-volcanic subaerial landslides								
Pontives	0.05			2		14.74		e.g., Griswold & Iverson (2008)
Poshivo	0.15	4.1	1.5		0.36		2.73	Hayashi & Self (1992)
Prayon	0.005			0.2		6.84		e.g., Griswold & Iverson (2008)
Puget Peak	0.00182			0.55		36.90		e.g., Griswold & Iverson (2008)
Saidmarreh	20	18.9	1.5		0.08		12.60	Hayashi & Self (1992)
San Giovanni	0.025			1.2		14.04		e.g., Griswold & Iverson (2008)
Schachental	0.0005	3.1	1.8		0.58		1.72	Hayashi & Self (1992)
Scimada Saoseo	0.08	5.5	1.5		0.27		3.67	Hayashi & Self (1992)
Sherman	0.03	6.2	1.3	8.25	0.21	85.45	4.77	e.g., Hayashi & Self (1992); Legros (2002)
Siders	1.5	17.4	2.4	28	0.14	21.37	7.25	e.g., Griswold & Iverson (2008)
St Andre	0.021			0.79		10.38		e.g., Griswold & Iverson (2008)
Tamins	1.3	13.5	1.3		0.10		10.38	Hayashi & Self (1992)
Torbole	0.03			1.1		11.39		e.g., Griswold & Iverson (2008)
Totalp	0.6			4.3		6.04		e.g., Griswold & Iverson (2008)
Tschirgant	0.21			13.2		37.36		e.g., Griswold & Iverson (2008)
Vaiont	0.25	1.5	0.5		0.34		3.00	Hayashi & Self (1992)
Vaiont	0.285			1.9		4.39		e.g., Griswold & Iverson (2008)
Val Brenta Alta	0.008			0.6		15.00		e.g., Griswold & Iverson (2008)
Val Lagone	0.00065	2.4	1.1		0.44		2.29	Hayashi & Self (1992)
Voralpsee	0.03	3.4	1.1	0.85	0.33	8.80	3.09	e.g., Griswold & Iverson (2008)
Wengen 1	0.0025	1.1	0.5		0.45		2.20	Hayashi & Self (1992)
Wengen 2	0.0055	1.4	0.6		0.42		2.37	Hayashi & Self (1992)
Winkelmatten	0.003			0.25		12.02		e.g., Griswold & Iverson (2008)
Submarine landslides								
Grant Banks	76	110.0	0.4		0.00		301.37	Hampton et al. (1996)
Kidnappers	8	11.0	0.1		0.05		220.00	Hampton et al. (1996)

Appendix I (continued). Physical parameters of the Ruapehu debris avalanches in relation to non-volcanic landslides, subaerial volcanic landslides (confined and unconfined), submarine landslides, block-and-ash flows, and pumice flows.

	V [km^3]	L_{max} [km]	H_{max} [km]	A [km^2]	H_{max}/L_{max}*	$A/V_{2/3}$**	L_{max}/H_{max}***	References
Submarine landslides								
Rockall	300	160.0	0.3		0.00		484.85	Hampton et al. (1996)
Magdalena	0.3	24.0	1.4		0.06		17.14	Hampton et al. (1996)
Valdez	0.075	1.3	0.2		0.13		7.62	Hampton et al. (1996)
Orkdalsfjord	0.025	22.5	0.5		0.02		45.00	Hampton et al. (1996)
Sandnesjoen	0.005	1.2	0.2		0.15		6.67	Hampton et al. (1996)
Sokkelvik	0.0005	2.5	0.1		0.05		20.83	Hampton et al. (1996)
Storegga	800	160.0	1.7		0.01		94.12	Hampton et al. (1996)
Blake Escarpment	600	42.0	3.6		0.09		11.67	Hampton et al. (1996)
East Break East	13	70.0	1.2		0.02		60.87	Hampton et al. (1996)
East Break West	160	110.0	1.1		0.01		100.00	Hampton et al. (1996)
Navarin Canyon	5	6.0	0.2		0.03		34.29	Hampton et al. (1996)
Seward	0.0027	3.0	0.2		0.07		15.00	Hampton et al. (1996)
Sur	10	70.0	0.8		0.01		93.33	Hampton et al. (1996)
Sanata Barbara	0.02	2.3	0.1		0.05		19.17	Hampton et al. (1996)
Alika-2****	300	95.0	4.8		0.05		19.79	Hampton et al. (1996)
Nuuanu****	5000	230.0	5.0		0.02		46.00	Hampton et al. (1996)
Tristan de Cunha****	150	50.0	3.8		0.08		13.33	Hampton et al. (1996)
Kitimat slide	0.2	6.0	0.2		0.03		30.00	Lipman et al. (1988)
A1	250	370.0	1.7		0.01		217.65	Lipman et al. (1988)
A2	22	160.0	1.5		0.01		106.67	Lipman et al. (1988)
A3	8.5	140.0	1.4		0.01		100.00	Lipman et al. (1988)
A4A	27	130.0	1.3		0.01		100.00	Lipman et al. (1988)
A4B	320	400.0	2.0		0.01		200.00	Lipman et al. (1988)
Kae Lae slide****	40	60.0	5.0		0.08		12.00	Lipman et al. (1988)
Molokai slide****	1100	130.0	5.2		0.04		25.00	Lipman et al. (1988)
Oahu slide****	1800	180.0	5.5		0.03		32.73	Lipman et al. (1988)
Alika slide****	1800	105.0	5.3		0.05		19.81	Lipman et al. (1988)

Appendix I (continued). Physical parameters of the Ruapehu debris avalanches in relation to non-volcanic landslides, subaerial volcanic landslides (confined and unconfined), submarine landslides, block-and-ash flows, and pumice flows.

	V [km^3]	L_{max} [km]	H_{max} [km]	A [km^2]	H_{max}/L_{max}*	$A/V_{2/3}$**	L_{max}/H_{max}***	References
Block-and-ash flows								
Soufriere Hills Volcano, Montserrat	0.0002	1.6	0.6	0.101	0.37	29.53	2.71	Calder et al. (1999)
Soufriere Hills Volcano, Montserrat	0.0004	2.9	0.9	0.175	0.31	32.24	3.19	Calder et al. (1999)
Soufriere Hills Volcano, Montserrat	0.0026	3.6	0.8	0.16	0.23	8.46	4.34	Calder et al. (1999)
Soufriere Hills Volcano, Montserrat	0.0003	2.5	0.9	0.109	0.34	24.32	2.91	Calder et al. (1999)
Soufriere Hills Volcano, Montserrat	0.0030	4.1	0.9	0.43	0.22	20.67	4.50	Calder et al. (1999)
Soufriere Hills Volcano, Montserrat	0.0004	3.1	0.9	0.192	0.28	35.37	3.60	Calder et al. (1999)
Soufriere Hills Volcano, Montserrat	0.0008	3.9	0.9	0.3	0.22	34.81	4.53	Calder et al. (1999)
Soufriere Hills Volcano, Montserrat	0.0064	6.7	1.0	0.784	0.15	22.74	6.63	Calder et al. (1999)
Soufriere Hills Volcano, Montserrat	0.0088	5.6	0.9	1.784	0.16	42.01	6.22	Calder et al. (1999)
Soufriere Hills Volcano, Montserrat	0.0143	6.0	0.9	2.357	0.15	40.01	6.52	Calder et al. (1999)
Merapi	0.0003	3.7	1.5	0.129	0.41	31.83	2.47	Swarzkopf & Schminke (2000)
Merapi	0.0003	3.0	1.5	0.057	0.48	13.16	2.07	Swarzkopf & Schminke (2000)
Merapi	0.0001	4.5	1.7	0.043	0.37	18.84	2.73	Swarzkopf & Schminke (2000)
Merapi	0.0000			0.087		114.30		Swarzkopf & Schminke (2000)
Merapi	0.0002	5.8	1.8	0.35	0.31	111.87	3.22	Swarzkopf & Schminke (2000)
Merapi	0.0004			0.123		23.95		Swarzkopf & Schminke (2000)
Merapi	0.0004	5.4	1.8	0.7	0.33	140.95	3.00	Swarzkopf & Schminke (2000)
Merapi	0.0012	4.5	1.8	0.320	0.40	28.50	2.51	Charbonnier & Gertisser (2011)
Merapi	0.0027	7.0	2.1	0.882	0.30	45.51	3.38	Charbonnier & Gertisser (2011)
Merapi	0.0009	4.4	1.8	0.278	0.40	29.82	2.50	Charbonnier & Gertisser (2011)
Merapi	0.0008	4.0	1.7	0.256	0.42	30.53	2.36	Charbonnier & Gertisser (2011)
Merapi	0.0007	3.7	1.6	0.244	0.44	30.03	2.26	Charbonnier & Gertisser (2011)
Merapi	0.0006	3.3	1.6	0.213	0.47	28.72	2.13	Charbonnier & Gertisser (2011)
Merapi	0.0006	3.0	1.5	0.187	0.50	27.47	2.00	Charbonnier & Gertisser (2011)
Merapi	0.0001	2.7	1.4	0.045	0.53	22.42	1.89	Charbonnier & Gertisser (2011)
Merapi	0.0002	2.6	1.4	0.102	0.54	27.59	1.86	Charbonnier & Gertisser (2011)
Merapi	0.0001	2.0	1.2	0.039	0.62	21.29	1.63	Charbonnier & Gertisser (2011)

Appendix I (continued). Physical parameters of the Ruapehu debris avalanches in relation to non-volcanic landslides, subaerial volcanic landslides (confined and unconfined), submarine landslides, block-and-ash flows, and pumice flows.

	V [km^3]	L_{max} [km]	H_{max} [km]	A [km^2]	H_{max}/L_{max}*	$A/V_{2/3}$**	L_{max}/H_{max}***	References
Block-and-ash flows								
Augustine	0.0100	5.0	1.1	3	0.21	64.63	4.67	Vallance et al. (2010)
Augustine	0.0030	3.8	1.0	1	0.26	48.07	3.90	Vallance et al. (2010)
Augustine	0.0000	3.0	1.1	0.63	0.36	736.85	2.80	Vallance et al. (2010)
Unzen	0.0008	3.6	1.0		0.28		3.56	Takarada (personal comm.)
Unzen	0.0002	3.0	1.0		0.32		3.13	Takarada (personal comm.)
Unzen	0.0014	5.6	1.2		0.21		4.75	Takarada (personal comm.)
Unzen	0.0015	6.5	1.4		0.21		4.74	Takarada (personal comm.)
Unzen	0.0001	1.7	0.7		0.42		2.38	Takarada (personal comm.)
Unzen	0.0002	3.6	1.0		0.29		3.50	Takarada (personal comm.)
Unzen	0.0002	0.9	0.4		0.44		2.28	Takarada (personal comm.)
Unzen	0.0001	0.9	0.4		0.44		2.28	Takarada (personal comm.)
Unzen	0.0002	3.6	1.0		0.29		3.50	Takarada (personal comm.)
Unzen	0.0001	2.1	0.8		0.39		2.57	Takarada (personal comm.)
Unzen	0.0002	1.7	0.7		0.42		2.38	Takarada (personal comm.)
Unzen	0.0001	2.4	0.9		0.36		2.78	Takarada (personal comm.)
Unzen	0.0002	1.8	0.7		0.40		2.52	Takarada (personal comm.)
Unzen	0.0006	2.4	0.9		0.36		2.78	Takarada (personal comm.)
Unzen	0.0002	2.4	0.9		0.36		2.78	Takarada (personal comm.)
Unzen	0.0001	2.1	0.8		0.39		2.57	Takarada (personal comm.)
Unzen	0.0006	3.7	1.0		0.27		3.66	Takarada (personal comm.)
Unzen	0.0001	2.1	0.8		0.39		2.57	Takarada (personal comm.)
Unzen	0.0001	1.8	0.7		0.40		2.52	Takarada (personal comm.)
Unzen	0.0001	2.1	0.8		0.39		2.57	Takarada (personal comm.)
Unzen	0.0001	2.4	0.9		0.36		2.78	Takarada (personal comm.)
Unzen	0.0002	1.8	0.7		0.40		2.52	Takarada (personal comm.)
Unzen	0.0001	2.4	0.9		0.36		2.78	Takarada (personal comm.)
Unzen	0.0001	1.8	0.7		0.40		2.52	Takarada (personal comm.)

Appendix I (continued). Physical parameters of the Ruapehu debris avalanches in relation to non-volcanic landslides, subaerial volcanic landslides (confined and unconfined), submarine landslides, block-and-ash flows, and pumice flows.

	V [km^3]	L_{max} [km]	H_{max} [km]	A [km^2]	H_{max}/L_{max}*	$A/V_{2/3}$**	L_{max}/H_{max}***	References
Block-and-ash flows								
Unzen	0.0001	1.8	0.7		0.40		2.52	Takarada (personal comm.)
Unzen	0.0001	2.4	0.9		0.36		2.78	Takarada (personal comm.)
Unzen	0.0001	2.4	0.9		0.36		2.78	Takarada (personal comm.)
Unzen	0.0001	1.8	0.7		0.40		2.52	Takarada (personal comm.)
Unzen	0.0001	2.4	0.9		0.36		2.78	Takarada (personal comm.)
Unzen	0.0001	2.4	0.9		0.36		2.78	Takarada (personal comm.)
Unzen	0.0001	2.4	0.8		0.35		2.86	Takarada (personal comm.)
Unzen	0.0003	2.4	0.9		0.36		2.78	Takarada (personal comm.)
Unzen	0.0002	3.1	1.0		0.31		3.19	Takarada (personal comm.)
Unzen	0.0002	2.4	0.9		0.36		2.78	Takarada (personal comm.)
Unzen	0.0001	1.7	0.7		0.42		2.38	Takarada (personal comm.)
Unzen	0.0003	2.4	0.9		0.36		2.78	Takarada (personal comm.)
Unzen	0.0001	2.4	0.9		0.36		2.78	Takarada (personal comm.)
Unzen	0.0001	2.4	0.9		0.36		2.78	Takarada (personal comm.)
Unzen	0.0003	2.4	0.9		0.36		2.78	Takarada (personal comm.)
Unzen	0.0003	3.7	1.0		0.27		3.66	Takarada (personal comm.)
Unzen	0.0001	1.8	0.7		0.40		2.52	Takarada (personal comm.)
Unzen	0.0002	2.1	0.8		0.39		2.57	Takarada (personal comm.)
Unzen	0.0001	3.7	1.0		0.27		3.66	Takarada (personal comm.)
Unzen	0.0001	1.7	0.7		0.42		2.38	Takarada (personal comm.)
Unzen	0.0002	2.4	0.9		0.36		2.78	Takarada (personal comm.)
Unzen	0.0003	1.8	0.7		0.40		2.52	Takarada (personal comm.)
Unzen	0.0001	2.4	0.9		0.36		2.78	Takarada (personal comm.)
Unzen	0.0002	2.4	0.9		0.36		2.78	Takarada (personal comm.)
Unzen	0.0002	1.8	0.7		0.40		2.52	Takarada (personal comm.)
Unzen	0.0002	2.4	0.9		0.36		2.78	Takarada (personal comm.)
Unzen	0.0001	2.4	0.9		0.36		2.78	Takarada (personal comm.)

Appendix I (continued). Physical parameters of the Ruapehu debris avalanches in relation to non-volcanic landslides, subaerial volcanic landslides (confined and unconfined), submarine landslides, block-and-ash flows, and pumice flows.

	V [km^3]	L_{max} [km]	H_{max} [km]	A [km^2]	H_{max}/L_{max}*	$A/V_{2/3}$**	L_{max}/H_{max}***	References
Block-and-ash flows								
Unzen	0.0002	1.7	0.7		0.42		2.38	Takarada (personal comm.)
Unzen	0.0002	2.4	0.9		0.36		2.78	Takarada (personal comm.)
Unzen	0.0001	3.6	1.0		0.29		3.50	Takarada (personal comm.)
Unzen	0.0002	2.4	0.9		0.36		2.78	Takarada (personal comm.)
Unzen	0.0001	1.8	0.7		0.40		2.52	Takarada (personal comm.)
Unzen	0.0001	1.8	0.7		0.40		2.52	Takarada (personal comm.)
Unzen	0.0002	2.4	0.9		0.36		2.78	Takarada (personal comm.)
Unzen	0.0001	2.4	0.9		0.37		2.69	Takarada (personal comm.)
Unzen	0.0003	2.4	0.9		0.36		2.78	Takarada (personal comm.)
Unzen	0.0001	2.4	0.8		0.35		2.86	Takarada (personal comm.)
Unzen	0.0004	3.6	1.0		0.29		3.50	Takarada (personal comm.)
Unzen	0.0002	2.9	1.0		0.33		3.03	Takarada (personal comm.)
Unzen	0.0001	2.4	0.9		0.36		2.78	Takarada (personal comm.)
Unzen	0.0001	3.1	1.0		0.31		3.19	Takarada (personal comm.)
Unzen	0.0002	3.1	1.0		0.31		3.19	Takarada (personal comm.)
Unzen	0.0002	3.1	1.0		0.31		3.19	Takarada (personal comm.)
Unzen	0.0001	2.4	0.8		0.35		2.86	Takarada (personal comm.)
Unzen	0.0001	1.8	0.7		0.40		2.52	Takarada (personal comm.)
Unzen	0.0001	1.8	0.7		0.40		2.52	Takarada (personal comm.)
Unzen	0.0001	3.7	1.0		0.27		3.66	Takarada (personal comm.)
Unzen	0.0001	3.1	1.0		0.31		3.19	Takarada (personal comm.)
Colima	0.0020	2.0		1.28		80.63		Saucedo et al. (2010)
Colima	0.0001	4.0	1.6	0.12	0.39	46.76	2.50	Saucedo et al. (2010)
Colima	0.0001	3.6	1.6	0.11	0.43	51.06	2.21	Saucedo et al. (2010)
Colima	0.0002	4.8	1.6	0.11	0.43	30.56	2.98	Saucedo et al. (2010)
Colima	0.0016	9.0	2.5	0.27	0.27	19.57	3.64	Saucedo et al. (2010)
Colima	0.0017	9.5	2.5	0.285	0.26	19.93	3.83	Saucedo et al. (2010)

Appendix I (continued). Physical parameters of the Ruapehu debris avalanches in relation to non-volcanic landslides, subaerial volcanic landslides (confined and unconfined), submarine landslides, block-and-ash flows, and pumice flows.

	V [km^3]	L_{max} [km]	H_{max} [km]	A [km^2]	H_{max}/L_{max}*	$A/V_{2/3}$**	L_{max}/H_{max}***	References
Block-and-ash flows								
Colima	0.0012	4.4	1.6	0.132	0.36	11.77	2.75	Saucedo et al. (2010)
Colima	0.0011	9.0	2.4	0.27	0.26	25.65	3.83	Saucedo et al. (2010)
Colima	0.0009	7.2	2.3	0.216	0.31	23.81	3.20	Saucedo et al. (2010)
Colima	0.0007	7.9	2.2	0.237	0.27	29.75	3.67	Saucedo et al. (2010)
Colima	0.0006	6.8	2.1	0.204	0.30	28.30	3.29	Saucedo et al. (2010)
Colima	0.0012	7.9	2.3	0.237	0.28	21.16	3.51	Saucedo et al. (2010)
Colima	0.0012	8.7	2.4	0.260	0.27	23.22	3.68	Saucedo et al. (2010)
Colima	0.0100	2.6		2.5		53.86		Saucedo et al. (2010)
Semeru	0.0064	10.0	2.9		0.29		3.42	Thouret et al. (2007)
Semeru	0.0062	10.0						Thouret et al. (2007)
Semeru	0.0063	11.5	2.9		0.25		3.93	Thouret et al. (2007)
Semeru	0.0055	11.5	2.8		0.25		4.06	Thouret et al. (2007)
Semeru	0.0035	9.0	2.9		0.33		3.08	Thouret et al. (2007)
Pumice flows								
Agung	0.01	9.0	2.5		0.28		3.60	Hayashi & Self (1992)
Agung	0.01	11.5	3.3		0.29		3.48	Hayashi & Self (1992)
Chokai	1	10.0	0.9		0.09		11.11	Hayashi & Self (1992)
Colima	0.0284	13.5	2.9	4.05	0.21		4.74	Saucedo et al. (2010)
Colima	0.0225	12.5	2.7	3.75	0.22	43.56	4.63	Saucedo et al. (2010)
Colima	0.0238	13.2	2.8	3.96	0.21	47.05	4.80	Saucedo et al. (2010)
Colima	0.0122	10.2	2.4	3.06	0.23	47.91	4.27	Saucedo et al. (2010)
Colima	0.0283	15.7	2.6	4.71	0.17	57.61	6.04	Saucedo et al. (2010)
Colima	0.0294	15.1	2.7	4.53	0.18	50.77	5.66	Saucedo et al. (2010)
Colima	0.0058	9.7	2.6	2.91	0.26	47.51	3.80	Saucedo et al. (2010)
Colima	0.0044	14.7	2.7	17.64	0.18	89.94	5.55	Saucedo et al. (2010)

Appendix I (continued). Physical parameters of the Ruapehu debris avalanches in relation to non-volcanic landslides, subaerial volcanic landslides (confined and unconfined), submarine landslides, block-and-ash flows, and pumice flows.

	V [km^3]	L_{max} [km]	H_{max} [km]	A [km^2]	H_{max}/L_{max}*	$A/V_{2/3}$**	L_{max}/H_{max}***	References
Pumice flows								
Colima	0.0135	9.0	2.3	2.7	0.26	655.95	3.91	Saucedo et al. (2010)
Colima	0.0248	15.0	2.8	4.5	0.18	47.62	5.42	Saucedo et al. (2010)
Colima	0.0239	15.9	2.9	4.77	0.18	52.99	5.58	Saucedo et al. (2010)
Colima	0.0090	2.5		1.8		57.57		Saucedo et al. (2010)
Mayon	0.0015	5.0	2.6		0.52		1.92	Hayashi & Self (1992)
MSH	0.0100	7.5		8.3		170.00		e.g., Hayashi & Self (1992)
MSH	0.0030	6.5	1.7	4.8	0.26	178.82	3.82	e.g., Hayashi & Self (1992)
MSH	0.0030	5.9	1.2		0.20	230.76	4.92	e.g., Hayashi & Self (1992)
MSH	0.0040	5.7	1.2	3.6	0.21		4.75	e.g., Hayashi & Self (1992)
MSH	0.0010	4.0		2.3		142.87		e.g., Hayashi & Self (1992)
Shirouma-Oike	0.0000	4.0	1.0		0.25		4.00	Hayashi & Self (1992)
Soufriere Hills Volcano	0.0001	4.6	1.2	0.471	0.27		3.77	Calder et al. (1999)
Soufriere Hills Volcano	0.0001	4.4	1.3	0.272	0.29	173.86	3.46	Calder et al. (1999)
Soufriere Hills Volcano	0.0000	3.0	1.1	0.066	0.35	144.11	2.86	Calder et al. (1999)
Soufriere Hills Volcano	0.0001	3.3	1.1	0.209	0.34	89.58	2.97	Calder et al. (1999)
Montserrat_Tar	0.0123	3.0	0.9		0.32	132.00	3.17	Calder et al. (1999)

*e.g. Scheidegger, 1973; Hsü, 1975

**Legros, 2002

***Iverson, 1997; Dade, 1998

****volcanic submarine landslides

APPENDIX I. REFERENCES

Begét, J. E., & Kienle, J. (1992). Cyclic formation of debris avalanches at Mount St Augustine volcano. Nature, 701-704.

Belousov, A., Belousova, M., & Voight, B. (1999). Multiple edifice failures, debris avalanches and associated eruptions in the Holocene history of Shiveluch volcano, Kamchatka, Russia. Bulletin of Volcanology, 61(5), 324-342.

Belousova, M. G. (1996). Large-scale edifice failure and associated eruptions in the history of Shiveluch volcano (Kamchatka). Proc Moskow Univ Geol Issue 2:23-26 (In Russian).

Bernard, B., De Vries, B. V. W., & Leyrit, H. (2009). Distinguishing volcanic debris avalanche deposits from their reworked products: the Perrier sequence (French Massif Central). Bulletin of Volcanology, 71(9), 1041-1056.

Bronto, S. (1989). Volcanic geology of Galunggung, West Java, Indonesia.

Campbell, C. S. (1989). Self-lubrication for long runout landslides. The Journal of Geology, 653-665.

Calder, E. S., Cole, P. D., Dade, W. B., Druitt, T. H., Hoblitt, R. P., Huppert, H. E., ... & Young, S. R. (1999). Mobility of pyroclastic flows and surges at the Soufriere Hills Volcano, Montserrat. Geophysical Research Letters, 26(5), 537-540.

Carrasco-Núñez, G. (1997). Lava flow growth inferred from morphometric parameters: a case study of Citlaltépetl volcano, Mexico. Geological Magazine, 134(2), 151-162.

Carrasco-Núñez, G., Díaz-Castellón, R., Siebert, L., Hubbard, B., Sheridan, M. F., & Rodríguez, S. R. (2006). Multiple edifice-collapse events in the Eastern Mexican Volcanic Belt: the role of sloping substrate and implications for hazard assessment. Journal of Volcanology and Geothermal Research, 158(1), 151-176.

Charbonnier, S. J., & Gertisser, R. (2011). Deposit architecture and dynamics of the 2006 block-and-ash flows of Merapi Volcano, Java, Indonesia. Sedimentology, 58(6), 1573-1612.

Clavero, J., Sparks, R., Huppert, H., & Dade, W. (2002). Geological constraints on the emplacement mechanism of the Parinacota debris avalanche, northern Chile. Bulletin of Volcanology, 64(1), 40-54.

Cortes, A., Macías, J. L., Capra, L., & Garduño-Monroy, V. H. (2010). Sector collapse of the SW flank of Volcán de Colima, México: The 3600yr BP La Lumbre–Los Ganchos debris avalanche and associated debris flows. Journal of Volcanology and Geothermal Research, 197(1), 52-66.

Crandell, D. R. (1989). Gigantic debris avalanche of Pleistocene age from ancestral Mount Shasta volcano, California, and debris-avalanche hazard zonation. US Government Printing Office, 32.

Gaylord, D. R., & Neall, V. E. (2012). Subedifice collapse of an andesitic stratovolcano: The Maitahi Formation, Taranaki Peninsula, New Zealand. Geological Society of America Bulletin, 124(1-2), 181-199.

Geronimo-Cantane, S. G. (1997). Debris avalanche in the Philippines: Their occurrence, hazards, and mitigation measures: Puerto Vallarta, Mexico. International Association of Volcanology and Chemistry of the Earth's Interior General Assembly. Abstract, p. 37.

Godoy, B. G., Clavero, J., Rojas, C., & Godoy, E. (2012). Volcanic facies of the debris avalanche deposit of Tata Sabaya Volcano, Central Andes. Andean Geology, 39(3), 394-406.

Griswold, J. P., & Iverson, R. M. (2008). Mobility statistics and automated hazard mapping for debris flows and rock avalanches. US Department of the Interior, US Geological Survey. Hampton, M. A., Lee, H. J., & Locat, J. (1996). Submarine landslides. Reviews of geophysics, 34(1), 33-59.

Hazlett, R. W., Buesch, D., Anderson, J. L., Elan, R., & Scandone, R. (1991). Geology, failure conditions, and implications of seismogenic avalanches of the 1944 eruption at Vesuvius, Italy. Journal of Volcanology and Geothermal Research, 47(3), 249-264.

Kawachi, S., & Hayatsu, K. (1994). Debris avalanche and lahar deposits in the Yatsugatake Volcanic Chain and Myoko Volcanic Group, Central Japan. Journal of Natural Disaster Science, 16(1), 55-69.

Lipman, P. W., Normark, W. R., Moore, J. G., Wilson, J. B., & Gutmacher, C. E. (1988). The giant submarine Alika debris slide, Mauna Loa, Hawaii. Journal of Geophysical Research: Solid Earth (1978–2012), 93(B5), 4279-4299.

Luhr, J. F., & Prestegaard, K. L. (1985). Caldera formation at Volcán de Colima, Mexico: a large Mt St Helens-type avalanche event 4300 yr ago. Eos, Transactions of the American Geophysical Union, San Francisco, CA, p. 411.

Macías, J. L., Sheridan, M. F., & Espíndola, J. M. (1997). Reappraisal of the 1982 eruptions of El Chichón Volcano, Chiapas, Mexico: new data from proximal deposits. Bulletin of Volcanology, 58(6), 459-471.

McMurtry, G. M., Herrero-Bervera, E., Cremer, M. D., Smith, J. R., Resig, J., Sherman, C., & Torresan, M. E. (1999). Stratigraphic constraints on the timing and emplacement of the Alika 2 giant Hawaiian submarine landslide. Journal of Volcanology and Geothermal Research, 94(1), 35-58.

Melekestsev, I. V., Litasova, S. N., & Sulerzhitskly, L. D. (1992). The age and scale of catastrophic eruptions of the directed explosion type in the Avacha volcano (Kamchatka) in the late Pleistocene. Volcanology and Seismology, 13(2): 135-146.

Morelli, S., Monroy, V. H. G., Gigli, G., Falorni, G., Rocha, E. A., & Casagli, N. (2010). The Tancitaro debris avalanche: characterization, propagation and modeling. Journal of Volcanology and Geothermal Research, 193(1), 93-105.

Moreno, R. (1991). The southern Andes volcanoes (33°-41°30'S), Chile: 6th Congreso Geológico Chileno-Guía de Excursión, PC-3, 26 p.

Naranjo, J. A., Scott, K. M., & Hildreth, W. E. (1997). Highly mobile catastrophic debris avalanche of Planchon-Peteroa volcanic complex, southern Andes, Chile: Puerto Vallarta, Mexico. International Association of Volcanology and Chemistry of the Earth's Interior General Assembly, Abstracts, p. 107.

Paguican, E. M. R., de Vries, B. V. W., & Lagmay, A. M. F. (2012). Volcano-tectonic controls and emplacement kinematics of the Iriga debris avalanches (Philippines). Bulletin of Volcanology, 74(9), 2067-2081.

Procter, J.N., Cronin, S.J., Zernack, A.V., Lube, G., Stewart, B., Nemeth, K., Keys, H., (in review). Debris flow evolution and activation of an explosive hydrothermal system; Te Maari, Tongariro, New Zealand. Journal of Volcanology and Geothermal Research.

Richter, D. H., Smith, R. I., Yehle, L. A., & Miller, T. P., (1979). Geologic map of the Gulkana A-2 quadrangle, Alaska: U.S. Geological Survey Geologic Quadrangle Map GQ-1260, scale 1:63 360, 1 sheet.

Rowland, S. K., & Munro, D. C. (1992). The caldera of Volcan Fernandina: a remote sensing study of its structure and recent activity. Bulletin of Volcanology, 55(1-2), 97-109.

Satake, K., & Kato, Y. (2001). The 1741 Oshima-Oshima Eruption: Extent and volume of submarine debris avalanche. Geophysical Research Letters, 28(3), 427-430.

Saucedo, R., Macías, J. L., Gavilanes, J. C., Arce, J. L., Komorowski, J. C., Gardner, J. E., & Valdez-Moreno, G. (2010). Eyewitness, stratigraphy, chemistry, and eruptive dynamics of the 1913 Plinian eruption of Volcán de Colima, México. Journal of Volcanology and Geothermal Research, 191(3), 149-166.

Schwarzkopf, L., & Schmincke, H. U. (2000). The 1998 eruption of Merapi volcano. Central Java, Indonesia: Volumes and structure of the deposits and implications for flow mechanisms: IAVCEI general assembly, Bali, Indonesia, Abstract volume, 166.

Shea, T., De Vries, B. V. W., & Pilato, M. (2008). Emplacement mechanisms of contrasting debris avalanches at Volcán Mombacho (Nicaragua), provided by structural and facies analysis. Bulletin of Volcanology, 70(8), 899-921.

Siebe, C., Komorowski, J. C., & Sheridan, M. F. (1992). Morphology and emplacement of an unusual debris-avalanche deposit at Jocotitlan volcano, Central Mexico. Bulletin of Volcanology, 54(7), 573-589.

Siebe, C., Komorowski, J. C., Navarro, C., McHone, J., Delgado, H., & Cortés, A. (1995). Submarine eruption near Socorro Island, Mexico: Geochemistry and scanning electron microscopy studies of floating scoria and reticulite. Journal of Volcanology and Geothermal Research, 68(4), 239-271.

Siebert, L., Begét, J. E., & Glicken, H. (1995). The 1883 and late-prehistoric eruptions of Augustine volcano, Alaska. Journal of Volcanology and Geothermal Research, 66(1), 367-395.

Siebert, L., Bronto, S., Supriatman, L., & Mutyana, R. (1996). Massive debris-avalanche deposit from Raung volcano, eastern Java, Indonesia [abs.]: Eos Transactions, American Geophysical Union), 77, p. S291.

Siebert, L., Kimberly, P., & Pullinger, C. R. (2004). The voluminous Acajutla debris avalanche from Santa Ana volcano, western El Salvador, and comparison with other Central American edifice-failure events. Special Papers – Geological Society of America, 5-24.

Silver, E., Day, S., Ward, S., Hoffmann, G., Llanes, P., Driscoll, N., ... & Saunders, S. (2009). Volcano collapse and tsunami generation in the Bismarck Volcanic Arc, Papua New Guinea. Journal of Volcanology and Geothermal Research, 186(3), 210-222.

Thouret, J. C., Wörner, G., Gunnell, Y., Singer, B., Zhang, X., & Souriot, T. (2007). Geochronologic and stratigraphic constraints on canyon incision and Miocene uplift of the Central Andes in Peru. Earth and Planetary Science Letters, 263(3), 151-166.

Vallance, J. W., Siebert, L., Rose, W. I., Girón, J. R., & Banks, N. G. (1995). Edifice collapse and related hazards in Guatemala. Journal of Volcanology and Geothermal Research, 66(1), 337-355.

Vallance, J. W., Gardner, C. A., Scott, W. E., Iverson, R. M., & Pierson, T. C. (2010). Mount St. Helens: A 30-Year Legacy of Volcanism. Eos, Transactions American Geophysical Union, 91(19), 169-170.

Voight, B., Komorowski, J. C., Norton, G. E., Belousov, A. B., Belousova, M., Boudon, G., ... & Young, S. R. (2002). The 26 December (Boxing Day) 1997 sector collapse and debris

avalanche at Soufriere Hills volcano, Montserrat. Memoirs – Geological Society of London, 21, 363-408.

Wadge, G., Francis, P. W., & Ramirez, C. F. (1995). The Socompa collapse and avalanche event. Journal of Volcanology and Geothermal Research, 66(1), 309-336.

Yehle, L. A., & Nichols, D. R. (1980). Reconnaissance map and description of the Chetaslina volcanic debris flow (new name), southeastern Copper River basin and adjacent areas, south-central Alaska. The Survey.

Yoshida, H., Sugai, T., & Ohmori, H. (2012). Size–distance relationships for hummocks on volcanic rockslide-debris avalanche deposits in Japan. Geomorphology, 136(1), 76-87.

Yoshimoto M., Furukawa, R., Nanayama, F., Nishimura, Y., Nishina, K., Uchida, Y., Takarada, S., Takahashi, R., & Kinoshita, H. (2003). Subaqeous distribution and volume estimation of the debris-avalanche deposit from the 1640 eruption of Hokkaido-Komagatake volcano, southwest Hokkaido, Japan. Journal of the Geophysical Society of Japan, 109:137-148.

Appendix II. Representative whole-rock analyses of the Ruapehu mass flows (XRF and ICP-MS combined)

	1	2	3	4	5	6	7	8	9	10	11
Formation	**Mataroa Formation**										
Deposit	**RG**	**RG**	**RG**	**VDA**	**VDA**	**VDA**	**VDA**	**VDA**	**DF**	**DF**	**DF**
Sample no.:	GWT	GW1a	GW1b	GW3a	GW3a*	GW3b	GW3gr	GW3kl	GW4	GW5a	GW5b
SiO_2	57.41	60.08	58.21	56.67	56.40	58.53	58.70	56.59	58.16	56.95	54.87
TiO_2	0.66	0.57	0.60	0.67	0.67	0.60	0.65	0.66	0.69	0.64	0.68
Al_2O_3	17.51	16.29	16.68	18.69	18.54	19.25	17.56	19.36	17.96	18.88	17.76
Fe_2O_3	8.22	6.55	7.61	7.46	7.76	5.78	6.87	6.95	7.38	6.48	8.23
MnO	0.13	0.11	0.13	0.12	0.12	0.09	0.11	0.11	0.12	0.10	0.13
MgO	4.03	3.50	4.47	3.47	3.61	2.08	3.73	2.81	3.14	3.08	4.69
CaO	7.35	6.59	7.37	7.94	7.97	7.33	7.16	7.93	6.45	6.82	6.70
Na_2O	3.40	3.48	3.27	3.48	3.43	3.70	3.58	3.53	3.34	3.53	3.15
K_2O	1.12	1.35	1.03	1.02	0.99	1.21	1.10	1.00	1.50	1.02	0.73
P_2O_5	0.12	0.13	0.11	0.12	0.12	0.12	0.11	0.12	0.14	0.11	0.09
H_2O	0.24	0.29	0.20	0.04	0.27	0.26	0.12	0.52	0.26	0.71	1.46
LOI	-0.31	0.96	0.24	0.22	0.02	0.94	0.20	0.30	0.75	1.56	1.41
Total	99.88	99.89	99.91	99.90	99.89	99.89	99.88	99.90	99.89	99.88	99.89
Be		0.87	0.68	0.76		0.84	0.85	0.72	1.19	1.07	
Cs	0.72	1.98	1.42	1.36	1.49	1.65	1.46	1.36	1.98	1.50	1.21
Ba	294	315	245	264	275	309	273	269	351	322	294
Rb	31	37	28	25	27	30	29	25	42	27	21
Sr	266	229	210	249	268	261	229	258	261	256	231
Pb	32.38	7.13	6.58	6.70	68.25	7.97	7.97	7.02	9.83	8.54	46.73
Th	3.38	3.66	2.34	2.51	2.63	2.75	2.77	2.46	4.34	3.27	2.94
U	0.91	1.29	0.81	0.70	0.73	0.85	0.83	0.78	1.11	0.89	0.74
Zr	85	93	67	68	77	72	73	67	96	88	84
Nb	3.13	3.75	2.99	3.08	3.15	3.22	3.39	3.18	4.72	3.73	3.23
Hf	2.32	2.51	1.85	1.85	2.08	2.00	2.04	1.86	2.62	2.40	2.31
Ta	0.24	0.46	1.06	0.32	0.23	0.31	0.34	0.26	0.38	0.36	0.25
Y	18	18	15	16	18	14	14	16	16	17	18
Sc	29.2	21.9	24.3	22.5	26.2	16.3	20.4	20.1	19.8	21.4	32.3
V	219	162	186	191	200	154	181	173	174	163	217
Cr	46	47	86	46	54	20	88	29	18	44	93
Co	57	67	59	46	114	58	42	41	34	59	62
Ni	18	18	39	23	32	15	35	19	14	22	42
Cu	36	21	42	42	46	31	35	50	23	46	52
Zn	129	76	87	85	202	72	77	77	85	68	161
Ga	17	16	16	17	17	17	17	17	18	17	17
La	9.39	9.39	7.13	7.42	7.97	8.18	7.73	7.60	11.51	9.34	8.14
Ce	19.18	20.83	15.75	16.75	16.83	17.79	17.50	17.21	26.27	20.18	17.00
Pr	2.42	2.55	1.94	2.03	2.12	2.14	2.04	2.10	3.02	2.58	2.18
Nd	11.14	11.37	8.52	9.35	10.01	9.50	9.06	9.33	12.93	11.03	10.13
Sm	2.76	2.72	2.18	2.27	2.49	2.45	2.32	2.38	3.06	2.84	2.60
Eu	0.81	0.78	0.66	0.77	0.81	0.74	0.70	0.77	0.86	0.86	0.82
Gd	2.82	2.86	2.20	2.48	2.91	2.34	2.25	2.54	2.72	2.88	2.82
Tb	0.49	0.46	0.36	0.39	0.51	0.39	0.38	0.41	0.44	0.45	0.50
Dy	3.30	3.04	2.68	2.80	3.17	2.52	2.46	2.80	2.99	3.16	3.19
Ho	0.67	0.66	0.56	0.58	0.67	0.53	0.55	0.60	0.63	0.65	0.65
Er	1.99	2.00	1.75	1.74	2.07	1.53	1.60	1.73	1.88	1.97	2.00
Tm	0.31	0.32	0.28	0.27	0.31	0.25	0.25	0.28	0.30	0.32	0.32
Yb	1.93	2.18	1.87	1.83	2.12	1.65	1.62	1.86	1.95	1.97	2.01
Lu	0.31	0.32	0.26	0.26	0.32	0.27	0.25	0.26	0.29	0.30	0.32

VDA= Volcanic debris-avalanche deposit
DF= Debris-flow deposit
HCF= Hyperconcentrated-flow deposit
RG= River gravel
MT= Marine-terrace gravel

Appendix II (continued). Representative whole-rock analyses of the Ruapehu mass flows (XRF and ICP-MS combined)

	12	13	14	15	16	17	18	19	20	21	22	23
Formation	Mataroa Formation									L. Whangaehu Form		
Deposit	**VDA**	**DF**	**DF**	**DF**	**DF**	**DF**	**DF**	**HCF**	**N/A**	**DF**	**DF**	**DF**
Sample no.:	MF1	MF1b	MF3b	JW2a	JW2b	JW2c	JW2d	HI2b	HI_FS	GP1a	GP1b	GP1c
SiO_2	56.60	56.20	58.71	55.43	58.72	57.94	55.48	55.39	56.75	57.71	53.44	55.80
TiO_2	0.64	0.76	0.73	0.61	0.58	0.61	0.74	0.85	0.71	0.72	0.81	0.62
Al_2O_3	17.81	17.95	17.90	16.95	17.22	17.27	17.29	17.73	17.56	18.62	17.59	18.28
Fe_2O_3	7.26	8.17	6.95	8.16	7.06	7.81	9.05	8.65	7.75	7.39	10.05	8.02
MnO	0.13	0.12	0.11	0.13	0.13	0.13	0.15	0.14	0.12	0.11	0.15	0.13
MgO	4.37	3.79	2.91	5.87	3.91	4.21	4.35	4.59	4.26	3.02	5.01	4.41
CaO	8.06	7.28	5.97	8.24	7.06	7.07	7.88	7.71	6.35	7.42	8.61	7.97
Na_2O	3.24	3.16	3.49	3.21	3.29	3.18	2.96	3.12	3.11	3.60	2.94	3.49
K_2O	0.71	1.39	1.47	0.64	1.09	0.95	0.98	1.00	1.30	1.10	0.85	0.75
P_2O_5	0.09	0.13	0.12	0.09	0.10	0.10	0.13	0.14	0.13	0.12	0.10	0.09
H_2O	0.53	0.48	0.74	0.18	0.19	0.24	0.34	0.24	1.06	0.25	0.33	0.33
LOI	0.45	0.44	0.78	0.37	0.58	0.37	0.51	0.33	0.77	-0.18	0.00	0.02
Total	99.89	99.88	99.88	99.88	99.91	99.89	99.87	99.88	99.87	99.89	99.89	99.90
Be	0.54	0.95		0.70	0.92	0.80	0.81	0.89				
Cs	0.94	1.95	2.76	0.81	1.79	1.42	1.30	1.46	1.17	1.11	0.94	1.25
Ba	240	319	402	181	282	263	258	309	370	282	260	216
Rb	16	37	48	13	30	25	24	26	32	31	19	18
Sr	226	272	253	221	221	222	254	257	252	283	279	244
Pb	9.16	9.85	68.20	5.49	8.06	10.87	6.85	7.41	46.48	22.44	9.59	9.70
Th	1.57	3.99	5.53	1.06	2.95	2.38	2.74	3.85	5.10	3.27	2.40	1.69
U	0.60	0.92	1.33	0.38	0.89	0.73	0.68	0.89	1.14	0.80	0.59	0.60
Zr	57	91	126	49	74	66	66	101	111	89	64	61
Nb	2.11	4.24	4.94	1.67	3.30	2.93	3.29	4.70	4.53	3.78	2.15	1.95
Hf	1.50	2.54	3.38	1.40	2.08	1.84	1.95	2.85	3.03	2.44	1.85	1.76
Ta	0.24	0.38	0.41	0.19	0.44	0.32	0.32	0.45	0.35	0.29	0.15	0.16
Y	19	19	20	14	15	14	16	17	22	19	20	17
Sc	29.6	25.1	23.7	28.8	23.9	25.9	29.8	32.0	29.9	23.1	41.8	28.6
V	201	211	188	215	179	204	241	250	205	198	315	221
Cr	42	19	39	175	66	69	48	54	59	42	49	48
Co	49	48	73	49	95	51	54	50	41	81	49	98
Ni	24	15	27	67	23	24	64	19	20	23	21	35
Cu	41	26	28	24	28	16	25	45	34	39	43	52
Zn	74	83	182	80	90	93	98	89	144	114	95	94
Ga	16	18	18	16	16	17	16	18	18	18	18	17
La	6.88	11.60	12.71	3.85	7.99	6.38	8.68	10.52	14.21	9.99	7.80	5.42
Ce	11.66	24.30	27.57	9.15	16.99	13.99	18.26	22.83	30.68	19.67	16.10	11.10
Pr	1.99	3.17	3.27	1.22	2.09	1.75	2.31	2.78	3.67	2.59	2.15	1.55
Nd	9.49	13.57	14.38	6.02	9.07	7.81	10.59	12.46	16.29	11.80	10.58	7.63
Sm	2.40	3.37	3.54	1.76	2.39	2.01	2.54	2.89	3.74	2.97	2.79	2.19
Eu	0.82	0.90	0.90	0.59	0.69	0.66	0.76	0.86	0.96	0.86	0.85	0.69
Gd	2.84	3.24	3.45	2.09	2.43	2.19	2.62	2.94	3.73	3.09	3.14	2.46
Tb	0.47	0.51	0.58	0.35	0.39	0.34	0.40	0.46	0.67	0.51	0.53	0.43
Dy	3.32	3.43	3.69	2.50	2.59	2.44	2.99	3.20	4.06	3.36	3.53	2.93
Ho	0.72	0.72	0.74	0.53	0.56	0.55	0.64	0.66	0.81	0.72	0.74	0.64
Er	2.11	2.10	2.20	1.57	1.76	1.52	1.95	1.90	2.44	2.03	2.17	1.85
Tm	0.30	0.32	0.33	0.25	0.27	0.24	0.31	0.28	0.36	0.31	0.33	0.28
Yb	2.11	2.17	2.25	1.76	1.77	1.69	1.96	2.03	2.32	2.03	2.09	1.86
Lu	0.34	0.31	0.33	0.25	0.26	0.27	0.29	0.29	0.35	0.32	0.33	0.29

VDA= Volcanic debris-avalanche deposit
DF= Debris-flow deposit
HCF= Hyperconcentrated-flow deposit
RG= River gravel
MT= Marine-terrace gravel

Appendix II (continued). Representative whole-rock analyses of the Ruapehu mass flows (XRF and ICP-MS combined)

	24	25	26	27	28	29	30	31	32	33	34	35
Formation	**Lower Whangaehu Formation**											
Deposit	**VDA**	**VDA**	**VDA**	**VDA**	**VDA**	**VDA**	**VDA**	**VDA**	**VDA**	**VDA**	**VDA**	**N/A**
Sample no.:	QU1	QU2	MP3	MP4	TF1	TF2	TF4	TF5	TF6	TF7	TF8	MA1
SiO_2	55.66	56.46	57.64	57.64	56.80	57.79	59.57	55.01	56.14	57.07	57.42	59.59
TiO_2	0.61	0.55	0.75	0.64	0.65	0.60	0.55	0.77	0.62	0.71	0.63	0.63
Al_2O_3	17.93	17.84	17.64	19.24	17.88	16.30	17.08	17.56	16.91	17.00	17.62	18.52
Fe_2O_3	8.21	7.38	7.82	6.68	8.40	7.67	6.53	9.55	8.88	8.15	8.01	6.58
MnO	0.13	0.12	0.12	0.10	0.13	0.13	0.11	0.14	0.14	0.13	0.13	0.11
MgO	4.69	3.88	3.54	2.74	4.01	4.75	3.76	4.52	5.25	4.53	4.15	2.24
CaO	7.87	6.82	6.95	7.83	7.75	7.27	6.75	8.40	8.21	7.32	7.46	6.24
Na_2O	3.33	3.11	3.31	3.67	3.34	3.05	3.55	3.12	3.03	3.21	3.36	3.60
K_2O	0.74	0.85	1.38	1.07	0.95	1.38	1.23	0.92	0.73	1.18	1.07	1.53
P_2O_5	0.09	0.11	0.12	0.13	0.12	0.11	0.10	0.11	0.10	0.10	0.11	0.13
H_2O	0.33	0.53	0.32	0.21	0.17	0.25	0.32	0.14	0.12	0.20	0.12	0.18
LOI	0.33	2.26	0.30	-0.06	-0.32	0.58	0.35	-0.36	-0.23	0.30	-0.20	0.56
Total	99.90	99.90	99.88	99.88	99.88	99.87	99.89	99.88	99.89	99.91	99.89	99.91
Be												
Cs	1.24	1.65	2.08	1.02	1.18	2.36	2.07	0.86	0.75	1.92	1.10	2.36
Ba	197	251	299	338	274	335	309	271	206	270	292	365
Rb	18	24	39	25	26	39	34	22	18	35	30	46
Sr	222	254	266	310	246	267	255	275	225	238	253	290
Pb	6.73	8.34	10.53	8.58	9.63	13.41	16.08	23.64	27.76	34.95	31.47	26.84
Th	1.56	3.01	4.43	3.39	3.26	4.28	3.48	2.67	1.75	3.72	3.20	5.41
U	0.51	0.71	0.98	0.78	0.86	1.08	0.88	0.67	0.48	0.85	0.83	1.17
Zr	62	80	102	80	80	94	91	71	62	90	82	117
Nb	1.88	2.82	4.14	2.89	2.72	3.45	3.22	2.37	2.12	3.46	2.98	5.26
Hf	1.69	2.16	2.80	2.16	2.18	2.54	2.51	2.06	1.75	2.44	2.23	3.08
Ta	0.16	0.22	0.33	0.21	0.20	0.29	0.27	0.19	0.16	0.28	0.24	0.41
Y	19	18	20	17	20	18	16	20	18	20	18	19
Sc	31.2	26.5	29.3	21.2	28.3	30.9	23.9	38.4	34.4	33.6	27.8	16.9
V	221	179	237	193	221	205	168	295	221	241	209	139
Cr	56	63	18	35	67	91	69	37	89	72	62	9
Co	47	122	42	40	51	48	65	51	51	44	50	26
Ni	30	29	11	20	32	29	26	20	40	24	23	6
Cu	43	30	18	41	56	21	31	38	45	27	32	10
Zn	80	80	88	76	85	97	103	121	135	168	237	139
Ga	17	16	18	18	17	17	17	18	16	17	17	18
La	4.91	8.62	11.12	10.27	8.96	11.55	8.86	7.86	6.01	9.35	9.02	13.80
Ce	9.88	16.22	22.58	19.96	17.97	20.96	17.76	15.53	12.14	19.24	17.94	27.87
Pr	1.49	2.05	2.81	2.63	2.34	2.71	2.16	2.21	1.68	2.42	2.34	3.33
Nd	7.47	9.16	12.38	11.71	10.85	11.64	9.41	10.41	8.21	10.84	10.39	14.46
Sm	2.18	2.19	3.12	2.78	2.85	2.82	2.37	2.85	2.27	2.75	2.65	3.28
Eu	0.72	0.72	0.86	0.89	0.85	0.79	0.71	0.87	0.75	0.78	0.81	0.86
Gd	2.56	2.54	3.15	2.82	2.87	3.00	2.49	3.03	2.71	3.06	2.67	3.13
Tb	0.47	0.45	0.54	0.49	0.53	0.50	0.43	0.54	0.47	0.51	0.49	0.50
Dy	3.24	3.21	3.70	3.24	3.47	3.21	2.90	3.59	3.19	3.54	3.18	3.52
Ho	0.71	0.69	0.77	0.68	0.75	0.68	0.61	0.75	0.69	0.73	0.69	0.72
Er	2.08	2.03	2.20	1.91	2.10	1.96	1.81	2.10	1.95	2.14	1.99	2.14
Tm	0.33	0.32	0.33	0.31	0.35	0.32	0.28	0.34	0.32	0.34	0.30	0.33
Yb	2.00	2.05	2.10	1.90	2.06	1.97	1.85	2.10	1.86	2.17	2.06	2.13
Lu	0.32	0.31	0.33	0.29	0.32	0.30	0.28	0.32	0.29	0.32	0.32	0.33

VDA= Volcanic debris-avalanche deposit
DF= Debris-flow deposit
HCF= Hyperconcentrated-flow deposit
RG= River gravel
MT= Marine-terrace gravel

Appendix II (continued). Representative whole-rock analyses of the Ruapehu mass flows (XRF and ICP-MS combined)

	36	37	38	39	40	41	42	43	44	45	46	47
Formation	**Lower Whangaehu Formation**					**Oreore Formation**						
Deposit	**N/A**	**N/A**	**MT**	**MT**	**MT**	**RG**	**RG**	**VDA**	**VDA**	**VDA**	**VDA**	**VDA**
Sample no.:	MA2	MA3	HAF3	HAF4	HAF5	OQ1	OQ3	AI2	AI3	AR1	KL1	KL2
SiO_2	57.02	55.02	58.53	55.84	56.61	54.16	55.85	59.27	56.75	58.91	57.42	57.14
TiO_2	0.65	0.69	0.74	0.65	0.67	0.67	0.58	0.56	0.57	0.67	0.61	0.58
Al_2O_3	17.77	17.15	17.89	17.74	17.11	17.77	16.42	17.58	17.54	18.52	17.91	17.49
Fe_2O_3	7.96	9.02	7.28	8.63	8.55	9.38	7.77	7.25	8.06	7.52	8.17	8.15
MnO	0.12	0.14	0.11	0.11	0.13	0.15	0.13	0.11	0.13	0.12	0.13	0.12
MgO	3.85	5.08	2.87	4.14	4.34	4.99	6.68	3.47	4.65	2.37	3.86	4.60
CaO	7.37	8.43	6.84	7.60	7.92	7.69	7.52	6.71	7.67	5.76	7.36	7.28
Na_2O	3.27	3.01	3.57	3.41	3.08	2.89	2.97	3.47	3.32	3.37	3.39	3.35
K_2O	1.12	0.89	1.38	0.80	1.05	0.66	0.65	1.19	0.84	1.55	0.89	0.95
P_2O_5	0.11	0.11	0.13	0.10	0.11	0.10	0.10	0.11	0.10	0.15	0.10	0.10
H_2O	0.36	0.16	0.21	0.59	0.23	0.77	0.39	0.24	0.28	0.52	0.26	0.24
LOI	0.33	0.20	0.36	0.29	0.10	0.66	0.82	-0.08	-0.01	0.44	-0.19	-0.10
Total	99.91	99.89	99.90	99.91	99.89	99.89	99.87	99.90	99.89	99.89	99.91	99.90
Be												
Cs	1.67	1.16	2.30	0.73	1.54	0.74	0.81	1.01	1.18	1.39	0.62	1.05
Ba	290	247	347	262	293	233	263	295	250	433	247	254
Rb	29	22	41	16	28	14	16	35	20	46	24	25
Sr	250	249	291	256	255	226	240	242	244	273	238	238
Pb	18.09	11.01	16.28	11.05	12.00	6.83	7.64	10.07	10.99	16.45	9.52	7.57
Th	3.18	2.35	4.37	2.06	3.03	2.17	2.79	3.71	2.69	5.64	2.37	2.78
U	0.83	0.58	1.02	0.62	0.73	0.48	0.61	0.95	0.67	1.26	0.65	0.73
Zr	82	71	105	66	83	68	77	90	71	116	72	74
Nb	3.09	2.51	4.31	2.04	3.03	2.36	2.91	3.66	2.95	5.18	2.67	2.95
Hf	2.27	1.99	2.91	1.93	2.27	1.99	2.14	2.45	1.96	3.05	1.99	2.04
Ta	0.25	0.19	0.33	0.17	0.23	0.17	0.22	0.29	0.21	0.38	0.22	0.21
Y	17	18	19	15	18	19	18	18	16	20	19	16
Sc	27.6	35.2	23.9	30.2	34.4	35.3	30.5	24.6	29.1	19.5	27.5	28.4
V	212	251	202	220	227	246	190	170	200	167	213	201
Cr	42	64	19	60	62	75	272	36	65	11	32	73
Co	42	57	41	38	55	52	61	53	60	46	42	64
Ni	19	30	15	37	29	35	91	19	31	10	17	33
Cu	29	68	37	42	66	44	40	26	44	11	29	42
Zn	117	99	245	236	211	84	79	85	88	94	91	86
Ga	17	16	18	17	17	17	16	17	16	19	17	17
La	8.73	7.57	11.53	6.12	8.82	7.02	7.89	12.22	8.25	14.54	7.23	8.40
Ce	17.39	15.64	24.53	12.30	18.61	14.49	15.76	21.14	16.55	30.81	14.48	16.36
Pr	2.24	2.10	3.02	1.78	2.41	2.13	2.43	3.08	2.07	3.72	2.13	2.13
Nd	9.99	9.67	13.51	8.33	11.14	10.36	11.19	13.55	9.24	16.14	10.03	9.74
Sm	2.50	2.48	3.24	2.34	2.68	2.79	2.89	3.08	2.35	3.75	2.57	2.51
Eu	0.79	0.83	0.91	0.78	0.82	0.86	0.86	0.88	0.70	0.96	0.81	0.77
Gd	2.73	2.71	3.22	2.65	2.85	2.98	2.98	3.12	2.32	3.36	2.86	2.43
Tb	0.56	0.47	0.53	0.42	0.50	0.53	0.53	0.52	0.41	0.57	0.50	0.45
Dy	3.04	3.20	3.42	2.80	3.23	3.67	3.46	3.44	2.81	3.75	3.37	2.97
Ho	0.67	0.68	0.72	0.58	0.70	0.75	0.70	0.71	0.61	0.77	0.73	0.63
Er	2.00	1.97	2.10	1.74	2.06	2.13	2.03	2.02	1.74	2.18	2.07	1.89
Tm	0.30	0.29	0.31	0.26	0.30	0.33	0.29	0.30	0.27	0.34	0.34	0.28
Yb	2.02	2.00	2.18	1.65	2.11	2.17	1.98	2.04	1.83	2.24	2.23	1.92
Lu	0.30	0.30	0.32	0.25	0.30	0.32	0.30	0.31	0.28	0.35	0.32	0.28

VDA= Volcanic debris-avalanche deposit
DF= Debris-flow deposit
HCF= Hyperconcentrated-flow deposit
RG= River gravel
MT= Marine-terrace gravel

Appendix II (continued). Representative whole-rock analyses of the Ruapehu mass flows (XRF and ICP-MS combined)

	48	49	50	51	52	53	54	55	56	57	58	59
Formation	**Oreore Formation**											
Deposit	**VDA**	**VDA**	**VDA**	**VDA**	**VDA**	**VDA**	**VDA**	**VDA**	**VDA**	**VDA**	**VDA**	**VDA**
Sample no.:	KL3	KL4	KL5	KL6	KL7	KL8	KL9	KL10	KL11	OH1	OH2	OH3
SiO_2	57.10	58.76	53.52	53.64	59.34	52.53	52.93	50.89	51.41	58.77	54.59	56.53
TiO_2	0.56	0.55	0.64	0.69	0.50	0.64	0.64	0.65	0.61	0.57	0.60	0.63
Al_2O_3	17.70	16.46	18.59	18.26	17.68	17.04	17.29	18.17	17.04	17.22	20.22	17.41
Fe_2O_3	8.23	7.13	9.63	8.88	6.70	8.36	8.42	8.83	8.39	7.29	7.51	8.40
MnO	0.13	0.11	0.15	0.14	0.12	0.14	0.13	0.14	0.14	0.12	0.13	0.13
MgO	4.15	5.06	4.98	5.48	3.68	6.26	6.32	6.62	6.55	4.03	2.68	4.57
CaO	7.53	6.49	7.67	7.92	6.54	8.15	8.14	8.26	8.10	6.37	4.91	7.95
Na_2O	3.24	3.24	2.91	2.77	3.50	3.11	3.08	2.74	3.03	3.47	2.90	3.21
K_2O	0.55	1.04	0.29	0.68	0.64	0.62	0.58	0.36	0.52	1.08	1.07	0.95
P_2O_5	0.09	0.11	0.08	0.08	0.09	0.06	0.06	0.04	0.05	0.10	0.12	0.11
H_2O	0.36	0.52	0.43	0.44	0.40	1.22	0.84	1.01	1.67	0.43	1.88	0.16
LOI	0.25	0.42	1.03	0.90	0.69	1.76	1.44	2.17	2.36	0.42	3.25	-0.15
Total	99.90	99.90	99.90	99.88	99.89	99.89	99.87	99.88	99.88	99.88	99.88	99.91
Be												
Cs	0.68	0.65	0.49	1.50	0.30	1.25	1.04	0.84	1.28	0.77	1.94	1.31
Ba	217	289	236	282	305	235	260	254	227	304	436	289
Rb	11	27	4	19	8	16	14	8	13	27	34	25
Sr	225	222	218	267	266	257	251	295	269	277	238	258
Pb	7.22	42.01	52.54	36.75	25.50	28.55	28.66	26.30	16.40	29.37	18.39	16.43
Th	1.48	2.63	1.84	4.28	1.87	3.41	3.43	3.53	3.30	2.47	5.10	2.76
U	0.41	0.80	0.39	0.85	0.41	0.87	0.91	0.83	0.89	0.79	1.11	0.77
Zr	60	81	64	96	64	85	84	89	82	75	109	70
Nb	1.84	2.72	2.15	3.97	2.05	3.23	3.23	3.16	3.13	2.41	4.86	2.52
Hf	1.69	2.29	1.81	2.67	1.80	2.41	2.34	2.50	2.33	2.11	3.05	1.99
Ta	0.14	0.23	0.17	0.31	0.15	0.24	0.26	0.24	0.24	0.19	0.37	0.19
Y	15	20	16	18	11	19	16	14	21	18	17	17
Sc	26.1	25.9	35.6	34.8	23.6	33.2	33.7	35.5	33.9	24.9	19.1	30.2
V	194	180	252	222	166	193	194	197	184	185	148	217
Cr	59	208	48	108	70	210	218	219	212	78	18	63
Co	42	52	41	54	36	76	62	67	75	48	56	63
Ni	30	77	25	35	27	65	59	62	56	43	14	32
Cu	33	38	48	41	26	45	40	34	37	31	21	44
Zn	79	139	177	180	163	168	164	172	192	102	224	216
Ga	17	16	17	18	17	17	17	18	17	17	20	16
La	4.54	9.17	4.84	11.13	4.91	8.77	8.25	8.02	9.26	8.18	11.16	7.95
Ce	9.20	14.86	11.43	23.54	12.18	20.27	20.49	20.44	20.10	15.75	26.27	16.73
Pr	1.33	2.52	1.77	3.09	1.39	2.47	2.45	2.48	2.57	2.26	2.90	2.09
Nd	6.54	11.66	8.61	13.76	6.36	11.25	10.82	10.70	11.55	10.38	12.61	9.80
Sm	1.79	2.97	2.49	3.35	1.68	2.89	2.73	2.80	3.02	2.61	3.01	2.47
Eu	0.67	0.82	0.85	0.92	0.60	0.78	0.82	0.84	0.82	0.79	0.85	0.75
Gd	1.99	3.04	2.68	3.20	1.85	2.88	2.86	2.71	3.19	2.89	2.88	2.55
Tb	0.37	0.49	0.47	0.57	0.32	0.53	2.05	0.49	0.55	0.50	0.48	0.46
Dy	2.63	3.32	3.19	3.64	2.02	3.31	3.29	3.38	3.56	3.10	3.27	3.01
Ho	0.56	0.73	0.65	0.76	0.43	0.74	0.69	0.67	0.77	0.64	0.65	0.62
Er	1.65	2.04	1.99	2.23	1.25	2.19	2.08	1.95	2.31	1.93	1.95	1.90
Tm	0.26	0.31	0.28	0.33	0.18	0.33	0.31	0.29	0.35	0.28	0.31	0.31
Yb	1.79	2.15	1.96	2.24	1.26	2.19	2.06	1.95	2.28	1.97	2.24	1.93
Lu	0.29	0.34	0.30	0.32	0.19	0.32	0.30	0.27	0.33	0.31	0.31	0.29

VDA= Volcanic debris-avalanche deposit
DF= Debris-flow deposit
HCF= Hyperconcentrated-flow deposit
RG= River gravel
MT= Marine-terrace gravel

Appendix II (continued). Representative whole-rock analyses of the Ruapehu mass flows (XRF and ICP-MS combined)

	60	61	62	63	64	65	66	67	68	69	70	71
Formation	**Oreore Formation**			**Piriaka Formation**								
Deposit	**VDA**	**VDA**	**VDA**	**VDA**	**VDA**	**VDA**	**VDA**	**VDA**	**DF**	**DF**	**VDA**	**VDA**
Sample no.:	OH4	OH5	OH6	PI1	PI2	PI3	PI4	PI5	PI7	PI8	PL1	PL2
SiO_2	54.93	55.23	53.79	56.89	56.55	57.30	57.53	56.28	57.08	54.41	56.73	57.28
TiO_2	0.57	0.55	0.55	0.62	0.72	0.62	0.55	0.67	0.65	0.70	0.69	0.58
Al_2O_3	18.65	18.29	18.36	17.96	17.43	17.43	17.55	16.91	17.26	18.28	18.36	16.85
Fe_2O_3	7.56	7.32	7.52	7.93	8.88	7.88	8.28	8.49	8.37	9.28	7.85	7.89
MnO	0.13	0.13	0.13	0.13	0.14	0.12	0.13	0.13	0.13	0.15	0.12	0.13
MgO	4.17	4.05	4.31	4.28	4.04	4.37	4.16	5.12	4.09	4.51	3.50	4.97
CaO	6.55	6.54	6.63	7.75	7.42	7.41	7.66	7.99	7.30	8.28	7.32	7.76
Na_2O	3.24	3.27	3.28	3.36	3.20	3.37	3.37	3.27	3.28	3.01	3.52	3.25
K_2O	0.62	0.64	0.58	0.87	1.30	1.03	0.64	0.88	1.09	0.66	1.09	0.93
P_2O_5	0.09	0.08	0.08	0.10	0.18	0.11	0.08	0.10	0.13	0.09	0.11	0.11
H_2O	1.04	1.26	1.63	0.16	0.12	0.20	0.15	0.16	0.38	0.25	0.26	0.16
LOI	2.34	2.53	3.03	-0.10	-0.09	0.06	-0.20	-0.11	0.11	0.29	0.35	-0.02
Total	99.89	99.90	99.89	99.92	99.89	99.90	99.91	99.89	99.88	99.90	99.90	99.88
Be												
Cs	1.03	1.08	0.91	0.86	1.15	1.43	0.34	1.01	1.10	1.04	1.73	1.24
Ba	285	243	280	247	356	264	200	251	289	186	284	283
Rb	16	16	15	20	32	26	14	20	28	17	28	24
Sr	253	253	270	243	297	250	219	256	236	214	273	249
Pb	13.93	13.72	12.14	11.05	14.30	24.86	31.45	33.30	5.98	4.77	27.71	25.56
Th	2.03	1.94	1.93	2.18	3.51	2.57	1.25	2.23	2.61	1.71	2.81	2.29
U	0.52	0.51	0.49	0.58	0.87	0.68	0.41	0.62	0.73	0.51	0.73	0.64
Zr	72	68	68	68	90	74	52	68	74	62	78	70
Nb	2.19	2.14	2.19	2.54	3.23	2.67	1.60	2.37	2.48	2.03	3.02	2.22
Hf	2.04	1.96	1.88	1.91	2.48	2.14	1.52	1.93	2.05	1.80	2.12	1.87
Ta	0.16	0.16	0.15	0.18	0.23	0.21	0.11	0.17	0.19	0.15	0.21	0.18
Y	13	13	12	16	20	17	14	16	16	16	17	16
Sc	25.9	25.1	25.5	27.9	30.1	27.0	28.1	30.9	25.8	30.0	23.1	28.8
V	183	175	182	203	234	201	205	222	202	232	202	197
Cr	81	77	85	47	36	73	44	113	59	30	30	127
Co	31	49	48	57	45	46	41	52	35	62	49	43
Ni	34	30	39	31	24	50	27	55	22	18	32	42
Cu	26	27	29	41	26	35	67	57	43	56	51	51
Zn	195	187	183	172	193	177	236	177	68	71	179	178
Ga	18	17	17	17	18	17	16	17	16	17	18	17
La	4.72	4.78	4.38	6.53	11.29	7.30	4.11	6.93	7.87	5.42	7.95	7.00
Ce	12.81	12.57	12.01	13.81	23.96	15.81	9.04	14.75	16.88	12.28	17.61	14.84
Pr	1.46	1.41	1.36	1.79	3.20	1.97	1.23	1.92	2.32	1.66	2.17	1.96
Nd	7.05	6.71	6.44	8.54	15.23	9.40	6.04	9.15	10.42	7.76	9.92	9.25
Sm	1.94	1.85	1.88	2.29	3.92	2.52	1.73	2.41	2.69	2.11	2.49	2.53
Eu	0.67	0.64	0.66	0.72	1.07	0.73	0.58	0.75	0.81	0.67	0.79	0.76
Gd	2.08	2.05	1.94	2.44	3.72	2.60	2.07	2.65	2.77	2.35	2.64	2.59
Tb	0.36	0.36	0.35	0.43	0.74	0.46	0.37	0.44	0.44	0.43	0.45	0.41
Dy	2.55	2.33	2.33	2.89	3.60	2.94	2.50	2.93	2.95	2.88	3.00	2.79
Ho	0.52	0.50	0.47	0.58	0.72	0.62	0.53	0.58	0.60	0.61	0.64	0.61
Er	1.53	1.48	1.52	1.88	2.15	1.88	1.56	1.77	1.70	1.77	1.96	1.76
Tm	0.25	0.22	0.23	0.27	0.31	0.28	0.24	0.26	0.27	0.28	0.28	0.27
Yb	1.68	1.63	1.55	1.80	2.16	1.90	1.66	1.82	1.85	1.87	2.05	1.77
Lu	0.26	0.25	0.24	0.28	0.31	0.29	0.25	0.28	0.27	0.27	0.29	0.27

VDA= Volcanic debris-avalanche deposit
DF= Debris-flow deposit
HCF= Hyperconcentrated-flow deposit
RG= River gravel
MT= Marine-terrace gravel

Appendix II (continued). Representative whole-rock analyses of the Ruapehu mass flows (XRF and ICP-MS combined)

	72	73	74	75	76	77	78	79	80	81	82	83
Formation						**Piriaka Formation**						
Deposit	**VDA**	**DF**	**DF**	**DF**	**N/A**	**N/A**	**N/A**	**DF**	**DF**	**DF**	**DF**	**VDA**
Sample no.:	PL3	KAI1	KAI2	KAI3	SpL2	SpU1	SpU2	KA1	KA2	KA3	KA4	SH4-1
SiO_2	58.14	57.79	57.63	59.24	54.48	56.22	56.51	57.52	57.06	56.36	54.97	58.37
TiO_2	0.61	0.62	0.70	0.63	0.68	0.68	0.73	0.64	0.63	0.65	0.62	0.78
Al_2O_3	17.77	16.17	16.26	17.26	18.27	18.20	17.39	17.35	17.05	16.89	16.92	16.30
Fe_2O_3	7.85	7.49	7.66	6.97	8.65	8.21	8.53	8.07	8.28	8.69	9.03	8.19
MnO	0.13	0.11	0.11	0.11	0.13	0.13	0.12	0.12	0.14	0.14	0.13	0.13
MgO	3.59	5.50	4.85	3.78	4.42	4.27	4.17	4.21	4.62	4.86	5.47	4.09
CaO	7.08	7.51	7.26	6.88	7.65	7.67	6.29	7.02	7.62	7.83	8.38	7.03
Na_2O	3.40	3.21	3.15	3.70	3.06	3.47	3.13	3.42	3.14	3.08	2.85	3.24
K_2O	1.03	1.14	1.20	1.21	0.74	0.79	1.11	1.04	0.82	0.97	0.65	1.48
P_2O_5	0.11	0.11	0.12	0.11	0.11	0.11	0.11	0.11	0.11	0.11	0.09	0.14
H_2O	0.25	0.28	0.60	0.03	0.66	0.23	0.75	0.31	0.30	0.29	0.33	0.12
LOI	-0.05	-0.04	0.34	-0.03	1.04	-0.09	1.03	0.07	0.13	0.01	0.46	-0.01
Total	99.90	99.88	99.89	99.88	99.89	99.89	99.89	99.89	99.89	99.87	99.89	99.87
Be												
Cs	0.74	0.87	1.21	2.16	1.09	0.41	1.19	1.01	0.40	1.38	0.27	2.38
Ba	292	288	373	336	244	262	286	260	224	268	186	298
Rb	28	32	29	36	17	16	31	28	20	26	14	45
Sr	267	246	299	329	314	255	225	236	252	231	197	249
Pb	24.19	19.82	18.39	17.11	6.59	3.66	5.40	5.71	3.41	6.05	3.59	8.00
Th	2.94	3.37	4.60	3.73	2.19	2.11	2.99	2.39	1.76	2.70	1.54	4.91
U	0.79	0.85	0.94	0.93	0.58	0.60	0.80	0.73	0.55	0.78	0.43	1.19
Zr	79	86	104	94	63	70	80	70	60	67	56	116
Nb	3.03	3.23	4.33	3.30	2.04	2.14	3.04	2.41	2.03	2.54	1.89	4.81
Hf	2.22	2.45	2.86	2.61	1.80	1.97	2.20	1.96	1.65	1.91	1.63	3.08
Ta	0.23	0.25	0.33	0.26	0.13	0.15	0.23	0.17	0.15	0.18	0.13	0.35
Y	16	16	17	16	16	15	29	18	18	20	15	20
Sc	25.6	29.8	30.7	26.4	29.1	24.7	28.9	25.1	28.1	30.8	31.8	26.3
V	188	193	184	196	234	210	227	200	215	229	228	194
Cr	32	180	115	43	50	39	43	76	91	75	98	88
Co	49	63	48	59	51	47	38	47	71	37	49	55
Ni	26	74	42	31	30	31	14	36	27	25	36	28
Cu	39	48	33	57	25	40	32	46	32	31	46	30
Zn	188	215	232	230	69	71	64	64	62	73	63	65
Ga	17	16	17	17	17	18	17	16	16	16	15	16
La	8.18	8.79	12.10	8.95	6.29	6.65	13.60	7.26	7.08	8.74	5.11	13.02
Ce	17.76	18.30	24.09	18.96	14.59	14.47	23.99	15.12	13.72	16.47	11.56	28.78
Pr	2.22	2.34	3.18	2.35	1.87	1.88	4.06	2.09	2.07	2.31	1.49	3.43
Nd	9.94	10.61	13.76	10.51	8.80	8.54	18.87	9.59	9.52	10.64	7.13	14.83
Sm	2.57	2.77	3.41	2.69	2.35	2.14	4.51	2.52	2.53	2.62	1.99	3.44
Eu	0.77	0.76	1.00	0.71	0.74	0.72	1.26	0.77	0.76	0.77	0.61	0.90
Gd	2.68	2.72	3.22	2.72	2.49	2.22	4.91	2.68	2.66	2.88	2.19	3.49
Tb	0.45	0.46	0.53	0.46	0.44	0.39	0.76	0.48	0.46	0.47	0.41	0.58
Dy	2.98	3.01	3.38	2.92	2.88	2.58	5.16	2.88	3.01	3.18	2.63	3.65
Ho	0.62	0.63	0.65	0.62	0.59	0.55	1.05	0.63	0.63	0.70	0.58	0.78
Er	1.84	1.84	1.94	1.87	1.85	1.65	2.97	1.89	1.91	2.06	1.69	2.23
Tm	0.29	0.26	0.29	0.26	0.25	0.24	0.45	0.28	0.28	0.29	0.26	0.33
Yb	2.02	1.83	1.83	1.87	1.78	1.67	2.94	1.91	1.92	2.07	1.85	2.31
Lu	0.29	0.26	0.27	0.28	0.28	0.25	0.44	0.29	0.29	0.32	0.27	0.33

VDA= Volcanic debris-avalanche deposit
DF= Debris-flow deposit
HCF= Hyperconcentrated-flow deposit
RG= River gravel
MT= Marine-terrace gravel

Appendix II (continued). Representative whole-rock analyses of the Ruapehu mass flows (XRF and ICP-MS combined)

	84	85	86	87	88	89	90	91	92	93	94	95
Formation	**Piriaka**	**Pukekaha Formation**										
Deposit	**VDA**	**VDA**	**VDA**	**VDA**	**VDA**	**VDA**	**VDA**	**VDA**	**VDA**	**VDA**	**HCF**	**HCF**
Sample no.:	SH4-2	HR1	HR2	RB2	RB4	RB5	RB6	MA1	MA2	MA3	WY1	WY3
SiO_2	56.72	55.27	59.02	58.16	59.09	57.91	56.95	57.97	56.43	57.95	55.08	57.97
TiO_2	0.68	0.75	0.64	0.77	0.76	0.72	0.80	0.72	0.73	0.74	0.72	0.49
Al_2O_3	17.17	16.36	17.45	16.72	14.94	14.74	16.62	15.20	17.70	14.85	17.32	18.10
Fe_2O_3	9.11	8.72	7.11	6.79	7.01	7.26	7.09	7.27	7.90	7.23	9.22	7.16
MnO	0.13	0.14	0.09	0.10	0.11	0.11	0.11	0.12	0.12	0.11	0.15	0.13
MgO	4.28	5.74	3.47	4.19	5.80	6.95	4.73	6.17	4.40	6.63	4.55	3.14
CaO	7.51	8.38	6.11	6.86	6.80	7.16	7.27	7.50	7.69	7.33	7.90	6.34
Na_2O	3.27	2.89	3.54	3.32	3.07	2.98	3.22	3.03	3.18	3.01	3.00	3.16
K_2O	0.71	0.92	1.25	1.78	1.91	1.62	1.69	1.60	1.13	1.60	0.89	0.66
P_2O_5	0.10	0.13	0.11	0.16	0.15	0.14	0.16	0.14	0.13	0.14	0.13	0.10
H_2O	0.26	0.38	0.53	0.40	0.09	0.08	0.32	0.12	0.50	0.19	0.39	0.92
LOI	-0.03	0.17	0.55	0.63	0.12	0.16	0.91	0.02	-0.04	0.04	0.55	1.73
Total	99.92	99.86	99.88	99.87	99.84	99.85	99.86	99.85	99.87	99.84	99.89	99.91
Be												
Cs	0.58	1.19	0.99	3.59	4.27	3.56	3.35	2.31	1.15	3.13	1.05	1.29
Ba	169	238	311	349	363	319	341	337	304	328	222	212
Rb	16	26	36	61	69	58	57	54	29	55	20	18
Sr	213	292	284	261	228	218	260	248	300	233	219	205
Pb	3.67	5.84	6.47	9.44	10.05	8.60	9.07	8.17	6.17	8.50	4.67	5.12
Th	1.25	2.98	3.45	5.94	6.56	5.41	5.46	5.28	3.35	5.14	2.07	1.94
U	0.38	0.70	0.92	1.61	1.82	1.53	1.46	1.47	0.84	1.46	0.56	0.58
Zr	55	81	87	128	134	114	121	115	85	115	67	63
Nb	1.61	3.37	2.93	4.67	4.92	4.10	4.61	4.07	3.49	4.05	2.53	2.48
Hf	1.56	2.23	2.46	3.45	3.62	3.17	3.21	3.12	2.40	3.19	1.83	1.71
Ta	0.11	0.23	0.23	0.35	0.39	0.32	0.33	0.31	0.25	0.32	0.17	0.18
Y	23	17	16	18	18	17	17	17	18	16	18	14
Sc	29.6	33.8	23.5	20.9	25.1	25.3	22.5	27.3	26.4	26.1	29.6	18.6
V	238	239	195	181	186	188	186	195	213	197	229	141
Cr	49	134	37	88	245	334	104	237	79	309	47	19
Co	44	47	35	63	38	63	37	43	52	40	66	44
Ni	25	44	26	51	90	125	59	86	34	105	24	10
Cu	15	59	44	41	63	54	41	45	71	78	46	26
Zn	76	66	54	54	53	51	53	53	63	54	76	72
Ga	16	16	16	17	15	15	16	15	17	15	16	16
La	7.02	10.32	9.95	13.23	13.80	11.60	12.51	10.93	10.61	11.21	6.98	6.01
Ce	15.51	21.85	21.44	28.66	30.10	24.74	27.32	23.59	22.49	24.46	15.80	12.32
Pr	2.22	2.74	2.77	3.48	3.55	2.97	3.29	2.90	2.88	2.94	2.09	1.57
Nd	10.89	12.28	11.97	14.86	15.26	13.03	14.37	12.43	12.60	12.77	9.60	6.95
Sm	3.08	2.94	2.85	3.34	3.60	3.15	3.28	2.95	3.03	2.93	2.61	1.74
Eu	0.79	0.85	0.77	0.83	0.80	0.72	0.85	0.79	0.86	0.75	0.78	0.58
Gd	3.40	2.96	2.92	3.20	3.32	3.00	3.10	2.86	2.90	2.82	2.83	2.05
Tb	0.57	0.58	0.47	0.51	0.53	0.49	0.50	0.49	0.49	0.47	0.48	0.35
Dy	3.90	3.24	3.02	3.25	3.38	3.06	3.20	3.09	3.18	2.97	3.06	2.39
Ho	0.80	0.67	0.61	0.64	0.69	0.61	0.67	0.62	0.67	0.60	0.66	0.54
Er	2.45	1.94	1.80	1.92	2.01	1.86	1.91	1.84	1.89	1.70	1.97	1.60
Tm	0.35	0.28	0.26	0.30	0.30	0.26	0.27	0.27	0.28	0.25	0.30	0.23
Yb	2.37	1.89	1.75	1.95	1.98	1.81	1.84	1.74	1.92	1.70	2.10	1.69
Lu	0.34	0.29	0.24	0.28	0.29	0.27	0.27	0.26	0.28	0.26	0.30	0.26

VDA= Volcanic debris-avalanche deposit
DF= Debris-flow deposit
HCF= Hyperconcentrated-flow deposit
RG= River gravel
MT= Marine-terrace gravel

Appendix II (continued). Representative whole-rock analyses of the Ruapehu mass flows (XRF and ICP-MS combined)

	96	97	98	99	100	101	102	103
Formation	**Pukekaha Formation**				**Turakina Formation**			
Deposit	**HCF**	**HCF**	**DF**	**DF**	**DF**	**DF**	**DF**	**DF**
Sample no.:	WY5	WY6	BR1	BR3	TUR_01	RAT_01	RAT_02	RAT_03
SiO_2	55.36	56.21	56.74	54.19	58.65	58.65	56.91	59.31
TiO_2	0.64	0.68	0.67	0.81	0.64	0.49	0.53	0.49
Al_2O_3	17.53	17.44	16.74	17.78	17.91	17.77	17.51	16.47
Fe_2O_3	8.21	9.04	7.55	9.67	6.80	7.00	7.30	6.69
MnO	0.14	0.15	0.12	0.15	0.11	0.12	0.11	0.11
MgO	4.49	4.25	5.04	4.71	3.36	3.05	4.22	4.13
CaO	7.58	7.15	7.58	8.21	7.15	6.67	7.47	6.89
Na_2O	3.04	3.02	3.06	3.03	3.49	3.45	3.23	3.48
K_2O	0.87	0.88	1.07	0.81	1.07	0.81	0.77	0.88
P_2O_5	0.13	0.11	0.10	0.08	0.11	0.10	0.09	0.10
H_2O	0.64	0.47	0.62	0.38	0.17	0.34	0.44	0.27
LOI	1.26	0.50	0.60	0.09	0.43	1.47	1.31	1.08
Total	99.89	99.90	99.88	99.89	99.88	99.91	99.88	99.90
Be								
Cs	1.26	0.68	1.52	1.24	1.75	1.60	1.43	1.32
Ba	270	234	264	204	296	234	247	276
Rb	21	24	28	21	31	25	22	22
Sr	238	218	244	224	265	212	243	247
Pb	5.69	4.52	6.15	4.98	14.31	23.58	32.63	39.54
Th	2.55	2.34	2.77	1.90	3.19	2.05	2.31	1.78
U	0.69	0.64	0.75	0.50	0.79	0.62	0.63	0.58
Zr	68	67	74	61	86	68	72	65
Nb	2.20	2.66	2.71	2.20	3.47	2.80	2.65	2.12
Hf	1.91	1.83	2.08	1.80	2.38	1.88	1.95	1.80
Ta	0.15	0.20	0.21	0.15	0.29	0.19	0.21	0.15
Y	16	18	16	17	16	15	13	13
Sc	25.9	28.4	30.2	36.4	23.1	20.3	26.9	24.0
V	208	221	194	284	178	147	174	164
Cr	85	43	76	49	85	23	142	126
Co	46	51	47	52	57	39	67	51
Ni	26	20	35	15	33	20	63	51
Cu	39	31	48	35	34	27	30	32
Zn	68	79	63	71	173	191	203	233
Ga	16	16	16	17	17	16	17	15
La	7.62	7.14	8.22	5.85	8.53	6.11	6.21	5.86
Ce	16.26	15.62	17.52	13.41	18.49	12.53	13.22	12.57
Pr	2.07	2.00	2.22	1.77	2.28	1.63	1.62	1.61
Nd	9.71	9.31	9.95	8.52	9.95	7.38	7.45	7.22
Sm	2.32	2.38	2.69	2.52	2.51	1.98	1.93	1.94
Eu	0.71	0.75	0.73	0.81	0.74	0.64	0.64	0.65
Gd	2.48	2.66	2.67	2.80	2.57	2.18	2.10	1.99
Tb	0.42	0.46	0.44	0.47	0.46	0.38	0.39	0.34
Dy	2.84	3.09	2.99	3.13	2.91	2.60	2.39	2.20
Ho	0.59	0.68	0.62	0.68	0.63	0.60	0.51	0.48
Er	1.70	1.99	1.77	1.91	1.86	1.74	1.55	1.42
Tm	0.26	0.30	0.25	0.31	0.29	0.29	0.24	0.22
Yb	1.83	2.11	1.75	2.03	1.87	1.96	1.55	1.53
Lu	0.27	0.31	0.26	0.29	0.28	0.31	0.24	0.23

VDA= Volcanic debris-avalanche deposit
DF= Debris-flow deposit
HCF= Hyperconcentrated-flow deposit
RG= River gravel
MT= Marine-terrace gravel

DRC 16

MASSEY UNIVERSITY
GRADUATE RESEARCH SCHOOL

STATEMENT OF CONTRIBUTION
TO DOCTORAL THESIS CONTAINING PUBLICATIONS

(To appear at the end of each thesis chapter/section/appendix submitted as an article/paper or collected as an appendix at the end of the thesis)

We, the candidate and the candidate's Principal Supervisor, certify that all co-authors have consented to their work being included in the thesis and they have accepted the candidate's contribution as indicated below in the *Statement of Originality*.

Name of Candidate: Manuela Tost

Name/Title of Principal Supervisor: Shane J. Cronin

Name of Published Research Output and full reference:

Impacts of catastrophic volcanic collapse on the erosion and morphology of a distal fluvial landscape: Hautapu River, Mount Ruapehu, New Zealand
M. Tost, S. J. Cronin, J. N. Procter, I. E. M. Smith, V. E. Neall, R. C. Price
Geological Society of America Bulletin, 127(1-2), 266-280.

In which Chapter is the Published Work: Chapter 3

Please indicate either:

- The percentage of the Published Work that was contributed by the candidate: 70%

  and / or

- Describe the contribution that the candidate has made to the Published Work:

  Field studies; Sampling and laboratory preparation of clasts; Manuscript preparation and writing

Manuela Tost
Digitally signed by Manuela Tost
DN: cn=Manuela Tost, o=Massey University, ou=Institute of Natural Resources, email=m.tost@massey.ac.nz, c=NZ
Date: 2015.03.13 10:04:41 +12'00'

Candidate's Signature

13.03.2015
Date

Shane Cronin
Digitally signed by Shane Cronin
DN: cn=Shane Cronin, o=University of Auckland, ou=School of Environment, email=s.cronin@auckland.ac.nz, c=NZ
Date: 2015.03.13 13:07:40 +13'00'

Principal Supervisor's signature

13/3/2015
Date

DRC 16

MASSEY UNIVERSITY
GRADUATE RESEARCH SCHOOL

STATEMENT OF CONTRIBUTION
TO DOCTORAL THESIS CONTAINING PUBLICATIONS

(To appear at the end of each thesis chapter/section/appendix submitted as an article/paper or collected as an appendix at the end of the thesis)

We, the candidate and the candidate's Principal Supervisor, certify that all co-authors have consented to their work being included in the thesis and they have accepted the candidate's contribution as indicated below in the *Statement of Originality*.

Name of Candidate: Manuela Tost

Name/Title of Principal Supervisor: Shane J. Cronin

Name of Published Research Output and full reference:

Transport and emplacement mechanisms of channelized long-runout debris avalanches, Ruapehu volcano, New Zealand
M.Tost, S.J. Cronin, J.N. Procter
Bulletin of Volcanology, 76(12), 1-14.

In which Chapter is the Published Work: Chapter 4

Please indicate either:

- The percentage of the Published Work that was contributed by the candidate 80%
  and / or
- Describe the contribution that the candidate has made to the Published Work:
  Field studies; Manuscript preparation and writing

Manuela Tost
Digitally signed by Manuela Tost
DN: cn=Manuela Tost, o=Massey University, ou=Institute of Natural Resources, email=m.tost@massey.ac.nz, c=NZ
Date: 2015.03.13 10:07:42 +12'00'

Candidate's Signature

13.03.2015
Date

Shane Cronin
Digitally signed by Shane Cronin
DN: cn=Shane Cronin, o=University of Auckland, ou=School of Environment, email=s.cronin@auckland.ac.nz, c=NZ
Date: 2015.03.13 13:06:56 +13'00'

Principal Supervisor's signature

13/03/2015
Date